Internal Combustion Engine Fundamentals

John B. Heywood

INTERNAL COMBUSTION ENGINE FUNDAMENTALS

McGraw-Hill Series in Mechanical Engineering

Jack P. Holman, *Southern Methodist University*
Consulting Editor

Anderson: *Modern Compressible Flow: With Historical Perspective*
Dieter: *Engineering Design: A Materials and Processing Approach*
Eckert and Drake: *Analysis of Heat and Mass Transfer*
Heywood: *Internal Combustion Engine Fundamentals*
Hinze: *Turbulence, 2/e*
Hutton: *Applied Mechanical Vibrations*
Juvinall: *Engineering Considerations of Stress, Strain, and Strength*
Kane and Levinson: *Dynamics: Theory and Applications*
Kays and Crawford: *Convective Heat and Mass Transfer*
Martin: *Kinematics and Dynamics of Machines*
Phelan: *Dynamics of Machinery*
Phelan: *Fundamentals of Mechanical Design, 3/e*
Pierce: *Acoustics: An Introduction to Its Physical Principles and Applications*
Raven: *Automatic Control Engineering, 4/e*
Rosenberg and Karnopp: *Introduction to Physics*
Schlichting: *Boundary-Layer Theory, 7/e*
Shames: *Mechanics of Fluids, 2/e*
Shigley: *Kinematic Analysis of Mechanisms, 2/e*
Shigley and Mitchell: *Mechanical Engineering Design, 4/e*
Shigley and Uicker: *Theory of Machines and Mechanisms*
Stoecker and Jones: *Refrigeration and Air Conditioning, 2/e*
Vanderplaats: *Numerical Optimization Techniques for Engineering Design: With Applications*

INTERNAL COMBUSTION ENGINE FUNDAMENTALS

John B. Heywood

Professor of Mechanical Engineering
Director, Sloan Automotive Laboratory
Massachusetts Institute of Technology

McGraw-Hill, Inc.
New York St. Louis San Francisco Auckland Bogotá
Caracas Lisbon London Madrid Mexico Milan
Montreal New Delhi Paris San Juan Singapore
Sydney Tokyo Toronto

INTERNAL COMBUSTION ENGINE FUNDAMENTALS

This book was set in Times Roman.
The editors were Anne Duffy and John M. Morriss; the designer was Joan E. O'Connor; the production supervisor was Denise L. Puryear. New drawings were done by ANCO.
Project Supervision was done by Santype International Ltd.
R. R. Donnelley & Sons Company was printer and binder.

See acknowledgements on page xxi.

7890 DOCDOC 93

ISBN 0-07-028637-X

Library of Congress Cataloging-in-Publication Data

Heywood, John B.
Internal combustion engine fundamentals.
(McGraw-Hill series in mechanical engineering)
Bibliography: p.
Includes index.
1. Internal combustion engines. I. Title. II. Series.
TJ755.H45 1988 621.43 87-15251

Dr. John B. Heywood
the Massachusetts Inst
doctoral year of resear
Electricity Generating
hydrodynamic power g
is Professor of Mecha
Automotive Laborator
Division of the Mech
Energy Program Direc
to the MIT Sports Car

Professor Heywoo
modynamics, combust
decades, his research a
fuels requirements of
been on computer mo
sions of spark-ignitio
experiments to develo
technology assessmen
mobile fuel utilization
the automotive and pe

His extensive rese
Army, Department
National Science Fou
petroleum companies.

ABOUT THE AUTHOR

Dr. John B. Heywood received the Ph.D. degree in mechanical engineering from the Massachusetts Institute of Technology in 1965. Following an additional post-doctoral year of research at MIT, he worked as a research officer at the Central Electricity Generating Board's Research Laboratory in England on magneto-hydrodynamic power generation. In 1968 he joined the faculty at MIT where he is Professor of Mechanical Engineering. At MIT he is Director of the Sloan Automotive Laboratory. He is currently Head of the Fluid and Thermal Science Division of the Mechanical Engineering Department, and the Transportation Energy Program Director in the MIT Energy Laboratory. He is faculty advisor to the MIT Sports Car Club.

Professor Heywood's teaching and research interests lie in the areas of thermodynamics, combustion, energy, power, and propulsion. During the past two decades, his research activities have centered on the operating characteristics and fuels requirements of automotive and aircraft engines. A major emphasis has been on computer models which predict the performance, efficiency, and emissions of spark-ignition, diesel, and gas turbine engines, and in carrying out experiments to develop and validate these models. He is also actively involved in technology assessments and policy studies related to automotive engines, automobile fuel utilization, and the control of air pollution. He consults frequently in the automotive and petroleum industries, and for the U.S. Government.

His extensive research in the field of engines has been supported by the U.S. Army, Department of Energy, Environmental Protection Agency, NASA, National Science Foundation, automobile and diesel engine manufacturers, and petroleum companies. He has presented or published over a hundred papers on

his research in technical conferences and journals. He has co-authored two previous books: *Open-Cycle MHD Power Generation* published by Pergamon Press in 1969 and *The Automobile and the Regulation of Its Impact on the Environment* published by University of Oklahoma Press in 1975.

He is a member of the American Society of Mechanical Engineers, an associate fellow of the American Institute of Aeronautics and Astronautics, a fellow of the British Institution of Mechanical Engineers, and in 1982 was elected a Fellow of the U.S. Society of Automotive Engineers for his technical contributions to automotive engineering. He is a member of the editorial boards of the journals *Progress in Energy and Combustion Science* and the *International Journal of Vehicle Design.*

His research publications on internal combustion engines, power generation, and gas turbine combustion have won numerous awards. He was awarded the Ayreton Premium in 1969 by the British Institution of Electrical Engineers. Professor Heywood received a Ralph R. Teetor Award as an outstanding young engineering educator from the Society of Automotive Engineers in 1971. He has twice been the recipient of an SAE Arch T. Colwell Merit Award for an outstanding technical publication (1973 and 1981). He received SAE's Horning Memorial Award for the best paper on engines and fuels in 1984. In 1984 he received the Sc.D. degree from Cambridge University for his published contributions to engineering research. He was selected as the 1986 American Society of Mechanical Engineers Freeman Scholar for a major review of "Fluid Motion within the Cylinder of Internal Combustion Engines."

as co-authored two pre-
hed by Pergamon Press
pact on the Environment

cal Engineers, an associ-
Astronautics, a fellow of
982 was elected a Fellow
chnical contributions to
l boards of the journals
nternational Journal of

gines, power generation,
ls. He was awarded the
lectrical Engineers. Pro-
an outstanding young
gineers in 1971. He has
Award for an outstand-
AE's Horning Memorial
In 1984 he received the
lished contributions to
an Society of Mechani-
luid Motion within the

THIS BOOK IS DEDICATED TO MY FATHER,
Harold Heywood:

I have followed many of the paths he took.

CONTENTS

Appendixes

Internal combustion
spark-ignition engine
engine. Since that tim
of engine processes
demand for new typ
engine use changed. I
and manufacture the
fields of power, propu
an explosive growth i
lution, fuel cost, and
tant. An enormous te
adequately organized

This book has be
to that need. It conta
principles which gov
attempts to provide
technical material th
engines, and at the sa
dimensions of this pr
sound knowledge of
tribute to this field, a
base which has been
research, developmen
about engines. The e
and chemistry, fluid
vant to internal comb
fuels requirements.

CHAPTER 2

ENGINE DESIGN AND OPERATING PARAMETERS

2.1 IMPORTANT ENGINE CHARACTERISTICS

In this chapter, some basic geometrical relationships and the parameters commonly used to characterize engine operation are developed. The factors important to an engine user are:

1. The engine's performance over its operating range
2. The engine's fuel consumption within this operating range and the cost of the required fuel
3. The engine's noise and air pollutant emissions within this operating range
4. The initial cost of the engine and its installation
5. The reliability and durability of the engine, its maintenance requirements, and how these affect engine availability and operating costs

These factors control total engine operating costs—usually the primary consideration of the user—and whether the engine in operation can satisfy environmental regulations. This book is concerned primarily with the performance, efficiency, and emissions characteristics of engines; the omission of the other factors listed above does not, in any way, reduce their great importance.

CHAPTER
2

ENGINE
DESIGN
)PERATING
RAMETERS

and the parameters com-
eloped. The factors impor-

ıg range and the cost of the

ıin this operating range

intenance requirements, and
costs

ısually the primary consider-
on can satisfy environmental
the performance, efficiency,
on of the other factors listed
:tance.

Engine performance is more precisely defined by

1. The maximum power (or the maximum torque) available at each speed within the useful engine operating range
2. The range of speed and power over which engine operation is satisfactory

The following performance definitions are commonly used:

Maximum rated power. The highest power an engine is allowed to develop for short periods of operation.

Normal rated power. The highest power an engine is allowed to develop in continuous operation.

Rated speed. The crankshaft rotational speed at which rated power is developed.

2.2 GEOMETRICAL PROPERTIES OF RECIPROCATING ENGINES

The following parameters define the basic geometry of a reciprocating engine (see Fig. 2-1):

Compression ratio r_c:

$$r_c = \frac{\text{maximum cylinder volume}}{\text{minimum cylinder volume}} = \frac{V_d + V_c}{V_c} \tag{2.1}$$

where V_d is the displaced or swept volume and V_c is the clearance volume.
Ratio of cylinder bore to piston stroke:

$$R_{bs} = \frac{B}{L} \tag{2.2}$$

Ratio of connecting rod length to crank radius:

$$R = \frac{l}{a} \tag{2.3}$$

In addition, the stroke and crank radius are related by

$$L = 2a$$

Typical values of these parameters are: $r_c = 8$ to 12 for SI engines and $r_c = 12$ to 24 for CI engines; $B/L = 0.8$ to 1.2 for small- and medium-size engines, decreasing to about 0.5 for large slow-speed CI engines; $R = 3$ to 4 for small- and medium-size engines, increasing to 5 to 9 for large slow-speed CI engines.

The cylinder volume V at any crank position θ is

$$V = V_c + \frac{\pi B^2}{4}(l + a - s) \tag{2.4}$$

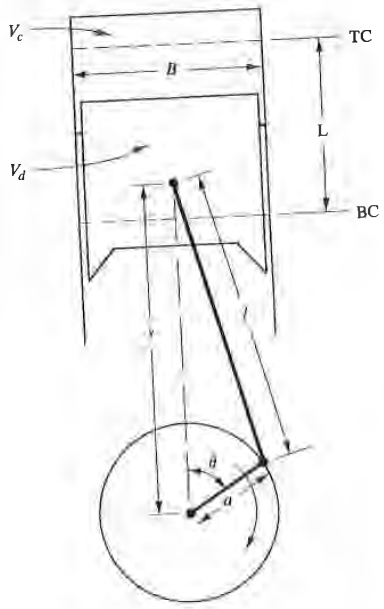

FIGURE 2-1
Geometry of cylinder, piston, connecting rod, and crankshaft where B = bore, L = stroke, l = connecting road length, a = crank radius, θ = crank angle.

where s is the distance between the crank axis and the piston pin axis (Fig. 2-1), and is given by

$$s = a \cos \theta + (l^2 - a^2 \sin^2 \theta)^{1/2} \tag{2.5}$$

The angle θ, defined as shown in Fig. 2-1, is called the *crank angle*. Equation (2.4) with the above definitions can be rearranged:

$$\frac{V}{V_c} = 1 + \tfrac{1}{2}(r_c - 1)[R + 1 - \cos \theta - (R^2 - \sin^2 \theta)^{1/2}] \tag{2.6}$$

The combustion chamber surface area A at any crank position θ is given by

$$A = A_{ch} + A_p + \pi B(l + a - s) \tag{2.7}$$

where A_{ch} is the cylinder head surface area and A_p is the piston crown surface area. For flat-topped pistons, $A_p = \pi B^2/4$. Using Eq. (2.5), Eq. (2-7) can be rearranged:

$$A = A_{ch} + A_p + \frac{\pi BL}{2}[R + 1 - \cos \theta - (R^2 - \sin^2 \theta)^{1/2}] \tag{2.8}$$

An important characteristic speed is the *mean piston speed* $\bar{S}_p$:

$$\bar{S}_p = 2LN \tag{2.9}$$

where N is the rotational speed of the crankshaft. Mean piston speed is often a

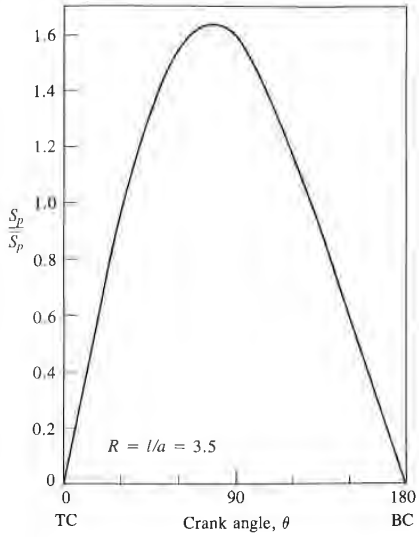

FIGURE 2-2
Instantaneous piston speed/mean piston speed as a function of crank angle for $R = 3.5$.

more appropriate parameter than crank rotational speed for correlating engine behavior as a function of speed. For example, gas-flow velocities in the intake and the cylinder all scale with $\bar{S}_p$. The *instantaneous* piston velocity S_p is obtained from

$$S_p = \frac{ds}{dt} \tag{2.10}$$

The piston velocity is zero at the beginning of the stroke, reaches a maximum near the middle of the stroke, and decreases to zero at the end of the stroke. Differentiation of Eq. (2.5) and substitution gives

$$\frac{S_p}{\bar{S}_p} = \frac{\pi}{2} \sin\theta \left[1 + \frac{\cos\theta}{(R^2 - \sin^2\theta)^{1/2}}\right] \tag{2.11}$$

Figure 2-2 shows how S_p varies over each stroke for $R = 3.5$.

Resistance to gas flow into the engine or stresses due to the inertia of the moving parts limit the maximum mean piston speed to within the range 8 to 15 m/s (1500 to 3000 ft/min). Automobile engines operate at the higher end of this range; the lower end is typical of large marine diesel engines.

2.3 BRAKE TORQUE AND POWER

Engine torque is normally measured with a dynamometer.[1] The engine is clamped on a test bed and the shaft is connected to the dynamometer rotor. Figure 2-3 illustrates the operating principle of a dynamometer. The rotor is

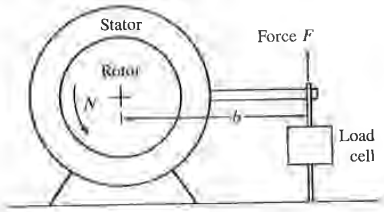

FIGURE 2-3
Schematic of principle of operation of dynamometer.

coupled electromagnetically, hydraulically, or by mechanical friction to a stator, which is supported in low friction bearings. The stator is balanced with the rotor stationary. The torque exerted on the stator with the rotor turning is measured by balancing the stator with weights, springs, or pneumatic means.

Using the notation in Fig. 2-3, if the torque exerted by the engine is T:

$$T = Fb \tag{2.12}$$

The power P delivered by the engine and absorbed by the dynamometer is the product of torque and angular speed:

$$P = 2\pi NT \tag{2.13a}$$

where N is the crankshaft rotational speed. In SI units:

$$P(\text{kW}) = 2\pi N(\text{rev/s})T(\text{N} \cdot \text{m}) \times 10^{-3} \tag{2.13b}$$

or in U.S. units:

$$P(\text{hp}) = \frac{N(\text{rev/min})\ T(\text{lbf} \cdot \text{ft})}{5252} \tag{2.13c}$$

Note that torque is a measure of an engine's ability to do work; power is the rate at which work is done.

The value of engine power measured as described above is called *brake power* P_b. This power is the usable power delivered by the engine to the load—in this case, a "brake."

2.4 INDICATED WORK PER CYCLE

Pressure data for the gas in the cylinder over the operating cycle of the engine can be used to calculate the work transfer from the gas to the piston. The cylinder pressure and corresponding cylinder volume throughout the engine cycle can be plotted on a p-V diagram as shown in Fig. 2-4. The *indicated work per cycle* $W_{c,i}$† (per cylinder) is obtained by integrating around the curve to obtain the

† The term indicated is used because such p-V diagrams used to be generated directly with a device called an engine indicator.

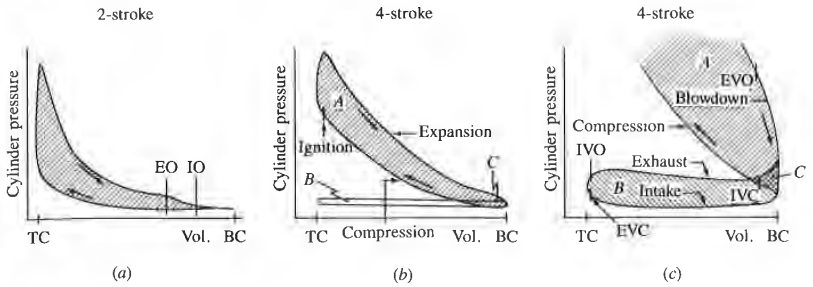

FIGURE 2-4
Examples of p-V diagrams for (*a*) a two-stroke cycle engine, (*b*) a four-stroke cycle engine; (*c*) a four-stroke cycle spark-ignition engine exhaust and intake strokes (pumping loop) at part load.

area enclosed on the diagram:

$$W_{c,i} = \oint p\, dV \tag{2.14}$$

With two-stroke cycles (Fig. 2-4*a*), the application of Eq. (2.14) is straightforward. With the addition of inlet and exhaust strokes for the four-stroke cycle, some ambiguity is introduced as two definitions of indicated output are in common use. These will be defined as:

Gross indicated work per cycle $W_{c,ig}$. Work delivered to the piston over the compression and expansion strokes only.

Net indicated work per cycle $W_{c,in}$. Work delivered to the piston over the entire four-stroke cycle.

In Fig. 2-4*b* and *c*, $W_{c,ig}$ is (area A + area C) and $W_{c,in}$ is (area A + area C) − (area B + area C), which equals (area A − area B), where each of these areas is regarded as a positive quantity. Area B + area C is the work transfer between the piston and the cylinder gases during the inlet and exhaust strokes and is called the *pumping work* W_p (see Chaps. 5 and 13). The pumping work transfer will be *to* the cylinder gases if the pressure during the intake stroke is less than the pressure during the exhaust stroke. This is the situation with naturally aspirated engines. The pumping work transfer will be *from* the cylinder gases to the piston if the exhaust stroke pressure is lower than the intake pressure, which is normally the case with highly loaded turbocharged engines.†

† With some two-stroke engine concepts there is a piston pumping work term associated with compressing the scavenging air in the crankcase.

The power per cylinder is related to the indicated work per cycle by

$$P_i = \frac{W_{c,i} N}{n_R} \tag{2.15}$$

where n_R is the number of crank revolutions for each power stroke per cylinder. For four-stroke cycles, n_R equals 2; for two-stroke cycles, n_R equals 1. This power is the indicated power; i.e., the rate of work transfer from the gas within the cylinder to the piston. It differs from the brake power by the power absorbed in overcoming engine friction, driving engine accessories, and (in the case of gross indicated power) the pumping power.

In discussing indicated quantities of the four-stroke cycle engine, such as work per cycle or power, the definition used for "indicated" (i.e., gross or net) *should always be explicitly stated.* The gross indicated output, the definition most commonly used, will be chosen where possible in this book for the following reasons. Indicated quantities are used primarily to identify the impact of the compression, combustion, and expansion processes on engine performance, etc. The gross indicated output is, therefore, the most appropriate definition. It represents the sum of the useful work available at the shaft and the work required to overcome all the engine losses. Furthermore, the standard engine test codes[2] define procedures for measuring brake power and friction power (the friction power test provides a close approximation to the total lost power in the engine). The sum of brake power and friction power provides an alternative way of estimating indicated power; the value obtained is a close approximation to the gross indicated power.

The terms brake and indicated are used to describe other parameters such as mean effective pressure, specific fuel consumption, and specific emissions (see the following sections) in a manner similar to that used for work per cycle and power.

2.5 MECHANICAL EFFICIENCY

We have seen that part of the gross indicated work per cycle or power is used to expel exhaust gases and induct fresh charge. An additional portion is used to overcome the friction of the bearings, pistons, and other mechanical components of the engine, and to drive the engine accessories. All of these power requirements are grouped together and called *friction power* P_f.† Thus:

$$P_{ig} = P_b + P_f \tag{2.16}$$

Friction power is difficult to determine accurately. One common approach for high-speed engines is to drive or motor the engine with a dynamometer (i.e., operate the engine without firing it) and measure the power which has to be

† The various components of friction power are examined in detail in Chap. 13.

supplied by the dynamometer to overcome *all* these frictional losses. The engine speed, throttle setting, oil and water temperatures, and ambient conditions are kept the same in the motored test as under firing conditions. The major sources of inaccuracy with this method are that gas pressure forces on the piston and rings are lower in the motored test than when the engine is firing and that the oil temperatures on the cylinder wall are also lower under motoring conditions.

The ratio of the brake (or useful) power delivered by the engine to the indicated power is called the *mechanical efficiency* η_m:

$$\eta_m = \frac{P_b}{P_{ig}} = 1 - \frac{P_f}{P_{ig}} \tag{2.17}$$

Since the friction power includes the power required to pump gas into and out of the engine, mechanical efficiency depends on throttle position as well as engine design and engine speed. Typical values for a modern automotive engine at wide-open or full throttle are 90 percent at speeds below about 30 to 40 rev/s (1800 to 2400 rev/min), decreasing to 75 percent at maximum rated speed. As the engine is throttled, mechanical efficiency decreases, eventually to zero at idle operation.

2.6 ROAD-LOAD POWER

A part-load power level useful as a reference point for testing automobile engines is the power required to drive a vehicle on a level road at a steady speed. Called *road-load power*, this power overcomes the rolling resistance which arises from the friction of the tires and the aerodynamic drag of the vehicle. Rolling resistance and drag coefficients, C_R and C_D, respectively, are determined empirically. An approximate formula for road-load power P_r is

$$P_r = (C_R M_v g + \tfrac{1}{2}\rho_a C_D A_v S_v^2) S_v \tag{2.18a}$$

where C_R = coefficient of rolling resistance ($0.012 < C_R < 0.015$)[3]
M_v = mass of vehicle [for passenger cars: curb mass plus passenger load of 68 kg (150 lbm); in U.S. units W_v = vehicle weight in lbf]
g = acceleration due to gravity
ρ_a = ambient air density
C_D = drag coefficient (for cars: $0.3 < C_D \lesssim 0.5$)[3]
A_v = frontal area of vehicle
S_v = vehicle speed

With the quantities in the units indicated:

$$P_r(\text{kW}) = [2.73 C_R M_v(\text{kg}) + 0.0126 C_D A_v(\text{m}^2) S_v(\text{km/h})^2] S_v(\text{km/h}) \times 10^{-3} \tag{2.18b}$$

or

$$P_r(\text{hp}) = \frac{[C_R W_v(\text{lbf}) + 0.0025 C_D A_v(\text{ft}^2) S_v(\text{mi/h})^2] S_v(\text{mi/h})}{375} \tag{2.18c}$$

2.7 MEAN EFFECTIVE PRESSURE

While torque is a valuable measure of a particular engine's ability to do work, it depends on engine size. A more useful relative engine performance measure is obtained by dividing the work per cycle by the cylinder volume displaced per cycle. The parameter so obtained has units of force per unit area and is called the *mean effective pressure* (mep). Since, from Eq. (2.15),

$$\text{Work per cycle} = \frac{Pn_R}{N}$$

where n_R is the number of crank revolutions for each power stroke per cylinder (two for four-stroke cycles; one for two-stroke cycles), then

$$\text{mep} = \frac{Pn_R}{V_d N} \tag{2.19a}$$

For SI and U.S. units, respectively,

$$\text{mep(kPa)} = \frac{P(\text{kW})n_R \times 10^3}{V_d(\text{dm}^3)N(\text{rev/s})} \tag{2.19b}$$

$$\text{mep(lb/in}^2) = \frac{P(\text{hp})n_R \times 396{,}000}{V_d(\text{in}^3)N(\text{rev/min})} \tag{2.19c}$$

Mean effective pressure can also be expressed in terms of torque by using Eq. (2.13):

$$\text{mep(kPa)} = \frac{6.28n_R T(\text{N}\cdot\text{m})}{V_d(\text{dm}^3)} \tag{2.20a}$$

or

$$\text{mep(lb/in}^2) = \frac{75.4n_R T(\text{lbf}\cdot\text{ft})}{V_d(\text{in}^3)} \tag{2.20b}$$

The maximum brake mean effective pressure of good engine designs is well established, and is essentially constant over a wide range of engine sizes. Thus, the actual bmep that a particular engine develops can be compared with this norm, and the effectiveness with which the engine designer has used the engine's displaced volume can be assessed. Also, for design calculations, the engine displacement required to provide a given torque or power, at a specified speed, can be estimated by assuming appropriate values for bmep for that particular application.

Typical values for bmep are as follows. For naturally aspirated spark-ignition engines, maximum values are in the range 850 to 1050 kPa ($\sim$ 125 to 150 lb/in^2) at the engine speed where maximum torque is obtained (about 3000 rev/min). At the maximum rated power, bmep values are 10 to 15 percent lower. For turbocharged automotive spark-ignition engines the maximum bmep is in the 1250 to 1700 kPa (180 to 250 lb/in^2) range. At the maximum rated power, bmep is in the 900 to 1400 kPa (130 to 200 lb/in^2) range. For naturally aspirated four-stroke diesels, the maximum bmep is in the 700 to 900 kPa (100 to 130

lb/in^2) range, with the bmep at the maximum rated power of about 700 kPa (100 lb/in^2). Turbocharged four-stroke diesel maximum bmep values are typically in the range 1000 to 1200 kPa (145 to 175 lb/in^2); for turbocharged aftercooled engines this can rise to 1400 kPa. At maximum rated power, bmep is about 850 to 950 kPa (125 to 140 lb/in^2). Two-stroke cycle diesels have comparable performance to four-stroke cycle engines. Large low-speed two-stroke cycle engines can achieve bmep values of about 1600 kPa.

An example of how the above engine performance parameters can be used to initiate an engine design is given below.

Example. A four-cylinder automotive spark-ignition engine is being designed to provide a maximum brake torque of 150 N·m (110 lbf·ft) in the mid-speed range (~ 3000 rev/min). Estimate the required engine displacement, bore and stroke, and the maximum brake power the engine will deliver.

Equation (2.20*a*) relates torque and mep. Assume that 925 kPa is an appropriate value for bmep at the maximum engine torque point. Equation (2.20*a*) gives

$$V(\text{dm}^3) = \frac{6.28 n_R T_{max}(\text{N}\cdot\text{m})}{\text{bmep}_{max}(\text{kPa})} = \frac{6.28 \times 2 \times 150}{925} = 2 \text{ dm}^3$$

For a four-cylinder engine, the displaced volume, bore, and stroke are related by

$$V_d = 4 \times \frac{\pi}{4} B^2 L$$

Assume $B = L$; this gives $B = L = 86$ mm.

The maximum rated engine speed can be estimated from an appropriate value for the maximum mean piston speed, 15 m/s (see Sec. 2.2):

$$\bar{S}_{pmax} = 2LN_{max} \rightarrow N_{max} = 87 \text{ rev/s (5200 rev/min)}$$

The maximum brake power can be estimated from the typical bmep value at maximum power, 800 kPa (116 lb/in^2), using Eq. (2.19*b*):

$$P_{bmax}(\text{kW}) = \frac{\text{bmep(kPa)}V(\text{dm}^3)N_{max}(\text{rev/s})}{n_R \times 10^3} = \frac{800 \times 2 \times 87}{2 \times 10^3} = 70 \text{ kW}$$

2.8 SPECIFIC FUEL CONSUMPTION AND EFFICIENCY

In engine tests, the fuel consumption is measured as a flow rate—mass flow per unit time $\dot{m}_f$. A more useful parameter is the *specific fuel consumption* (sfc)—the fuel flow rate per unit power output. It measures how efficiently an engine is using the fuel supplied to produce work:

$$\text{sfc} = \frac{\dot{m}_f}{P} \tag{2.21}$$

With units,

$$\text{sfc(mg/J)} = \frac{\dot{m}_f(\text{g/h})}{P(\text{kW})} \tag{2.22a}$$

or

$$\text{sfc(g/kW} \cdot \text{h)} = \frac{\dot{m}_f(\text{g/h})}{P(\text{kW})} = 608.3 \text{ sfc(lbm/hp} \cdot \text{h)} \tag{2.22b}$$

or

$$\text{sfc(lbm/hp} \cdot \text{h)} = \frac{\dot{m}_f(\text{lbm/h})}{P(\text{hp})} = 1.644 \times 10^3 \text{ sfc(g/kW} \cdot \text{h)} \tag{2.22c}$$

Low values of sfc are obviously desirable. For SI engines typical best values of brake specific fuel consumption are about 75 μg/J = 270 g/kW · h = 0.47 lbm/hp · h. For CI engines, best values are lower and in large engines can go below 55 μg/J = 200 g/kW · h = 0.32 lbm/hp · h.

The specific fuel consumption has units. A dimensionless parameter that relates the desired engine output (work per cycle or power) to the necessary input (fuel flow) would have more fundamental value. The ratio of the work produced per cycle to the amount of fuel energy supplied per cycle that can be released in the combustion process is commonly used for this purpose. It is a measure of the engine's efficiency. The fuel energy supplied which can be released by combustion is given by the mass of fuel supplied to the engine per cycle times the heating value of the fuel. The heating value of a fuel, Q_{HV}, defines its energy content. It is determined in a standardized test procedure in which a known mass of fuel is fully burned with air, and the thermal energy released by the combustion process is absorbed by a calorimeter as the combustion products cool down to their original temperature.

This measure of an engine's "efficiency," which will be called the *fuel conversion efficiency* η_f,† is given by

$$\eta_f = \frac{W_c}{m_f Q_{HV}} = \frac{(P n_R/N)}{(\dot{m}_f n_R/N) Q_{HV}} = \frac{P}{\dot{m}_f Q_{HV}} \tag{2.23}$$

where m_f is the mass of fuel inducted per cycle. Substitution for $P/\dot{m}_f$ from Eq (2.21) gives

$$\eta_f = \frac{1}{\text{sfc } Q_{HV}} \tag{2.24a}$$

† This empirically defined engine efficiency has previously been called thermal efficiency or enthalpy efficiency. The term fuel conversion efficiency is preferred because it describes this quantity more precisely, and distinguishes it clearly from other definitions of engine efficiency which will be developed in Sec. 3.6. Note that there are several different definitions of heating value (see Sec. 3.5). The numerical values do not normally differ by more than a few percent, however. In this text, the lower heating value at constant pressure is used in evaluating the fuel conversion efficiency.

or with units:

$$\eta_f = \frac{1}{\text{sfc(mg/J)}Q_{\text{HV}}\text{(MJ/kg)}} \tag{2.24b}$$

$$\eta_f = \frac{3600}{\text{sfc(g/kW} \cdot \text{h)}Q_{\text{HV}}\text{(MJ/kg)}} \tag{2.24c}$$

$$\eta_f = \frac{2545}{\text{sfc(lbm/hp} \cdot \text{h)}Q_{\text{HV}}\text{(Btu/lbm)}} \tag{2.24d}$$

Typical heating values for the commercial hydrocarbon fuels used in engines are in the range 42 to 44 MJ/kg (18,000 to 19,000 Btu/lbm). Thus, specific fuel consumption is inversely proportional to fuel conversion efficiency for normal hydrocarbon fuels.

Note that the fuel energy supplied to the engine per cycle is not fully released as thermal energy in the combustion process because the actual combustion process in incomplete. When enough air is present in the cylinder to oxidize the fuel completely, almost all (more than about 96 percent) of this fuel energy supplied is transferred as thermal energy to the working fluid. When insufficient air is present to oxidize the fuel completely, lack of oxygen prevents this fuel energy supplied from being fully released. This topic is discussed in more detail in Secs. 3.5 and 4.9.4.

2.9 AIR/FUEL AND FUEL/AIR RATIOS

In engine testing, both the air mass flow rate $\dot{m}_a$ and the fuel mass flow rate $\dot{m}_f$ are normally measured. The ratio of these flow rates is useful in defining engine operating conditions:

$$\text{Air/fuel ratio } (A/F) = \frac{\dot{m}_a}{\dot{m}_f} \tag{2.25}$$

$$\text{Fuel/air ratio } (F/A) = \frac{\dot{m}_f}{\dot{m}_a} \tag{2.26}$$

The normal operating range for a conventional SI engine using gasoline fuel is $12 \leq A/F \leq 18$ $(0.056 \leq F/A \leq 0.083)$; for CI engines with diesel fuel, it is $18 \leq A/F \leq 70$ $(0.014 \leq F/A \leq 0.056)$.

2.10 VOLUMETRIC EFFICIENCY

The intake system—the air filter, carburetor, and throttle plate (in a spark-ignition engine), intake manifold, intake port, intake valve—restricts the amount of air which an engine of given displacement can induct. The parameter used to measure the effectiveness of an engine's induction process is the *volumetric efficiency* η_v. Volumetric efficiency is only used with four-stroke cycle engines which have a distinct induction process. It is defined as the volume flow rate of air into

the intake system divided by the rate at which volume is displaced by the piston:

$$\eta_v = \frac{2\dot{m}_a}{\rho_{a,i} V_d N} \tag{2.27a}$$

where $\rho_{a,i}$ is the inlet air density. An alternative equivalent definition for volumetric efficiency is

$$\eta_v = \frac{m_a}{\rho_{a,i} V_d} \tag{2.27b}$$

where m_a is the mass of air inducted into the cylinder per cycle.

The inlet density may either be taken as atmosphere air density (in which case η_v measures the pumping performance of the entire inlet system) or may be taken as the air density in the inlet manifold (in which case η_v measures the pumping performance of the inlet port and valve only). Typical maximum values of η_v for naturally aspirated engines are in the range 80 to 90 percent. The volumetric efficiency for diesels is somewhat higher than for SI engines. Volumetric efficiency is discussed more fully in Sec. 6.2.

2.11 ENGINE SPECIFIC WEIGHT AND SPECIFIC VOLUME

Engine weight and bulk volume for a given rated power are important in many applications. Two parameters useful for comparing these attributes from one engine to another are:

$$\text{Specific weight} = \frac{\text{engine weight}}{\text{rated power}} \tag{2.28}$$

$$\text{Specific volume} = \frac{\text{engine volume}}{\text{rated power}} \tag{2.29}$$

For these parameters to be useful in engine comparisons, a consistent definition of what components and auxiliaries are included in the term "engine" must be adhered to. These parameters indicate the effectiveness with which the engine designer has used the engine materials and packaged the engine components.[4]

2.12 CORRECTION FACTORS FOR POWER AND VOLUMETRIC EFFICIENCY

The pressure, humidity, and temperature of the ambient air inducted into an engine, at a given engine speed, affect the air mass flow rate and the power output. Correction factors are used to adjust measured wide-open-throttle power and volumetric efficiency values to standard atmospheric conditions to provide a more accurate basis for comparisons between engines. Typical standard ambient

conditions used are:

Dry air pressure	Water vapour pressure	Temperature
736.6 mmHg	9.65 mmHg	29.4°C
29.00 inHg	0.38 inHg	85°F

The basis for the correction factor is the equation for one-dimensional steady compressible flow through an orifice or flow restriction of effective area A_E (see App. C):

$$\dot{m} = \frac{A_E p_0}{\sqrt{RT_0}} \left\{ \frac{2\gamma}{\gamma - 1} \left[\left(\frac{p}{p_0} \right)^{2/\gamma} - \left(\frac{p}{p_0} \right)^{(\gamma+1)/\gamma} \right] \right\}^{1/2} \tag{2.30}$$

In deriving this equation, it has been assumed that the fluid is an ideal gas with gas constant R and that the ratio of specific heats ($c_p/c_v = \gamma$) is a constant; p_0 and T_0 are the total pressure and temperature upstream of the restriction and p is the pressure at the throat of the restriction.

If, in the engine, p/p_0 is assumed constant at wide-open throttle, then for a given intake system and engine, the mass flow rate of dry air $\dot{m}_a$ varies as

$$\dot{m}_a \propto \frac{p_0}{\sqrt{T_0}} \tag{2.31}$$

For mixtures containing the proper amount of fuel to use all the air available (and thus provide maximum power), the indicated power at full throttle P_i will be proportional to $\dot{m}_a$, the *dry* air flow rate. Thus if

$$P_{i,s} = C_F P_{i,m} \tag{2.32}$$

where the subscripts s and m denote values at the standard and measured conditions, respectively, the correction factor C_F is given by

$$C_F = \frac{p_{s,d}}{p_m - p_{v,m}} \left(\frac{T_m}{T_s} \right)^{1/2} \tag{2.33}$$

where $p_{s,d}$ = standard dry-air absolute pressure
p_m = measured ambient-air absolute pressure
$p_{v,m}$ = measured ambient–water vapour partial pressure
T_m = measured ambient temperature, K
T_s = standard ambient temperature, K

The rated *brake* power is corrected by using Eq. (2.33) to correct the *indicated* power and making the assumption that friction power is unchanged. Thus

$$P_{b,s} = C_F P_{i,m} - P_{f,m} \tag{2.34}$$

Volumetric efficiency is proportional to $\dot{m}_a/\rho_a$ [see Eq. (2.27)]. Since ρ_a is proportional to p/T, the correction factor for volumetric efficiency, C'_F, is

$$C'_F = \frac{\eta_{v,s}}{\eta_{v,m}} = \left(\frac{T_s}{T_m} \right)^{1/2} \tag{2.35}$$

2.13 SPECIFIC EMISSIONS AND EMISSIONS INDEX

Levels of emissions of oxides of nitrogen (nitric oxide, NO, and nitrogen dioxide, NO_2, usually grouped together as NO_x), carbon monoxide (CO), unburned hydrocarbons (HC), and particulates are important engine operating characteristics.

The concentrations of gaseous emissions in the engine exhaust gases are usually measured in parts per million or percent by volume (which corresponds to the mole fraction multiplied by 10^6 or by 10^2, respectively). Normalized indicators of emissions levels are more useful, however, and two of these are in common use. *Specific emissions* are the mass flow rate of pollutant per unit power output:

$$s\mathrm{NO}_x = \frac{\dot{m}_{\mathrm{NO}_x}}{P} \tag{2.36a}$$

$$s\mathrm{CO} = \frac{\dot{m}_{\mathrm{CO}}}{P} \tag{2.36b}$$

$$s\mathrm{HC} = \frac{\dot{m}_{\mathrm{HC}}}{P} \tag{2.36c}$$

$$s\mathrm{Part} = \frac{\dot{m}_{\mathrm{part}}}{P} \tag{2.36d}$$

Indicated and brake specific emissions can be defined. Units in common use are μg/J, g/kW · h, and g/hp · h.

Alternatively, emission rates can be normalized by the fuel flow rate. An *emission index* (EI) is commonly used: e.g.,

$$\mathrm{EI}_{\mathrm{NO}_x} = \frac{\dot{m}_{\mathrm{NO}_x}(\mathrm{g/s})}{\dot{m}_f(\mathrm{kg/s})} \tag{2.37}$$

with similar expressions for CO, HC, and particulates.

2.14 RELATIONSHIPS BETWEEN PERFORMANCE PARAMETERS

The importance of the parameters defined in Secs. 2.8 to 2.10 to engine performance becomes evident when power, torque, and mean effective pressure are expressed in terms of these parameters. From the definitions of engine power [Eq. (2.13)], mean effective pressure [Eq. (2.19)], fuel conversion efficiency [Eq. (2.23)], fuel/air ratio [Eq. (2.26)], and volumetric efficiency [Eq. (2.27)], the following relationships between engine performance parameters can be developed. For power P:

$$P = \frac{\eta_f m_a N Q_{\mathrm{HV}}(F/A)}{n_R} \tag{2.38}$$

For four-stroke cycle engines, volumetric efficiency can be introduced:

$$P = \frac{\eta_f \eta_v N V_d Q_{HV} \rho_{a,i}(F/A)}{2} \tag{2.39}$$

For torque T:

$$T = \frac{\eta_f \eta_v V_d Q_{HV} \rho_{a,i}(F/A)}{4\pi} \tag{2.40}$$

For mean effective pressure:

$$\text{mep} = \eta_f \eta_v Q_{HV} \rho_{a,i}(F/A) \tag{2.41}$$

The power per unit piston area, often called the *specific power*, is a measure of the engine designer's success in using the available piston area regardless of cylinder size. From Eq. (2.39), the specific power is

$$\frac{P}{A_p} = \frac{\eta_f \eta_v N L Q_{HV} \rho_{a,i}(F/A)}{2} \tag{2.42}$$

Mean piston speed can be introduced with Eq. (2.9) to give

$$\frac{P}{A_p} = \frac{\eta_f \eta_v \bar{S}_p Q_{HV} \rho_{a,i}(F/A)}{4} \tag{2.43}$$

Specific power is thus proportional to the product of mean effective pressure and mean piston speed.

These relationships illustrate the direct importance to engine performance of:

1. High fuel conversion efficiency
2. High volumetric efficiency
3. Increasing the output of a given displacement engine by increasing the inlet air density
4. Maximum fuel/air ratio that can be usefully burned in the engine
5. High mean piston speed

2.15 ENGINE DESIGN AND PERFORMANCE DATA

Engine ratings usually indicate the highest power at which manufacturers expect their products to give satisfactory economy, reliability, and durability under service conditions. Maximum torque, and the speed at which it is achieved, is usually given also. Since both of these quantities depend on displaced volume, for comparative analyses between engines of different displacements in a given engine category normalized performance parameters are more useful. The following measures, at the operating points indicated, have most significance:[4]

TABLE 2.1
Typical design and operating data for internal combustion engines

	Operating cycle	Compression ratio	Bore, m	Stroke/ bore	Rated maximum: Speed, rev/min	Rated maximum: bmep, atm	Rated maximum: Power per unit volume kW/dm³	Weight/ power ratio, kg/kW	Approx. best bsfc, g/kW · h
Spark-ignition engines:									
Small (e.g., motorcycles)	2S,4S	6–11	0.05–0.085	1.2–0.9	4500–7500	4–10	20–60	5.5–2.5	350
Passenger cars	4S	8–10	0.07–0.1	1.1–0.9	4500–6500	7–10	20–50	4–2	270
Trucks	4S	7–9	0.09–0.13	1.2–0.7	3600–5000	6.5–7	25–30	6.5–2.5	300
Large gas engines	2S,4S	8–12	0.22–0.45	1.1–1.4	300–900	6.8–12	3–7	23–35	200
Wankel engines	4S	≈ 9	0.57 dm³ per chamber		6000–8000	9.5–10.5	35–45	1.6–0.9	300
Diesel engines:									
Passenger cars	4S	17–23	0.075–0.1	1.2–0.9	4000–5000	5–7.5	18–22	5–2.5	250
Trucks (NA)	4S	16–22	0.1–0.15	1.3–0.8	2100–4000	6–9	15–22	7–4	210
Trucks (TC)	4S	14–20	0.1–0.15	1.3–0.8	2100–4000	12–18	18–26	7–3.5	200
Locomotive, industrial, marine	4S,2S	12–18	0.15–0.4	1.1–1.3	425–1800	7–23	5–20	6–18	190
Large engines, marine and stationary	2S	10–12	0.4–1	1.2–3	110–400	9–17	2–8	12–50	180

1. At maximum or normal rated point:

   Mean piston speed. Measures comparative success in handling loads due to inertia of the parts, resistance to air flow, and/or engine friction.

   Brake mean effective pressure. In naturally aspirated engines bmep is not stress limited. It then reflects the product of volumetric efficiency (ability to induct air), fuel/air ratio (effectiveness of air utilization in combustion), and fuel conversion efficiency. In supercharged engines bmep indicates the degree of success in handling higher gas pressures and thermal loading.

   Power per unit piston area. Measures the effectiveness with which the piston area is used, regardless of cylinder size.

   Specific weight. Indicates relative economy with which materials are used.

   Specific volume. Indicates relative effectiveness with which engine space has been utilized.

2. At all speeds at which the engine will be used with full throttle or with maximum fuel-pump setting:

   Brake mean effective pressure. Measures ability to obtain/provide high air flow and use it effectively over the full range.

3. At all useful regimes of operation and particularly in those regimes where the engine is run for long periods of time:

   Brake specific fuel consumption or *fuel conversion efficiency.*
   Brake specific emissions.

Typical performance data for spark-ignition and diesel engines over the normal production size range are summarized in Table 2.1.[4] The four-stroke cycle dominates except in the smallest and largest engine sizes. The larger engines are turbocharged or supercharged. The maximum rated engine speed decreases as engine size increases, maintaining the maximum mean piston speed in the range of about 8 to 15 m/s. The maximum brake mean effective pressure for turbocharged and supercharged engines is higher than for naturally aspirated engines. Because the maximum fuel/air ratio for spark-ignition engines is higher than for diesels, their naturally aspirated maximum bmep levels are higher. As engine size increases, brake specific fuel consumption decreases and fuel conversion efficiency increases, due to reduced importance of heat losses and friction. For the largest diesel engines, brake fuel conversion efficiencies of about 50 percent and indicated fuel conversion efficiencies of over 55 percent can be obtained.

PROBLEMS

2.1. Explain why the brake mean effective pressure of a naturally aspirated diesel engine is lower than that of a naturally aspirated spark-ignition engine. Explain why the bmep is lower at the maximum rated power for a given engine than the bmep at the maximum torque.

Trucks (NA)	4S	14–20	0.1–0.15	1.3–0.8	2100–4000	12–18	190
Trucks (TC)	4S	12–18	0.15–0.4	1.1–1.3	425–1800	7–23	5–20	6–18	180
Locomotive, industrial, marine	4S,2S							12–50	
Large engines, marine and stationary	2S	10–12	0.4–1	1.2–3	110–400	9–17	2–8		

2.2. Describe the impact on air flow, maximum torque, and maximum power of changing a spark-ignition engine cylinder head from 2 valves per cylinder to 4 valves (2 inlet and 2 exhaust) per cylinder.

2.3. Calculate the mean piston speed, bmep, and specific power of the spark-ignition engines in Figs. 1-4, 1-9, and 1-12 at their maximum rated power.

2.4. Calculate the mean piston speed, bmep, and specific power of the diesel engines in Figs. 1-20, 1-21, 1-22, 1-23, and 1-24 at their maximum rated power. Briefly explain any significant differences.

2.5. Develop an equation for the power required to drive a vehicle at constant speed up a hill of angle α, in terms of vehicle speed, mass, frontal area, drag coefficient, coefficient of rolling resistance, α, and acceleration due to gravity. Calculate this power when the car mass is 1500 kg, the hill angle is 15 degrees, and the vehicle speed is 50 mi/h.

2.6. The spark-ignition engine in Fig. 1-4 is operating at a mean piston speed of 10 m/s. The measured air flow is 60 g/s. Calculate the volumetric efficiency based on atmospheric conditions.

2.7. The diesel engine of Fig. 1-20 is operating with a mean piston speed of 8 m/s. Calculate the air flow if the volumetric efficiency is 0.92. If (F/A) is 0.05 what is the fuel flow rate, and the mass of fuel injected per cylinder per cycle?

2.8. The brake fuel conversion efficiency of a spark-ignition engine is 0.3, and varies little with fuel type. Calculate the brake specific fuel consumption for isooctane, gasoline, methanol, and hydrogen (relevant data are in App. D).

2.9. You are doing a preliminary design study of a turbocharged four-stroke diesel engine. The maximum rated power is limited by stress considerations to a brake mean effective pressure of 1200 kPa and maximum value of the mean piston speed of 12 m/s.

(*a*) Derive an equation relating the engine inlet pressure (pressure in the inlet manifold at the turbocharger compressor exit) to the fuel/air ratio at this maximum rated power operating point. Other reciprocating engine parameters (e.g., volumetric efficiency, fuel conversion efficiency, bmep, etc.) appear in this equation also.

(*b*) The maximum rated brake power requirement for this engine is 400 kW. Estimate sensible values for number of cylinders, cylinder bore, stroke, and determine the maximum rated speed of this preliminary engine design.

(*c*) If the pressure ratio across the compressor is 2, estimate the overall fuel/air and air/fuel ratios at the maximum rated power. Assume appropriate values for any other parameters you may need.

2.10. In the reciprocating engine, during the power or expansion stroke, the gas pressure force acting on the piston is transmitted to the crankshaft via the connecting rod. List the forces acting on the piston during this part of the operating cycle. Show the direction of the forces acting on the piston on a sketch of the piston, cylinder, connecting rod, crank arrangement. Write out the force balance for the piston (*a*) along the cylinder axis and (*b*) transverse to the cylinder axis in the plane containing the connecting rod. (You are not asked to manipulate or solve these equations.)

2.11. You are designing a four-stroke cycle diesel engine to provide a brake power of 300 kW naturally aspirated at its maximum rated speed. Based on typical values for brake mean effective pressure and maximum mean piston speed, estimate the required engine displacement, and the bore and stroke for sensible cylinder geometry and number of engine cylinders. What is the maximum rated engine speed (rev/min)

for your design? What would be the brake torque (N · m) and the fuel flow rate (g/h) at this maximum speed? Assume a maximum mean piston speed of 12 m/s is typical of good engine designs.

2.12. The power per unit piston area P/A_p (often called the specific power) is a measure of the designer's success in using the available piston area regardless of size.
(*a*) Derive an expression for P/A_p in terms of mean effective pressure and mean piston speed for two-stroke and four-stroke engine cycles.
(*b*) Compute typical maximum values of P/A_p for a spark-ignition engine (e.g., Fig. 1-4), a turbocharged four-stroke cycle diesel engine (e.g., Fig. 1-22), and a large marine diesel (Fig. 1-24). Table 2-1 may be helpful. State your assumptions clearly.

2.13. Several velocities, time, and length scales are useful in understanding what goes on inside engines. Make estimates of the following quantities for a 1.6-liter displacement four-cylinder spark-ignition engine, operating at wide-open throttle at 2500 rev/min.
(*a*) The mean piston speed and the maximum piston speed.
(*b*) The maximum charge velocity in the intake port (the port area is about 20 percent of the piston area).
(*c*) The time occupied by one engine operating cycle, the intake process, the compression process, the combustion process, the expansion process, and the exhaust process. (*Note*: The word *process* is used here not the word *stroke*.)
(*d*) The average velocity with which the flame travels across the combustion chamber.
(*e*) The length of the intake system (the intake port, the manifold runner, etc.) which is filled by one cylinder charge just before the intake valve opens and this charge enters the cylinder (i.e., how far back from the intake valve, in centimeters, one cylinder volume extends in the intake system).
(*f*) The length of exhaust system filled by one cylinder charge after it exits the cylinder (assume an average exhaust gas temperature of 425°C).
You will have to make several appropriate geometric assumptions. The calculations are straightforward, and only approximate answers are required.

2.14. The values of mean effective pressure at rated speed, maximum mean piston speed, and maximum specific power (engine power/total piston area) are essentially independent of cylinder size for naturally aspirated engines of a given type. If we also assume that engine weight per unit displaced volume is essentially constant, how will the *specific weight* of an engine (engine weight/maximum rated power) at fixed total displaced volume vary with the number of cylinders? Assume the bore and stroke are equal.

REFERENCES

1. Obert, E.F.: *Internal Combustion Engines and Air Pollution*, chap. 2, Intext Educational Publishers, New York, 1973.
2. SAE Standard: "Engine Test Code—Spark Ignition and Diesel," SAE J816b, *SAE Handbook*.
3. Bosch: *Automotive Handbook*, 2nd English edition, Robert Bosch GmbH, Stuttgart, 1986.
4. Taylor, C.F.: *The Internal Combustion Engine in Theory and Practice*, vol. II, MIT Press, Cambridge, Mass., 1968.

ns," *Ind. Engng. Chem.*, vol. 40, pp.

967.
rs," Ethyl technical note PCDTN

16–22, American Chemical Society,

"Additives, Engine Fuel," in J. J.
emical Processing and Design, vol. 2,

e Trends in Automotive Fuels and
International Pacific Conference on
-10, 1983.
ement Increase," SAE paper 750933,

CHAPTER 10

COMBUSTION IN COMPRESSION-IGNITION ENGINES

10.1 ESSENTIAL FEATURES OF PROCESS

The essential features of the compression-ignition or diesel engine combustion process can be summarized as follows. Fuel is injected by the fuel-injection system into the engine cylinder toward the end of the compression stroke, just before the desired start of combustion. Figures 1-17, 1-18, and 1-19 illustrate the major components of common diesel fuel-injection systems. The liquid fuel, usually injected at high velocity as one or more jets through small orifices or nozzles in the injector tip, atomizes into small drops and penetrates into the combustion chamber. The fuel vaporizes and mixes with the high-temperature high-pressure cylinder air. Since the air temperature and pressure are above the fuel's ignition point, spontaneous ignition of portions of the already-mixed fuel and air occurs after a delay period of a few crank angle degrees. The cylinder pressure increases as combustion of the fuel-air mixture occurs. The consequent compression of the unburned portion of the charge shortens the delay before ignition for the fuel and air which has mixed to within combustible limits, which then burns rapidly. It also reduces the evaporation time of the remaining liquid fuel. Injection continues until the desired amount of fuel has entered the cylinder. Atomization, vaporization, fuel-air mixing, and combustion continue until essentially all the fuel has passed through each process. In addition, mixing of the air remaining in the cylinder with burning and already burned gases continues throughout the combustion and expansion processes.

It will be clear from this summary that the compression-ignition combustion process is extremely complex. The details of the process depend on the characteristics of the fuel, on the design of the engine's combustion chamber and fuel-injection system, and on the engine's operating conditions. It is an unsteady, heterogeneous, three-dimensional combustion process. While an adequate conceptual understanding of diesel engine combustion has been developed, to date an ability to describe many of the critical individual processes in a quantitative manner is lacking.

Some important consequences of this combustion process on engine operation are the following:

1. Since injection commences just before combustion starts, there is no knock limit as in the spark-ignition engine resulting from spontaneous ignition of the premixed fuel and air in the end-gas. Hence a higher engine compression ratio can be used in the compression-ignition engine, improving its fuel conversion efficiency relative to the SI engine.
2. Since injection timing is used to control combustion timing, the delay period between the start of injection and start of combustion must be kept short (and reproducible). A short delay is also needed to hold the maximum cylinder gas pressure below the maximum the engine can tolerate. Thus, the spontaneous ignition characteristics of the fuel-air mixture must be held within a specified range. This is done by requiring that diesel fuel have a cetane number (a measure of the ease of ignition of that fuel in a typical diesel environment, see Sec. 10.6.2) above a certain value.
3. Since engine torque is varied by varying the amount of fuel injected per cycle with the engine air flow essentially unchanged, the engine can be operated unthrottled. Thus, pumping work requirements are low, improving part-load mechanical efficiency relative to the SI engine.
4. As the amount of fuel injected per cycle is increased, problems with air utilization during combustion lead to the formation of excessive amounts of soot which cannot be burned up prior to exhaust. This excessive soot or black smoke in the exhaust constrains the fuel/air ratio at maximum engine power to values 20 percent (or more) lean of stoichiometric. Hence, the maximum indicated mean effective pressure (in a naturally aspirated engine) is lower than values for an equivalent spark-ignition engine.
5. Because the diesel always operates with lean fuel/air ratios (and at part load with very lean fuel/air ratios), the effective value of γ ($=c_p/c_v$) over the expansion process is higher than in a spark-ignition engine. This gives a higher fuel conversion efficiency than the spark-ignition engine, for a given expansion ratio (see Sec. 5.5.3).

The major problem in diesel combustion chamber design is achieving sufficiently rapid mixing between the injected fuel and the air in the cylinder to complete combustion in the appropriate crank angle interval close to top-center. The

foregoing discussion indicates (and more detailed analysis will confirm) that mixing rates control the fuel burning rate. Commercial diesel engines are made with a very large range of cylinder sizes, with cylinder bores varying from about 70 to 900 mm. The mean piston speed at maximum rated power is approximately constant over this size range (see Sec. 2.2), so the maximum rated *engine* speed will be inversely proportional to the stroke [see Eq. (2.9)]. For a fixed crank angle interval for combustion (of order 40 to 50° to maintain high fuel conversion efficiency), the time available for combustion will, therefore, scale with the stroke. Thus, at the small end of the diesel engine size range, the mixing between the injected fuel and the air must take place on a time scale some 10 times shorter than in engines at the large end of this range. It would be expected, therefore, that the design of the engine combustion chamber (including the inlet port and valve) and the fuel-injection system would have to change substantially over this size range to provide the fuel and air motion inside the cylinder required to achieve the desired fuel-air mixing rate. As engine size decreases, more vigorous air motion is required while less fuel jet penetration is necessary. It is this logic, primarily, that leads to the different diesel combustion chamber designs and fuel injection systems found in practice over the large size range of commercial diesel engines.

10.2 TYPES OF DIESEL COMBUSTION SYSTEMS

Diesel engines are divided into two basic categories according to their combustion chamber design: (1) *direct-injection (DI) engines*, which have a single open combustion chamber into which fuel is injected directly; (2) *indirect-injection (IDI) engines*, where the chamber is divided into two regions and the fuel is injected into the "prechamber" which is connected to the main chamber (situated above the piston crown) via a nozzle, or one or more orifices. IDI engine designs are only used in the smallest engine sizes. Within each category there are several different chamber geometry, air-flow, and fuel-injection arrangements.

10.2.1 Direct-Injection Systems

In the largest-size engines, where mixing rate requirements are least stringent, quiescent direct-injection systems of the type shown in Fig. 10-1a are used. The momentum and energy of the injected fuel jets are sufficient to achieve adequate fuel distribution and rates of mixing with the air. Additional organized air motion is not required. The combustion chamber shape is usually a shallow bowl in the crown of the piston, and a central multihole injector is used.

As engine size decreases, increasing amounts of air swirl are used to achieve faster fuel-air mixing rates. Air swirl is generated by suitable design of the inlet port (see Sec. 8.3); the swirl rate can be increased as the piston approaches TC by forcing the air toward the cylinder axis, into a bowl-in-piston type of combustion

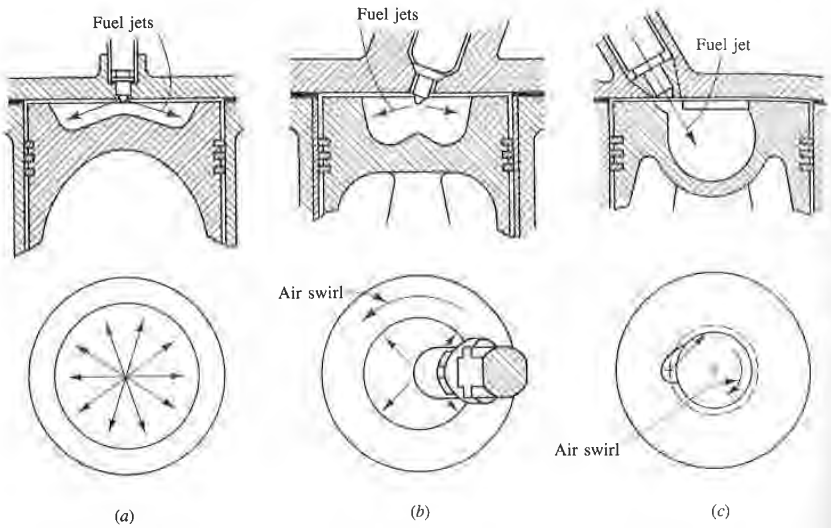

FIGURE 10-1
Common types of direct-injection compression-ignition or diesel engine combustion systems: (*a*) quiescent chamber with multihole nozzle typical of larger engines; (*b*) bowl-in-piston chamber with swirl and multihole nozzle; (*c*) bowl-in-piston chamber with swirl and single-hole nozzle. (*b*) and (*c*) used in medium to small DI engine size range.

chamber. Figure 10-1b and *c* shows the two types of DI engine with swirl in common use. Figure 10-1*b* shows a DI engine with swirl, with a centrally located multihole injector nozzle. Here the design goal is to hold the amount of liquid fuel which impinges on the piston cup walls to a minimum. Figure 10-1*c* shows the M.A.N. "M system" with its single-hole fuel-injection nozzle, oriented so that most of the fuel is deposited on the piston bowl walls. These two types of designs are used in medium-size (10- to 15-cm bore) diesels and, with increased swirl, in small-size (8- to 10-cm bore) diesels.

10.2.2 Indirect-Injection Systems

Inlet generated air swirl, despite amplification in the piston cup, has not provided sufficiently high fuel-air mixing rates for small high-speed diesels such as those used in automobiles. Indirect-injection or divided-chamber engine systems have been used instead, where the vigorous charge motion required during fuel injection is generated during the compression stroke. Two broad classes of IDI systems can be defined: (1) swirl chamber systems and (2) prechamber systems, as illustrated in Fig. 10-2*a* and *b*, respectively. During compression, air is forced from the main chamber above the piston into the auxiliary chamber, through the nozzle or orifice (or set of orifices). Thus, toward the end of compression, a vigorous flow in the auxiliary chamber is set up; in swirl chamber systems the connect-

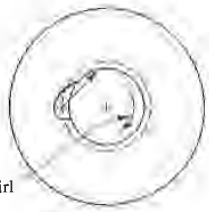

(*c*)

engine combustion systems: (*a*)
(*b*) bowl-in-piston chamber with
nd single-hole nozzle. (*b*) and (*c*)

f DI engine with swirl in
rl, with a centrally located
hold the amount of liquid
imum. Figure 10-1*c* shows
on nozzle, oriented so that
These two types of designs
ıd, with increased swirl, in

ston cup, has not provided
peed diesels such as those
ımber engine systems have
required during fuel injec-
wo broad classes of IDI
(2) prechamber systems, as
compression, air is forced
liary chamber, through the
nd of compression, a vigor-
amber systems the connect-

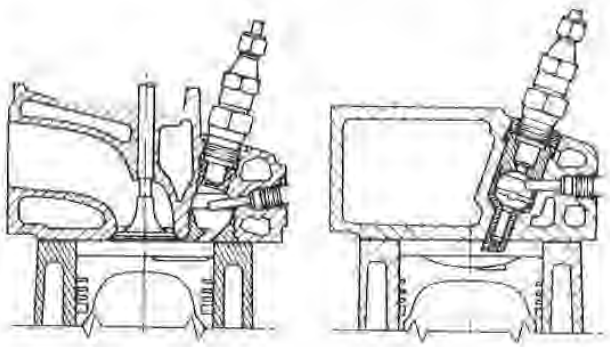

(*a*) (*b*)

FIGURE 10-2
Two common types of small indirect-injection diesel engine combustion system: (*a*) swirl prechamber; (*b*) turbulent prechamber.

ing passage and chamber are shaped so that this flow within the auxiliary chamber rotates rapidly.

Fuel is usually injected into the auxiliary chamber at lower injection-system pressure than is typical of DI systems through a pintle nozzle as a single spray, as shown in Fig. 1-18. Combustion starts in the auxiliary chamber; the pressure rise associated with combustion forces fluid back into the main chamber where the jet issuing from the nozzle entrains and mixes with the main chamber air. The glow plug shown on the right of the prechamber in Fig. 10-2 is a cold-starting aid. The plug is heated prior to starting the engine to ensure ignition of fuel early in the engine cranking process.

10.2.3 Comparison of Different Combustion Systems

The number of different combustion chamber types proposed and tried since the beginnings of diesel engine development is substantial. Over the years, however, through the process of evolution and the increased understanding of the physical and chemical processes involved, only a few designs based on a sound principle have survived. The important characteristics of those chambers now most commonly used are summarized in Table 10.1. The numbers for dimensions and operating characteristics are typical ranges for each different type of diesel engine and combustion system.

The largest, slowest speed, engines for power generation or marine applications use open quiescent chambers which are essentially disc shaped; the motion of the fuel jets is responsible for distributing and mixing the fuel. These are usually two-stroke cycle engines. In the next size range, in large truck and locomotive engines, a quiescent chamber consisting of a shallow dish or bowl in the

TABLE 10.1
Characteristics of Common Diesel Combustion Systems

	Direct injection				Indirect injection	
System	Quiescent	Medium swirl	High swirl "M"	High swirl multispray	Swirl chamber	Pre-chamber
Size	Largest	Medium	Medium—smaller	Medium—small	Smallest	Smallest
Cycle	2-/4-stroke	4-stroke	4-stroke	4-stroke	4-stroke	4-stroke
Turbocharged/supercharged/naturally aspirated	TC/S	TC/NA	TC/NA	NA/TC	NA/TC	NA/TC
Maximum speed, rev/min	120–2100	1800–3500	2500–5000	3500–4300	3600–4800	4500
Bore, mm	900–150	150–100	130–80	100–80	95–70	95–70
Stroke/bore	3.5–1.2	1.3–1.0	1.2–0.9	1.1–0.9	1.1–0.9	1.1–0 9
Compression ratio	12–15	15–16	16–18	16–22	20–24	22–24
Chamber	Open or shallow dish	Bowl-in-piston	Deep bowl-in-piston	Deep bowl-in-piston	Swirl pre-chamber	Single/multi-orifice pre-chamber
Air-flow pattern	Quiescent	Medium swirl	High swirl	Highest swirl	Very high swirl in pre-chamber	Very turbulent in pre-chamber
Number of nozzle holes	Multi	Multi	Single	Multi	Single	Single
Injection pressure	Very high	High	Medium	High	Lowest	Lowest

piston crown is often used. The air utilization in these engines is low, but they are invariably supercharged or turbocharged to obtain high power density.

In the DI category, as engine size decreases and maximum speed rises, swirl is used increasingly to obtain high-enough fuel-air mixing rates. The swirl is generated by suitably shaped inlet ports, and is amplified during compression by forcing most of the air toward the cylinder axis into the deep bowl-in-piston combustion chamber. In about the same size range, an alternative system to the multihole nozzle swirl system is the M.A.N. "M" system (or wall-wetting system), where most of the fuel from the single-hole pintle nozzle is placed on the wall of the spherical bowl in the piston crown.

In the smallest engine sizes, the IDI engine has traditionally been used to obtain the vigorous air motion required for high fuel-air mixing rates. There are several different geometries in use. These either generate substantial swirl in the

	Indirect injection	
	Swirl chamber	Pre-chamber
	Smallest	Smallest
	4-stroke	4-stroke
	NA/TC	NA/TC
)	3600–4800	4500
	95–70	95–70
	1.1–0.9	1.1–0.9
	20–24	22–24
l- n	Swirl pre-chamber	Single/ multi-orifice pre-chamber
	Very high swirl in pre-chamber	Very turbulent in pre-chamber
	Single	Single
	Lowest	Lowest

ıgines is low, but they are
power density.
ıaximum speed rises, swirl
ng rates. The swirl is gen-
d during compression by
the deep bowl-in-piston
alternative system to the
ı (or wall-wetting system),
.e is placed on the wall of

raditionally been used to
ir mixing rates. There are
te substantial swirl in the

auxiliary chamber during the latter part of the compression stroke, using a nozzle or connecting passage that enters the auxiliary chamber tangentially, or they generate intense turbulence in the prechamber through use of several small orifices and obstructions to the flow within the prechamber. The most common design of swirl chamber is the Ricardo Comet design shown in Fig. 10-2*a*. An alternative IDI engine to the two types listed in Table 10-1 is the air cell system. In that system the fuel is injected into the main chamber and not the auxiliary "air cell." The auxiliary chamber acts as a turbulence generator as gas flows into and out of the cell.

10.3 PHENOMENOLOGICAL MODEL OF COMPRESSION-IGNITION ENGINE COMBUSTION

Studies of photographs of diesel engine combustion, combined with analyses of engine cylinder pressure data, have led to a widely accepted descriptive model of the compression-ignition engine combustion process. The concept of *heat-release rate* is important to understanding this model. It is defined as the rate at which the chemical energy of the fuel is released by the combustion process. It can be calculated from cylinder pressure versus crank angle data, as the energy release required to create the measured pressure, using the techniques described in Sec. 10.4. The combustion model defines four separate phases of diesel combustion, each phase being controlled by different physical or chemical processes. Although the relative importance of each phase does depend on the combustion system used, and engine operating conditions, these four phases are common to all diesel engines.

10.3.1 Photographic Studies of Engine Combustion

High-speed photography at several thousand frames per second has been used extensively to study diesel engine combustion. Some of these studies have been carried out in combustion chambers very close to those used in practice, under normal engine operating conditions (e.g., Refs. 1 and 2). Sequences of individual frames from movies provide valuable information on the nature of the combustion process in the different types of diesel engines. Figure 10-3 shows four combustion chamber geometries that have been studied photographically. These are: (*a*) a quiescent chamber typical of diesel engines in the 3 to 20 dm^3/cylinder displacement used for industrial, marine, and rail traction applications (only the burning of a single fuel spray of the multispray combustion system could be studied[2]); (*b*) a smaller high-speed DI engine with swirl and four fuel jets centrally injected; (*c*) an M.A.N. "M" DI system; and (*d*) a Ricardo Comet V swirl chamber IDI system.[3]

The combustion sequences were recorded on color film and show the following features:

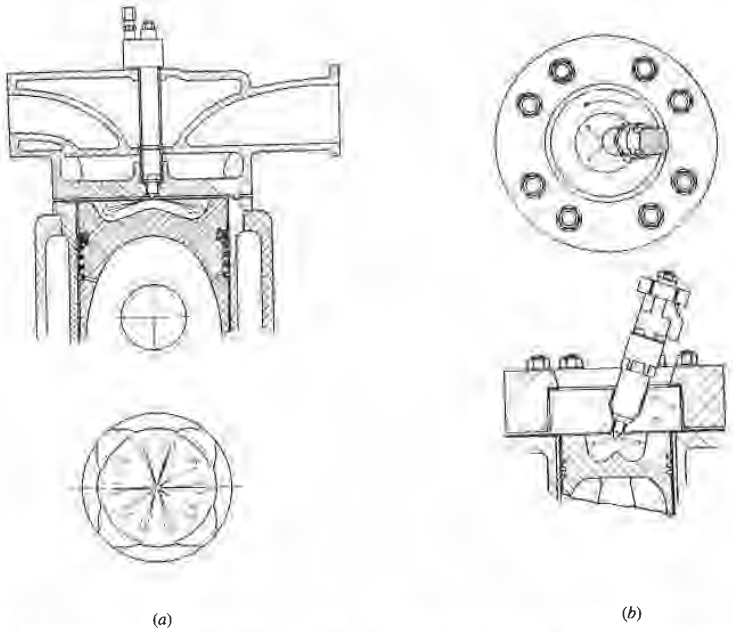

(*a*) (*b*)

FIGURE 10-3
Four diesel combustion chambers used to obtain photographs of the compression-ignition combustion process shown in Fig. 10-4 on color plate: (*a*) quiescent DI chamber; (*b*) multihole nozzle DI chamber with swirl; on p. 499 | (c) M.A.N. "M" DI chamber; (*d*) Ricardo Comet IDI swirl chamber.[1,2]

Fuel spray(s). The fuel droplets reflect light from spot lamps and define the extent of the liquid fuel spray prior to complete vaporization.

Premixed flame. These regions are of too low a luminosity to be recorded with the exposure level used. The addition of a copper additive dope to the fuel gives these normally blue flames a green color bright enough to render them visible.

Diffusion flame. The burning high-temperature carbon particles in this flame provide more than adequate luminosity and appear as yellow-white. As the flame cools, the radiation from the particles changes color through orange to red.

Over-rich mixture. The appearance of a brown region, usually surrounded by a white diffusion flame, indicates an excessively rich mixture region where substantial soot particle production has occurred. Where this fuel-rich soot-laden cloud contacts unburned air there is a hot white diffusion flame.

Table 10.2 summarizes the characteristics of these different regions, discernable in the photographs shown in Fig. 10-4 on the color plate.

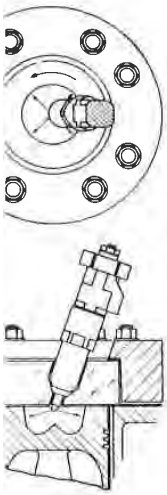

(*b*)

of the compression-ignition com-
chamber; (*b*) multihole nozzle DI
ardo Comet IDI swirl chamber.[1,2]

spot lamps and define the
zation.

luminosity to be recorded
er additive dope to the fuel
ht enough to render them

arbon particles in this flame
; yellow-white. As the flame
rough orange to red.

region, usually surrounded
rich mixture region where
ere this fuel-rich soot-laden
ion flame.

erent regions, discernable in

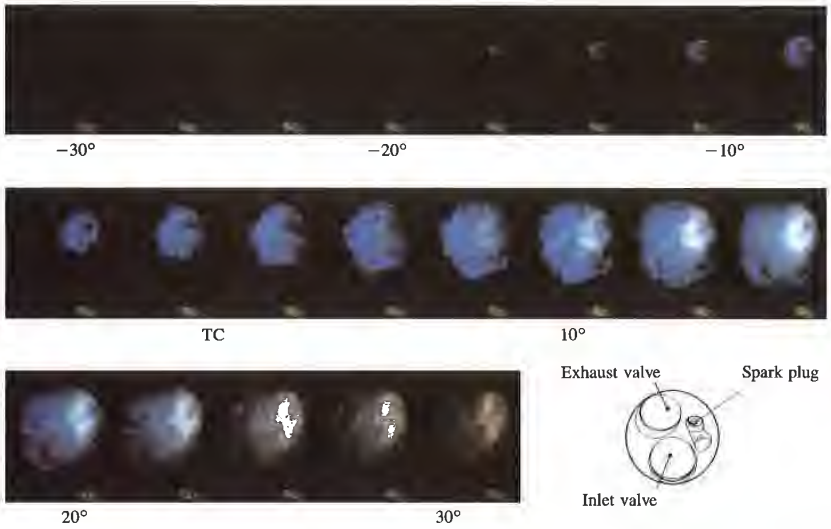

FIGURE 9-1

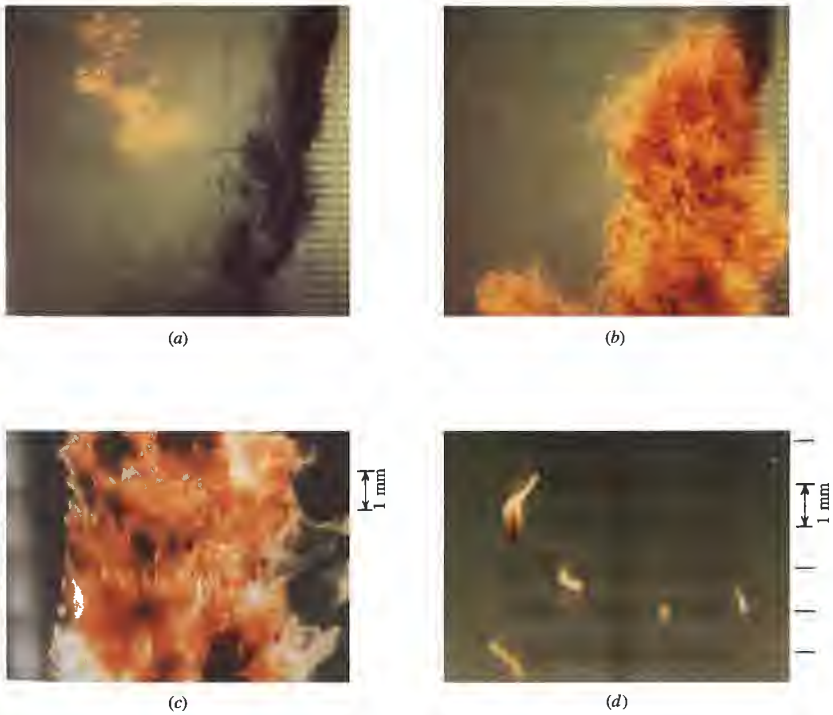

(*a*) (*b*) (*c*) (*d*)

FIGURE 10-5

FIGURE 10-4

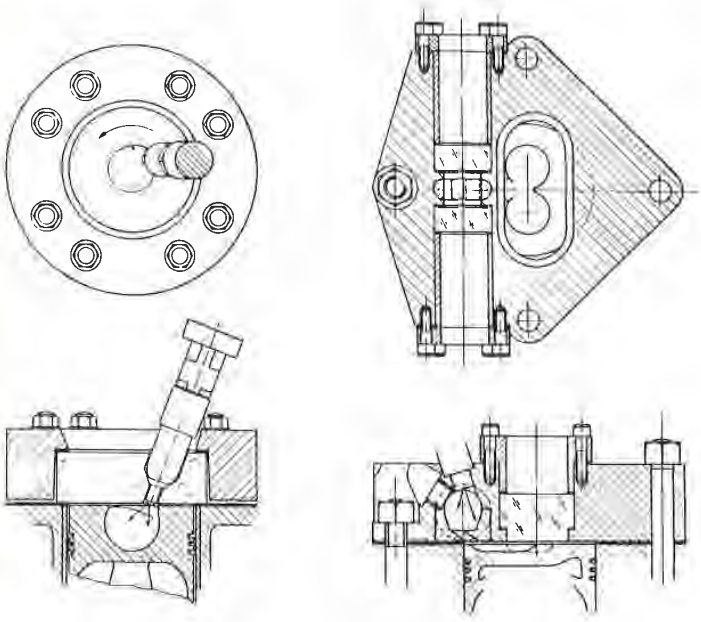

(c) (d)

Figure 10-4*a* shows a sequence of photographs from one combustion event of the single spray, burning under conditions typical of a large quiescent DI engine. The fuel spray is shown penetrating into the chamber. Ignition occurs at $-8°$ in the fuel-air mixture left behind on the edge of the spray not far from the injector. The flame then spreads rapidly ($-7°$) along the outside of the spray to the spray tip. Here some of the fuel, which has had a long residence time in the chamber, burns with a blue-green low-luminosity flame (colored green by the copper fuel additive). The flame engulfing the remainder of the spray is brilliant white-yellow from the burning of the soot particles which have been formed in

FIGURE 10-4 (On Color Plate, facing this page)
Sequence of photographs from high-speed movies taken in special visualization diesel engines shown in Fig. 10-3: (*a*) combustion of single spray burning under large DI engine conditions; (*b*) combustion of four sprays in DI engine with counterclockwise swirl; (*c*) combustion of single spray in M.A.N. "M" DI diesel; (*d*) combustion in prechamber (on left) and main chamber (on right) in Ricardo Comet IDI swirl chamber diesel. 1250 rev/min, imep = 827 kPa (120 lb/in^2)[1, 2] (*Courtesy Ricardo Consulting Engineers.*)

TABLE 10.2
Interpretation of diesel engine combustion color photographs[1]

Color	Interpretation
Grey	Background; the gas (air in early stages, combustion products later) is transparent and not glowing
Green	Early in combustion process; low luminosity "premixed"-type flame, rendered visible by copper added to fuel. Later; burned gas above about 1800°C
White, and yellow-white	Carbon particle burnup in diffusion flame, 2000–2500°C
Yellow, orange-red	Carbon burnup in diffusion flame at lower temperatures; last visible in film at 1000°C
Brown	Soot clouds from very fuel-rich mixture regions. Where these meet air (grey) there is always a white fringe of hot flame

the fuel-rich spray core. At this stage ($-1°$), about 60 percent of the fuel has been injected. The remainder is injected into this enflamed region, producing a very fuel-rich zone apparent as the dark brown cloud (11°). This soot cloud moves to the outer region of the chamber (11° to 20°); white-yellow flame activity continues near the injector, probably due to combustion of ligaments of fuel which issued from the injector nozzle as the injector needle was seating. Combustion continues well into the expansion stroke (31°C).

This sequence shows that fuel distribution is always highly nonuniform during the combustion process in this type of DI engine. Also the air which is between the individual fuel sprays of the quiescent open-chamber diesel mixes with each burning spray relatively slowly, contributing to the poor air utilization with this type of combustion chamber.

Figure 10-4*b* shows a combustion sequence from the DI engine with swirl (the chamber shown in Fig. 10-3*b*). The inner circle corresponds to the deep bowl in the piston crown, the outer circle to the cylinder liner. The fuel sprays (of which two are visible without obstruction from the injector) first appear at $-13°$. At $-7°$ they have reached the wall of the bowl; the tips of the sprays have been deflected slightly by the anticlockwise swirl. The frame at $-3°$ shows the first ignition. Bright luminous flame zones are visible, one on each spray. Out by the bowl walls, where fuel vapor has been blown around by the swirl, larger greenish burning regions indicating the presence of premixed flame can be seen. The fuel downstream of each spray is next to ignite, burning yellow-white due to the soot

formed by the richer mixture. Flame propagation back to the injector follows extremely rapidly and at TC the bowl is filled with flame. At 5° ATC the flame spreads out over the piston crown toward the cylinder wall due to combustion-produced gas expansion and the reverse squish flow (see Sec. 8.4). The brown regions (13°) are soot-laden fuel-rich mixture originating from the fuel which impinges on the wall. The last frame (30° ATC) shows the gradual diminution of the soot-particle-laden regions as they mix with the excess air and burn up. The last dull-red flame visible on the film is at about 75° ATC, well into the expansion stroke.

Figure 10-4*c* shows the combustion sequence for the M.A.N. "M"-type DI engine. In the version of the system used for these experiments, the fuel was injected through a two-hole nozzle which produces a main jet directed tangentially onto the walls of the spherical cup in the piston crown, and an auxiliary spray which mixes a small fraction of the fuel directly with the swirling air flow. More recent "M" systems use a pintle nozzle with a single variable orifice.[3] At $-5°$ the fuel spray is about halfway round the bowl. Ignition has just occurred of fuel adjacent to the wall which has mixed sufficiently with air to burn. The flame spreads rapidly ($-2°$, 1°) to envelop the fuel spray, and is convected round the cup by the high swirl air flow. By shortly after TC the flame has filled the bowl and is spreading out over the piston crown. A soot cloud is seen near the top right of the picture at 5° ATC which spreads out around the circumference of the enflamed region. There is always a rim of flame between the soot cloud and the cylinder liner as excess air is mixed into the flame zone (10.5°). The flame is of the carbon-burning type throughout; little premixed green flame is seen even at the beginning of the combustion process.

Figure 10-4*d* shows the combustion sequence in a swirl chamber IDI engine of the Ricardo Comet V design. The swirl chamber (on the left) is seen in the view of the lower drawing of Fig. 10-3*d* (with the connecting passageway entering the swirl chamber tangentially at the bottom left to produce clockwise swirl). The main chamber is seen in the plan view of the upper drawing of Fig. 10-3*d*. Two sprays emerge from the Pintaux nozzle after the start of injection at $-11°$. The smaller auxiliary spray which is radial is sharply deflected by the high swirl. Frame 1 shows how the main spray follows the contour of the chamber; the auxiliary spray has evaporated and can no longer be seen. The first flame occurs at $-1°$ in the vaporized fuel from the auxiliary spray and is a green premixed flame. The flame then spreads to the main spray (TC), becoming a yellow-white carbon-particle-burning flame with a green fringe. At 4° ATC the swirl chamber appears full of carbon-burning flame, which is being blown down the throat and into the recesses in the piston crown by the combustion generated pressure rise in the prechamber. The flame jet impinges on the piston recesses entraining the air in the main chamber, leaving green patches where all carbon is burned out (4°, 11°, 15°). A brown soot cloud is emerging from the throat. By 15° ATC this soot cloud has spread around the cylinder, with a bright yellow-white flame at its periphery. This soot then finds excess air and burns up, while the yellow-white

flame becomes yellow and then orange-red as the gases cool on expansion. By 38° ATC most of the flame is burnt out.

Magnified color photographs of the flame around a single fuel spray under conditions typical of a direct-injection diesel engine, shown in Fig. 10-5 on the color plate, provide additional insight into the compression-ignition and flame-development processes.[4] These photographs were obtained in a rapid compression machine: this device is a cylinder-piston apparatus in which air is rapidly compressed by moving the piston to temperatures and pressures similar to those in the diesel engine combustion chamber at the time of injection. A single fuel spray was then injected into the disc-shaped combustion chamber. The air flow prior to compression was forced to swirl around the cylinder axis and much of that swirl remains after compression.

Figure 10-5*a* shows a portion of the liquid fuel spray (which appears black due to back lighting) and the rapidly developing flame 0.4 ms after ignition occurs. Ignition commences in the *fuel vapor*–air mixture region, set up by the jet motion and swirling air flow, away from the liquid core of the spray. In this region the smaller fuel droplets have evaporated in the hot air atmosphere that surrounds them and mixed with sufficient air for combustion to occur. Notice that the fuel vapor concentration must be nonuniform; combustion apparently occurs around small "lumps" of mixture of the appropriate composition and temperature. Figure 10-5*b* shows the same flame at a later time, 3.2 ms after ignition. The flame now surrounds most of the liquid spray core. Its irregular boundary reflects the turbulent character of the fuel spray and its color variation indicates that the temperature and composition in the flame region are not uniform.

Figure 10-5*c* shows a portion of this main flame region enlarged to show its internal structure. A highly convoluted flame region is evident, which has a similar appearance to a gaseous turbulent diffusion flame. The major portion of the diesel engine flame has this character, indicative of the burning of fuel vapor–air pockets or lumps or eddies of the appropriate composition. Only at the end of the combustion process is there visible evidence of individual fuel droplets burning with an envelope flame. Figure 10-5*d* shows the same region of the combustion chamber as Fig. 10-5*c*, but at the end of the burning process well after injection has been completed. A few large droplets are seen burning with individual droplet flames. It is presumed that such large drops were formed at the end of the injection process as the injector nozzle was closing.

FIGURE 10-5 (On Color Plate, facing page 498)
Photographs from high-speed movie of single fuel spray injected into a swirling air flow in a rapid-compression machine. (*a*) Spray and flame 0.4 ms after ignition; scale on right in millimeters. (*b*) Flame surrounding spray 3.2 ms after ignition. (*c*) Magnified photograph of main portion of flame. (*d*) Individual droplet burning late in combustion process after injection completed. Air temperature ~500°C. 50 mg fuel injected.[4] (*Courtesy Professor M. Ogasawara, Osaka University.*)

10.3.2 Combustion in Direct-Injection, Multispray Systems

Figure 10-6 shows typical data for cylinder pressure (p), fuel-injector needle-lift, and fuel pressure in the nozzle gallery through the compression and expansion strokes of a direct-injection diesel. The engine had central fuel injection through a four-hole nozzle into a disc-shaped bowl-in-piston combustion chamber. The rate of fuel injection can be obtained from the fuel-line pressure, cylinder pressure, nozzle geometry, and needle-lift profiles by considering the injector as one or more flow restrictions;[5] it is similar in phasing and comparable in shape to the needle-lift profile. There is a delay of 9° between the start of injection and start of combustion [identified by the change in slope of the $p(\theta)$ curve]. The pressure rises rapidly for a few crank angle degrees, then more slowly to a peak value about 5° after TC. Injection continues after the start of combustion. A rate-of-heat-release diagram† from the same study, corresponding to this rate of fuel injection and cylinder pressure data, is shown in Fig. 10-7. The general shape of the rate-of-heat-release curve is typical of this type of DI engine over its load and speed range. The heat-release-rate diagram shows negligible heat release until toward the end of compression when a slight loss of heat during the delay period (which is due to heat transfer to the walls and to fuel vaporization and heating) is

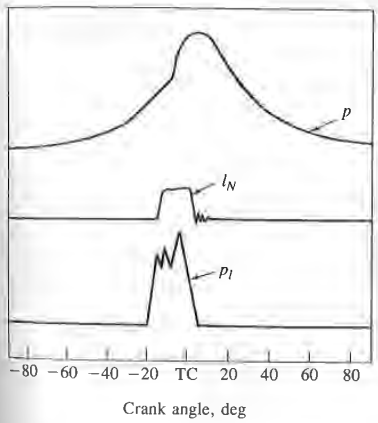

FIGURE 10-6
Cylinder pressure p, injector needle lift l_N, and injection-system fuel-line pressure p_l, as functions of crank angle for small DI diesel engine.[5]

† The heat-release rate plotted here is the net heat-release rate (see Sec. 10.4). It is the sum of the change of sensible internal energy of the cylinder gases and the work done on the piston. It differs from the rate of fuel energy released by combustion by the heat transferred to the combustion chamber walls. The heat loss to the walls is 10 to 25 percent of the fuel heating value in smaller engines; it is less in larger engine sizes. This net heat release can be used as an indicator of actual heat release when the heat loss is small.

evident. During the combustion process the burning proceeds in three distinguishable stages. In the first stage, the rate of burning is generally very high and lasts for only a few crank angle degrees. It corresponds to the period of rapid cylinder pressure rise. The second stage corresponds to a period of gradually decreasing heat-release rate (though it initially may rise to a second, lower, peak as in Fig. 10-7). This is the main heat-release period and lasts about 40°. Normally about 80 percent of the total fuel energy is released in the first two periods. The third stage corresponds to the "tail" of the heat-release diagram in which a small but distinguishable rate of heat release persists throughout much of the expansion stroke. The heat release during this period usually amounts to about 20 percent of the total fuel energy.

From studies of rate-of-injection and heat-release diagrams such as those in Fig. 10-7, over a range of engine loads, speeds, and injection timings, Lyn[6] developed the following summary observations. First, the total burning period is much longer than the injection period. Second, the absolute burning rate increases proportionally with increasing engine speed; thus on a crank angle basis, the burning interval remains essentially constant. Third, the magnitude of the initial peak of the burning-rate diagram depends on the ignition delay period, being higher for longer delays. These considerations, coupled with engine combustion photographic studies, lead to the following model for diesel combustion.

Figure 10-8 shows schematically the rate-of-injection and rate-of-burning diagrams, where the injected fuel as it enters the combustion chamber has been divided into a number of elements. The first element which enters mixes with air and becomes "ready for burning" (i.e., mixes to within combustible limits), as shown conceptually by the lowest triangle along the abscissa in the rate-of-burning figure. While some of this fuel mixes rapidly with air, part of it will mix much more slowly. The second and subsequent elements will mix with air in a similar manner, and the total "ready-for-burning" diagram, enclosed by the dashed line, is obtained. The total area of this diagram is equal to that of the rate-of-injection diagram. Ignition does not occur until after the delay period is over, however. At the ignition point, some of the fuel already injected has mixed with enough air to be within the combustible limits. That "premixed" fuel-air

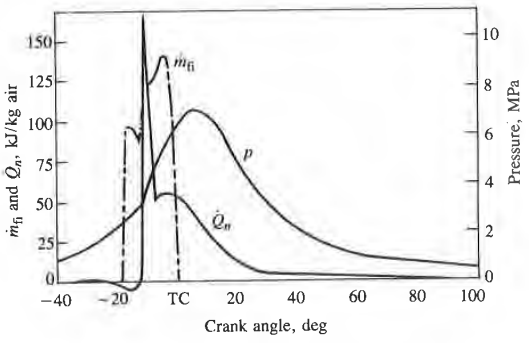

FIGURE 10-7
Cylinder pressure p, rate of fuel injection $\dot{m}_{fi}$, and net heat-release rate $\dot{Q}_n$ calculated from p for small DI diesel engine, 1000 rev/min, normal injection timing, bmep = 620 kPa.[5]

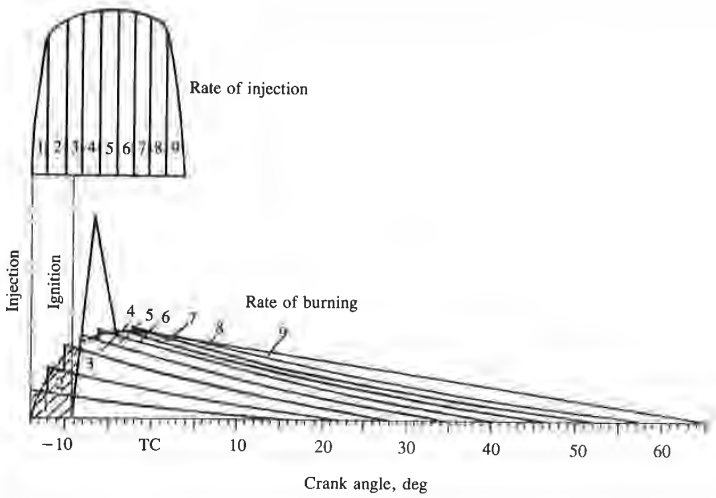

FIGURE 10-8
Schematic of relationship between rate of fuel injection and rate of fuel burning or energy release.[6]

mixture (the shaded region in Fig. 10-8) is then added to the mixture which becomes ready for burning after the end of the delay period, producing the high initial rate of burning as shown. Such a heat-release profile is generally observed with this type of naturally aspirated DI diesel engine. Photographs (such as those in Fig. 10-4*a* and *b*) show that up to the heat-release-rate peak, flame regions of low green luminosity are apparent because the burning is predominantly of the premixed part of the spray. After the peak, as the amount of premixed mixture available for burning decreases and the amount of fresh mixture mixed to be "ready for burning" increases, the spray burns essentially as a turbulent diffusion flame with high yellow-white or orange luminosity due to the presence of carbon particles.

To summarize, the following stages of the overall compression-ignition diesel combustion process can be defined. They are identified on the typical heat-release-rate diagram for a DI engine in Fig. 10-9.

Ignition delay (*ab*). The period between the start of fuel injection into the combustion chamber and the start of combustion [determined from the change in slope on the p-θ diagram, or from a heat-release analysis of the $p(\theta)$ data, or from a luminosity detector].

Premixed or rapid combustion phase (*bc*). In this phase, combustion of the fuel which has mixed with air to within the flammability limits during the ignition delay period occurs rapidly in a few crank angle degrees. When this burning mixture is added to the fuel which becomes ready for burning and burns during this phase, the high heat-release rates characteristic of this phase result.

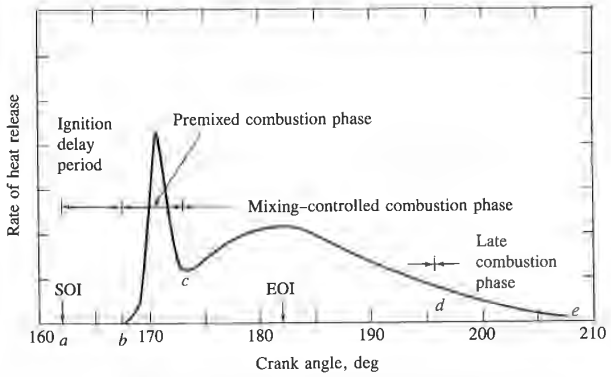

FIGURE 10-9
Typical DI engine heat-release-rate diagram identifying different diesel combustion phases.

Mixing-controlled combustion phase (*cd*). Once the fuel and air which premixed during the ignition delay have been consumed, the burning rate (or heat-release rate) is controlled by the rate at which mixture becomes available for burning. While several processes are involved—liquid fuel atomization, vaporization, mixing of fuel vapor with air, preflame chemical reactions—the rate of burning is controlled in this phase primarily by the fuel vapor–air mixing process. The heat-release rate may or may not reach a second (usually lower) peak in this phase; it decreases as this phase progresses.

Late combustion phase (*de*). Heat release continues at a lower rate well into the expansion stroke. There are several reasons for this. A small fraction of the fuel may not yet have burned. A fraction of the fuel energy is present in soot and fuel-rich combustion products and can still be released. The cylinder charge is nonuniform and mixing during this period promotes more complete combustion and less-dissociated product gases. The kinetics of the final burnout processes become slower as the temperature of the cylinder gases fall during expansion.

10.3.3 Application of Model to Other Combustion Systems

In the M.A.N. "M" DI engine system, and in IDI systems, the shapes of the heat-release-rate curve are different from those of the quiescent or moderate swirl DI shown in Figs. 10-7 and 10-9. With the "M" system, the initial heat-release "spike" is much less pronounced (in spite of the fact that a large fraction of the fuel is injected during the delay period) though the total burning period is about the same. Lyn[6] has suggested that the lower initial burning rate is due to the fact that the smaller number of nozzle holes (one or two instead of about four or more) and the directing of the main spray tangentially to the wall substantially reduce the free mixing surface area of the fuel jets. However, since the burning

rates after ignition are relatively high, mixing must speed up. This occurs due to the centrifugal forces set up in the swirling flow. Initially, the fuel is placed near the wall, and mixing is inhibited by the effect of the high centrifugal forces on the fuel vapor which is of higher density than the air and so tends to remain near the wall. Once ignition occurs, the hot burning mixture expands, decreases in density, and is then moved rapidly toward the center of the chamber. This strong radial mixing is the rate-determining process. An additional delaying mechanism exists if significant fuel is deposited on the wall. At compression air temperatures, the heat transferred to the fuel film on the wall from the gases in the cylinder is too small to account for the observed burning rates. Only after combustion starts will the gas temperature and heat-transfer rates be high enough to evaporate the fuel off the wall at an adequate rate.

In the swirl chamber IDI engine, where the air in the main chamber is not immediately available for mixing, again the rate-determining processes are different.[6] There is no initial spike on the rate-of-heat-release curve as was the case with DI engines. The small size of the chamber, together with the high swirl rate generated just before injection, results in considerable fuel impingement on the walls. This and the fact that the ignition delay is usually shorter with the IDI engine due to the higher compression ratio used account for the low initial burning rate.

Based on the above discussion Lyn[6] proposed three basic injection, mixing, and burning patterns important in diesel engines:

A. Fuel injection across the chamber with substantial momentum. Mixing proceeds immediately as fuel enters the chamber and is little affected by combustion.

B. Fuel deposition on the combustion chamber walls. Negligible mixing during the delay period due to limited evaporation. After ignition, evaporation becomes rapid and its rate is controlled by access of hot gases to the surface, radial mixing being induced by differential centrifugal forces. Burning is therefore delayed by the ignition lag.

C. Fuel distributed near the wall: mixing proceeds during the delay, but at a rate smaller than in mechanism A. After ignition, mixing is accelerated by the same mechanism as in mechanism B.

Figure 10-10 shows, schematically, the construction of the burning-rate or heat-release-rate diagrams (from the same injection-rate diagram) for the DI diesel combustion system with a central multihole nozzle, for the "M"-type DI diesel, and for the swirl chamber IDI. For the DI engine with multihole nozzle, mechanism A is predominant. For the DI engine with fuel sprayed tangentially to the wall, mechanisms B and C prevail; the delayed mixing prevents excessively high initial burning rates. For the IDI swirl chamber engine, the shorter ignition delay together with mixing process C during the delay period produces a gradual increase in burning rate, as shown in Fig. 10-10c.

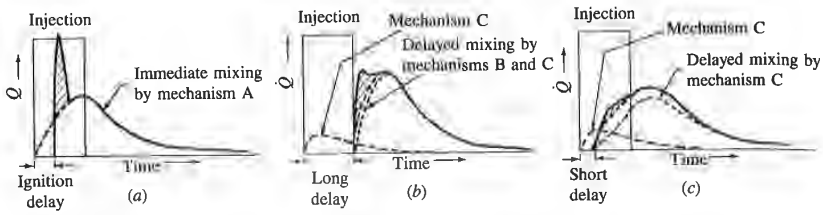

FIGURE 10-10
Schematic injection-rate and burning-rate diagrams in three different types of naturally aspirated diesel combustion system: (*a*) DI engine with central multihole nozzle; (*b*) DI "M"-type engine with fuel injected on wall; (*c*) IDI swirl chamber engine. Mechanisms A, B, and C defined in text.[6]

10.4 ANALYSIS OF CYLINDER PRESSURE DATA

Cylinder pressure versus crank angle data over the compression and expansion strokes of the engine operating cycle can be used to obtain quantitative information on the progress of combustion. Suitable methods of analysis which yield the rate of release of the fuel's chemical energy (often called heat release), or rate of fuel burning, through the diesel engine combustion process will now be described. The methods of analysis are similar to those described in Sec. 9.2.2 for spark-ignition engines and start with the first law of thermodynamics for an open system which is quasi static (i.e., uniform in pressure and temperature). The first law for such a system (see Fig. 9-11) is

$$\frac{dQ}{dt} - p\frac{dV}{dt} + \sum_i \dot{m}_i h_i = \frac{dU}{dt} \tag{10.1}$$

where dQ/dt is the heat-transfer rate across the system boundary into the system, $p(dV/dt)$ is the rate of work transfer done by the system due to system boundary displacement, $\dot{m}_i$ is the mass flow rate into the system across the system boundary at location i (flow out of the system would be negative), h_i is the enthalpy of flux i entering or leaving the system, and U is the energy of the material contained inside the system boundary.

The following problems make the application of this equation to diesel combustion difficult:

1. Fuel is injected into the cylinder. Liquid fuel is added to the cylinder which vaporizes and mixes with air to produce a fuel/air ratio distribution which is nonuniform and varies with time. The process is not quasi static.
2. The composition of the burned gases (also nonuniform) is not known.
3. The accuracy of available correlations for predicting heat transfer in diesel engines is not well defined (see Chap. 12).
4. Crevice regions (such as the volumes between the piston, rings, and cylinder wall) constitute a few percent of the clearance volume. The gas in these regions is cooled to close to the wall temperature, increasing its density and, therefore,

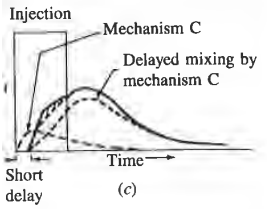

ent types of naturally aspirated
le; (b) DI "M"-type engine with
and C defined in text.[6]

mpression and expansion
tain quantitative informa-
of analysis which yield the
ed heat release), or rate of
cess will now be described.
ed in Sec. 9.2.2 for spark-
modynamics for an open
nd temperature). The first

(10.1)

boundary into the system,
n due to system boundary
cross the system boundary
, h_i is the enthalpy of flux i
of the material contained

of this equation to diesel

lded to the cylinder which
ratio distribution which is
t quasi static.
rm) is not known.
ing heat transfer in diesel

piston, rings, and cylinder
ne. The gas in these regions
g its density and, therefore,

the relative importance of these crevices. Thus crevices increase heat transfer and contain a nonnegligible fraction of the cylinder charge at conditions that are different from the rest of the combustion chamber.

Due to difficulties in dealing with these problems, both sophisticated methods of analysis and more simple methods give only approximate answers.

10.4.1 Combustion Efficiency

In both heat-release and fuel mass burned estimations, an important factor is the completeness of combustion. Air utilization in diesels is limited by the onset of black smoke in the exhaust. The smoke is soot particles which are mainly carbon. While smoke and other incomplete combustion products such as unburned hydrocarbons and carbon monoxide represent a combustion inefficiency, the magnitude of that inefficiency is small. At full load conditions, if only 0.5 percent of the fuel supplied is present in the exhaust as black smoke, the result would be unacceptable. Hydrocarbon emissions are the order of or less than 1 percent of the fuel. The fuel energy corresponding to the exhausted carbon monoxide is about 0.5 percent. Thus, the combustion inefficiency [Eq. (4.69)] is usually less than 2 percent; the combustion efficiency is usually greater than about 98 percent (see Fig. 3-9). While these emissions are important in terms of their air-pollution impact (see Chap. 11), from the point of view of energy conversion it is a good approximation to regard combustion and heat release as essentially complete.

10.4.2 Direct-Injection Engines

For this type of engine, the cylinder contents are a single open system. The only mass flows across the system boundary (while the intake and exhaust valves are closed) are the fuel and the crevice flow. An approach which incorporates the crevice flow has been described in Sec. 9.2.2; crevice flow effects will be omitted here. Equation (10.1) therefore becomes

$$\frac{dQ}{dt} - p\frac{dV}{dt} + \dot{m}_f h_f = \frac{dU}{dt} \tag{10.2}$$

Two common methods are used to obtain combustion information from pressure data using Eq. (10.2). In both approaches, the cylinder contents are assumed to be at a uniform temperature at each instant in time during the combustion process. One method yields fuel energy- or heat-release rate; the other method yields a fuel mass burning rate. The term *apparent* is often used to describe these quantities since both are approximations to the real quantities which cannot be determined exactly.

HEAT-RELEASE ANALYSIS. If U and h_f in Eq. (10.2) are taken to be the sensible internal energy of the cylinder contents and the sensible enthalpy of the injected

fuel, respectively,† then dQ/dt becomes the difference between the chemical energy or heat released by combustion of the fuel (a positive quantity) and the heat transfer from the system (in engines, the heat transfer is from the system and by thermodynamic convention is a negative quantity). Since $h_{s,f} \approx 0$, Eq. (10.2) becomes

$$\frac{dQ_n}{dt} = \frac{dQ_{ch}}{dt} - \frac{dQ_{ht}}{dt} = p\frac{dV}{dt} + \frac{dU_s}{dt} \tag{10.3}$$

The apparent *net heat-release* rate, dQ_n/dt, which is the difference between the apparent *gross heat-release* rate dQ_{ch}/dt and the heat-transfer rate to the walls dQ_{ht}/dt, equals the rate at which work is done on the piston plus the rate of change of sensible internal energy of the cylinder contents.

If we further assume that the contents of the cylinder can be modeled as an ideal gas, then Eq. (10.3) becomes

$$\frac{dQ_n}{dt} = p\frac{dV}{dt} + mc_v\frac{dT}{dt} \tag{10.4}$$

From the ideal gas law, $pV = mRT$, with R assumed constant, it follows that

$$\frac{dp}{p} + \frac{dV}{V} = \frac{dT}{T} \tag{10.5}$$

Equation (10.5) can be used to eliminate T from Eq. (10.4) to give

$$\frac{dQ_n}{dt} = \left(1 + \frac{c_v}{R}\right)p\frac{dV}{dt} + \frac{c_v}{R}V\frac{dp}{dt}$$

or

$$\frac{dQ_n}{dt} = \frac{\gamma}{\gamma - 1}p\frac{dV}{dt} + \frac{1}{\gamma - 1}V\frac{dp}{dt} \tag{10.6}$$

Here γ is the ratio of specific heats, c_p/c_v. An appropriate range for γ for diesel heat-release analysis is 1.3 to 1.35; Eq. (10.6) is often used with a constant value of γ within this range. More specifically, we would expect γ for diesel engine heat-release analysis to have values appropriate to air at end-of-compression-stroke temperatures prior to combustion ($\approx$1.35) and to burned gases at the overall equivalence ratio following combustion ($\approx$1.26–1.3). The appropriate values for γ during combustion which will give most accurate heat-release information are not well defined.[7, 8]

More complete methods of heat-release analysis based on Eq. (10.2) have been proposed and used. These use more sophisticated models for the gas properties before, during, and after combustion, and for heat transfer and crevice effects.[8] However, it is also necessary to deal with the additional issues of: (1) mixture nonuniformity (fuel/air ratio nonuniformity *and* burned and unburned gas nonuniformities); (2) accuracy of any heat-transfer model used (see Chap. 12);

† That is, $U = U_s = U(T) - U(298\text{ K})$ and $h_f = h_{s,f} = h_f(T) - h_f(298\text{ K})$; see Sec. 5.5 for definition.

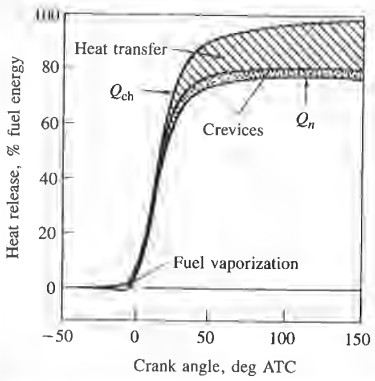

FIGURE 10-11
Gross and net heat-release profile during combustion, for a turbocharged DI diesel engine in mid-load, mid-speed range, showing relative magnitude of heat transfer, crevice, and fuel vaporization and heatup effects.

and (3) the effects of the crevice regions. These additional phenomena must be dealt with at an equivalent level of accuracy for more complex heat-release models to be worth while. For many engineering applications, Eq. (10.6) is adequate for diesel engine combustion analysis.

Additional insight can be obtained by incorporating a model for the largest of the effects omitted from Eq. (10.6), the heat transfer dQ_{ht}/dt (see Chap. 12); we thereby obtain a close approximation to the *gross* heat-release rate. The integral of the gross heat-release rate over the complete combustion process should then equal (to within a few percent only, since the analysis is not exact) the mass of fuel injected m_f times the fuel lower heating value Q_{LHV}: i.e.,

$$Q_{ch} = \int_{t_{start}}^{t_{end}} \frac{dQ_{ch}}{dt}\, dt = m_f Q_{LHV} \tag{10.7}$$

Of course, Eqs. (10.1) to (10.4), (10.6), and (10.7) also hold with crank angle θ as the independent variable instead of time t.

Figure 10-11 illustrates the relative magnitude of gross and net heat release, heat transfer, crevice effects, and heat of vaporization and heating up of the fuel for a turbocharged DI diesel engine operating in the mid-load, mid-speed range. The net heat release is the gross heat release due to combustion, less the heat transfer to the walls, crevice effects, and the effect of fuel vaporization and heatup (which was omitted above by neglecting the mass addition term in dU/dt). This last term is sufficiently small to be neglected. The enthalpy of vaporization of diesel fuel is less than 1 percent of its heating value; the energy change associated with heating up fuel vapor from injection temperature to typical compression air temperatures is about 3 percent of the fuel heating value. The heat transfer integrated over the duration of the combustion period is 10 to 25 percent of the total heat released.

FUEL MASS BURNING RATE ANALYSIS. If the internal energies of the fuel, air, and burned gases in Eq. (10.1) are evaluated relative to a consistent datum (such

as that described in Sec. 4.5.2), then this equation can be used to obtain an apparent *fuel mass burning rate* from cylinder pressure versus crank angle data. (With such a species energy datum the "heat release" is properly accounted for in the internal energy and enthalpy terms.) Following Krieger and Borman,[9] Eq. (10.2) can be written as

$$\frac{d}{dt}(mu) = -p\frac{dV}{dt} + \frac{dQ}{dt} + h_f\frac{dm}{dt} \tag{10.8}$$

Here Q is the heat transfer to the gas within the combustion chamber (that is, $Q = -Q_{ht}$), m is the mass within the combustion chamber, and dm/dt has been substituted for $\dot{m}_f$.

Since the properties of the gases in the cylinder during combustion (assumed to be uniform and in chemical equilibrium at the pressure p and average temperature T) are in general a function of p, T, and the equivalence ratio ϕ,

$$u = u(T, p, \phi) \qquad \text{and} \qquad R = R(T, p, \phi)$$

Therefore

$$\frac{du}{dt} = \frac{\partial u}{\partial T}\frac{dT}{dt} + \frac{\partial u}{\partial p}\frac{dp}{dt} + \frac{\partial u}{\partial \phi}\frac{d\phi}{dt} \tag{10.9a}$$

$$\frac{dR}{dt} = \frac{\partial R}{\partial T}\frac{dT}{dt} + \frac{\partial R}{\partial p}\frac{dp}{dt} + \frac{\partial R}{\partial \phi}\frac{d\phi}{dt} \tag{10.9b}$$

Also,

$$\phi = \phi_0 + \left(\frac{m}{m_0} - 1\right)\frac{1 + (F/A)_0}{(F/A)_s} \tag{10.10}$$

and

$$\frac{d\phi}{dt} = \frac{1 + (F/A)_0}{(F/A)_s m_0}\frac{dm}{dt} \tag{10.11}$$

(F/A) is the fuel/air ratio; the subscript 0 denotes the initial value prior to fuel injection and the subscript s denotes the stoichiometric value. It then follows that

$$\frac{1}{m}\frac{dm}{dt} = \frac{-(RT/V)(dV/dt) - (\partial u/\partial p)(dp/dt) + (1/m)(dQ/dt) - CB}{u - h_f + D(\partial u/\partial \phi) - C[1 + (D/R)(\partial R/\partial \phi)]} \tag{10.12}$$

where

$$B = \frac{1}{p}\frac{dp}{dt} - \frac{1}{R}\frac{\partial R}{\partial p}\frac{dp}{dt} + \frac{1}{V}\frac{dV}{dt}$$

$$C = \frac{T(\partial u/\partial T)}{1 + (T/R)(\partial R/\partial T)}$$

$$D = \frac{[1 + (F/A)_0]m}{(F/A)_s m_0}$$

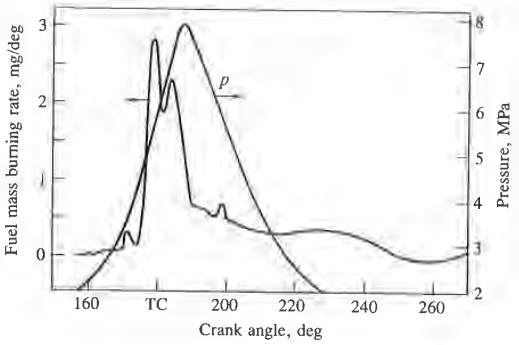

FIGURE 10-12
Cylinder pressure p and fuel mass burning rate calculated from p, as a function of crank angle, using the Krieger and Borman method[9] for DI diesel engine at 3200 rev/min and full load.

Equation (10.12) can be solved numerically for $m(t)$ given m_0, ϕ_0, $p(t)$, and appropriate models for the working fluid properties (see Sec. 4.7) and for the heat-transfer term dQ/dt (see Chap. 12).

Figure 10-12 shows cylinder pressure data for an open chamber DI diesel and fuel mass burning rate $dm/d\theta$ calculated from that data using the above method. The heat-transfer model of Annand was used (see Sec. 12.4.3). The result obtained is an *apparent* fuel mass burning rate. It is best interpreted, after multiplying by the heating value of the fuel, as the fuel chemical-energy or heat-release rate. The *actual* fuel burning rate is unknown because not all the fuel "burns" with sufficient air available locally to produce products of *complete* combustion. About 60 percent of the fuel has burned in the first one-third of the total combustion period. The integral of the fuel mass burning rate over the combustion process should equal the total fuel mass burned; in this case it is 3 percent less than the total fuel mass injected. Note that chemical energy continues to be released well into the expansion process. The accuracy of this type of calculation then decreases, however, since errors in estimating heat transfer significantly affect the apparent fuel burning rate.

Krieger and Borman also carried out sensitivity analyses for the critical assumptions and variables. They found that the effect of dissociation of the product gases was negligible. This permits a substantial simplification of Eq. (10.12). With no dissociation, $u = u(T, \phi)$, and $R = \tilde{R}/M$ can be taken as constant, since the molecular weight M changes little. Then

$$\frac{dm}{dt} = \frac{[1 + (c_v/R)]p(dV/dt) + (c_v/R)V(dp/dt) - (dQ/dt)}{h_f + (c_v/R)(pV/m) - u - D(\partial u/\partial \phi)} \tag{10.13}$$

where D, as before, is $[1 + (F/A)_0]m/[(F/A)_s m_0]$. Given the uncertainties inherent in the heat-transfer model and the neglect of nonuniformities and crevices, Eq. (10.13) represents an adequate level of sophistication.

The other sensitivity variations studied by Krieger and Borman were: shifting of the phasing of the pressure data 2° forward and 2° backward; translating the pressure data ± 34 kPa (5 lb/in^2); changing the heat transfer ± 50 percent;

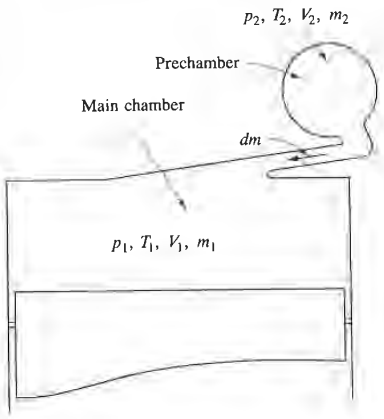

FIGURE 10-13
Schematic defining variables in main chamber (subscript 1) and prechamber (subscript 2) for IDI engine heat-release analysis.

increasing the initial mass 5 percent. The initial mass change had a negligible effect on the fuel burning rate calculations. The heat-transfer changes of ± 50 percent changed the mass of fuel burned by about ± 5 percent. The change in phasing of the pressure data was more significant. It needs to be stressed that *accurate* (in magnitude and phasing) pressure data are a most important requirement for useful heat-release or fuel mass burning rate analysis.

10.4.3 Indirect-Injection Engines

In IDI diesel engines, the pressures in each of the two chambers, main and auxiliary, are not the same during the combustion process. Since combustion starts in the auxiliary or prechamber, the fuel energy release in the prechamber causes the pressure there to rise above the main chamber pressure. Depending on combustion chamber design and operating conditions, the prechamber pressure rises to be 0.5 to 5 atm above that in the main chamber. This pressure difference causes a flow of fuel, air, and burning and burned gases into the main chamber, where additional energy release now occurs. The analysis of the DI diesel in the previous section was based on uniform pressure throughout the combustion chamber. For IDI engines the effect of the pressure difference between the chambers must usually be included.

Figure 10-13 shows an IDI combustion chamber divided at the nozzle into two open systems. Applying the first law [Eq. (10.1)] to the *main chamber* yields

$$\frac{dQ_1}{dt} - p_1 \frac{dV_1}{dt} + h_{2,1} \frac{dm}{dt} = \frac{dU_1}{dt} \tag{10.14}$$

and to the *auxiliary chamber* yields

$$\frac{dQ_2}{dt} - h_{2,1} \frac{dm}{dt} + h_f \frac{dm_f}{dt} = \frac{dU_2}{dt} \tag{10.15}$$

Here dm/dt is the mass flow rate between the chambers with positive flow from the prechamber to the main chamber. If $dm/dt > 0$, $h_{2,1} = h_2$; if $dm/dt < 0$, $h_{2,1} = h_1$. If we define U_1 and U_2 as sensible internal energies and h_f as the sensible enthalpy of the fuel, then dQ_1/dt and dQ_2/dt represent the net heat-release rates—the difference between the combustion energy-release rates and the rates of heat transfer to the walls.

If we use an ideal gas model for the working fluid in each chamber, with c_v, c_p, and M constant, the relation $p_1V_1 = m_1RT_1$ and $p_2V_2 = m_2RT_2$ can be used to eliminate m and T from the dU/dt terms and, with the fact that $h_{s,f} = 0$, can be used to write Eqs. (10.14) and (10.15) as

$$\frac{dQ_1}{dt} = \frac{\gamma}{\gamma - 1} p_1 \frac{dV_1}{dt} + \frac{1}{\gamma - 1} V_1 \frac{dp_1}{dt} - c_p T_{2,1} \frac{dm}{dt} \tag{10.16}$$

$$\frac{dQ_2}{dt} = \frac{1}{\gamma - 1} V_2 \frac{dp_2}{dt} + c_p T_{2,} \frac{dm}{dt} \tag{10.17}$$

When Eqs. (10.16) and (10.17) are added together, the term representing the enthalpy flux between the two chambers cancels out, and the following equation for *total* net heat-release results:

$$\frac{dQ}{dt} = \frac{dQ_1}{dt} + \frac{dQ_2}{dt} = \frac{\gamma}{\gamma - 1} p_1 \frac{dV_1}{dt} + \frac{1}{\gamma - 1} \left(V_1 \frac{dp_1}{dt} + V_2 \frac{dp_2}{dt} \right) \tag{10.18}$$

The comments made in the previous section regarding the interpretation of the net heat release (it is the gross heat release due to combustion less the heat transfer to the walls, and other smaller energy transfers due to crevices, fuel vaporization, and heatup) also hold here.

In practice, Eq. (10.18) is difficult to use since it requires experimental data for both the main and auxiliary chamber pressures throughout the combustion process. Access for two pressure transducers through the cylinder head is not often available; even when access can be achieved, the task of obtaining pressure data from two different transducers under the demanding thermal loading conditions found in IDI diesels, of sufficient accuracy such that the difference between the pressures (of order 0.5 to 5 atm) at pressure levels of 60 to 80 atm can be interpreted, requires extreme diligence in technique.[10, 11] Figure 10-14*a* and *b* shows apparent net heat-release rate profiles for an IDI diesel obtained using Eq. (10.18) with $\gamma = 1.35$.[11] Curves of dQ/dt and $dQ/d\theta$ are shown at three different speeds and essentially constant fuel mass injected per cycle. While the absolute heat-release rates increase with increasing speed, the relative rates are essentially independent of speed, indicating that combustion rates, which depend on fuel-air mixing rates, scale approximately with engine speed.

Equation (10.18) (or its equivalent) has been used assuming $p_2 = p_1$ and using either main chamber or auxiliary chamber pressure data alone. The error associated with this approximation can be estimated as follows. If we write $p_2 =$

variables in main chamber
echamber (subscript 2) for IDI
nalysis.

change had a negligible
-transfer changes of ±50
5 percent. The change in
needs to be stressed that
a most important require-
ıalysis.

chambers, main and aux-
s. Since combustion starts
in the prechamber causes
ssure. Depending on com-
prechamber pressure rises
. This pressure difference
es into the main chamber,
/sis of the DI diesel in the
roughout the combustion
ference between the cham-

divided at the nozzle into
the *main chamber* yields

$\frac{I_1}{t}$ (10.14)

$\frac{I_2}{t}$ (10.15)

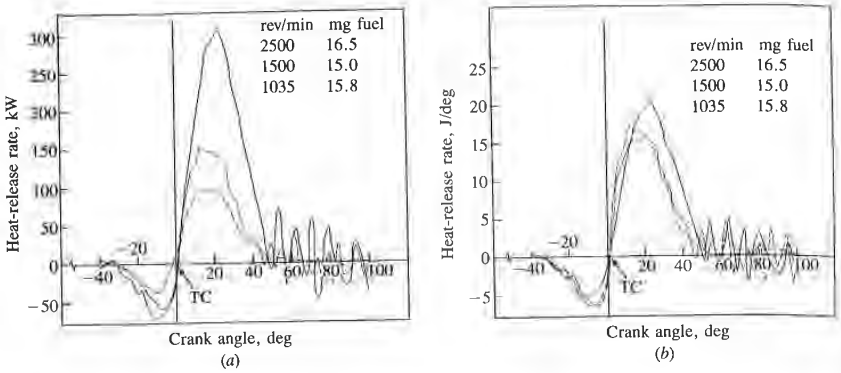

FIGURE 10-14
Calculated net heat-release-rate profiles for IDI diesel engine at constant load ($0.29 \leq \phi \leq 0.32$). (*a*) Heat-release rate in kilowatts. (*b*) Heat-release rate in joules per degree.[11]

$p_1 + \Delta p$ then Eq. (10.18) becomes

$$\frac{dQ}{dt} = \frac{\gamma}{\gamma - 1} p_1 \frac{dV_1}{dt} + \frac{V_1 + V_2}{\gamma - 1} \frac{dp_1}{dt} + \frac{V_2}{\gamma - 1} \frac{d(\Delta p)}{dt} \tag{10.19}$$

If the last term is omitted, Eq. (10.19) is identical to Eq. (10.6) derived for the DI diesel. Since the term $V(dp_1/dt)/(\gamma - 1)$ is much larger than the first term on the right-hand side of Eq. (10.19) during the early stages of the combustion process, the error involved in omitting the last term is given to a good approximation by $[V_2/(V_1 + V_2)]d(\Delta p)/dp_1$. In the initial stages of combustion this error can be quite large (of order 0.25 based on data in Ref. 10 close to TC). Later in the combustion process it becomes negligible (of order a few percent after 20° ATC).[10] Thus, neglecting Δp will lead to errors in predicting the initial heat-release *rate*. The magnitude of the error will depend on the design of the combustion chamber and on engine speed and load (with more restricted passageways, higher loads and speeds, giving higher values of Δp and, therefore, greater error). Later in the combustion process the error is much less, so *integrated* heat-release data derived ignoring Δp will show a smaller error.

A model analogous to the above, but using the approach of Krieger and Borman[9] (see Sec. 10.4.2), for the IDI diesel has been developed and used by Watson and Kamel.[10] The energy conservation equation for an *open* system developed in Sec. 14.2.2, with energy and enthalpy modeled using a consistent datum (see Sec. 4.5.2), with appropriate models for convective and radiation heat transfer and for gas properties, was applied to the main chamber and also to the prechamber. These equations were solved using accurately measured main chamber and prechamber pressure data to determine the apparent rate of heat release (here, the rate of fuel burning multiplied by the fuel heating value) in the main chamber and prechambers through the combustion process. The engine was a Ricardo Comet swirl chamber IDI design. Some results are shown in Fig.

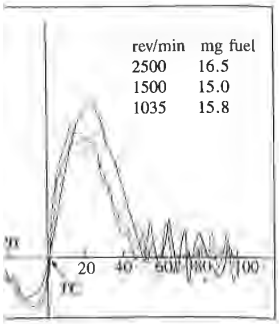

Crank angle, deg
(*b*)

nstant load ($0.29 \leq \phi \leq 0.32$). (*a*)
ee.[11]

$$\frac{V_2}{-1}\frac{d(\Delta p)}{dt} \qquad (10.19)$$

q. (10.6) derived for the DI
than the first term on the
of the combustion process,
) a good approximation by
stion this error can be quite
to TC). Later in the com-
percent after 20° ATC).[10]
the initial heat-release *rate*.
of the combustion chamber
passageways, higher loads
greater error). Later in the
ed heat-release data derived

e approach of Krieger and
en developed and used by
uation for an *open* system
modeled using a consistent
nvective and radiation heat
in chamber and also to the
accurately measured main
e the apparent rate of heat
ne fuel heating value) in the
ion process. The engine was
results are shown in Fig.

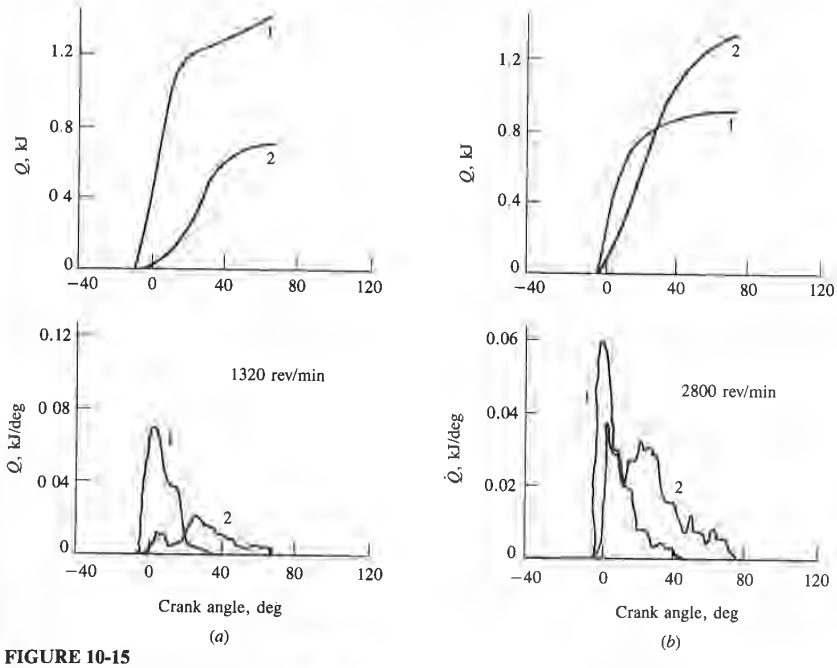

FIGURE 10-15
Calculated gross heat-release rates in IDI swirl-chamber diesel engine at full load. 1 Prechamber heat release. 2 Main chamber heat release. Top figures: integrated heat release. Bottom figures: heat-release rate. (*a*) 1320 rev/min; (*b*) 2800 rev/min.[10]

10-15. For this particular engine, at low engine speeds two-thirds of the heat release occurs in the prechamber; at higher engine speeds about two-thirds of the heat release occurs in the main chamber.

10.5 FUEL SPRAY BEHAVIOR

10.5.1 Fuel Injection

The fuel is introduced into the cylinder of a diesel engine through a nozzle with a large pressure differential across the nozzle orifice. The cylinder pressure at injection is typically in the range 50 to 100 atm. Fuel injection pressures in the range 200 to 1700 atm are used depending on the engine size and type of combustion system employed. These large pressure differences across the injector nozzle are required so that the injected liquid fuel jet will enter the chamber at sufficiently high velocity to (1) atomize into small-sized droplets to enable rapid evaporation and (2) traverse the combustion chamber in the time available and fully utilize the air charge.

Examples of common diesel fuel-injection systems were described briefly in Sec. 1.7 and illustrated in Figs. 1-17 to 1-19. (See also Refs. 12 and 13 for more

extensive descriptions of diesel fuel-injection systems.) The task of the fuel-injection system is to meter the appropriate quantity of fuel for the given engine speed and load to each cylinder, each cycle, and inject that fuel at the appropriate time in the cycle at the desired rate with the spray configuration required for the particular combustion chamber employed. It is important that injection begin and end cleanly, and avoid any secondary injections.

To accomplish this task, fuel is usually drawn from the fuel tank by a supply pump, and forced through a filter to the injection pump. The injection pump sends fuel under pressure to the nozzle pipes which carry fuel to the injector nozzles located in each cylinder head. Excess fuel goes back to the fuel tank. Figures 1-17 and 1-19 show two common versions of fuel systems used with multicylinder engines in the 20 to 100 kW per cylinder brake power range which operate with injection pressures between about 300 and 1200 atm.

In-line injection pumps (Fig. 1-17) are used in engines in the 40 to 100 kW per cylinder maximum power range. They contain a plunger and barrel assembly for each engine cylinder. Each plunger is raised by a cam on the pump camshaft and is forced back by the plunger return spring. The plunger stroke is fixed. The plunger fits sufficiently accurately within the barrel to seal without additional sealing elements, even at high pressures and low speeds. The amount of fuel delivered is altered by varying the *effective* plunger stroke. This is achieved by means of a control rod or rack, which moves in the pump housing and rotates the plunger via a ring gear or linkage lever on the control sleeve. The plunger chamber above the plunger is always connected with the chamber below the plunger helix by a vertical groove or bore in the plunger. Delivery ceases when the plunger helix exposes the intake port (port opening), thus connecting the plunger chamber with the suction gallery. When this takes place depends on the rotational position of the plunger. In the case of a lower helix, delivery always starts (port closing) at the same time, but ends sooner or later depending on the rotational position of the plunger. With a plunger with an upper helix, port closing (start of delivery) not port opening is controlled by the helix and is varied by rotating the plunger. Figure 1-18 illustrates how the plunger helix controls fuel delivery.[14]

Distributor-type fuel-injection pumps (such as that illustrated in Fig. 1-19) are normally used in multicylinder engines with less than 30 kW per cylinder maximum power with injection pressures up to 750 atm. These pumps have only one plunger and barrel. The pump plunger is made to describe a combined rotary and stroke movement by the rotating cam plate. The fuel is accurately metered to each injection nozzle in turn by this plunger which simultaneously acts as the distributor. Such units are more compact and cheaper than in-line pumps but cannot achieve such high injection pressures. The distributor-type fuel-injection pump is combined with the automatic timing device, governor, and supply pump to form a single unit.

Single-barrel injection pumps are used on small one- and two-cylinder diesel engines, as well as large engines with outputs of more than 100 kW per cylinder. Figure 10-16 shows the layout of the injection system and a section

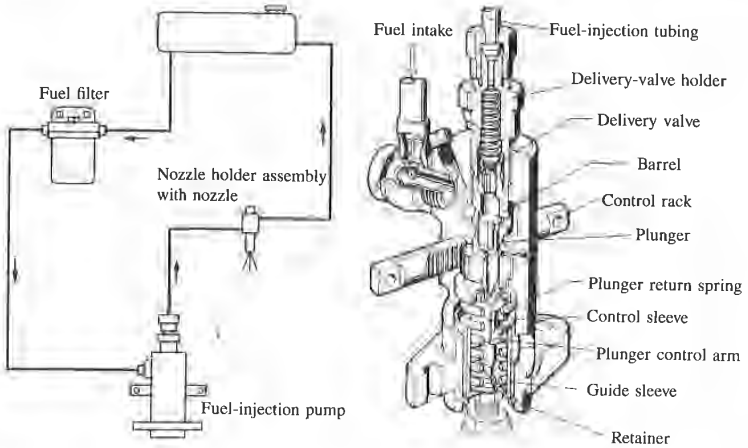

FIGURE 10-16
Fuel-injection system with single-barrel pump. Left: system layout. Right: section through fuel-injection pump. (*Courtesy Robert Bosch GmbH and SAE.*[14])

through the fuel-injection pump.[14] Such pumps are driven by an auxiliary cam on the engine camshaft. Also used extensively on larger engines are unit injectors where the pump and injector nozzle are combined into a single unit. An example of a unit injector and its driving mechanism used on a large two-stroke cycle diesel engine is shown in Fig. 10-17. Fuel, supplied to the injector through a fuel-distributing manifold, enters the cavity or plunger chamber ahead of the plunger through a metering orifice. When fuel is to be injected, the cam via the rocker arm pushes down the plunger, closing the metering orifice and compressing the fuel, causing it to flow through check valves and discharge into the cylinder through the injector nozzles or orifices. The amount of fuel injected is controlled by the rack, which controls the spill of fuel into the fuel drain manifold by rotating the plunger with its helical relief section via the gear.

The most important part of the injection system is the nozzle. Examples of different nozzle types and a nozzle holder assembly are shown in Fig. 1-18. The nozzles shown are fluid-controlled needle valves where the needle is forced against the valve seat by a spring. The pressure of the fuel in the pressure chamber above the nozzle aperture opens the nozzle by the axial force it exerts on the conical surface of the nozzle needle. Needle valves are used to prevent dribble from the nozzles when injection is not occurring. It is important to keep the volume of fuel left between the needle and nozzle orifices (the sac volume) as small as possible to prevent any fuel flowing into the cylinder after injection is over, to control hydrocarbon emissions (see Sec. 11.4.4). Multihole nozzles are used with most direct-injection systems; the M.A.N. "M" system uses a single-hole nozzle. Pintle nozzles, where the needle projects into and through the nozzle hole, are used in indirect-injection engine systems. The shape of the pin on the

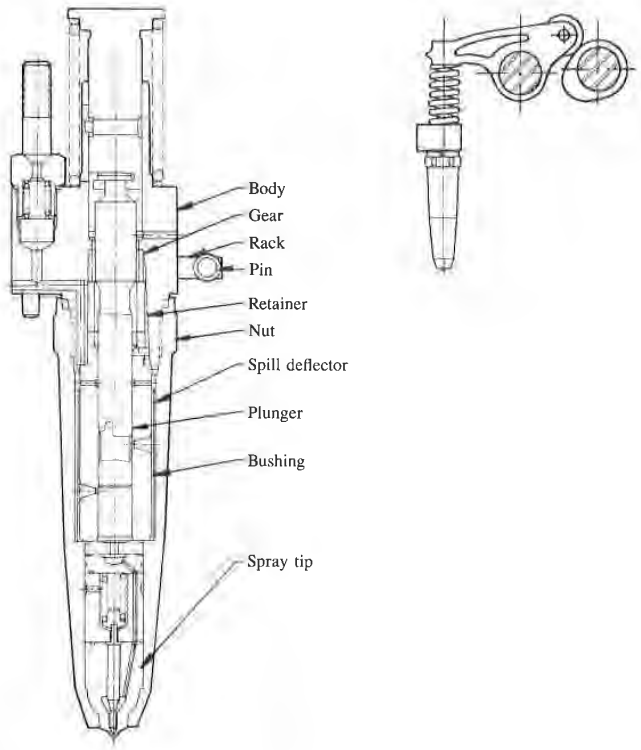

FIGURE 10-17
Unit fuel injector and its driving mechanism, typically used in large diesel engines.[15]

end of the nozzle needle controls the spray pattern and fuel-delivery characteristics. Auxiliary nozzle holes are sometimes used to produce an auxiliary smaller spray to aid ignition and starting. Open nozzle orifices, without a needle, are also used.

The technology for electronic control of injection is now available. In an electronic injector, such as that shown in Fig. 10-18, a solenoid operated control valve performs the injection timing and metering functions in a fashion analogous to the ports and helices of the mechanical injector. Solenoid valve closure initiates pressurization and injection, and opening causes injection pressure decay and end of injection. Duration of valve closure determines the quantity of fuel injected. The unit shown uses camshaft/rocker arm driven plungers to generate the injection pressure, and employs needle-valve nozzles of conventional design. Increased flexibility in fuel metering and timing and simpler injector mechanical design are important advantages.[16]

Accurate predictions of fuel behavior within the injection system require

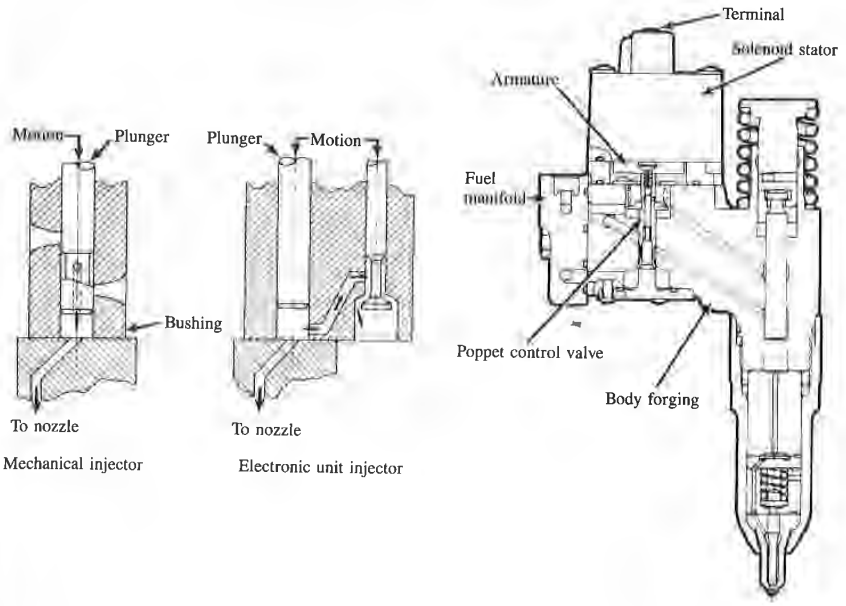

FIGURE 10-18
Electronically controlled unit fuel-injection system.[16]

sophisticated hydraulic models: Hiroyasu[17] provides an extensive reference list of such models. However, approximate estimates of the injection rate through the injector nozzles can be made as follows. If the pressure upstream of the injector nozzle(s) can be estimated or measured, and assuming the flow through each nozzle is quasi steady, incompressible, and one dimensional, the mass flow rate of fuel injected through the nozzle $\dot{m}_f$ is given by

$$\dot{m}_f = C_D A_n \sqrt{2\rho_f \Delta p} \tag{10.20}$$

where A_n is the nozzle minimum area, C_D the discharge coefficient, ρ_f the fuel density, and Δp the pressure drop across the nozzle. If the pressure drop across the nozzle and the nozzle open area are essentially constant during the injection period, the mass of fuel injected is then

$$m_f = C_D A_n \sqrt{2\rho_f \Delta p} \frac{\Delta\theta}{360N} \tag{10.21}$$

where $\Delta\theta$ is the nozzle open period in crank angle degrees and N is engine speed. Equations (10.20) and (10.21) illustrate the dependence of injected amounts of fuel on injection system and engine parameters.

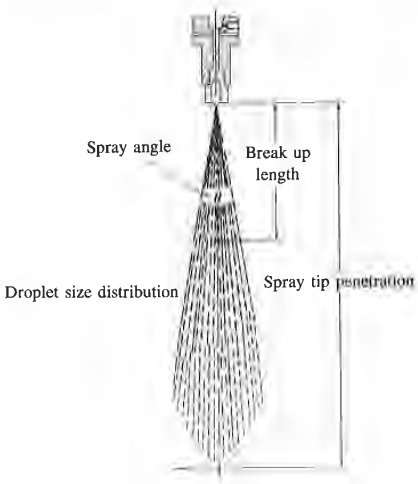

FIGURE 10-19
Schematic of diesel fuel spray defining its major parameters.[18]

10.5.2 Overall Spray Structure

The fuel is introduced into the combustion chamber of a diesel engine through one or more nozzles or orifices with a large pressure differential between the fuel supply line and the cylinder. Different designs of nozzle are used (e.g., single-orifice, multiorifice, throttle, or pintle; see Fig. 1-18), depending on the needs of the combustion system employed. Standard diesel injectors usually operate with fuel-injection pressures between 200 and 1700 atm. At time of injection, the air in the cylinder has a pressure of 50 to 100 atm, temperature about 1000 K, and density between 15 and 25 kg/m^3. Nozzle diameters cover the range 0.2 to 1 mm diameter, with length/diameter ratios from 2 to 8. Typical distillate diesel fuel properties are: relative specific gravity of 0.8, viscosity between 3 and 10 kg/m·s and surface tension about 3×10^{-2} N/m (at 300 K). Figure 10-19 illustrates the structure of a typical DI engine fuel spray. As the liquid jet leaves the nozzle it becomes turbulent and spreads out as it entrains and mixes with the surrounding air. The initial jet velocity is greater than 10^2 m/s. The outer surface of the jet breaks up into drops of order 10 μm diameter, close to the nozzle exit. The liquid column leaving the nozzle disintegrates within the cylinder over a finite length called the *breakup length* into drops of different sizes. As one moves away from the nozzle, the mass of air within the spray increases, the spray diverges, its width increases, and the velocity decreases. The fuel drops evaporate as this air-entrainment process proceeds. The tip of the spray penetrates further into the combustion chamber as injection proceeds, but at a decreasing rate. Figure 10-20 shows photographs of a diesel fuel spray injected into quiescent air in a rapid-compression machine which simulates diesel conditions.[19] Two different pho-

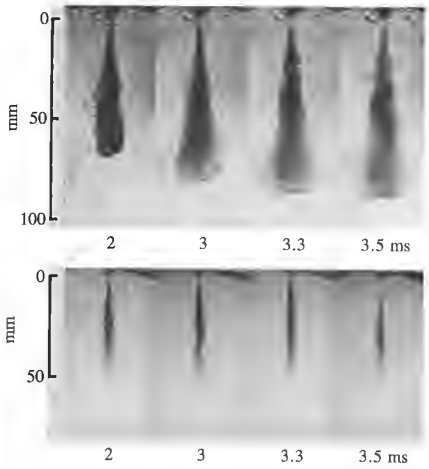

FIGURE 10-20
Shadowgraph and back-illuminated photographs of evaporating spray injected into nitrogen at 3.4 MPa and 670 K in rapid-compression machine. Times in milliseconds are after start of injection: injection duration 3.3 ms. Top (shadowgraph) photographs show full vapor and liquid region. Bottom (back-illuminated) photographs only show liquid-containing core.[19]

tographic techniques, back lighting and shadowgraph,† have been used to distinguish the liquid-containing core of the jet and the extent of the fuel vapor region of the spray which surrounds the liquid core. The region of the jet closest to the nozzle (until injection ceases at 3.3 ms) contains liquid drops and ligaments; the major region of the spray is a substantial vapor cloud around this narrow core which contains liquid fuel.

Different spray configurations are used in the different diesel combustion systems described earlier in this chapter. The simplest configuration involves multiple sprays injected into quiescent air in the largest-size diesels (Fig. 10-1*a*). Figures 10-19 and 10-20 illustrate the essential features of each spray under these circumstances until interactions with the wall occur. Each liquid fuel jet atomizes into drops and ligaments at the exit from the nozzle orifice (or shortly thereafter). The spray entrains air, spreads out, and slows down as the mass flow in the spray increases. The droplets on the outer edge of the spray evaporate first, creating a fuel vapor–air mixture sheath around the liquid-containing core. The highest velocities are on the jet axis. The equivalence ratio is highest on the centerline (and fuel-rich along most of the jet), decreasing to zero (unmixed air) at the spray boundary. Once the sprays have penetrated to the outer regions of the combustion chamber, they interact with the chamber walls. The spray is then forced to flow tangentially along the wall. Eventually the sprays from multihole nozzles

† The back lighting identifies regions where sufficient liquid fuel (as ligaments or drops) is present to attenuate the light. The shadowgraph technique responds to density gradients in the test section, so it identifies regions where fuel vapor exists.

of a diesel engine through
differential between the fuel
ozzle are used (e.g., single-
depending on the needs of
jectors usually operate with
t time of injection, the air in
erature about 1000 K, and
over the range 0.2 to 1 mm
Typical distillate diesel fuel
y between 3 and 10 kg/m · s
Figure 10-19 illustrates the
quid jet leaves the nozzle it
mixes with the surrounding
The outer surface of the jet
o the nozzle exit. The liquid
ylinder over a finite length
s. As one moves away from
the spray diverges, its width
ops evaporate as this air-
penetrates further into the
lecreasing rate. Figure 10-20
ito quiescent air in a rapid-
tions.[19] Two different pho-

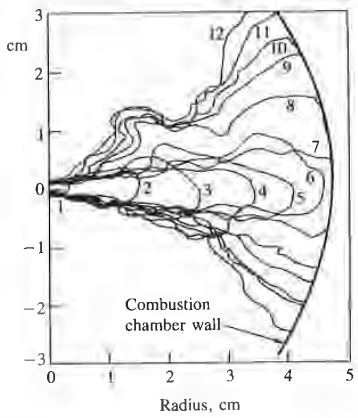

FIGURE 10-21
Sketches of outer vapor boundary of diesel fuel spray from 12 successive frames of rapid-compression-machine high-speed shadowgraph movie showing interaction of vaporizing spray with cylindrical wall of combustion chamber. Injection pressure 60 MPa. Time between frames 0.14 ms.[20]

interact with one another. Figure 10-21 shows diesel fuel sprays interacting with the cylindrical outer wall of a disc-shaped combustion chamber in a rapid-compression machine, under typical diesel-injection conditions. The cylinder wall causes the spray to split with about half flowing circumferentially in either direction. Adjacent sprays then interact forcing the flow radially inward toward the chamber axis.[20]

Most of the other combustion systems in Figs. 10-1 and 10-2 use air swirl to increase fuel-air mixing rates. A schematic of the spray pattern which results when a fuel jet is injected radially outward into a swirling flow is shown in Fig. 10-22. Because there is now relative motion in both radial and tangential directions between the initial jet and the air, the structure of the jet is more complex. As the spray entrains air and slows down it becomes increasingly bent toward the swirl direction; for the same injection conditions it will penetrate less with swirl than without swirl. An important feature of the spray is the large vapor-containing region downstream of the liquid-containing core. Figure 10-23 shows schlieren photographs of four fuel jets injected on the axis of an IDI diesel engine

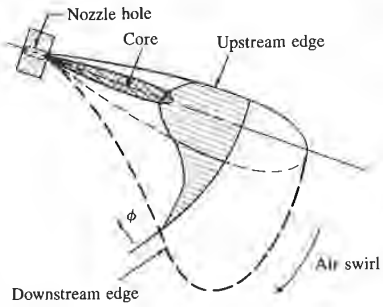

FIGURE 10-22
Schematic of fuel spray injected radially outward from the chamber axis into swirling air flow. Shape of equivalence ratio (ϕ) distribution within jet is indicated.

FIGURE 10-23
Schlieren photographs of vaporizing sprays injected into swirling air flow in transparent prechamber of special IDI diesel.[21] Left: high sensitivity, showing boundaries of the vapor regions of spray. Right: low sensitivity, showing liquid-containing core (dark) in relation to vapor regions (mottled).

prechamber with high clockwise swirl. The photograph on the left, with high sensitivity, shows the outer boundary of the fuel vapor region of the spray; the low-sensitivity photograph on the right locates the liquid phase regions of the spray.[21] The interaction between the swirl and both liquid and vapor spray regions is evident, as is the spray interaction with the chamber wall.

Other spray flow patterns are used. The spray may enter the swirling air flow tangentially as in the M.A.N. "M" system shown in Fig. 10-1*c*. The spray then interacts immediately with the combustion chamber walls.

To couple the spray-development process with the ignition phase of the combustion, it is important to know which regions of the spray contain the fuel injected at the beginning of the injection process. These regions of the sprays are likely to autoignite first. Each spray develops as follows. At the start of injection the liquid fuel enters the quiescent air charge, atomizes, moves outward from the nozzle, and slows down rapidly as air is entrained into the spray and accelerated. This start-up process forms a vortex or "puff" at the head of the spray. The injected fuel which follows encounters less resistance; thus drops from that fuel overtake the drops from first-injected fuel, forcing them outward toward the periphery of the spray. At the tip of the unsteady spray the drops meet the highest aerodynamic resistance and slow down, but the spray continues to penetrate the air charge because droplets retarded at the tip are continually replaced by new higher-momentum later-injected drops.[22] Accordingly, droplets in the periphery of the spray and behind the tip of the spray come from the earliest injected fuel.[23] As Figs. 10-20 and 10-23 indicate, these drops evaporate quickly.

10.5.3 Atomization

Under diesel engine injection conditions, the fuel jet usually forms a cone-shaped spray at the nozzle exit. This type of behavior is classified as the atomization breakup regime, and it produces droplets with sizes very much less than the nozzle exit diameter. This behavior is different from other modes of liquid jet

breakup. At low jet velocity, in the Rayleigh regime, breakup is due to the unstable growth of surface waves caused by surface tension and results in drops larger than the jet diameter. As jet velocity is increased, forces due to the relative motion of the jet and the surrounding air augment the surface tension force, and lead to drop sizes of the order of the jet diameter. This is called the first wind-induced breakup regime. A further increase in jet velocity results in breakup characterized by divergence of the jet spray after an intact or undisturbed length downstream of the nozzle. In this second wind-induced breakup regime, the unstable growth of short-wavelength waves induced by the relative motion between the liquid and surrounding air produces droplets whose average size is much less than the jet diameter. Further increases in jet velocity lead to breakup in the atomization regime, where the breakup of the outer surface of the jet occurs at, or before, the nozzle exit plane and results in droplets whose average diameter is much smaller than the nozzle diameter. Aerodynamic interactions at the liquid/gas interface appear to be one major component of the atomization mechanism in this regime.[22, 24]

A sequence of very short time exposure photographs of the emergence of a liquid jet from a nozzle of 0.34 mm diameter and $L_n/d_n = 4$ into high-pressure nitrogen at ambient temperature is shown in Fig. 10-24. The figure shows how the spray tip penetrates and the spray spreads during the early part of its travel.[25] Data such as these were used to examine the dependence of the spray development on gas and liquid density, liquid viscosity, and nozzle geometry.[24–26] The effects of the most significant variables, gas/liquid density ratio and nozzle geometry, on initial jet spreading angle are shown in Fig. 10-25. For a given geometry (cylindrical hole and length/diameter = 4), the initial jet spreading or spray angle increases with increasing gas/liquid density ratio as shown in Fig. 10-25*a*. Typical density ratios for diesel injection conditions are between 15×10^{-3} and 30×10^{-3}. Of several different nozzle geometry parameters examined, the length/diameter ratio proved to be the most significant (see Fig. 10-25*b*).

For jets in the atomization regime, the spray angle θ was found to follow the relationship

$$\tan \frac{\theta}{2} = \frac{1}{A} 4\pi \left(\frac{\rho_g}{\rho_l}\right)^{1/2} \frac{\sqrt{3}}{6} \tag{10.22}$$

where ρ_g and ρ_l are gas and liquid densities and A is a constant for a given nozzle geometry.† The data in Fig. 10-25*a* are fitted by $A = 4.9$. This behavior is in accord with the theory that aerodynamic interactions are largely responsible for jet breakup. Note that the data in Fig. 10-25*b* show a continuous trend as the jet breakup regime makes a transition from second wind-induced breakup (solid

† An empirical equation for A is $A = 3.0 + 0.28\ (L_n/d_n)$, where L_n/d_n is the length/diameter ratio of the nozzle.[25]

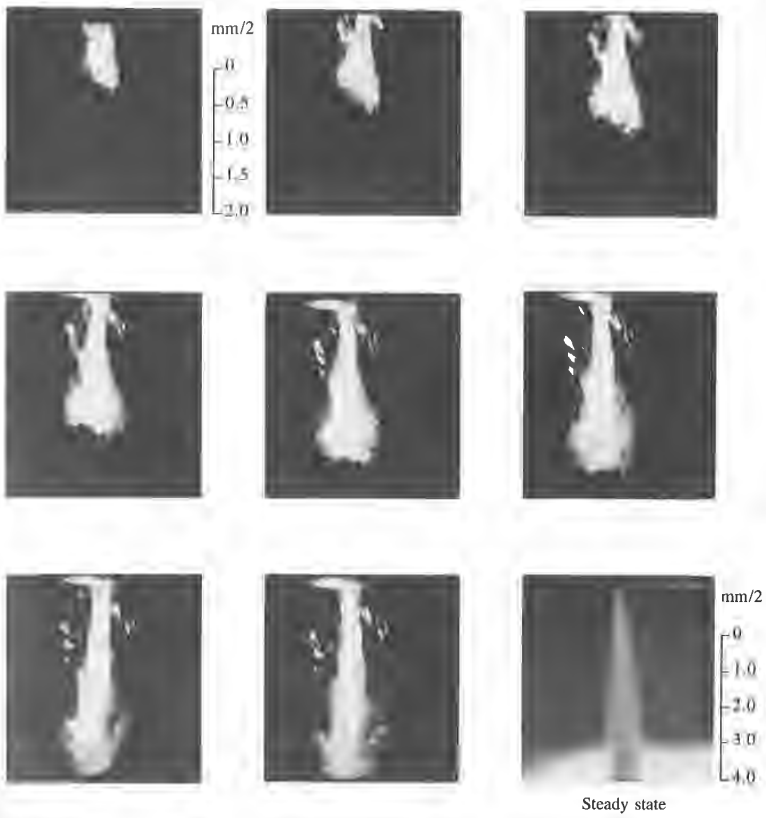

FIGURE 10-24
Photographs showing initial emergence and steady state (bottom right) of high-pressure liquid spray. Time between frames 2.1 μs. Liquid: water. Gas: nitrogen at 1380 kPa. Δp across nozzle 11 MPa. Nozzle diameter 0.34 mm.[25]

symbols) to atomization regime breakup (open symbols). The growth of aerodynamic surface waves is known to be responsible for jet breakup in the second wind-induced breakup regime. Such a mechanism can explain the observed data trends in the atomization regime, if an additional mechanism is invoked to explain nozzle geometry effects. One possible additional mechanism is liquid cavitation. A criterion for the onset of jet atomization at the nozzle exit plane was developed. For $(\rho_l/\rho_g)(\mathrm{Re}_l/\mathrm{We}_l)^2 > 1$ (which is true for distillate fuel injection applications) the design criterion is

$$\left(\frac{\rho_l}{\rho_g}\right)^{1/2} < k \tag{10.23}$$

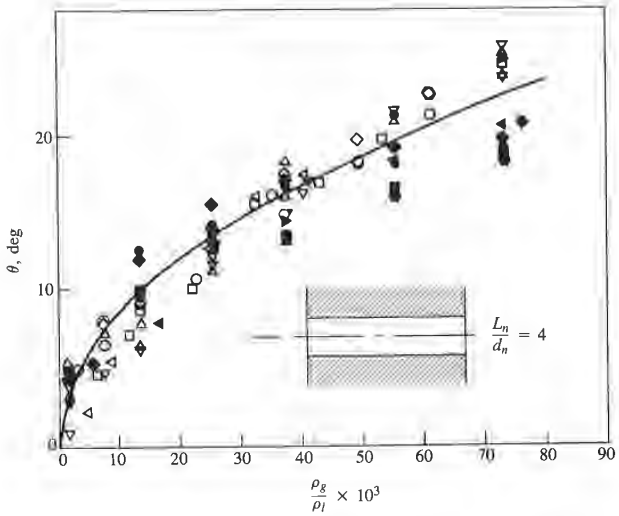

(*a*)

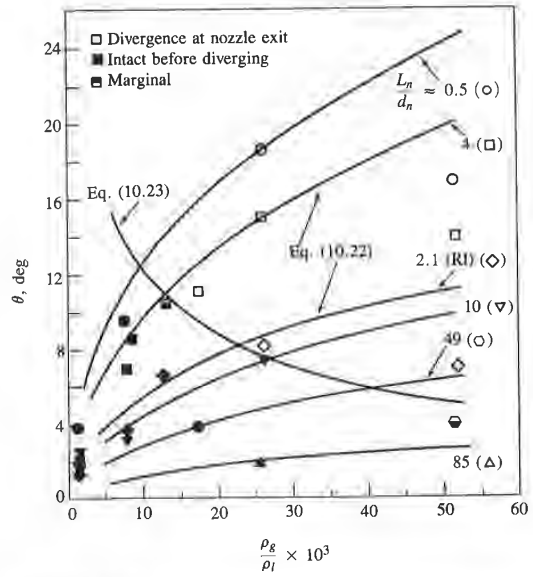

(*b*)

FIGURE 10-25
(*a*) Initial spray angle of atomizing jets versus density ratio (ρ_g/ρ_l = gas density/liquid density) for fixed nozzle geometry shown. Various fluids and gases at liquid pressures of 3.4–92 MPa. Nozzle diameters $d_n = 0.254$, 0.343, and 0.61 mm.[22] (*b*) Initial spray angle versus density ratio for a wide range of nozzle geometries. L_n/d_n = nozzle length/diameter ratio (RI = rounded inlet geometry). Solid symbols indicate jets which break up and diverge downstream of nozzle exit. Open symbols indicate jet breakup at nozzle exit.[25]

where k is an empirical constant depending on nozzle geometry in the range 6 to 12 ($k = 18.3/\sqrt{A}$).

Jet breakup trends can be summarized as follows. The initial jet divergence angles increase with increasing gas density. Divergence begins progressively closer to the nozzle as gas density increases until it reaches the nozzle exit. Jet divergence angles increase with decreasing fuel viscosity; divergence begins at the nozzle exit once the liquid viscosity is below a certain level. Nozzle design affects the onset of the jet atomization regime. Jet divergence angles decrease with increasing nozzle length. For the same length, rounded inlet nozzles produce less divergent jets than sharp-edged inlet nozzles. The initial jet divergence angle and intact spray length are quasi steady with respect to changes in operating conditions which occur on time scales longer than about 20 μs.[25] Note that while all these results were obtained under conditions where evaporation was not occurring, the initial spray-development processes are not significantly affected by evaporation (see Sec. 10.5.6).

10.5.4 Spray Penetration

The speed and extent to which the fuel spray penetrates across the combustion chamber has an important influence on air utilization and fuel-air mixing rates. In some engine designs, where the walls are hot and high air swirl is present, fuel impingement on the walls is desired. However, in multispray DI diesel combustion systems, overpenetration gives impingement of liquid fuel on cool surfaces which, especially with little or no air swirl, lowers mixing rates and increases emissions of unburned and partially burned species. Yet underpenetration results in poor air utilization since the air on the periphery of the chamber does not then contact the fuel. Thus, the penetration of liquid fuel sprays under conditions typical of those found in diesel engines has been extensively studied.

Many correlations based on experimental data and turbulent gas jet theory have been proposed for fuel spray penetration.[17] These predict the penetration S of the fuel spray tip across the combustion chamber for injection into quiescent air, as occurs in larger DI engines, as a function of time. An evaluation of these correlations[27] indicated that the formula developed by Dent,[28] based on a gas jet mixing model for the spray, best predicts the data:†

$$S = 3.07\left(\frac{\Delta p}{\rho_g}\right)^{1/4}(t d_n)^{1/2}\left(\frac{294}{T_g}\right)^{1/4} \tag{10.24}$$

where Δp is the pressure drop across the nozzle, t is time after the start of injection, and d_n is the nozzle diameter. All quantities are expressed in SI units: t in

† For nozzles where $2 \le L_n/d_n \le 4$, and for $t > 0.5$ ms. At exceptionally high chamber densities ($p > 100$ atm) Eq. (10.24) overpredicts penetration.

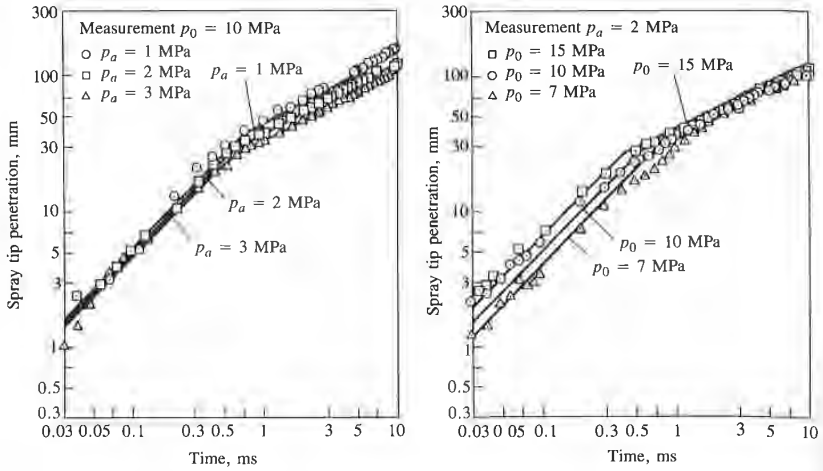

FIGURE 10-26
Spray tip penetration as function of time at various ambient pressures (p_a) and injection pressures (p_0). Fuel jets injected into quiescent air at room temperature.[29]

seconds, S and d_n in meters, Δp in pascals, ρ_g in kilograms per cubic meter, and T_g in kelvins.

More detailed studies have examined the spray tip location as a function of time, following start of a diesel injection process in high-pressure bombs. Data taken by Hiroyasu *et al.*,[29] shown in Fig. 10-26, illustrate the sensitivity of the spray tip position as a function of time to ambient gas state and injection pressure for fuel jets injected into quiescent air at room temperature. These data show that the initial spray tip penetration increases linearly with time t (i.e., the spray tip velocity is constant) and, following jet breakup, then increase as $\sqrt{t}$. Injection pressure has a more significant effect on the initial motion before breakup; ambient gas density has its major impact on the motion after breakup. Hiroyasu *et al.* correlated their data for spray tip penetration S(m) versus time as

$$\begin{aligned} t < t_{\text{break}}: \quad & S = 0.39\left(\frac{2\Delta p}{\rho_l}\right)^{1/2} t \\ t > t_{\text{break}}: \quad & S = 2.95\left(\frac{\Delta p}{\rho_g}\right)^{1/4} (d_n t)^{1/2} \end{aligned} \tag{10.25}$$

where

$$t_{\text{break}} = \frac{29 \rho_l d_n}{(\rho_g \Delta p)^{1/2}} \tag{10.26}$$

and Δp is the pressure drop across the nozzle (pascals), ρ_l and ρ_g are the liquid and gas densities, respectively (in kilograms per cubic meter), d_n is the nozzle

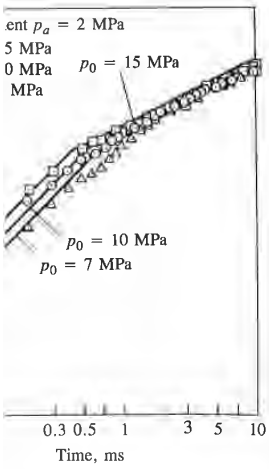

es (p_a) and injection pressures (p_0).

ıms per cubic meter, and T_g

ip location as a function of
ıigh-pressure bombs. Data
ıstrate the sensitivity of the
as state and injection pres-
ıperature. These data show
with time t (i.e., the spray
ɔn increase as $\sqrt{t}$. Injection
ıl motion before breakup;
on after breakup. Hiroyasu
n) versus time as

(10.25)

(10.26)

ls), ρ_l and ρ_g are the liquid
ɔic meter), d_n is the nozzle

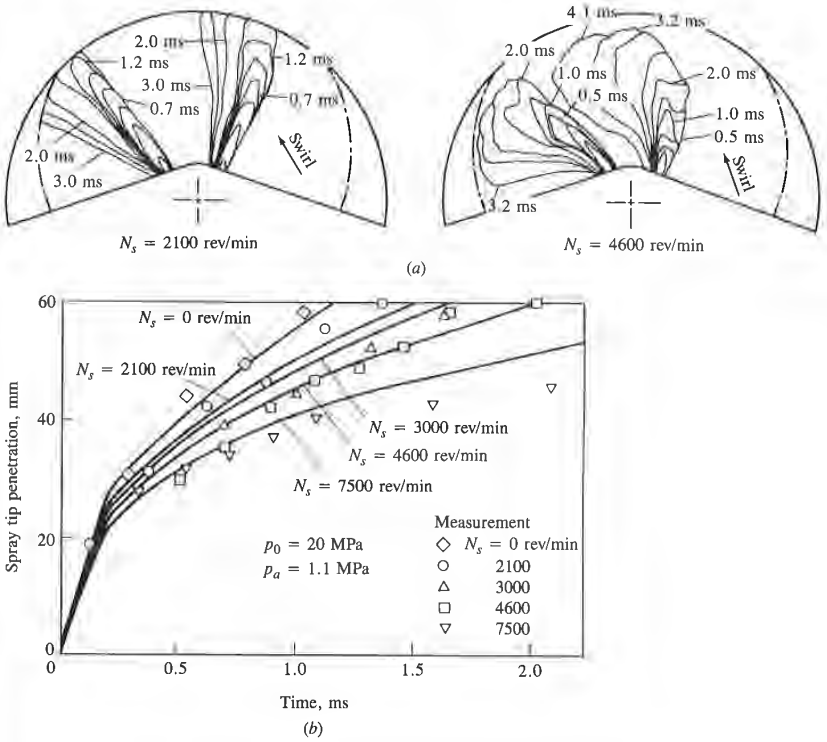

FIGURE 10-27
(*a*) Measured outer boundary of sprays injected into swirling air flow. (*b*) Spray tip penetration as a function of time for different swirl rates. Solid lines show Eq. (10.27).[29]

diameter (meters), and t is time (seconds). The results of Reitz and Bracco[25] indicate that the breakup or intact length depends on nozzle geometry details in addition to the diameter (see Fig. 10-25*b*). Note that under high injection pressures and nozzle geometries with short length/diameter ratios, the intact or breakup length becomes very short; breakup can occur at the nozzle exit plane.

The effect of combustion air swirl on spray penetration is shown in Fig. 10-27. Figure 10-27*a* shows how the spray shape and location changes as swirl is increased; Fig. 10-27*b* shows how spray tip penetration varies with time and swirl rate.[29] These authors related their data on spray tip penetration with swirl, S_s, through a correlation factor to the equivalent penetration, S, without swirl given by Eq. (10.25):

$$\frac{S_s}{S} = \left(1 + \frac{\pi R_s N S}{30 v_j}\right)^{-1} \tag{10.27}$$

where R_s is the swirl ratio which equals the swirl rate in revolutions per minute divided by the engine speed N (revolutions per minute), and v_j is the initial fuel jet velocity (meters per second). The curves in Fig. 10-27*b* correspond to Eq. (10.27). Swirl both reduces the penetration of the spray and spreads out the spray more rapidly.

10.5.5 Droplet Size Distribution

Previous sections in Sec. 10.5 have discussed the overall characteristics of the diesel engine fuel spray—its spreading rate and penetration into the combustion chamber. While the distribution of fuel via the spray trajectory throughout the combustion chamber is important, atomization of the liquid fuel into a large number of small drops is also necessary to create a large surface area across which liquid fuel can evaporate. Here we review how the drop size distribution in the fuel spray depends on injection parameters and the air and fuel properties. Since the measurement of droplet characteristics in an operating diesel engine is extremely difficult, most results have come from studies of fuel injection into constant-volume chambers filled with high-pressure quiescent air at room temperature.

During the injection period, the injection conditions such as injection pressure, nozzle orifice area, and injection rate may vary. Consequently, the droplet size distribution at a given location in the spray may also change with time during the injection period. In addition, since the details of the atomization process are different in the spray core and at the spray edge, and the trajectories of individual drops depend on their size, initial velocity, and location within the spray, the drop size distribution will vary with position within the spray.[29] None of these variations has yet been adequately quantified.

The aerodynamic theory of jet breakup in the atomization regime summarized in Sec. 10.5.3 (which is based on work by G. I. Taylor) leads to the prediction that the initial average drop diameter D_d is proportional to the length of the most unstable surface waves:[22]

$$\bar{D}_d = C \frac{2\pi\sigma}{\rho_g v_r^2} \lambda^* \tag{10.28}$$

where σ is the liquid-fuel surface tension, ρ_g is the gas density, v_r is the relative velocity between the liquid and gas (taken as the mean injection velocity v_j), C is a constant of order unity, and λ^* is the dimensionless wavelength of the fastest growing wave. λ^* is a function of the dimensionless number $(\rho_l/\rho_g)(\mathrm{Re}_j/\mathrm{We}_j)^2$, where the jet Reynolds and Weber numbers are given by $\mathrm{Re}_j = \rho_l v_j d_n/\mu_l$ and $\mathrm{We}_j = \rho_l v_j^2 d_n/\sigma$ and d_n is the nozzle orifice diameter. λ^* goes to 3/2 as this number increases above unity. Near the edge of the spray close to the nozzle, this equation predicts observed drop size trends with respect to injection velocity, fuel properties, nozzle L/d, and nozzle diameter, though measured mean drop sizes are larger by factors of 2 to 3.[30] However, within the dense early region of the spray, secondary atomization phenomena—coalescence and breakup—occur

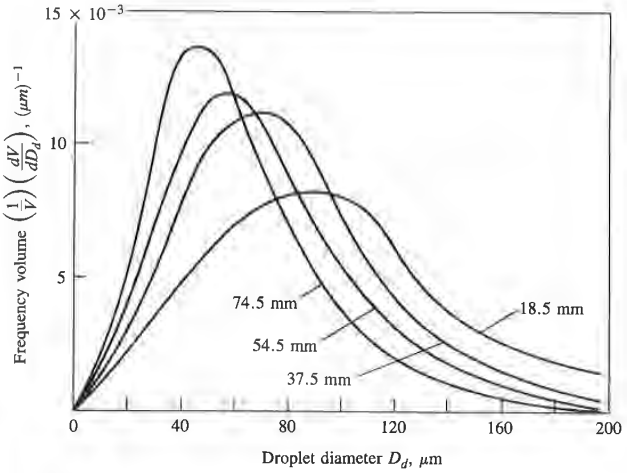

FIGURE 10-28
Droplet size distribution in diesel fuel spray injected through throttling pintle nozzle into quiescent room-temperature air at 11 atm. Nozzle opening pressure 9.9 MPa. Pump speed 500 rev/min. Droplets are sampled well downstream of injector at given radial distances from spray axis.[32]

which will change the droplet size distribution and mean diameter. The downstream drop size in the solid-cone sprays used in diesel-injection systems is markedly influenced by both drop coalescence and breakup. Eventually a balance is reached as coalescence decreases (due to the expansion of the spray) and breakup ceases (due to the reduced relative velocity between the drops and the entrained gas).[31]

Measurements of droplet size distributions within a simulated diesel spray indicate how size varies with location. Figure 10-28 shows the variation in drop size distribution with radial distance from the spray axis, at a fixed axial location. The drop sizes were measured with a liquid immersion technique where a sample of drops is collected in a small cell filled with an immiscible liquid. Size distributions can be expressed in terms of:

1. The incremental number of drops Δn within the size range $D_d - \Delta D_d/2 < D_d < D_d + \Delta D_d/2$
2. The incremental volume ΔV of drops in this size range
3. The cumulative number of drops n less than a given size D_d
4. The cumulative volume V of drops less than a given size D_d

Since the drops are spherical:

$$\frac{dn}{dD_d} = \frac{6}{\pi D_d^3}\frac{dV}{dD_d} \tag{10.29}$$

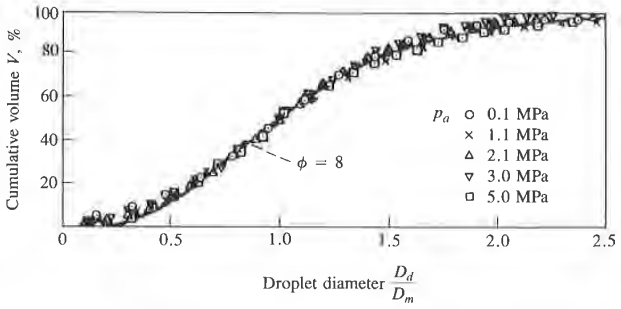

FIGURE 10-29
Normalized drop-size cumulative frequency distribution in spray injected into ambient-temperature air for air pressures from 0.1 to 5 MPa. Throttling pintle nozzle with nozzle opening pressure of 9.9 MPa. Median drop diameter $D_m = 1.224D_{SM}$.[32]

The distributions shown in the figure are frequency distributions of drop volume.[32] The peak in the distribution shifts to larger drop diameters as the radial position decreases: on average, the drops are smaller at the periphery of the spray.

To characterize the spray, expressions for drop size distribution and mean diameter are desirable. An appropriate and commonly used mean diameter is the *Sauter mean diameter:*

$$D_{SM} = \left(\int D_d^3 \, dn\right) \Big/ \left(\int D_d^2 \, dn\right) \tag{10.30}$$

where dn is the number of drops with diameter D_d in the range $D_d - dD_d/2 < D_d < D_d + dD_d/2$. The integration is usually carried out by summing over an appropriate number of drop size groups. The Sauter mean diameter is the diameter of the droplet that has the same surface/volume ratio as that of the total spray.

Various expressions for the distribution of drop sizes in liquid sprays have been proposed. One proposed by Hiroyasu and Kadota[32] based on the chi-square statistical distribution fits the available experimental data. Figure 10-29 shows how the chi-square distribution with a degree of freedom equal to 8 fits well to experimental measurements of the type shown in Fig. 10-28. Here D_m is the median drop diameter which for this chi-square curve is $1.224D_{SM}$. The nondimensional expression for drop size distribution in sprays injected through hole nozzles, pintle nozzles, and throttling pintle nozzles given by the chi-square distribution is

$$\frac{dV}{V} = 13.5\left(\frac{D_d}{D_{SM}}\right)^3 \exp\left[-3\left(\frac{D_d}{D_{SM}}\right)\right] d\left(\frac{D_d}{D_{SM}}\right) \tag{10.31}$$

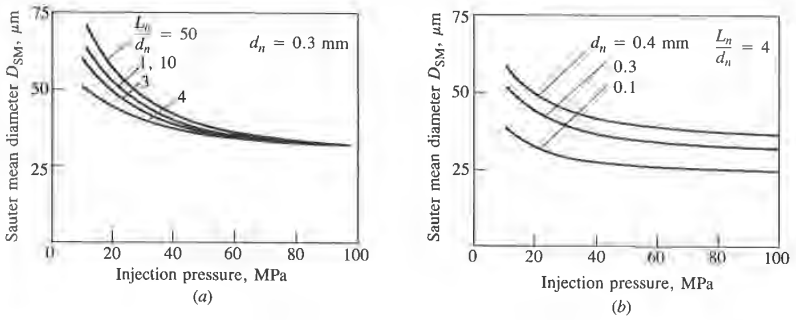

FIGURE 10-30
Effect of fuel-injection pressure and nozzle geometry and size on Sauter mean drop diameter. (*a*) Effect of nozzle length/diameter ratio L_n/d_n and injection pressure. (*b*) Effect of nozzle diameter d_n and injection pressure.[18]

An empirical expression for the Sauter mean diameter D_{SM} (in micrometers) for typical diesel fuel properties given by Hiroyasu and Kadota[32] is

$$D_{SM} = A(\Delta p)^{-0.135}\rho_a^{0.121}V_f^{0.131} \tag{10.32}$$

where Δp is the mean pressure drop across the nozzle in megapascals, ρ_a is the air density in kilograms per cubic meter, and V_f is the amount of fuel delivered per cycle per cylinder in cubic millimeters per stroke. A is a constant which equals 25.1 for pintle nozzles, 23.9 for hole nozzles, and 22.4 for throttling pintle nozzles. Other expressions for predicting D_{SM} can be found in Ref. 17.

The effects of injection pressure, nozzle geometry and size, air conditions, and fuel properties on Sauter mean diameter in sprays obtained with diesel fuel-injection nozzles have been extensively studied. Various immersion, photographic, and optical techniques for making such measurements have been used.[17] Some of the major effects are illustrated in Figs. 10-30 and 10-31 which show

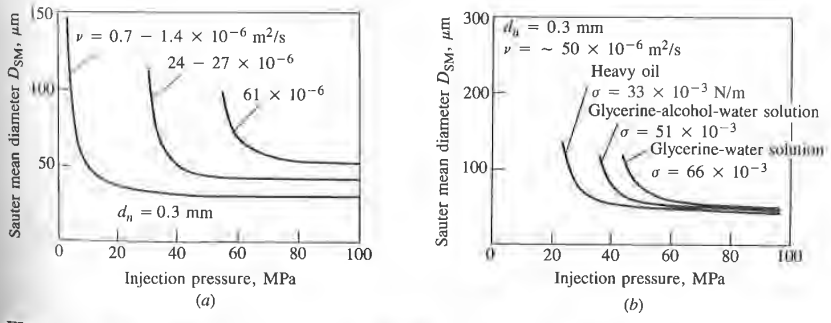

FIGURE 10-31
Effect of (*a*) liquid viscosity ν and (*b*) liquid surface tension σ on Sauter mean drop diameter as a function of injection pressure. Air conditions: 3 MPa and ambient temperature.[17]

average Sauter mean diameters determined optically from studies of steady diesel fuel sprays in a pressurized vessel. Figure 10-30 shows that nozzle size affects the mean drop size in the expected direction. Nozzle length/diameter ratio is also shown to be important: an $L_n/d_n = 4$ gives the minimum mean drop size at low and intermediate injection pressures. This L_n/d_n also corresponds to the minimum value of spray breakup length and to the maximum spray cone angle. Fuel viscosity and surface tension also affect mean drop size as shown in Fig. 10-31, with the effects being most significant at lower injection pressures.

10.5.6 Spray Evaporation

The injected liquid fuel, atomized into small drops near the nozzle exit to form a spray, must evaporate before it can mix with air and burn. Figure 10-20 showed the basic structure of an evaporating diesel spray under conditions typical of a large direct-injection engine. Back illumination showed that a core exists along the axis of the spray where the liquid fuel ligaments or drops are sufficiently dense to attenuate the light beam. Once the start-up phase of the injection process is over, the length of this core remains essentially constant until injection ends. This core is surrounded by a much larger vapor-containing spray region which continues to penetrate deeper into the combustion chamber: the core extends only partway to the spray tip. Additional insight into the physical structure of evaporating sprays can be obtained from the schlieren photographs taken just after the end of injection in a prechamber engine with air swirl, shown in Fig. 10-32. The lowest magnification picture (A) shows the overall structure of the spray. The only liquid-containing region evident is that part of the core nearest the nozzle which shows black on the left of the photograph. The spreading vapor region of the spray, carried around the chamber by the swirling air flow, appears mottled due to local turbulent vapor concentration and temperature fluctuations. The dark region within the spray vapor region is due to soot formed where the fuel vapor concentration is sufficiently high. It is probable that, after the breakup length, the dense black liquid core of the spray is composed of individual droplets but the concentration is so high along the optical path that the light beam is fully extinguished. However, the last part of the core close to the nozzle tip (B) disperses sufficiently for individual features to be resolved. The small black dots are liquid fuel drops in the size range 20 to 100 μm. Fuel drop vapor trails can be observed in the highest magnification photo (C) corresponding to various stages of evaporation. These range from drops showing little surrounding vapor to vapor trails with little liquid remaining at the head. The vapor trails show random orientations relative to the spray axis, presumably due to local air turbulence. The process of droplet evaporation under normal engine operating conditions appears to be rapid relative to the total combustion period.[21]

Let us examine the drop evaporation process in more detail. Consider a liquid drop at close to ambient temperature injected into air at typical end-of-compression engine conditions. Three phenomena will determine the history of the drop under these conditions:

om studies of steady diesel
that nozzle size affects the
gth/diameter ratio is also
um mean drop size at low
rresponds to the minimum
pray cone angle. Fuel vis-
shown in Fig. 10-31, with
sures.

r the nozzle exit to form a
burn. Figure 10-20 showed
ler conditions typical of a
d that a core exists along
s or drops are sufficiently
up phase of the injection
ılly constant until injection
or-containing spray region
ustion chamber: the core
ght into the physical struc-
chlieren photographs taken
vith air swirl, shown in Fig.
ne overall structure of the
at part of the core nearest
graph. The spreading vapor
e swirling air flow, appears
d temperature fluctuations.
to soot formed where the
able that, after the breakup
posed of individual droplets
that the light beam is fully
e to the nozzle tip (B) dis-
d. The small black dots are
el drop vapor trails can be
sponding to various stages
ttle surrounding vapor to
ıd. The vapor trails show
ably due to local air turbu-
nal engine operating condi-
on period.[21]
in more detail. Consider a
into air at typical end-of-
ill determine the history of

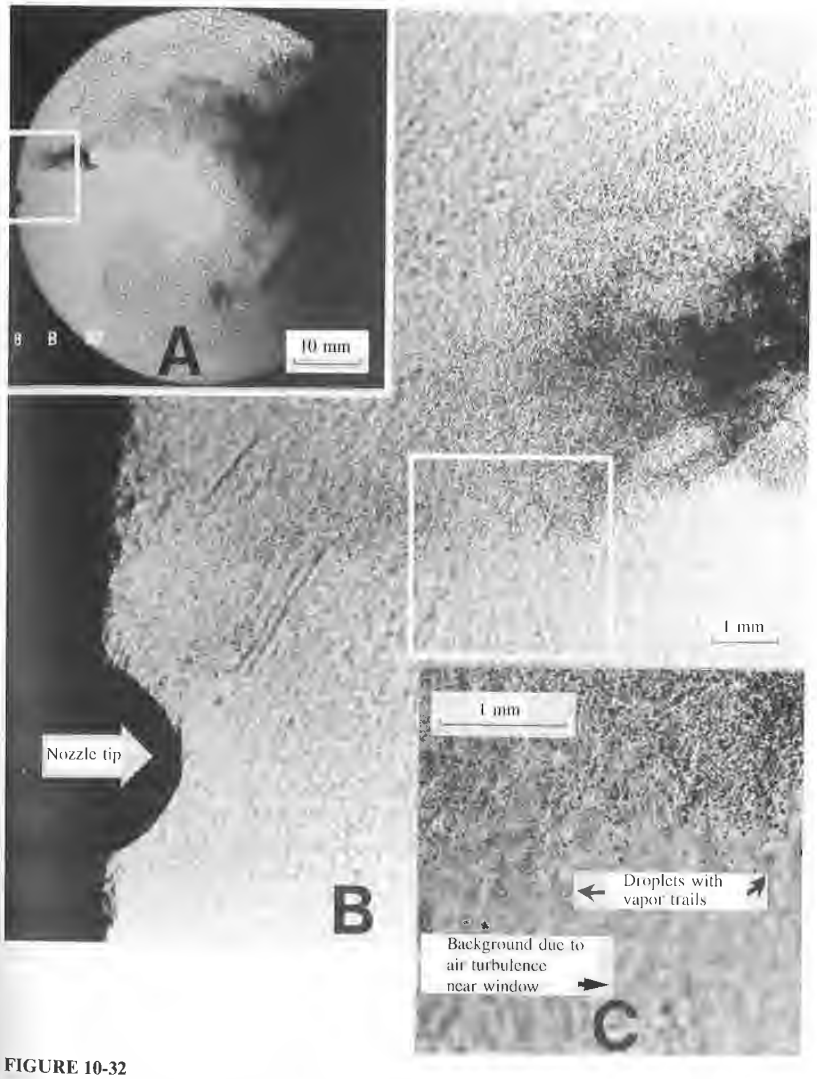

FIGURE 10-32
Shadowgraph photographs at three magnifications taken just after the end of injection of diesel-fuel spray into swirling air flow in prechamber of special diesel engine. Nozzle hole diameter = 0.25 mm.[21]

1. Deceleration of the drop due to aerodynamic drag
2. Heat transfer to the drop from the air
3. Mass transfer of vaporized fuel away from the drop

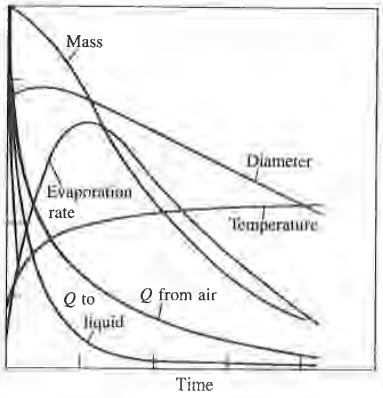

FIGURE 10-33
Schematic of variation of mass, diameter, temperature, evaporation rate, heat-transfer rate from air, and heat-transfer rate to liquid drop core as function of time during evaporation process of individual drop in diesel environment at the time of injection.

As the droplet temperature increases due to heat transfer, the fuel vapor pressure increases and the evaporation rate increases. As the mass transfer rate of vapor away from the drop increases, so the fraction of the heat transferred to the drop surface which is available to increase further the drop temperature decreases. As the drop velocity decreases, the convective heat-transfer coefficient between the air and the drop decreases. The combination of these factors gives the behavior shown in Fig. 10-33 where drop mass, temperature, velocity, vaporization rate, and heat-transfer rate from the air are shown schematically as a function of time following injection.[33] Analysis of individual fuel drops 25 μm in diameter, injected into air at typical diesel conditions, indicates that evaporation times are usually less than 1 ms.[34]

Such an analysis is relevant to drops that are widely separated (e.g., at the edge of the spray). In the spray core, where drop number densities are high, the evaporation process has a significant effect on the temperature and fuel-vapor concentration in the air within the spray. As fuel vaporizes, the local air temperature will decrease and the local fuel vapor pressure will increase. Eventually thermodynamic equilibrium would pertain: this is usually called adiabatic saturation.[33] Calculated thermodynamic equilibrium temperatures for diesel spray conditions are plotted in Fig. 10-34 as a function of the fuel/air mass ratio for *n*-dodecane and *n*-heptane. The initial liquid fuel temperature was 300 K. The ratio of fuel vapor to air mass at these equilibrium conditions is also shown. To the left of the peaks in the m_{fv}/m_a curves, only fuel vapor is present. To the right of these peaks, liquid fuel is also present because the vapor phase is saturated.[35] Liquid fuel vaporization causes substantial reductions in gas temperature. While this equilibrium situation may not be reached within the spray, these results are useful for understanding the temperature distribution within an evaporating spray.

To quantify accurately the fuel vaporization rate within a diesel fuel spray requires the solution of the coupled conservation equations for the liquid drop-

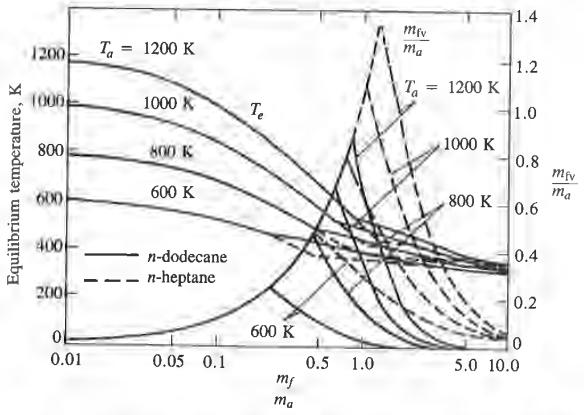

FIGURE 10-34
Adiabatic-saturation conditions for equilibrium mixtures formed by injecting *n*-dodecane and *n*-heptane, initially liquid at 300 K, into air at initial temperature T_a between 600 and 1200 K and initial density 6.5 kg/m^3. Equilibrium mixture temperature (T_e) and ratio of fuel vapor mass (m_{fv}) to air mass (m_a) shown as function of ratio of total fuel mass m_f to m_a. Fuel vapor only present to left of peaks in m_{fv}/m_a curves; liquid fuel also present to right of peaks.[35]

lets and the air within the combustion chamber. Various phenomenological models and computational fluid dynamic models have been developed for this purpose (see Secs. 14.4.3 and 14.5.5). In the most sophisticated of these, the spray is assumed to be composed of discrete computational particles each of which represents a group of droplets of similar size, temperature, etc. The distribution functions in droplet size, velocity, temperature, etc., produced by the fuel injector are statistically sampled and the resulting discrete particles are followed along lagrangian trajectories as they interact and exchange mass, momentum, and energy with the surrounding gas. Drops interact directly with each other via collisions and indirectly via evaporation by modifying the ambient vapor concentration and gas temperature. Studies with such models indicate that, under normal diesel engine conditions, 70 to 95 percent of the injected fuel is in the vapor phase at the start of combustion. Evaporation is more than 90 percent complete after 1 ms. However, only 10 to 35 percent of the vaporized fuel has mixed to within flammability limits in a typical medium-speed DI diesel engine. Thus combustion is largely mixing-limited, rather than evaporation-limited.[36] Of course, under cold-starting conditions, evaporation becomes a major constraint.

10.6 IGNITION DELAY

10.6.1 Definition and Discussion

The ignition delay in a diesel engine was defined as the time (or crank angle) interval between the start of injection and the start of combustion. The start of

injection is usually taken as the time when the injector needle lifts off its seat (determined by a needle-lift indicator). The start of combustion is more difficult to determine precisely. It is best identified from the change in slope of the heat-release rate, determined from cylinder pressure data using the techniques described in Sec. 10.4, which occurs at ignition. Depending on the character of the combustion process, the pressure data alone may indicate when pressure change due to combustion first occurs; in DI engines under normal conditions ignition is well defined, but in IDI engines the ignition point is harder to identify. Flame luminosity detectors are also used to determine the first appearance of the flame. Experience has shown that under normal conditions, the point of appearance of the flame is later than the point of pressure rise and results in greater uncertainty or error in determining the ignition point.

Both physical and chemical processes must take place before a significant fraction of the chemical energy of the injected liquid fuel is released. The physical processes are: the atomization of the liquid fuel jet; the vaporization of the fuel droplets; the mixing of fuel vapor with air. The chemical processes are the precombustion reactions of the fuel, air, residual gas mixture which lead to autoignition. These processes are affected by engine design and operating variables, and fuel characteristics, as follows.

Good atomization requires high fuel-injection pressure, small injector hole diameter, optimum fuel viscosity, and high cylinder air pressure at the time of injection (see Sec. 10.5.3). The rate of vaporization of the fuel droplets depends on the size of the droplets, their distribution, and their velocity, the pressure and temperature inside the chamber, and the volatility of the fuel. The rate of fuel-air mixing is controlled largely by injector and combustion chamber design. Some combustion chamber and piston head shapes are designed to amplify swirl and create turbulence in the air charge during compression. Some engine designs use a prechamber or swirl chamber to create the vigorous air motion necessary for rapid fuel-air mixing (see Sec. 10.2). Also, injector design features such as the number and spatial arrangement of the injector holes determine the fuel spray pattern. The details of each nozzle hole affect the spray cone angle. The penetration of the spray depends on the size of the fuel droplets, the injection pressure, the air density, and the air-flow characteristics. The arrangement of the sprays, the spray cone angle, the extent of spray penetration, and the air flow all affect the rate of air entrainment into the spray. These physical aspects of fuel-injection and fuel-spray behavior are reviewed in Sec. 10.5.

The chemical component of the ignition delay is controlled by the precombustion reactions of the fuel. A fundamental discussion of autoignition or spontaneous hydrocarbon oxidation in premixed fuel-air mixtures is given in Sec. 9.6.2. Since the diesel engine combustion process is heterogeneous, its spontaneous ignition process is even more complex. Though ignition occurs in vapor phase regions, oxidation reactions can proceed in the liquid phase as well between the fuel molecules and the oxygen dissolved in the fuel droplets. Also, cracking of large hydrocarbon molecules to smaller molecules is occurring. These chemical processes depend on the composition of the fuel and the cylinder charge tem-

perature and pressure, as well as the physical processes described above which govern the distribution of fuel throughout the air charge.

Since the ignition characteristics of the fuel affect the ignition delay, this property of a fuel is very important in determining diesel engine operating characteristics such as fuel conversion efficiency, smoothness of operation, misfire, smoke emissions, noise, and ease of starting. The ignition quality of a fuel is defined by its cetane number. Cetane number is determined by comparing the ignition delay of the fuel with that of primary reference fuel mixtures in a standardized engine test (see below). For low cetane fuels with too long an ignition delay, most of the fuel is injected before ignition occurs, which results in very rapid burning rates once combustion starts with high rates of pressure rise and high peak pressures. Under extreme conditions, when autoignition of most of the injected fuel occurs, this produces an audible knocking sound, often referred to as "diesel knock." For fuels with very low cetane numbers, with an exceptionally long delay, ignition may occur sufficiently late in the expansion process for the burning process to be quenched, resulting in incomplete combustion, reduced power output, and poor fuel conversion efficiency. For higher cetane number fuels, with shorter ignition delays, ignition occurs before most of the fuel is injected. The rates of heat release and pressure rise are then controlled primarily by the rate of injection and fuel-air mixing, and smoother engine operation results.

10.6.2 Fuel Ignition Quality

The ignition quality of a diesel fuel is defined by its *cetane number*. The method used to determine the ignition quality in terms of cetane number is analogous to that used for determining the antiknock quality of gasoline in terms of octane number. The cetane number scale is defined by blends of two pure hydrocarbon reference fuels. Cetane (*n*-hexadecane, $C_{16}H_{34}$), a hydrocarbon with high ignition quality, represents the top of the scale with a cetane number of 100. An isocetane, heptamethylnonane (HMN), which has a very low ignition quality, represents the bottom of the scale with a cetane number of 15.† Thus, cetane number (CN) is given by

$$\text{CN} = \text{percent } n\text{-cetane} + 0.15 \times \text{percent HMN} \tag{10.33}$$

The engine used in cetane number determination is a standardized single-cylinder, variable compression ratio engine with special loading and accessory equipment and instrumentation. The engine, the operating conditions, and the test procedure are specified by ASTM Method D613.[37] The operating requirements include: engine speed—900 rev/min; coolant temperature—100°C; intake air temperature—65.6°C (150°F); injection timing—13° BTC; injection

† In the original procedure α-methylnaphthalene ($C_{11}H_{10}$) with a cetane number of zero represented the bottom of the scale. Heptamethylnonane, a more stable compound, has replaced it.

pressure—10.3 MPa (1500 lb/in^2). With the engine operating under these conditions, on the fuel whose cetane number is to be determined, the compression ratio is varied until combustion starts at TC: i.e., an ignition delay period of 13° (2.4 ms at 900 rev/min) is produced. The above procedure is then repeated using reference fuel blends. Each time a reference fuel is tried, the compression ratio is adjusted to give the same 13° ignition delay. When the compression ratio required by the actual fuel is bracketed by the values required by two reference blends differing by less than five cetane numbers, the cetane number of the fuel is determined by interpolation between the compression ratios required by the two reference blends.

Because of the expense of the cetane number test, many correlations which predict ignition quality based on the physical properties of diesel fuels have been developed.[38, 39] A calculated *cetane index* (CCI) is often used to estimate ignition quality of diesel fuels (ASTM D976[40]). It is based on API gravity and the mid-boiling point (temperature 50 percent evaporated). It is applicable to straight-run fuels, catalytically cracked stocks, and blends of the two. Its use is suitable for most diesel fuels and gives numbers that correspond quite closely to cetane number. A *diesel index* is also used. It is based on the fact that ignition quality is linked to hydrocarbon composition: *n*-paraffins have high ignition quality, and aromatic and napthenic compounds have low ignition quality. The aniline point (ASTM D611[41]—the lowest temperature at which equal volumes of the fuel and aniline become just miscible) is used, together with the API gravity, to give the diesel index:

$$\text{Diesel index} = \text{aniline point (°F)} \times \frac{\text{API gravity}\dagger}{100} \tag{10.34}$$

The diesel index depends on the fact that aromatic hydrocarbons mix completely with aniline at comparatively low temperatures, whereas paraffins require considerably higher temperatures before they are completely miscible. Similarly, a high API gravity denotes low specific gravity and high paraffinicity, and, again, good ignition quality. The diesel index usually gives values slightly above the cetane number. It provides a reasonable indication of ignition quality in many (but not all) cases.

10.6.3 Autoignition Fundamentals

Basic studies in constant-volume bombs, in steady-flow reactors, and in rapid-compression machines have been used to study the autoignition characteristics of fuel-air mixtures under controlled conditions. In some of these studies the fuel and air were premixed; in some, fuel injection was used. Studies with fuel injec-

† API gravity is based on specific gravity and is calculated from: API gravity, deg = (141.5/specific gravity at 60°F) − 131.5.

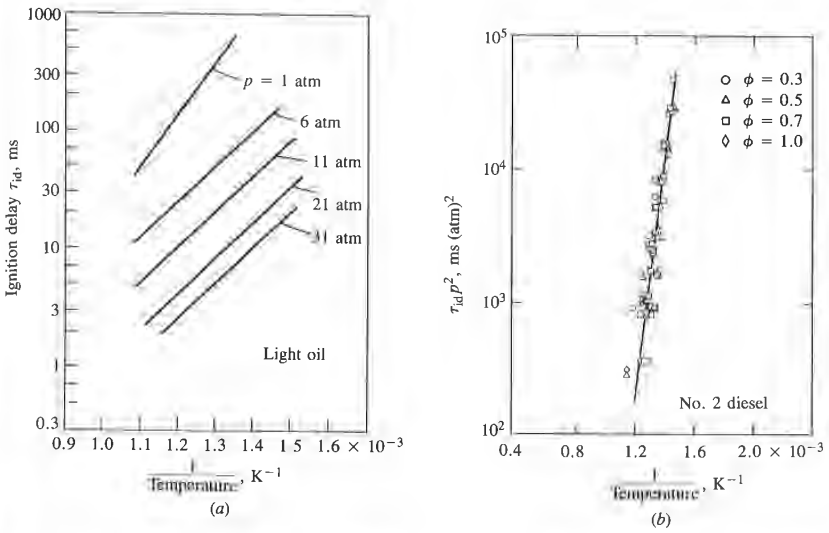

FIGURE 10-35
(*a*) Ignition delay as function of reciprocal air temperature for light oil spray injected into constant-volume combustion bomb. Injection pressure 9.8 MPa (100 atm). Air pressures indicated.[42] (*b*) Ignition delay × (pressure)^2 measured in steady-flow reactor for No. 2 diesel fuel as function of reciprocal temperature. Fuel/air equivalence ratio ϕ varied from 0.3 to 1.0.[43]

tion into constant-temperature and pressure environments have shown that the temperature and pressure of the air are the most important variables for a given fuel composition. Ignition delay data from these experiments have usually been correlated by equations of the form:

$$\tau_{id} = Ap^{-n} \exp\left(\frac{E_A}{\tilde{R}T}\right) \tag{10.35}$$

where τ_{id} is the ignition delay (the time between the start of injection and the start of detectable heat release), E_A is an apparent activation energy for the fuel autoignition process, $\tilde{R}$ is the universal gas constant, and A and n are constants dependent on the fuel (and, to some extent, the injection and air-flow characteristics).

Figure 10-35*a* shows ignition delay data obtained by injecting liquid fuel sprays into a high-pressure heated constant-volume bomb.[42] Figure 10-35*b* shows ignition delay data from a steady-flow high-pressure reactor where vaporized fuel was mixed rapidly with the heated air stream.[43] The match between the form of Eq. (10.35) and the data is clear. Figure 10-35*b* also shows an equivalence ratio dependence of the ignition delay. Representative values for A, n, and E_A for Eq. (10.35), taken from these and other studies, are given in Table 10.3. Ignition delay times calculated with these formulas for various diesel engines are given in

TABLE 10.3
Constants for Arrhenius equation for ignition delay:[44]
$$\tau_{id}(\text{ms}) = Ap^{-n} \exp\,[E_A/(\tilde{R}T)]$$

	Conditions				Parameters		
Investigator	Apparatus	Fuel	p, atm	T, K	n	A	$E_A/\tilde{R}$, K
Spadaccini and TeVelde[43] No. 1	Steady flow	No. 2 diesel	10–30	650–900	2	2.43×10^{-9}	20,926
Spadaccini and TeVelde[43] No. 2	Steady flow	No. 2 diesel	10–30	650–900	1	4.00×10^{-10}	20,080
Stringer *et al.*[45]	Steady flow	Diesel 45–50 cetane number	30–60	770–980	0.757	0.0405	5,473
Wolfer[46]	Constant-volume bomb	Fuel with cetane number >50	8–48	590–782	1.19	0.44	4,650
Hiroyasu *et al.*[29]	Constant-volume bomb	Kerosene	1–30	673–973	1.23	0.0276	7,280

Table 10.4. Air pressures and temperatures at TC piston position were estimated from measured cylinder pressure data. Measured ignition delay times in these types of engines are: 0.6 to 3 ms for low-compression-ratio DI diesel engines over a wide range of operating conditions; 0.4 to 1 ms for high-compression-ratio and turbocharged DI diesel engines; 0.6 to 1.5 ms for IDI diesel engines.[44]

The variation in the calculated delay times can be attributed to several factors:

1. In some cases the correlations are being extrapolated outside their original range of operating conditions.
2. The methods used to detect the start of combustion, and hence the duration of the delay, are not identical.
3. The experimental apparatus and the method of fuel-air mixture preparation are different.

The third factor is probably the most significant. As has been explained, the phenomenon of autoignition of a fuel spray consists of sequences of physical and chemical processes of substantial complexity. The relative importance of each process depends on the ambient conditions, on fuel properties, and on how the fuel-air mixture is prepared. For example, fuel evaporation times are significant in cold engines, but not under fully warmed-up conditions. Thus, an equation of the simple form of Eq. (10.35) can only fit the data over a limited range of conditions. The correlations of Spadaccini and TeVelde[43] have much higher activation energies. Normally, lower values of $E_A/\tilde{R}$ imply that physical processes such as vaporization and mixing are important and relevant to chemical processes. Thus, fuel preparation, mixture inhomogeneity, heat loss, and nonuniform flow patterns

TABLE 10.4
Calculated ignition delay times[44]

Engine	Conditions			τ_{id}, ms				
				Spadaccini and TeVelde[43]				
	Speed, rev/min	p, atm	T, K	No. 1	No. 2	Stringer *et al.*[45]	Wolfer[46]	Hiroyasu *et al.*[29]
IDI Diesel								
1. Low swirl	600	45.6	690	17.3	38.2	6.26	3.94	9.60
	1200	49.3	747	1.47	3.83	3.22	2.15	3.90
	1800	52.5	758	0.86	2.44	2.76	1.82	3.13
2. High swirl	600	45.2	674	36.3	76.9	7.60	4.68	12.5
	1200	48.4	721	4.18	10.3	4.25	2.75	5.67
	1800	51.8	744	1.47	4.07	3.19	2.08	3.82
DI Diesel								
1. Low compression ratio		42.8	781	0.57	1.37	2.60	1.92	2.39
2. High compression ratio	1500	58.8	975	0.0015	0.0060	0.508	0.407	0.322

affect the ignition delay. While the work of Spadaccini and TeVelde probably describes the chemical ignition delay more accurately, since great care was taken to obtain a uniform mixture and flow, the experiments in constant-volume bombs with diesel-type fuel injectors are more relevant to the diesel engine compression-ignition combustion process because they include the appropriate physical and chemical processes. The available engine ignition delay data suggest that for delays less than about 1 ms, the rate of decrease in delay with increasing temperature becomes much less than that indicated by the data in Fig. 10-35. This is due to the increasing relative importance of physical processes relative to chemical processes during the delay period. Thus relations of the form of Eq. (10.35) should be used with caution.

In general, τ_{id} is a function of mixture temperature, pressure, equivalence ratio, and fuel properties (though no accepted form for the variation with equivalence ratio is yet established). In the above referenced studies, the fuel was injected into a uniform air environment where the pressure and temperature only changed due to the cooling effect of the fuel-vaporization and fuel-heating processes. In an engine, pressure and temperature change during the delay period due to the compression resulting from piston motion. To account for the effect of changing conditions on the delay the following empirical integral relation is usually used:

$$\int_{t_{si}}^{t_{si}+\tau_{id}} \left(\frac{1}{\tau}\right) dt = 1 \tag{10.36}$$

where t_{si} is the time of start of injection, τ_{id} is the ignition delay period, and τ is the ignition delay at the conditions pertaining at time t. Whether the variation in conditions is significant depends on the amount of injection advance before TC that is used and the length of the delay.

10.6.4 Physical Factors Affecting Delay

The physical factors that affect the development of the fuel spray and the air charge state (its pressure, temperature, and velocity) will influence the ignition delay. These quantities depend on the design of the fuel-injection system and combustion chamber, and the engine operating conditions. The injection system variables affecting the fuel-spray development are injection timing, quantity, velocity, rate, drop size, and spray form or type. The relevant charge conditions depend on the combustion system employed, the details of the combustion chamber design, inlet air pressure and temperature, compression ratio, injection timing, the residual gas conditions, coolant and oil temperature, and engine speed. Data on these interactions are available for different types of diesel engines. The trends observed with the different diesel combustion systems are generally similar, though some of the details are different. In this section the ignition delay trends during normal (fully warmed-up) engine operation are considered. The dependence of the ignition delay on engine design and operating variables during engine starting and warm-up is also very important, and may be different from fully warmed-up behavior due to lower air temperature and pressure.

INJECTION TIMING. At normal engine conditions (low to medium speed, fully warmed engine) the minimum delay occurs with the start of injection at about 10 to 15° BTC.[47] The increase in the delay with earlier or later injection timing occurs because the air temperature and pressure change significantly close to TC. If injection starts earlier, the initial air temperature and pressure are lower so the delay will increase. If injection starts later (closer to TC) the temperature and pressure are initially slightly higher but then decrease as the delay proceeds. The most favorable conditions for ignition lie in between.

INJECTION QUANTITY OR LOAD. Figure 10-36 shows the effect of increasing injection quantity or engine load on ignition delay. The delay decreases approximately linearly with increasing load for this DI engine. As load is increased, the residual gas temperature and the wall temperature increase. This results in higher charge temperature (and also, to a lesser extent, charge pressure) at injection, thus shortening the ignition delay. When adjustment is made for this increasing temperature, it is found that increasing the quantity of fuel injected has no significant effect on the delay period under normal operating conditions. Under engine starting conditions, however, the delay increases due to the larger drop in mixture temperature associated with evaporating and heating the increased amount of fuel.[47] This latter result should be expected since it is the first part of the injected fuel which ignites first; subsequent injected fuel (above the minimum required to maintain the fuel-air mixture within the flammability limits during the delay) does not influence the delay.

DROP SIZE, INJECTION VELOCITY, AND RATE. These quantities are determined by injection pressure, injector nozzle hole size, nozzle type, and geometry.

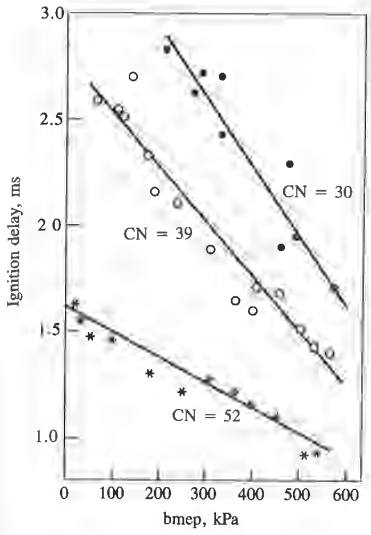

FIGURE 10-36
Ignition delays measured in a small four-stroke cycle DI diesel engine with $r_c = 16.5$ as a function of load at 1980 rev/min. Fuel cetane numbers 30, 39, and 52.[48]

Experiments by Lyn and Valdmanis[47] have shown that none of these factors has a significant effect on the delay. At normal operating conditions, increasing injection pressure produces only modest decreases in the delay. Doubling the nozzle hole diameter at constant injection pressure to increase the fuel flow rate (by a factor of about 4) and increase the drop size (by about 30 percent) had no significant effect on the delay. Studies of different nozzle hole geometries showed that the length/diameter ratio of the nozzle was not significant; nor did changes in nozzle type (multihole, pintle, pintaux) cause any substantial variation in delay at normal engine conditions.

INTAKE AIR TEMPERATURE AND PRESSURE. Figure 10-35 showed values of ignition delay for diesel fuels plotted against the reciprocal of charge temperature for several charge pressures at the time of injection. The intake air temperature and pressure will affect the delay via their effect on charge conditions during the delay period. Figure 10-37 shows the effects of inlet air pressure and temperature as a function of engine load. The fundamental ignition data available show a strong dependence of ignition delay on charge temperatures below about 1000 K at the time of injection. Above about 1000 K, the data suggest that the charge temperature is no longer so significant. Through this temperature range there is an effect of pressure at the time of injection on delay: the higher the pressure the shorter the delay, with the effect decreasing as charge temperatures increase and delay decreases. Since air temperature and pressure during the delay period are such important variables, other engine variables that affect the relation between the inlet air state and the charge state at the time of injection will influence the delay. Thus, an increase in the compression ratio will decrease the ignition delay,

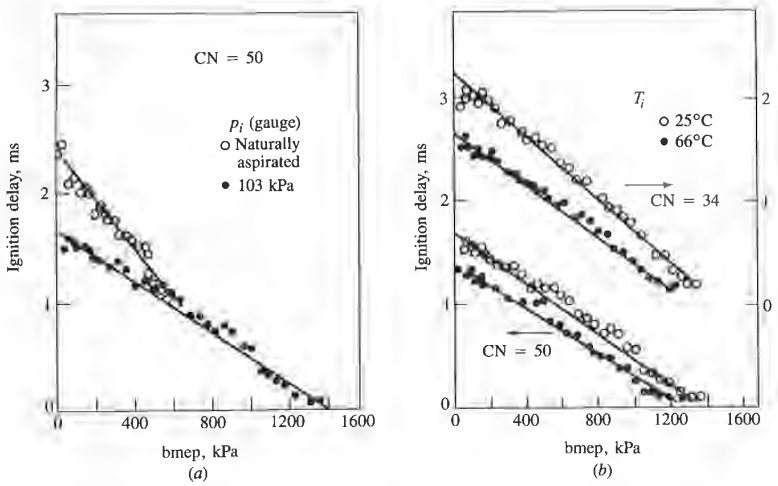

FIGURE 10-37
Effect of inlet air pressure and temperature on ignition delay over load range of small DI diesel at 1980 rev/min. (*a*) Engine naturally aspirated and with 1 atm boost; inlet air temperature $T_i = 25°C$; 50 cetane number fuel. (*b*) Engine naturally aspirated; $T_i = 25$ and 66°C; 34 and 50 cetane number fuel.[48]

and injection timing will affect the delay (as was discussed earlier), largely due to the changes in charge temperature and pressure at the time of injection.

ENGINE SPEED. Increases in engine speed at constant load result in a slight decrease in ignition delay when measured in milliseconds; in terms of crank angle degrees, the delay increases almost linearly.[48] A change in engine speed changes the temperature/time and pressure/time relationships. Also, as speed increases, injection pressure increases. The peak compression temperature increases with increasing speed due to smaller heat loss during the compression stroke.[47]

COMBUSTION CHAMBER WALL EFFECTS. The impingement of the spray on the combustion chamber wall obviously affects the fuel evaporation and mixing processes. Impingement of the fuel jet on the wall occurs, to some extent, in almost all of the smaller, higher speed engines. With the "M" system, this impingement is desired to obtain a smooth pressure rise. The ignition delay with the "M" system is longer than in conventional DI engine designs.[47] Engine and combustion bomb experiments have been carried out to examine the effect of wall impingement on the ignition delay. Figure 10-38 shows the effect of jet wall impingement on ignition delay measured in a constant-volume combustion bomb, for a range of air pressures and temperatures, and wall temperatures.[20] The wall was perpendicular to the spray and was placed 100 mm from the nozzle tip. The data shows that the presence of the wall reduces the delay at the lower

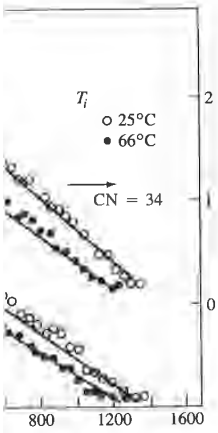

load range of small DI diesel at
; inlet air temperature $T_i = 25°C$;
66°C; 34 and 50 cetane number

ssed earlier), largely due to
time of injection.

ant load result in a slight
ıds; in terms of crank angle
ge in engine speed changes
;. Also, as speed increases,
temperature increases with
mpression stroke.[47]

pingement of the spray on
ıel evaporation and mixing
occurs, to some extent, in
'ith the "M" system, this
ise. The ignition delay with
ıgine designs.[47] Engine and
ıt to examine the effect of
shows the effect of jet wall
nstant-volume combustion
s, and wall temperatures.[29]
:ed 100 mm from the nozzle
luces the delay at the lower

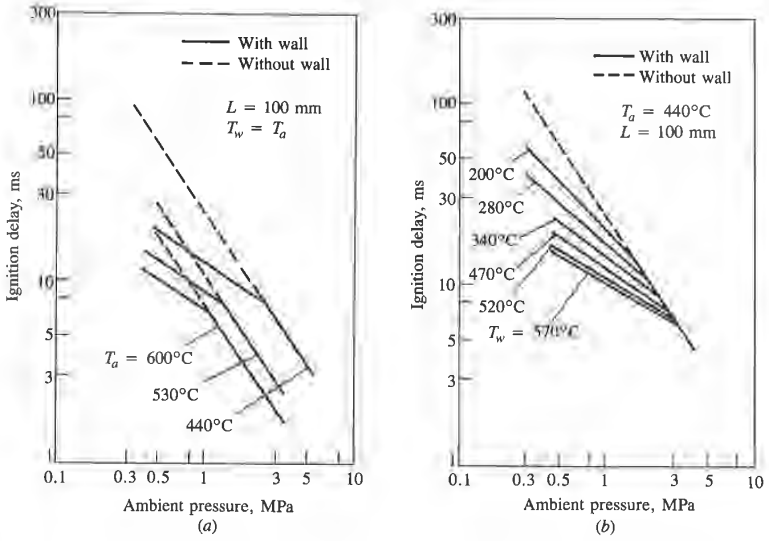

FIGURE 10-38
Effect of spray impingement on wall 100 mm from nozzle on ignition delay from combustion bomb studies. (*a*) Effect of air temperature as a function of air pressure; $T_w = T_{air}$. (*b*) Effect of wall temperature at 440°C air temperature.[29]

pressures and temperatures studied, but has no significant effect at the high pressures and temperatures more typical of normal diesel operation. Engine experiments where the delay was measured while the jet impingement process was varied showed analogous trends. The jet impingement angle (the angle between the fuel jet axis and the wall) was varied from almost zero (jet and wall close to parallel) to perpendicular. The delay showed a tendency to become longer as the impingement angle decreased. The most important result is not so much the modest change in delay but the difference in the initial rate of burning that results from the differences in fuel evaporation and fuel-air mixing rates.

SWIRL RATE. Changes in swirl rate change the fuel evaporation and fuel-air mixing processes. They also affect wall heat transfer during compression and, hence, the charge temperature at injection. Only limited engine studies of the effect of swirl rate variations on ignition delay have been made. At normal operating engine speeds, the effect of swirl rate changes on the delay are small. Under engine starting conditions (low engine speeds and compression temperatures) the effect is much more important,[47] due presumably to the higher rates of evaporation and mixing obtained with swirl.

OXYGEN CONCENTRATION. The oxygen concentration in the charge into which the fuel is injected would be expected to influence the delay. The oxygen concentration is changed, for example, when exhaust gas is recycled to the intake

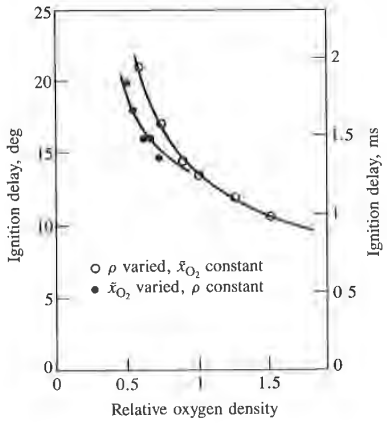

FIGURE 10-39
Effect of oxygen density in gas on ignition delay in single-cylinder DI engine of 1.3-dm^3 displacement with $r_c = 15$ at 1800 rev/min. Oxygen density changed by recycling exhaust gas at constant inlet density and by varying inlet pressure from 0.5 to 3 atm with air.[49]

for the control of oxides of nitrogen emissions (see Chap. 11). Results of a study carried out in a single-cylinder DI engine operated at a constant air/fuel ratio (30 : 1), manifold temperature, injection timing, and speed (1800 rev/min), where the oxygen concentration was varied by recirculating known amounts of cooled exhaust, are shown in Fig. 10-39.[49] Oxygen density is normalized by the naturally aspirated no-recirculation test value. As oxygen concentration is decreased, ignition delay increases.

10.6.5 Effect of Fuel Properties

Since both physical and chemical processes take place during the ignition delay, the effects of changes in the physical and chemical properties of fuels on the delay period have been studied. The chemical characteristics of the fuel are much the more important. The ignition quality of the fuel, defined by its cetane number, will obviously affect the delay. The dependence of cetane number on fuel molecular structure is as follows. Straight-chain paraffinic compounds (normal alkanes) have the highest ignition quality, which improves as the chain length increases. Aromatic compounds have poor ignition quality as do the alcohols (hence, the difficulties associated with using methanol and ethanol, possible alternative fuels, in compression-ignition engines). Figure 10-40 illustrates these effects. A base fuel was blended with pure paraffinic (normal, iso-, and cycloalkanes), aromatic, and olefinic hydrocarbons of various carbon numbers, by up to 20 percent by volume. The base fuel, a blend of 25 percent *n*-hexadecane and 75 percent isooctane, had a cetane number of 38.3. The figure shows that the resulting ignition delays correlate well as a function of cetane number at constant compression ratio and engine operating conditions. Addition of normal alkanes (excluding *n*-pentane and lower carbon number alkanes) improve the ignition quality. As the chain length of the added paraffin gets longer (higher carbon number) the cetane number improve-

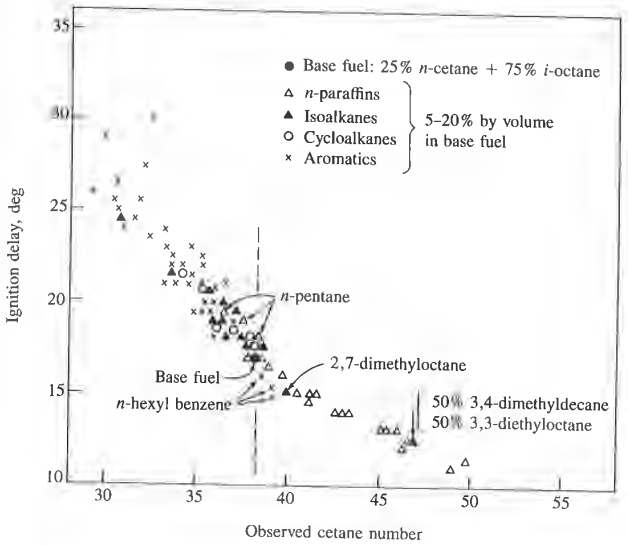

FIGURE 10-40
Effect of type of hydrocarbon structure on ignition quality of fuels in DI diesel combustion process at constant compression ratio and engine operating conditions.[50]

ment increases. Isoalkanes, depending on the degree of branching, degrade ignition quality (unless the branching is concentrated at one end of the molecule, when these types of isoalkanes improve ignition quality). Cycloalkanes and aromatics generally reduce the cetane number, unless they have a long *n*-alkane chain attached to the ring. The cetane number of a fuel (a measure of its ability to autoignite) generally varies inversely with its octane number (a measure of its ability to resist autoignition; see Fig. 9-69 for the effect of hydrocarbon structure on knock). The cetane number of commercial diesel fuel is normally in the range 40 to 55.

Engine ignition delay data with diesel fuels of different cetane number, at various constant loads and speeds, shown in Fig. 10-41, demonstrate similar trends. Within the normal diesel fuel cetane number range of 40 to 55, an approximately linear variation is evident. However, decreasing fuel cetane number below about 38 may result in a more rapid increase in ignition delay.

Cetane number is controlled by the source of crude oil, by the refining process, and by additives or ignition accelerators. Just as it is possible to reduce the tendency to knock or autoignite in spark-ignition engine fuels by adding antiknock agents, so there are additives that improve the ignition quality of compression-ignition engine fuels. Generally, substances that increase the tendency to knock enhance ignition, and vice versa. Ignition-accelerating additives include organic peroxides, nitrates, nitrites, and various sulfur compounds. The most important of these commercially are the alkyl nitrates (isopropyl nitrate,

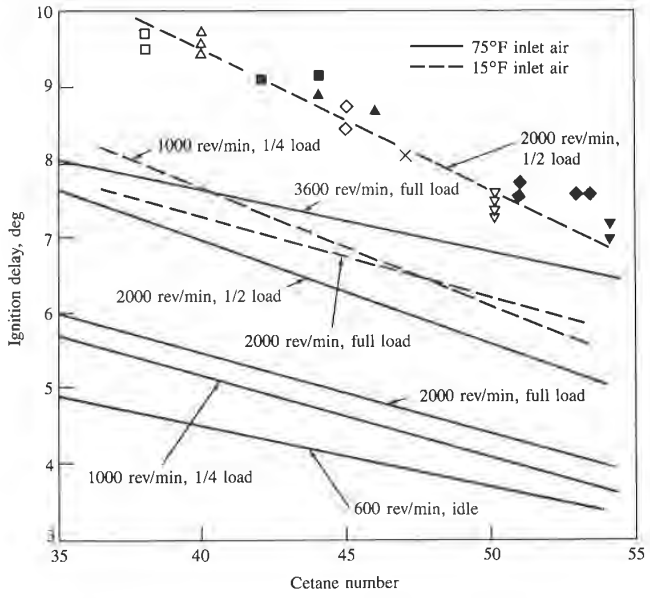

FIGURE 10-41
Effect of fuel cetane number on ignition delay over the load and speed range of 6.2-dm^3 eight-cylinder IDI swirl-chamber diesel engine. Top curve indicates typical fit between data and least-squares straight line over this cetane number range.[51]

primary amyl nitrates, primary hexyl nitrates, octyl nitrate).[52] Typically, about 0.5 percent of these additives by volume in a distillate fuel gives about a 10 cetane number increase in a fuel's ignition quality, though their effectiveness may depend on the composition of the base fuel. The incremental effect of increasing amounts of ignition-accelerating additives on cetane number decreases.[48] Usually, the ignition delay obtained with cetane improved blends are found to be equivalent to those obtained with natural diesel fuels of the same cetane number. Two potential practical uses for ignition accelerators are in upgrading the ignition characteristics of poorer quality diesel fuel and (in much larger amounts) making possible the use of alcohols in compression-ignition engines.

The physical characteristics of diesel fuel do not significantly affect the ignition delay in fully or partially warmed-up engines. Tests with fuels of different front-end volatility (over the cetane number range 38 to 53), and with substantially different front-end ignition quality for the same average cetane number, showed no discernible differences. Fuel viscosity variations over a factor of 2.5 were also tested and showed no significant effect.[48] Thus, in a warmed-up engine, variations in fuel atomization, spray penetration, and vaporization rate over reasonable ranges do not appear to influence the duration of the delay period significantly (see also Sec. 10.5.6 on fuel vaporization).

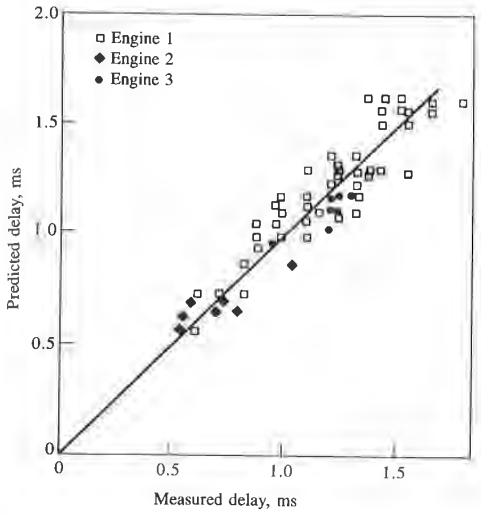

FIGURE 10-42
Comparison of engine ignition delays predicted with Eq. (10.37) with corresponding measured values.[54]

10.6.6 Correlations for Ignition Delay in Engines

Many correlations have been proposed for predicting ignition delay as a function of engine and air charge variables. These usually have the form of Eq. (10.35) and have been based on data from more fundamental experiments in combustion bombs and flow reactors. An important factor in assessing the appropriateness of any correlation is how it is to be used to predict the magnitude of the delay. If an equation for predicting the complete delay process (including all the physical and chemical processes from injection to combustion) is required, then the data show that such a simple form for the equation is unlikely to be adequate for the full range of engine conditions (see Table 10.4). However, if a model for the autoignition process of a premixed fuel-air mixture during the delay period is required, for use in conjunction with models for the physical processes of fuel evaporation and fuel-air mixing, then correlations such as those listed in Table 10.3 may be sufficiently accurate.

An empirical formula, developed by Hardenberg and Hase[53] for predicting the duration of the ignition delay period in DI engines, has been shown to give good agreement with experimental data over a wide range of engine conditions (see Fig. 10-42).[54] This formula gives the ignition delay (in crank angle degrees) in terms of charge temperature T (kelvins) and pressure p (bars) during the delay (taken as TC conditions) as

$$\tau_{id}(\text{CA}) = (0.36 + 0.22\bar{S}_p) \exp\left[E_A\left(\frac{1}{\bar{R}T} - \frac{1}{17{,}190}\right)\left(\frac{21.2}{p - 12.4}\right)^{0.63}\right] \quad (10.37)$$

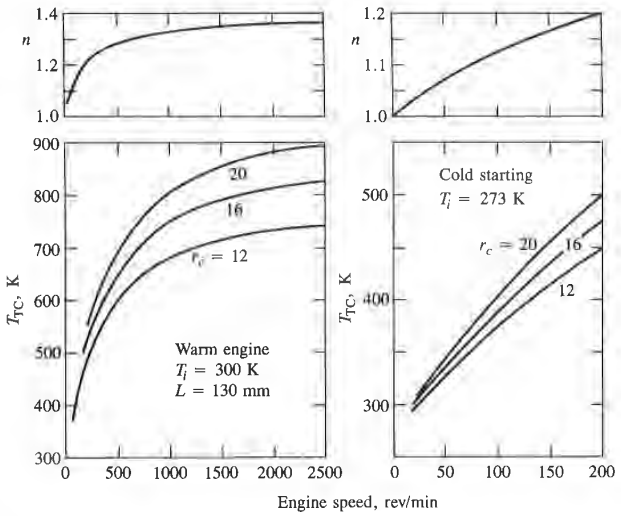

FIGURE 10-43
Exponent n for polytropic model of compression process in Eq. (10.39) and corresponding end-of-compression air temperature at TC. Warm and cold DI diesel engine with 130 mm stroke.[53]

where $\bar{S}_p$ is the mean piston speed (meters per second) and $\tilde{R}$ is the universal gas constant (8.3143 J/mol · K). E_A (joules per mole) is the apparent activation energy, and is given by

$$E_A = \frac{618{,}840}{\text{CN} + 25} \tag{10.38}$$

where CN is the fuel cetane number. The apparent activation energy decreases with increasing fuel cetane number. The delay in milliseconds is given by

$$\tau_{\text{id}}(\text{ms}) = \frac{\tau_{\text{id}}(\text{CA})}{0.006N}$$

where N, engine speed, is in revolutions per minute. Values for T and p can be estimated using a polytropic model for the compression process:

$$T_{\text{TC}} = T_i r_c^{n-1} \qquad p_{\text{TC}} = p_i r_c^n \tag{10.39a,b}$$

where n is the polytropic exponent (see Sec. 9.2.2), r_c is the compression ratio, and the subscript i denotes intake manifold conditions. Values of the polytropic exponent are given in Fig. 10-43 for a direct-injection diesel under warm and cold engine operating conditions.[49,53]

10.7 MIXING-CONTROLLED COMBUSTION

10.7.1 Background

Earlier sections of this chapter have developed our current understanding of the individual processes which together make up the total injection-mixing-burning sequence—atomization, vaporization, fuel spray development, air entrainment, ignition, and combustion. While the phenomenological model developed by Lyn[6] provides satisfactory logical links between these processes, quantitative links are still lacking. Especially difficult to quantify are the relations between fuel spray behavior, flame structure, and fuel burning rate—the area of focus of this section. The color photographs of the compression-ignition combustion process in different types of diesel engines in Figs. 10-4 and 10-5 (see color plate between 498 and 499) show how the flame immediately following ignition spreads rapidly and envelops the spray. Depending on the spray configuration, the visible flame may then fill almost the entire combustion chamber. The flame and spray geometries are closely related. Mixing processes are also critical during the ignition delay period: while the duration of the delay period is not influenced in a major way by the rates of spray processes which together control "mixing," the amount of fuel mixed with air to within combustible limits during the delay (which affects the rate of pressure rise once ignition has occurred) obviously is directly related to mixing rates. Thus substantial observational evidence supports the mixing-controlled character of diesel engine combustion.

However, while it is well accepted that diesel combustion is normally controlled by the fuel-air mixing rate, fundamentally based quantitatively accurate models for this coupled mixing and combustion process are not yet available. The difficulties are twofold. First, the spray geometry in real diesel combustion systems is extremely complex. Second, the phenomena which must be described (and especially the unsteady turbulent diffusion diesel engine flame) are inadequately understood. Current capabilities for modeling these phenomena are reviewed in Chap. 14. Thermodynamic-based models of the diesel combustion process with atomization, vaporization, and spray development described by empirical or turbulent-jet-based submodels have been developed and used to predict burning rates. These are described in Secs. 14.4.3 and 14.4.4, and show reasonable but not precise agreement with data. Fluid-mechanic-based models of air flow, fuel spray behavior, and combustion are under active development (see Sec. 14.5). While realistic air-flow predictions are now feasible, predictions of spray behavior are less well developed and combustion-rate predictions are still exploratory.

In the following sections, the evidence linking spray characteristics to flame structure and burning rates is summarized.

10.7.2 Spray and Flame Structure

The structure of each fuel spray is that of a narrow liquid-containing core (densely filled with drops of order 20 μm in diameter) surrounded by a much

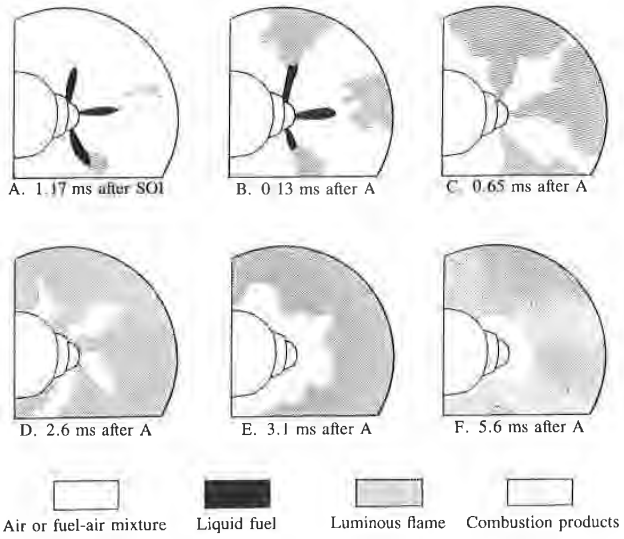

FIGURE 10-44
Tracings of outer boundary of liquid fuel spray and flame from high-speed movies of diesel combustion taken in a rapid-compression machine, looking down on piston through transparent head. First occurrence of luminous flame at A, 1.17 ms after start of injection. End of injection at D.[57]

larger gaseous-jet region containing fuel vapor (see Fig. 10-20). The fuel concentration in the core is extremely high: local fuel/air equivalence ratios near the nozzle of order 10 have been measured during the injection period. Fuel concentrations within the spray decrease with increasing radial and axial position at any given time, and with time at a fixed location once injection has ended.[55] The fuel distribution within the spray is controlled largely by turbulent-jet mixing processes. Fuel vapor concentration contours determined from interferometric studies of unsteady vaporizing diesel-like sprays, presented by Lakshminarayan and Dent,[56] confirm this gaseous turbulent-jet-like structure of the spray, with its central liquid-containing core which evaporates relatively quickly once fuel injection ends.

The location of the autoignition sites and subsequent spreading of the enflamed region in relation to the fuel distribution in the spray provides further evidence of the mixing-controlled character of combustion. Figure 10-44 shows how this process occurs under conditions typical of direct-injection quiescent-chamber diesel engines. It shows tracings of the liquid fuel spray and flame boundaries taken from high-speed movies of the injection and combustion processes with central injection of five fuel jets into a disc-shaped chamber in a rapid-compression machine.[57] These and other similar studies show that autoignition first occurs toward the edge of the spray, between the spray tip (which may by then have interacted with the combustion chamber walls, and which contains

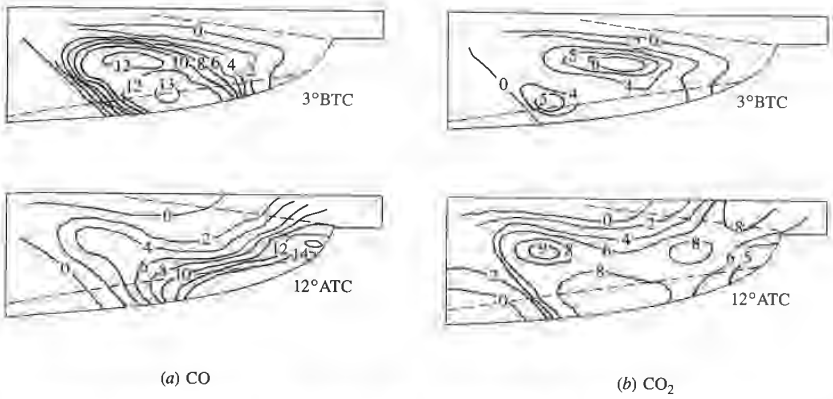

(*a*) CO (*b*) CO_2

FIGURE 10-45
Contours of constant CO and CO_2 concentration in a plane along the spray axis calculated from gas composition data obtained with a rapid-acting sampling valve in a large 30.5-cm-bore DI quiescent-chamber diesel engine with $r_c = 12.85$ operated at 500 rev/min. Injection starts 17° BTC, ignition occurs 8° BTC, injection ends 5° ATC.[60]

later-injected fuel as explained in Sec. 10.5.2) and the injector nozzle. Experiments where air/fuel ratio contours for a gaseous fuel jet injected into a swirling air flow in a rig simulated the fuel-air mixing process in open-chamber diesels,[58] under conditions chosen to match a set of diesel combustion rapid-compression-machine experiments where the autoignition sites and subsequent flame development were recorded on movies,[59] showed that autoignition occurred in a concentration band between the equivalence ratios of 1 and 1.5. Subsequent flame development, along mixture contours close to stoichiometric, occurs rapidly, as indicated in Fig. 10-44. Initially, this is thought to be due to spontaneous ignition of regions close to the first ignition site due to the temperature rise associated with the strong pressure wave which emanates from each ignition site due to local rapid chemical energy release. Also, spontaneous ignition at additional sites on the same spray, well separated from the original ignition location, can occur. Turbulent mixing provides another flame-spreading mechanism. From this point flame development is rapid, and the gas expansion which occurs on burning deforms the original spray form. These processes take place in each fuel spray in a closely comparable though not necessarily identical manner. Combustion movies such as those in Figs. 10-4 and 10-44 show that flame rapidly envelops each spray once spontaneous ignition occurs.

Gas-sampling data indicate that the burned gases within the flame-enveloped spray are only partially reacted and may be fuel-rich. Figure 10-45 shows CO and CO_2 concentration contours determined from rapid-acting sample valve measurements from the combustion chamber of a large quiescent-chamber two-stroke cycle diesel engine.[60] The contour maps shown correspond to the centerline of one of the five injected fuel sprays. Injection commenced at

17° BTC and ended about 5° ATC; ignition occurred at 8° BTC. The contours at 3° BTC show high CO concentrations in the burned gases which now occupy most of the spray region, indicating locally very fuel-rich conditions. Later, at 12° ATC, fuel injection has ceased, this rich core has moved outward to the piston-bowl wall, and combustion within the expanded spray region is much more complete. This oxidation of CO, as air is entrained into the spray region, mixes, and burns, releases substantial additional chemical energy.

The role of air swirl in promoting much more rapid fuel-air mixing in medium-size and smaller diesel engines is evident from similar gas-sampling studies in engines with these different combustion systems. The variation of gas species and unburned hydrocarbon concentrations within critical regions of the combustion chamber have been mapped out by a number of investigators.[61–63] These data show that during the early stages of injection and combustion, the boundaries of the individual sprays can be identified as they are convected around the combustion chamber bowl by the swirl. The fuel distribution within the combustion chamber is highly nonuniform. However, within each spray, sufficient air has mixed into the spray to bring the peak fuel/air equivalence ratios within the spray, in the outer regions of the chamber, to close to stoichiometric values.[63] This substantially different character of the spray with swirl is clear from the data in Fig. 10-46. Figure 10-46*a* shows equivalence ratio values determined from gas sampling, versus crank angle, from several studies with different designs of combustion chamber. While the local values obviously depend on the relation of the sample valve location to spray position at any given crank angle, the much lower values of equivalence ratio with swirl relative to quiescent chambers, during injection and the early stages of combustion, clearly indicate that swirl enhances mixing rates substantially. As combustion ends, these data indicate relatively uniform fuel distribution within the combustion chamber, at least on a gross geometric scale. However, early in the combustion process the high CO levels, found in all these combustion systems as shown in Fig. 10-46*b*, indicate that the burned gases are only partially reacted. With quiescent chambers this is largely due to lack of oxygen. With swirl, however, substantial oxygen is present. Whether the high CO with swirl is due to kinetic limitations or to smaller-scale mixture nonhomogeneities is unclear.

10.7.3 Fuel-Air Mixing and Burning Rates

The model of diesel combustion obtained from heat-release analyses of cylinder pressure data identifies two main stages of combustion (see Fig. 10-9). The first is the premixed-combustion phase, when the fuel which has mixed sufficiently with air to form an ignitable mixture during the delay period is consumed. The second is the mixing-controlled combustion phase, where rates of burning (at least in naturally aspirated engines) are lower. Experimental evidence from heat-release analysis indicates that the majority of the fuel (usually more than 75 percent) burns during the second mixing-controlled phase. Such evidence forms the basis for the heat-release models used in diesel engine cycle simulations. For example,

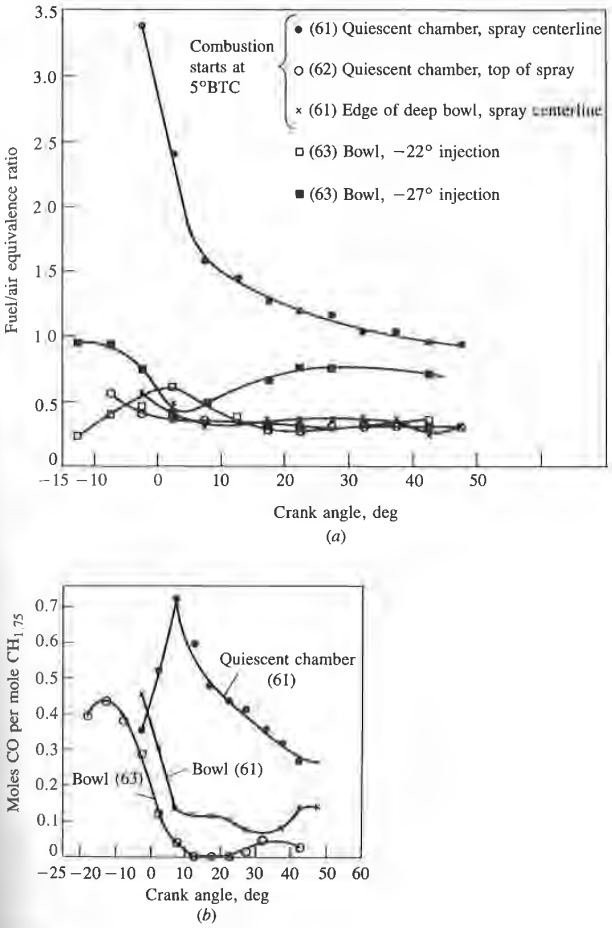

FIGURE 10-46
Time and space-resolved gas-composition data obtained from rapid-acting sampling valves from within the combustion chambers of quiescent and high-swirl bowl-in-piston DI diesel engines. (*a*) Local fuel/air equivalence ratios on spray centerline and periphery with quiescent chamber, edge of deep bowl with swirl, and within a shallow bowl with swirl, three-quarters of the way out to the bowl wall, for two injection timings (−22° and −27°). (*b*) CO concentration on spray centerline with quiescent chamber, edge of deep bowl, and within shallow bowl with swirl.[61–63]

the fraction of the fuel β which burns in the premixed phase has been correlated by Watson *et al.* (see Sec. 14.4.3) by the relation

$$\beta = 1 - \frac{a\phi^b}{\tau_{id}^c} \tag{10.40}$$

where ϕ is the fuel/air equivalence ratio, τ_{id} the ignition delay (in milliseconds), and $a \approx 0.9$, $b \approx 0.35$, and $c \approx 0.4$ are constants depending on engine design. Equation (10.40) shows the expected trends for the premixed fraction, with changes in the overall equivalence ratio ϕ (increasing injection duration as load is increased) and changes in the ignition delay.

That the fuel-burning or heat-release rate is predominantly mixing controlled is supported by the following types of evidence. Estimates of the rate at which fuel-air mixture with composition within the combustible limits is produced in diesel sprays under typical engine conditions, based on a variety of turbulent-jet models of the spray (e.g., see Refs. 29, 36, and 59 and also Sec. 14.4.3), show that mixing rates and burning rates are comparable in magnitude. Estimates of characteristic times for the turbulent-jet mixing processes in diesel combustion chambers show these to be comparable to the duration of the heat-release process, and much longer than characteristic times for evaporation and the combustion chemical kinetics.[36, 44]

Then, measured diesel-combustion heat-release profiles show trends with engine design and operating parameter changes that correspond to fuel-air mixing being the primary controlling factor. Examples of heat-release profiles measured in rapid-compression-machine studies of diesel combustion, shown in Fig. 10-47, illustrate this clearly. The rapid-compression machine had a disc-shaped chamber of 10 cm diameter with a 3.1 cm clearance height at the end of a compression process through a volume ratio of 15.4; a five-hole centrally located fuel-injector nozzle was used. Figure 10-47*a* shows the heat-release profiles for different initial air temperatures which produce different ignition delays. Longer delays allow more fuel to mix to within combustible limits during the delay, so the peak premixed heat-release rate increases. However, the mixing-controlled-phase heat-release-rate magnitudes are essentially the same because the spray-mixing processes are little affected by these changes in air temperature. Figure 10-47*b* and *c* shows that heat-release rates throughout the combustion process are increased by increased fuel-injection rate (achieved by increasing the fuel-injection pressure) and by swirl. Both these changes increase the fuel-air mixing rates within the fuel spray and therefore increase the heat-release rate during the mixing-controlled combustion phase.

Diesel engine heat-release rate trends, as design and operating variables are changed, can be related to mixing rates in analogous fashion. Table 10.5 summarizes the trends that have been investigated. The directional effects of changes in engine parameters on the ignition delay period and the fuel-air mixing rate are all consistent with the measured changes in premixed and mixing-controlled heat-release rates. The controlling role of fuel-air mixing in the diesel engine fuel spray on combustion is clear.

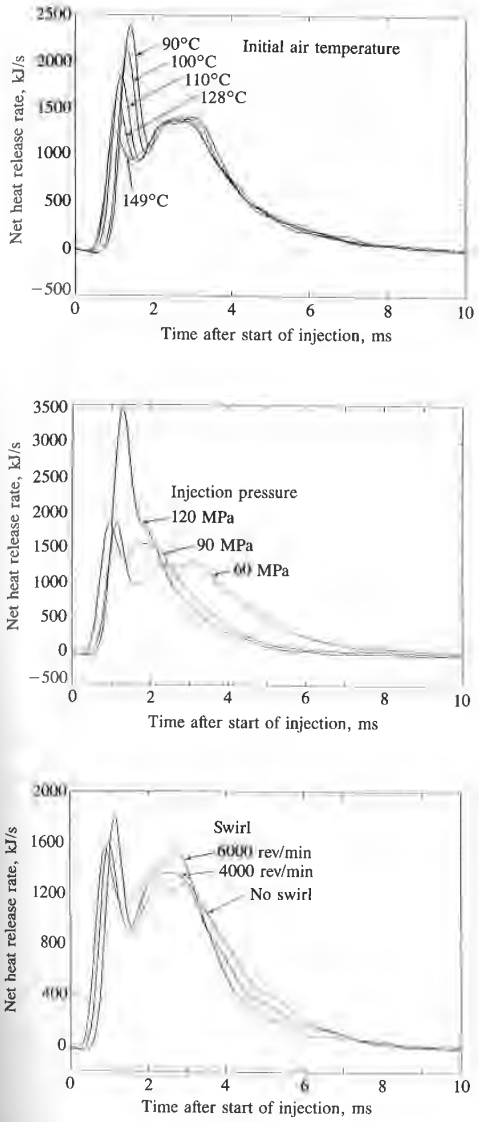

FIGURE 10-47
Net heat-release rates, as a function of time after start of injection, calculated from cylinder pressure data from rapid-compression-machine studies of DI diesel combustion. (*a*) Effect of varying initial air temperature: 4000 rev/min swirl, injection pressure 60 MPa. (*b*) Effect of varying injection pressure: no swirl. (*c*) Effect of varying swirl: injection pressure 60 MPa.[20]

TABLE 10.5
Effects of engine design and operating variables on heat-release rates

		Effect on			
Reference	Parameter varied	τ_{id}	$\dot{m}_m$	$\dot{Q}_p$	$\dot{Q}_m$
5, 64	Injection rate ↑	*	↑	↑	↑
65	Turbocharger boost ↑	↓	*	↓	*
66	Compression ratio ↓	↑	*	↑	*
66	Number of injector holes ↑	*	↑	↑	↑
67, 68	Injection advance ↑	↑	*	↑	*
67, 68	Swirl ↑	*	↑	↑	↑
67	Intake-air temperature ↓	↑	*	↑	*
68, 69	Injection pressure ↑	*	↑	↑	↑
11, 69	Speed ↑	*	↑	↑	↑

τ_{id}, ignition delay; $\dot{m}_m = (dm/dt)_m$, fuel-air mixing rate; $\dot{Q}_p = (dQ/dt)_p$, heat-release rate during premixed-combustion phase; $\dot{Q}_m = (dQ/dt)_m$, heat-release rate during mixing-controlled-combustion phase. ↑ increase; ↓ decrease; * minor effect.
Source: From Plee and Ahmad.[44]

PROBLEMS

10.1. Describe the sequence of processes which must occur before the liquid fuel in the injection system in a direct-injection compression-ignition engine is fully burned.

10.2. Small high-swirl direct-injection CI engines have fuel conversion efficiencies which are about 10 percent higher than values typical of equivalent indirect-injection engines. (IDI engines are used because they achieve higher bmep.) What combustion-system-related differences contribute to this higher efficiency?

10.3. In a diesel engine, because the fuel distribution is nonuniform the burned gas temperature is nonuniform. Consider small fuel-air mixture elements initially at 1000 K and 6.5 MPa at top-center with a range of equivalence ratios. Each element burns at essentially constant pressure. Calculate (using the charts in Chap. 4, or an appropriate chemical equilibrium thermodynamic computer code) the burned gas temperature for mixture equivalence ratios of 0.4, 0.6, 0.8, 1.0, 1.2. Assume the fuel is isooctane.

10.4. The levels of combustible species in the exhaust of a direct-injection diesel engine are: HC, 0.8 g/kW · h; CO, 3 g/kW · h; particulates, 0.7 g/kW · h. If the specific fuel consumption is 210 g/kW · h calculate the combustion efficiency.

10.5. Consider the naturally aspirated direct-injection diesel engine in Fig. 1-23 operating at 2300 rev/min and an equivalence ratio of 0.7. Estimate the following:
(*a*) Mass of air in each cylinder per cycle, mass, and volume (as liquid) of diesel fuel injected per cylinder per cycle.
(*b*) Estimate the average drop size [e.g., use Eq. (10.32)]. The cylinder pressure at time of injection (close to TC) is 50 atm; the fuel injection pressure is 500 atm.
(*c*) Assuming all fuel droplets are the same size as the average drop, how many drops are produced per injection? If these drops are uniformly distributed throughout the air charge at TC, what is the approximate distance between drops? (Neither of these assumptions is correct; however, the calculations illustrate the difficulty of the fuel-air mixing process.)

10.6. Estimate the following quantities for a typical direct-injection diesel fuel spray. The injection pressure is 500 atm; the cylinder pressure during injection is 50 atm.
(*a*) Assuming that the flow through the nozzle orifice is incompressible and quasi steady, estimate the liquid fuel velocity at the orifice exit. At this velocity, how long would the fuel take to reach the cylinder wall? The bore is 125 mm.
(*b*) Each nozzle orifice diameter d_n is 0.34 mm and $L_n/d_n = 4$. Determine the spray angle and plot spray tip penetration versus time.
(*c*) Use Eq. (10.32) to estimate the initial average drop size assuming that the injection process in (*a*) above continues for 1 millisecond and the injector nozzle has four orifices.

10.7. Diesel fuel is injected as a liquid at room temperature into air at 50 atm and 800 K, close to TC at the end of compression. If the overall equivalence ratio is 0.7, estimate the reduction in average air temperature which would occur when the fuel is fully vaporized and uniformly mixed. Assume such mixing takes place at constant volume prior to any combustion.

10.8. Using Eq. (10.37) estimate the ignition delay in milliseconds and crank angle degrees for these operating conditions in Table 10.4: low swirl IDI diesel 600 and 1800 rev/min; high swirl IDI diesel 1800 rev/min; DI diesel low and high compression ratio. The fuel cetane number is 45; stroke = 0.1 m. Discuss whether the predicted trends with speed, swirl, and compression ratio are consistent with Sec. 10.6.4.

10.9. The compression ratio of truck diesel engines must be set at about 18 so that the engine will start when cold. Using Eqs. (10.37) to (10.39) develop a graph of τ_{id} (in degrees) as a function of compression ratio for $r_c = 12$ to 20. Assume $p_i = 1$ atm, $T_i = 255$ K, $n = 1.13$, speed = 100 rev/min, bore = stroke = 120 mm, fuel cetane number = 45. If the ignition delay must be less than 20° CA for satisfactory starting, what compression ratio is required?

10.10. Equation (10.40) predicts the fraction β of the fuel injected into a direct-injection diesel engine which burns in the premixed phase. Plot β as a function of τ_{id} for $\phi = 0.4$. Show that for turbocharged DI diesel engines where τ_{id} is 0.4 to 1 ms, the premixed combustion phase is much less important than it normally is for naturally aspirated engines where τ_{id} is between 0.7 and 3 ms.

REFERENCES

1. Alcock, J. F., and Scott, W. M.: "Some More Light on Diesel Combustion," *Proc. Auto. Div., Instn Mech. Engrs*, No. 5, pp. 179–191, 1962–1963.
2. Scott, W. M.: "Understanding Diesel Combustion through the Use of High Speed Moving Pictures in Color," SAE paper 690002, *SAE Trans.*, vol. 78, 1969.
3. Neitz, A., and D'Alfonso, N.: "The M.A.N. Combustion System with Controlled Direct Injection for Passenger Car Diesel Engines," SAE paper 810479, 1979.
4. Ogasawara, M., Tokunaga, Y., Horio, K., Uryu, M., and Hirofumi, N.: "Photographic Study on the Intermittent Spray Combustion by a Rapid Compression Machine" (in Japanese), *Internal Combustion Engine*, vol. 15, 1976.
5. Austen, A. E. W., and Lyn, W.-T.: "Relation between Fuel Injection and Heat Release in a Direct-Injection Engine and the Nature of the Combustion Processes," *Proc. Instn Mech. Engrs*, No. 1, pp. 47–62, 1960–1961.
6. Lyn, W.-T.: "Study of Burning Rate and Nature of Combustion in Diesel Engines," in *Proceedings of Ninth International Symposium on Combustion*, pp. 1069–1082, The Combustion Institute, 1962.
7. Cheng, W., and Gentry, R.: "Effects on Charge Non-Uniformity on Diesel Heat Release Analysis," SAE paper 861568, 1986.

8. Gatowski, J. A., Balles, E. N., Chun, K. M., Nelson, F. E., Ekchian, J. A., and Heywood, J. B.: "Heat Release Analysis of Engine Pressure Data," SAE paper 841359, *SAE Trans.*, vol. 93, 1984.
9. Krieger, R. B., and Borman, G. L.: "The Computation of Apparent Heat Release for Internal Combustion Engines," ASME paper 66-WA/DGP-4, in *Proc. Diesel Gas Power*, ASME, 1966.
10. Watson, N., and Kamel, M.: "Thermodynamic Efficiency Evaluation of an Indirect Injection Diesel Engine," SAE paper 790039, *SAE Trans.*, vol. 88, 1979.
11. Kort, R. T., Mansouri, S. H., Heywood, J. B., and Ekchian, J. A.: "Divided-Chamber Diesel Engine, Part II: Experimental Validation of a Predictive Cycle-Simulation and Heat Release Analysis," SAE paper 820274, *SAE Trans.*, vol. 91, 1982.
12. Obert, E. F.: *Internal Combustion Engines and Air Pollution*, Intext Educational Publishers, 1973 edition.
13. Weathers, Jr., T., and Hunter, C.: *Diesel Engines for Automobiles and Small Trucks*, Reston Publishing Company, a Prentice-Hall Company, Reston, Va. 1981.
14. Bosch: *Automotive Handbook*, 1st English ed., Robert Bosch GmbH, 1976.
15. Williams, Jr., H. A.: "The GM/EMD Model 710G Series Engine," in *Marine Engine Development*, SP-625, SAE, 1985. Also ASME paper 85-GGP-24, 1985.
16. Hames, R. J., Straub, R. D., and Amann, R. W.: "DDEC Detroit Diesel Electronic Control," SAE paper 850542, 1985.
17. Hiroyasu, H.: "Diesel Engine Combustion and Its Modeling," in *Diagnostics and Modeling of Combustion in Reciprocating Engines*, pp. 53–75, COMODIA 85, Proceedings of Symposium, Tokyo, Sept. 4–6, 1985.
18. Arai, M., Tabata, M., and Hiroyasu, H.: "Disintegrating Process and Spray Characterization of Fuel Jet Injected by a Diesel Nozzle," SAE paper 840275, *SAE Trans.*, vol. 93, 1984.
19. Kamimoto, T., Kobayashi, H., and Matsuoka, S.: "A Big Size Rapid Compression Machine for Fundamental Studies of Diesel Combustion," SAE paper 811004, *SAE Trans.*, vol. 90, 1981.
20. Balles, E.: "Fuel-Air Mixing and Diesel Combustion in a Rapid Compression Machine," Ph.D. Thesis, Department of Mechanical Engineering, MIT, June 1987.
21. Browne, K. R., Partridge, I. M., and Greeves, G.: "Fuel Property Effects on Fuel/Air Mixing in an Experimental Diesel Engine," SAE paper 860223, 1986.
22. Bracco, F. V.: "Modeling of Engine Sprays," SAE paper 850394, 1985.
23. Kuo, T., and Bracco, F. V.: "Computations of Drop Sizes in Pulsating Sprays and of Liquid-Core Length in Vaporizing Sprays," SAE paper 820133, *SAE Trans.*, vol. 91, 1982.
24. Reitz, R. D., and Bracco, F. V.: "Mechanism of Atomization of a Liquid Jet," *Phys. Fluid*, vol. 25, no. 10, pp. 1730–1742, 1982.
25. Reitz, R. D., and Bracco, F. V.: "On the Dependence of Spray Angle and Other Spray Parameters on Nozzle Design and Operating Conditions," SAE paper 790494, 1979.
26. Wu, K.-J., Su, C.-C., Steinberger, R. L., Santavicca, D. A., and Bracco, F. V.: "Measurements of the Spray Angle of Atomizing Jets," *J. Fluids Engng*, vol. 105, pp. 406–413, 1983.
27. Hay, N., and Jones, P. L.: "Comparison of the Various Correlations for Spray Penetration," SAE paper 720776, 1972.
28. Dent, J. C.: "Basis for the Comparison of Various Experimental Methods for Studying Spray Penetration," SAE paper 710571, *SAE Trans.*, vol. 80, 1971.
29. Hiroyasu, H., Kadota, T., and Arai, M.: "Supplementary Comments: Fuel Spray Characterization in Diesel Engines," in James N. Mattavi and Charles A. Amann (eds.), *Combustion Modeling in Reciprocating Engines*, pp. 369–408, Plenum Press, 1980.
30. Wu, K.-J., Reitz, R. D., and Bracco, F. V.: "Measurements of Drop Size at the Spray Edge near the Nozzle in Atomizing Liquid Jets," *Phys. Fluids*, vol. 29, no. 4, pp. 941–951, 1986.
31. Reitz, R. D., and Diwakar, R.: "Effect of Drop Breakup on Fuel Sprays," SAE paper 860469, 1986.
32. Hiroyasu, H., and Kadota, T.: "Fuel Droplet Size Distribution in Diesel Combustion Chamber," SAE paper 740715, *SAE Trans.*, vol. 83, 1974.
33. El Wakil, M. M., Myers, P. S., and Uyehara, O. A.: "Fuel Vaporization and Ignition Lag in Diesel Combustion," in *Burning a Wide Range of Fuels in Diesel Engines*, *SAE Progress in Technol.*, vol. 11, pp. 30–44, SAE, 1967.

34. Borman, G. L., and Johnson, J. H.: "Unsteady Vaporization Histories and Trajectories of Fuel Drops Injected into Swirling Air," in *Burning a Wide Range of Fuels in Diesel Engines. SAE Progress in Technology*, vol. 11, pp. 13–29, SAE, 1967; also SAE paper 598C, 1962.
35. Kamimoto, T., and Matsuoka, S.: "Prediction of Spray Evaporation in Reciprocating Engines," SAE paper 770413, *SAE Trans.*, vol. 86, 1977.
36. Kuo, T., Yu, R. C., and Shahed, S. M.: "A Numerical Study of the Transient Evaporating Spray Mixing Process in the Diesel Environment," SAE paper 831735, *SAE Trans.*, vol. 92, 1983.
37. ASTM Method D613, Cetane Test Procedure.
38. Henein, N. A., and Fragoulis, A. N.: "Correlation between Physical Properties and Autoignition Parameters of Alternate Fuels," SAE paper 850266, 1985.
39. Gulder, O. L., Glavincevski, B., and Burton, G. F.: "Ignition Quality Rating Methods for Diesel Fuels—A Critical Appraisal," SAE paper 852080, 1985.
40. ASTM D976, Calculated Cetane Index.
41. ASTM D611.
42. Igura, S., Kadota, T., and Hiroyasu, H.: "Spontaneous Ignition Delay of Fuel Sprays in High Pressure Gaseous Environments," *Trans. Japan Soc. Mech. Engrs*, vol. 41, no. 345, pp. 24–31, 1975.
43. Spadaccini, L. J., and TeVelde, J. A.: "Autoignition Characteristics of Aircraft-Type Fuels," *Combust. Flame*, vol. 46, pp. 283–300, 1982.
44. Ploe, S. L., and Ahmad, T.: "Relative Roles of Premixed and Diffusion Burning in Diesel Combustion," SAE paper 831733, *SAE Trans.*, vol. 92, 1983.
45. Stringer, F. W., Clarke, A. E., and Clarke, J. S.: "The Spontaneous Ignition of Hydrocarbon Fuels in a Flowing System," *Proc. Instn Mech. Engrs*, vol. 184, pt. 3J, 1969–1970.
46. Wolfer, H. H.: "Ignition Lag in Diesel Engines," VDI-Forschungsheft 392, 1938; Translated by Royal Aircraft Establishment, Farnborough Library No. 358, UDC 621–436.047, August 1959.
47. Lyn, W.-T., and Valdmanis, E.: "Effects of Physical Factors on Ignition Delay," SAE paper 680102, 1968.
48. Wong, C. L., and Steere, D. E.: "The Effects of Diesel Fuel Properties and Engine Operating Conditions on Ignition Delay," SAE paper 821231, *SAE Trans.*, vol. 91, 1982.
49. Andree, A., and Pachernegg, S. J.: "Ignition Conditions in Diesel Engines," SAE paper 690253, *SAE Trans.*, vol. 78, 1969.
50. Glavincevski, B., Gülder, O. L., and Gardner, L.: "Cetane Number Estimation of Diesel Fuels from Carbon Type Structural Composition," SAE paper 841341, 1984.
51. Olree, R., and Lenane, D.: "Diesel Combustion Cetane Number Effects," SAE paper 840108, *SAE Trans.*, vol. 93, 1984.
52. Schaefer, A. J., and Hardenberg, H. O.: "Ignition Improvers for Ethanol Fuels," SAE paper 810249, *SAE Trans.*, vol. 90, 1981.
53. Hardenberg, H. O., and Huse, F. W.: "An Empirical Formula for Computing the Pressure Rise Delay of a Fuel from its Cetane Number and from the Relevant Parameters of Direct-Injection Diesel Engines," SAE paper 790493, *SAE Trans.*, vol. 88, 1979.
54. Dent, J. C., and Mehta, P. S.: "Phenomenological Combustion Model for a Quiescent Chamber Diesel Engine," SAE paper 811235, *SAE Trans.*, vol. 90, 1981.
55. Chang, Y. J., Kobayashi, H., Matsuzawa, K., and Kamimoto, T.: "A Photographic Study of Soot Formation and Combustion in a Diesel Flame with a Rapid Compression Machine," in *Diagnostics and Modeling of Combustion in Reciprocating Engines*, pp. 149–157, COMODIA 85, Proceedings of Symposium, Tokyo, Sept. 4–6, 1985.
56. Lakshminarayan, P. A., and Dent, J. C.: "Interferometric Studies of Vaporising and Combustion Sprays," SAE paper 830244, *SAE Trans.*, vol. 92, 1983.
57. Coletta, K. J., Balles, E. N., Ekchian, J. A., Cheng, W. K., and Heywood, J. B.: "A Rapid Compression Machine Study of the Influence of Charge Temperature on Diesel Combustion," SAE paper 870587, 1987.
58. Morris, C. J., and Dent, J. C.: "The Simulation of Air Fuel Mixing in High Swirl Open Chamber Diesel Engines," *Proc. Instn Mech. Engrs*, vol. 190, no. 47/76, pp. 503–513, 1976.
59. Rife, J., and Heywood, J. B.: "Photographic and Performance Studies of Diesel Combustion with

a Rapid Compression Machine," SAE paper 740948, *SAE Trans.*, vol. 83, 1974.
60. Whitehouse, N. D., Cough, E., and Jeje, A. B.: "The Study of Combustion in a Quiescent Combustion Chamber Diesel Engine," ASME paper 82-HT-35, 1982.
61. Nightingale, D. R.: "A Fundamental Investigation into the Problem of NO Formation in Diesel Engines," SAE paper 750848, *SAE Trans.*, vol. 84, 1975.
62. Bennethum, J. E., Mattavi, J. N., and Toepel, R. R.: "Diesel Combustion Chamber Sampling-Hardware, Procedures, and Data Interpretation," SAE paper 750849, *SAE Trans.*, vol. 84, 1975.
63. Rhee, K. T., Myers, P. S., and Uyehara, O. A.: "Time- and Space-Resolved Species Determination in Diesel Combustion Using Continuous Flow Gas Sampling," SAE paper 780226, *SAE Trans.*, vol. 87, 1978.
64. Shipinsky, J., Uyehara, O. A., and Myers, P. S.: "Experimental Correlation between Rate-of-Injection and Rate-of-Heat-Release in a Diesel Engine," ASME paper 68–DGP-11, 1968.
65. Grigg, H. C., and Syed, M. H.: "The Problem of Predicting Rate of Heat Release in Diesel Engine," *Proc. Instn Mech. Engrs*, vol. 184, pt. 3J, 1969–1970.
66. Whitehouse, N. D., Clough, E., and Way, J. B.: "The Effect of Changes in Design and Operating Conditions on Heat Release in Direct-Injection Diesel Engines," SAE paper 740085, 1974.
67. Meguerdichian, M., and Watson, N.: "Prediction of Mixture Formation and Heat Release in Diesel Engines," SAE paper 780225, 1978.
68. Kamimoto, T., Aoyagi, Y., Matsui, Y., and Matsuoka, S.: "The Effects of Some Engine Variables on Measured Rates of Air Entrainment and Heat Release in a DI Diesel Engine," SAE paper 8000253, *SAE Trans.*, vol. 89, 1980.
69. Dent, J. C., Mehta, P. S., and Swan, J.: "A Predictive Model for Automotive DI Diesel Engine Performance and Smoke Emissions," paper C126/82, presented at the International Conference on *Diesel Engines for Passenger Cars and Light Duty Vehicles*, Institution of Mechanical Engineers, London, England, Oct. 5–7, 1982.

E Trans., vol. 83, 1974.
udy of Combustion in a Quiescent Com-
5, 1982.
the Problem of NO Formation in Diesel

'Diesel Combustion Chamber Sampling-
aper 750849, SAE Trans., vol. 84, 1975.
e- and Space-Resolved Species Determi-
Gas Sampling," SAE paper 780226, SAE

perimental Correlation between Rate-of-
ASME paper 68–DGP-11, 1968.
edicting Rate of Heat Release in Diesel
1970.
ffect of Changes in Design and Operating
ngines," SAE paper 740085, 1974.
Mixture Formation and Heat Release in

.: "The Effects of Some Engine Variables
ease in a DI Diesel Engine," SAE paper

Model for Automotive DI Diesel Engine
presented at the International Conference
Vehicles, Institution of Mechanical Engi-

CHAPTER 11

POLLUTANT FORMATION AND CONTROL

11.1 NATURE AND EXTENT OF PROBLEM

Spark-ignition and diesel engines are a major source of urban air pollution. The spark-ignition engine exhaust gases contain oxides of nitrogen (nitric oxide, NO, and small amounts of nitrogen dioxide, NO_2—collectively known as NO_x), carbon monoxide (CO), and organic compounds which are unburned or partially burned hydrocarbons (HC). The relative amounts depend on engine design and operating conditions but are of order: NO_x, 500 to 1000 ppm or 20 g/kg fuel; CO, 1 to 2 percent or 200 g/kg fuel; and HC, 3000 ppm (as C_1) or 25 g/kg fuel. Piston blowby gases, and fuel evaporation and release to the atmosphere through vents in the fuel tank and carburetor after engine shut-down, are also sources of unburned hydrocarbons. However, in most modern engines these nonexhaust sources are effectively controlled by returning the blowby gases from the crankcase to the engine intake system and by venting the fuel tank and carburetor float bowl through a vapor-absorbing carbon cannister which is purged by some of the engine intake air during normal engine operation. In diesel engine exhaust, concentrations of NO_x are comparable to those from SI engines. Diesel hydrocarbon emissions are significant though exhaust concentrations are lower by about a factor of 5 than typical SI engine levels. The hydrocarbons in the exhaust may also condense to form white smoke during engine starting and warm-up.

Specific hydrocarbon compounds in the exhaust gases are the source of diesel odor. Diesel engines are an important source of particulate emissions; between about 0.2 and 0.5 percent of the fuel mass is emitted as small (~ 0.1 μm diameter) particles which consist primarily of soot with some additional absorbed hydrocarbon material. Diesel engines are not a significant source of carbon monoxide.

Use of alcohol fuels in either of these engines substantially increases aldehyde emissions. While these are not yet subject to regulation, aldehydes would be a significant pollutant if these fuels were to be used in quantities comparable to gasoline and diesel. Currently used fuels, gasoline and diesel, contain sulfur: gasoline in small amounts (≤ 600 ppm by weight S), diesel fuel in larger amounts (≤ 0.5 percent). The sulphur is oxidized (or burned) to produce sulfur dioxide, SO_2, of which a fraction can be oxidized to sulfur trioxide, SO_3, which combines with water to form a sulfuric acid aerosol.

In general, the concentrations of these pollutants in internal combustion engine exhaust differ from values calculated assuming chemical equilibrium. Thus the detailed chemical mechanisms by which these pollutants form and the kinetics of these processes are important in determining emission levels. For some pollutant species, e.g., carbon monoxide, organic compounds, and particulates, the formation and destruction reactions are intimately coupled with the primary fuel combustion process. Thus an understanding of the formation of these species requires knowledge of the combustion chemistry. For nitrogen oxides and sulfur oxides, the formation and destruction processes are not part of the fuel combustion process. However, the reactions which produce these species take place in an environment created by the combustion reactions, so the two processes are still intimately linked. A summary of the mechanisms by which these pollutants form in internal combustion engines provides an introduction to this chapter. In subsequent sections, the details of the basic formation mechanisms of each pollutant and the application of these mechanisms to the combustion process in both spark-ignition and compression-ignition engines will be developed.

The processes by which pollutants form within the cylinder of a conventional spark-ignition engine are illustrated qualitatively in Fig. 11-1. The schematic shows the combustion chamber during four different phases of the engine operating cycle: compression, combustion, expansion, and exhaust. Nitric oxide (NO) forms throughout the high-temperature burned gases behind the flame through chemical reactions involving nitrogen and oxygen atoms and molecules, which do not attain chemical equilibrium. The higher the burned gas temperature, the higher the rate of formation of NO. As the burned gases cool during the expansion stroke the reactions involving NO freeze, and leave NO concentrations far in excess of levels corresponding to equilibrium at exhaust conditions. Carbon monoxide also forms during the combustion process. With rich fuel-air mixtures, there is insufficient oxygen to burn fully all the carbon in the fuel to CO_2; also, in the high-temperature products, even with lean mixtures, dissociation ensures there are significant CO levels. Later, in the expansion stroke, the CO oxidation process also freezes as the burned gas temperature falls.

The unburned hydrocarbon emissions have several different sources.

gases are the source of diesel particulate emissions; between d as small (~0.1 μm diameter) ıe additional absorbed hydro- t source of carbon monoxide. ɛs substantially increases alde- ɛgulation, aldehydes would be ɛd in quantities comparable to and diesel, contain sulfur: gas- , diesel fuel in larger amounts ed) to produce sulfur dioxide, trioxide, SO_3, which combines

utants in internal combustion ing chemical equilibrium. Thus ıese pollutants form and the ining emission levels. For some compounds, and particulates, ıtely coupled with the primary f the formation of these species For nitrogen oxides and sulfur are not part of the fuel com- duce these species take place in ions, so the two processes are sms by which these pollutants ntroduction to this chapter. In ıtion mechanisms of each pol- to the combustion process in ıes will be developed.

in the cylinder of a conventionly in Fig. 11-1. The schemate ent phases of the engine oper- and exhaust. Nitric oxide (NO) ases behind the flame through atoms and molecules, which do burned gas temperature, the d gases cool during the expand leave NO concentrations far at exhaust conditions. Carbon ɛss. With rich fuel-air mixtures bon in the fuel to CO_2; also, in mixtures, dissociation ensures ısion stroke, the CO oxidation falls.

ıve several different sources

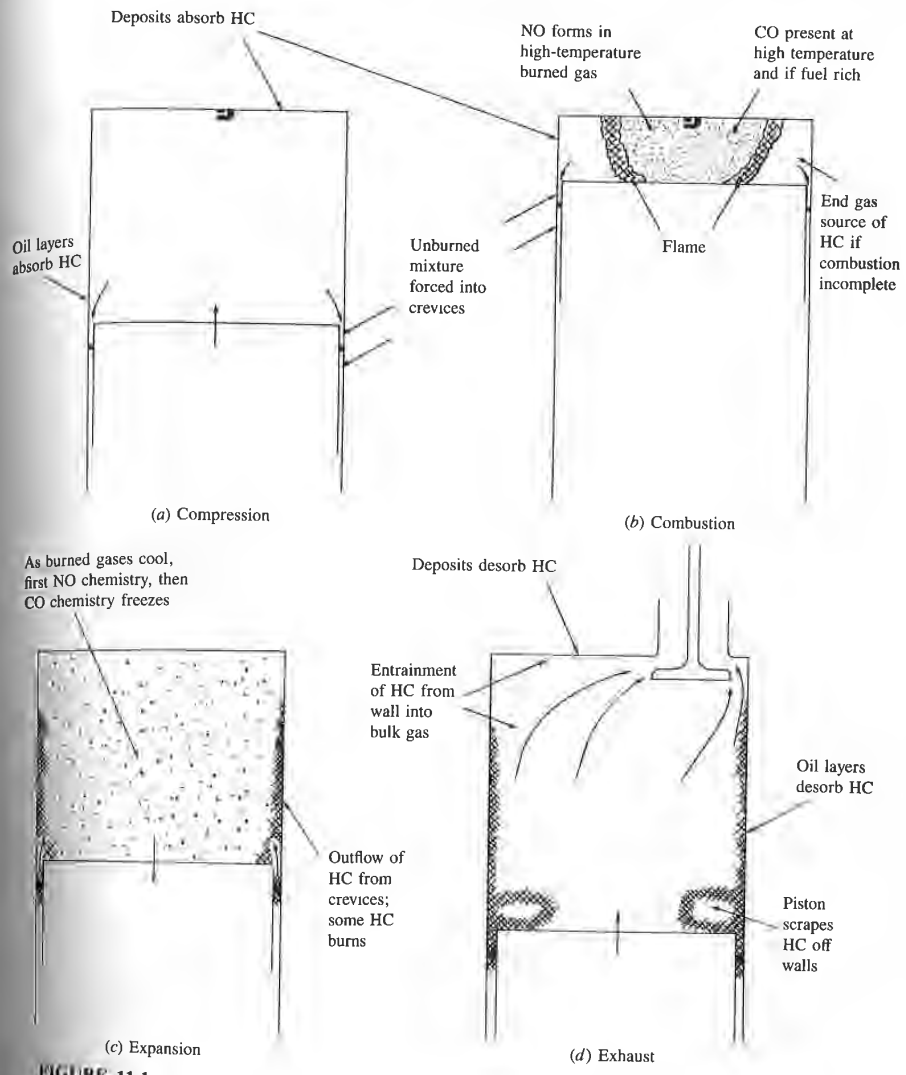

FIGURE 11-1
Summary of HC, CO, and NO pollutant formation mechanisms in a spark-ignition engine.

During compression and combustion, the increasing cylinder pressure forces some of the gas in the cylinder into crevices, or narrow volumes, connected to the combustion chamber: the volumes between the piston, rings, and cylinder wall are the largest of these. Most of this gas is unburned fuel-air mixture; much of it

escapes the primary combustion process because the entrance to these crevices is too narrow for the flame to enter. This gas, which leaves these crevices later in the expansion and exhaust processes, is one source of unburned hydrocarbon emissions. Another possible source is the combustion chamber walls. A quench layer containing unburned and partially burned fuel-air mixture is left at the wall when the flame is extinguished as it approaches the wall. While it has been shown that the unburned HC in these thin (≤ 0.1 mm) layers burn up rapidly when the combustion chamber walls are clean, it has also been shown that the porous deposits on the walls of engines in actual operation do increase engine HC emissions. A third source of unburned hydrocarbons is believed to be any engine oil left in a thin film on the cylinder wall, piston and perhaps on the cylinder head. These oil layers can absorb and desorb fuel hydrocarbon components, before and after combustion, respectively, thus permitting a fraction of the fuel to escape the primary combustion process unburned. A final source of HC in engines is incomplete combustion due to bulk quenching of the flame in that fraction of the engine cycles where combustion is especially slow (see Sec. 9.4.3). Such conditions are most likely to occur during transient engine operation when the air/fuel ratio, spark timing, and the fraction of the exhaust recycled for emission control may not be properly matched.

The unburned hydrocarbons exit the cylinder by being entrained in the bulk-gas flow during blowdown and at the end of the exhaust stroke as the piston pushes gas scraped off the wall out of the exhaust valve. Substantial oxidation of the hydrocarbons which escape the primary combustion process by any of the above processes can occur during expansion and exhaust. The amount of oxidation depends on the temperature and oxygen concentration time histories of these HC as they mix with the bulk gases.

One of the most important variables in determining spark-ignition engine emissions is the fuel/air equivalence ratio, ϕ. Figure 11-2 shows qualitatively how NO, CO, and HC exhaust emissions vary with this parameter. The spark-ignition engine has normally been operated close to stoichiometric, or slightly fuel-rich, to ensure smooth and reliable operation. Figure 11-2 shows that leaner mixtures give lower emissions until the combustion quality becomes poor (and eventually misfire occurs), when HC emissions rise sharply and engine operation becomes erratic. The shapes of these curves indicate the complexities of emission control. In a cold engine, when fuel vaporization is slow, the fuel flow is increased to provide an easily combustible fuel-rich mixture in the cylinder. Thus, until the engine warms up and this enrichment is removed, CO and HC emissions are high. At part-load conditions, lean mixtures could be used which would produce lower HC and CO emissions (at least until the combustion quality deteriorates) and moderate NO emissions. Use of recycled exhaust to dilute the engine intake mixture lowers the NO levels, but also deteriorates combustion quality. Exhaust gas recirculation (EGR) is used with stoichiometric mixtures in many engine control systems. Note that the highest power levels are obtained from the engine with slightly rich-of-stoichiometric mixtures and no recycled exhaust to dilute the incoming charge. As we will see, several emission control techniques are required

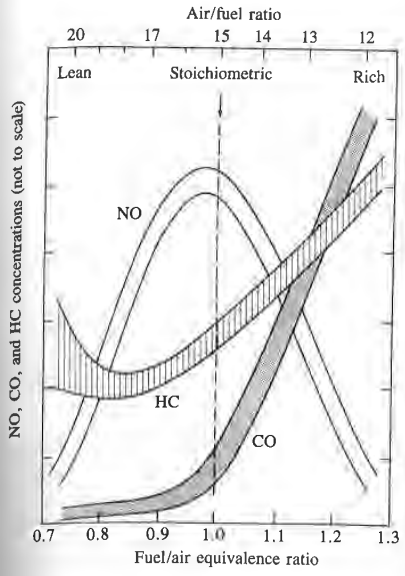

FIGURE 11-2
Variation of HC, CO, and NO concentration in the exhaust of a conventional spark-ignition engine with fuel/air equivalence ratio.

to reduce emissions of all three pollutants, over all engine operating modes, and achieve acceptable average levels.

In the diesel engine, the fuel is injected into the cylinder just before combustion starts, so throughout most of the critical parts of the cycle the fuel distribution is nonuniform. The pollutant formation processes are strongly dependent on the fuel distribution and how that distribution changes with time due to mixing. Figure 11-3 illustrates how various parts of the fuel jet and the flame affect the formation of NO, unburned HC, and soot (or particulates) during the "premixed" and "mixing-controlled" phases of diesel combustion in a direct-injection engine with swirl. Nitric oxide forms in the high-temperature burned gas regions as before, but temperature and fuel/air ratio distributions within the burned gases are now nonuniform and formation rates are highest in the close-to-stoichiometric regions. Soot forms in the rich unburned-fuel-containing core of the fuel sprays, within the flame region, where the fuel vapor is heated by mixing with hot burned gases. Soot then oxidizes in the flame zone when it contacts unburned oxygen, giving rise to the yellow luminous character of the flame. Hydrocarbons and aldehydes originate in regions where the flame quenches both on the walls and where excessive dilution with air prevents the combustion process from either starting or going to completion. Fuel that vaporizes from the nozzle sac volume during the later stages of combustion is also a source of HC. Combustion generated noise is controlled by the early part of the combustion process, the initial rapid heat release immediately following the ignition-delay period.

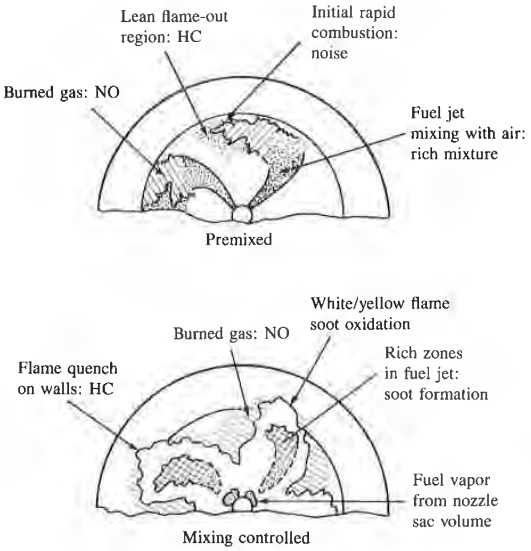

FIGURE 11-3
Summary of pollutant formation mechanisms in a direct-injection compression-ignition engine during "premixed" and "mixing-controlled" combustion phases.

11.2 NITROGEN OXIDES

11.2.1 Kinetics of NO Formation

While nitric oxide (NO) and nitrogen dioxide (NO_2) are usually grouped together as NO_x emissions, nitric oxide is the predominant oxide of nitrogen produced inside the engine cylinder. The principal source of NO is the oxidation of atmospheric (molecular) nitrogen. However, if the fuel contains significant nitrogen, the oxidation of the fuel nitrogen-containing compounds is an additional source of NO. Gasolines contain negligible amounts of nitrogen; although diesel fuels contain more nitrogen, current levels are not significant.

The mechanism of NO formation from atmospheric nitrogen has been studied extensively.[1] It is generally accepted that in combustion of near-stoichiometric fuel-air mixtures the principal reactions governing the formation of NO from molecular nitrogen (and its destruction) are†

$$O + N_2 = NO + N \tag{11.1}$$

$$N + O_2 = NO + O \tag{11.2}$$

$$N + OH = NO + H \tag{11.3}$$

† This is often called the extended Zeldovich mechanism. Zeldovich[1] was the first to suggest the importance of reactions (11.1) and (11.2). Lavoie *et al.*[2] added reaction (11.3) to the mechanism; it does contribute significantly.

TABLE 11.1
Rate constants for NO formation mechanism[1]

Reaction	Rate constant, $cm^3/mol \cdot s$	Temperature range, K	Uncertainty, factor of or %
(1) $O + N_2 \rightarrow NO + N$	$7.6 \times 10^{13} \exp[-38{,}000/T]$	2000–5000	2
(−1) $N + NO \rightarrow N_2 + O$	1.6×10^{13}	300–5000	±20% at 300 K 2 at 2000–5000 K
(2) $N + O_2 \rightarrow NO + O$	$6.4 \times 10^{9}\ T \exp[-3150/T]$	300–3000	±30% 300–1500 K 2 at 3000 K
(−2) $O + NO \rightarrow O_2 + N$	$1.5 \times 10^{9}\ T \exp[-19{,}500/T]$	1000–3000	±30% at 1000 K 2 at 3000 K
(3) $N + OH \rightarrow NO + H$	4.1×10^{13}	300–2500	±80%
(−3) $H + NO \rightarrow OH + N$	$2.0 \times 10^{14} \exp[-23{,}650/T]$	2200–4500	2

The forward and reverse rate constants (k_i^+ and k_i^-, respectively) for these reactions have been measured in numerous experimental studies. Recommended values for these rate constants taken from a critical review of this published data are given in Table 11.1. Note that the equilibrium constant for each reaction, $K_{c,i}$ (see Sec. 3.7.2), is related to the forward and reverse rate constants by $K_{c,i} = k_i^+/k_i^-$. The rate of formation of NO via reactions (11.1) to (11.3) is given by [see Eqs. (3.55) and (3.58)]

$$\frac{d[NO]}{dt} = k_1^+[O][N_2] + k_2^+[N][O_2] + k_3^+[N][OH] - k_1^-[NO][N] - k_2^-[NO][O] - k_3^-[NO][H] \quad (11.4)$$

where [ ] denote species concentrations in moles per cubic centimeter when k_i have the values given in Table 11.1. The forward rate constant for reaction (11.1) and the reverse rate constants for reactions (11.2) and (11.3) have large activation energies which results in a strong temperature dependence of NO formation rates.

A similiar relation to (11.4) can be written for $d[N]/dt$:

$$\frac{d[N]}{dt} = k_1^+[O][N_2] - k_2^+[N][O_2] - k_3^+[N][OH] - k_1^-[NO][N] + k_2^-[NO][O] + k_3^-[NO][H] \quad (11.5)$$

Since [N] is much less than the concentrations of other species of interest ($\sim 10^{-8}$ mole fraction), the steady-state approximation is appropriate: $d[N]/dt$ is set equal to zero and Eq. (11.5) used to eliminate [N]. The NO formation rate then becomes

$$\frac{d[NO]}{dt} = 2k_1^+[O][N_2]\frac{1 - [NO]^2/(K[O_2][N_2])}{1 + k_1^-[NO]/(k_2^+[O_2] + k_3^+[OH])} \quad (11.6)$$

where $K = (k_1^+/k_1^-)(k_2^+/k_2^-)$.

FIGURE 11-3
Summary of pollutant formation mechanisms in a direct-injection compression-ignition engine during "premixed" and "mixing-controlled" combustion phases.

TABLE 11.2
Typical values of R_1, R_1/R_2, and $R_1/(R_2 + R_3)$†

Equivalence ratio	R_1‡	R_1/R_2	$R_1/(R_2 + R_3)$
0.8	5.8×10^{-5}	1.2	0.33
1.0	2.8×10^{-5}	2.5	0.26
1.2	7.6×10^{-6}	9.1	0.14

† At 10 atm pressure and 2600 K.
‡ Units gmol/cm^3 · s.

NO forms in both the flame front and the postflame gases. In engines, however, combustion occurs at high pressure so the flame reaction zone is extremely thin ($\sim$0.1 mm) and residence time within this zone is short. Also, the cylinder pressure rises during most of the combustion process, so burned gases produced early in the combustion process are compressed to a higher temperature than they reached immediately after combustion. Thus, NO formation in the postflame gases almost always dominates any flame-front–produced NO. It is, therefore, appropriate to assume that the combustion and NO formation processes are decoupled and to approximate the concentrations of O, O_2, OH, H, and N_2 by their equilibrium values at the local pressure and equilibrium temperature.

To introduce this equilibrium assumption it is convenient to use the notation $R_1 = k_1^+[O]_e[N_2]_e = k_1^-[NO]_e[N]_e$, where $[\ ]_e$ denotes equilibrium concentration, for the one-way equilibrium rate for reaction (11.1), with similiar definitions for $R_2 = k_2^+[N]_e[O_2]_e = k_2^-[NO]_e[O]_e$ and $R_3 = k_3^+[N]_e[OH]_e = k_3^-[NO]_e[H]_e$. Substituting $[O]_e$, $[O_2]_e$, $[OH]_e$, $[H]_e$, and $[N_2]_e$ for [O], $[O_2]$, [OH], [H], and $[N_2]$ in Eq. (11.6) yields

$$\frac{d[NO]}{dt} = \frac{2R_1\{1 - ([NO]/[NO]_e)^2\}}{1 + ([NO]/[NO]_e)R_1/(R_2 + R_3)} \tag{11.7}$$

Typical values of R_1, R_1/R_2 and $R_1/(R_2 + R_3)$ are given in Table 11.2. The difference between R_1/R_2 and $R_1/(R_2 + R_3)$ indicates the relative importance of adding reaction (11.3) to the mechanism.

The strong temperature dependence of the NO formation rate can be demonstrated by considering the initial value of $d[NO]/dt$ when $[NO]/[NO]_e \ll 1$. Then, from Eq. (11.7),

$$\frac{d[NO]}{dt} = 2R_1 = 2k_1^+[O]_e[N_2]_e \tag{11.8}$$

The equilibrium oxygen atom concentration is given by

$$[O]_e = \frac{K_{p(O)}[O_2]_e^{1/2}}{(\bar{R}T)^{1/2}} \tag{11.9}$$

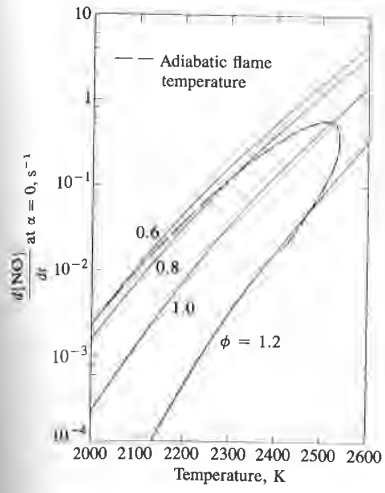

FIGURE 11-4
Initial NO formation rate, mass fraction per second (for $[NO]/[NO]_e \ll 1$), as a function of temperature for different equivalence ratios (ϕ) and 15 atm pressure. Dashed line shows adiabatic flame temperature for kerosene combustion with 700 K, 15 atm air.[3]

where $K_{p(O)}$ is the equilibrium constant for the reaction

$$\tfrac{1}{2}O_2 = O$$

and is given by

$$K_{p(O)} = 3.6 \times 10^3 \exp\left(\frac{-31{,}090}{T}\right) \quad \text{atm}^{1/2} \tag{11.10}$$

The initial NO formation rate may then be written [combining Eqs. (11.8), (11.9), and (11.10) with k_1^+ from Table 11.1] as

$$\frac{d[NO]}{dt} = \frac{6 \times 10^{16}}{T^{1/2}} \exp\left(\frac{-69{,}090}{T}\right)[O_2]_e^{1/2}[N_2]_e \quad \text{mol/cm}^3 \cdot \text{s} \tag{11.11}$$

The strong dependence of $d[NO]/dt$ on temperature in the exponential term is evident. High temperatures and high oxygen concentrations result in high NO formation rates. Figure 11-4 shows the NO formation rate as a function of gas temperature and fuel/air equivalence ratio in postflame gases. Also shown is the adiabatic flame temperature attained by a fuel-air mixture initially at 700 K at a constant pressure of 15 atm. For adiabatic constant-pressure combustion (an appropriate model for each element of fuel that burns in an engine), this initial NO formation rate peaks at the stoichiometric composition, and decreases rapidly as the mixture becomes leaner or richer.

A characteristic time for the NO formation process, τ_{NO}, can be defined by

$$\tau_{NO}^{-1} = \frac{1}{[NO]_e}\frac{d[NO]}{dt} \tag{11.12}$$

$[NO]_e$ can be obtained from the equilibrium constant

$$K_{NO} = 20.3 \times \exp(-21{,}650/T)$$

for the reaction

$$O_2 + N_2 = 2NO$$

as $[NO]_e = (K_{NO}[O_2]_e[N_2]_e)^{1/2}$. Equations (11.11) and (11.12) can be combined to give

$$\tau_{NO} = \frac{8 \times 10^{-16} T \exp(58{,}300/T)}{p^{1/2}} \tag{11.13}$$

where τ_{NO} is in seconds, T in kelvins, and p in atmospheres. Use has been made of the fact that $\bar{x}_{N_2} \approx 0.71$. For engine combustion conditions, τ_{NO} is usually comparable to or longer than the times characteristic of changes in engine conditions so the formation process is kinetically controlled. However, for close-to-stoichiometric conditions at the maximum pressures and burned gas temperatures, τ_{NO} is of the same order as typical combustion times (1 ms) and equilibrium NO concentrations may be attained.

Evidence that this formation model is valid under conditions typical of those found in engines is provided by high-pressure combustion bomb studies. Newhall and Shahed[4] have measured the NO production, using the q-band absorption technique, behind hydrogen-air and propane-air planar flames propagating axially in a cylindrical bomb. Some results are compared with predictions made with this kinetic scheme (coupled with an "unmixed" combustion calculation to determine local pressure and temperature; see Sec. 9.2.1) in Fig. 11-5. The agreement is excellent. Note that the NO concentration rises smoothly from

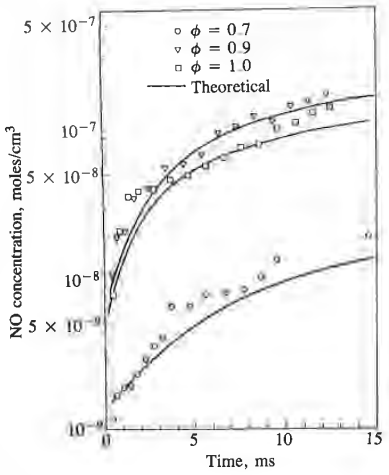

FIGURE 11-5
Measured and calculated rate-limited NO concentrations behind flame in high-pressure cylindrical bomb experiments with H_2-air mixtures. ϕ = equivalence ratio.[4]

TABLE 11.3
Typical nitrogen content of distillate fuels[1]

Fraction	Average nitrogen, wt %	Range, wt %
Crude	0.65	—
Heavy distillates	1.40	0.60–2.15
Light distillates	0.07	0–0.60

close to zero, indicating that at these high pressures there is negligible NO production within the flame front itself.

Fuel nitrogen is also a source of NO via a different and yet to be fully explained mechanism. Table 11.3 shows the typical nitrogen content of petroleum-derived fuels. During distillation, the fuel nitrogen is concentrated in the higher boiling fractions. In distillate fuels, the nitrogen can exist as amines and ring compounds (e.g., pyridine, quinoline, and carbazoles). During combustion these compounds are likely to undergo some thermal decomposition prior to entering the combustion zone. The precursors to NO formation will therefore be low molecular weight nitrogen-containing compounds such as NH_3, HCN, and CN. The detailed information on the kinetics of NO formation from these compounds is limited. Oxidation to NO is usually rapid, occurring on a time scale comparable to that of the combustion reactions. The NO yield (amount of fuel nitrogen converted to NO) is sensitive to the fuel/air equivalence ratio. Relatively high NO yields (approaching 100 percent) are obtained for lean and stoichiometric mixtures; relatively low yields are found for rich mixtures. NO yields are only weakly dependent on temperature, in contrast to the strong temperature dependence of NO formed from atmospheric nitrogen.[1]

11.2.2 Formation of NO_2

Chemical equilibrium considerations indicate that for burned gases at typical flame temperatures, NO_2/NO ratios should be negligibly small. While experimental data show this is true for spark-ignition engines, in diesels NO_2 can be 10 to 30 percent of the total exhaust oxides of nitrogen emissions.[5] A plausible mechanism for the persistence of NO_2 is the following.[6] NO formed in the flame zone can be rapidly converted to NO_2 via reactions such as

$$NO + HO_2 \rightarrow NO_2 + OH \tag{11.14}$$

Subsequently conversion of this NO_2 to NO occurs via

$$NO_2 + O \rightarrow NO + O_2 \tag{11.15}$$

Unless the NO_2 formed in the flame is quenched by mixing with cooler fluid. This explanation is consistent with the highest NO_2/NO ratio occurring at light load in diesels, when cooler regions which could quench the conversion back to NO are widespread.[5]

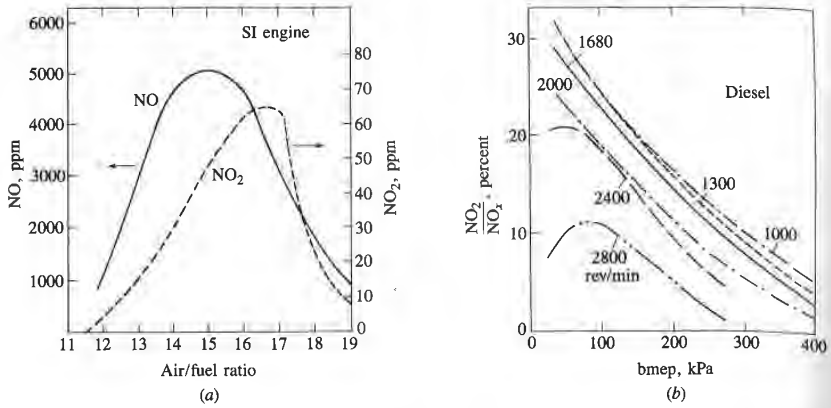

FIGURE 11-6
(*a*) NO and NO_2 concentrations in SI engine exhaust as function of air/fuel ratio, 1500 rev/min, wide-open throttle; (*b*) NO_2 as percent of total NO_x in diesel exhaust as function of load and speed.[5]

Figure 11-6 shows examples of NO and NO_2 emissions data from a spark-ignition and a diesel engine. The maximum value for the ratio (NO_2/NO) for the SI engine is 2 percent, at an equivalence ratio of about 0.85. For the diesel this ratio is higher, and is highest at light load and depends on engine speed.

It is customary to measure total oxides of nitrogen emissions, NO plus NO_2, with a chemiluminescence analyzer and call the combination NO_x. It is always important to check carefully whether specific emissions data for NO_x are given in terms of mass of NO or mass of NO_2, which have molecular weights of 30 and 46, respectively.

11.2.3 NO Formation in Spark-Ignition Engines

In conventional spark-ignition engines the fuel and air (and any recycled exhaust) are mixed together in the engine intake system, and vigorous mixing with the residual gas within the cylinder occurs during the intake process. Thus the fuel/air ratio and the amount of diluent (residual gas plus any recycled exhaust) is approximately uniform throughout the charge within the cylinder during combustion.† Since the composition is essentially uniform, the nature of the NO formation process within the cylinder can be understood by coupling the kinetic mechanism developed in Sec. 11.2.1 with the burned gas temperature distribution and pressure in the cylinder during the combustion and expansion processes. The

† It is well known that the mixture composition within the cylinder is not completely uniform and varies from one cycle to the next. Both these factors contribute to cycle-by-cycle combustion variations. For the present discussion, the assumption of mixture uniformity is adequate.

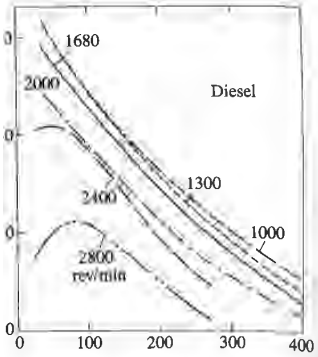

nction of air/fuel ratio, 1500 rev/min, haust as function of load and speed.[5]

$_2$ emissions data from a spark- for the ratio (NO_2/NO) for the about 0.85. For the diesel this ends on engine speed.

f nitrogen emissions, NO plus ıll the combination NO_x. It is ific emissions data for NO_x are hich have molecular weights of

nes

d air (and any recycled exhaust) and vigorous mixing with the e intake process. Thus the fuel/ s plus any recycled exhaust) is ithin the cylinder during com- form, the nature of the NO for- rstood by coupling the kinetic ed gas temperature distribution n and expansion processes. The

cylinder is not completely uniform and te to cycle-by-cycle combustion varia- niformity is adequate.

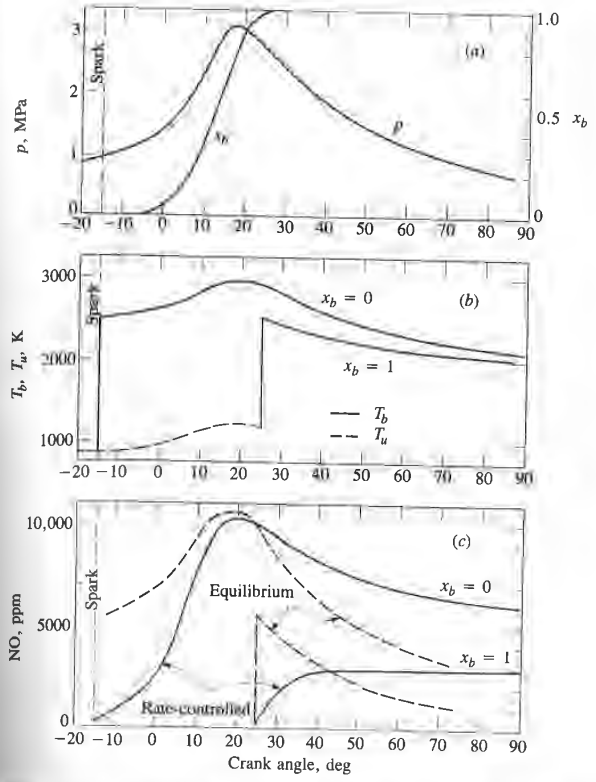

FIGURE 11-7
Illustration of SI engine NO formation model: (*a*) measured cylinder pressure p and calculated mass fraction burned x_b; (*b*) calculated temperature of unburned gas T_u and burned gas T_b in early- and late-burning elements; (*c*) calculated NO concentrations in early- and late-burning elements for rate-controlled model and at equilibrium.[7]

temperature distribution which develops in the burned gases due to the passage of the flame across the combustion chamber has been discussed in Sec. 9.2.1. Mixture which burns early is compressed to higher temperatures after combustion, as the cylinder pressure continues to rise; mixture which burns later is compressed primarily as unburned mixture and ends up after combustion at a lower burned gas temperature. Figure 11-7*a* and *b* shows measured cylinder pressure data from an operating engine, with estimates of the mass fraction burned (x_b) and the temperatures of a gas element which burned just after spark discharge and a gas element which burned at the end of the burning process. The model used to estimate these temperatures assumed no mixing between mixture elements which burn at different times. This assumption is more realistic than the

alternative idealization that the burned gases mix rapidly and are thus uniform (see Sec. 9.2.1). If the NO formation kinetic model [Eq. (11.7)] is used to calculate NO concentrations in these burned gas elements, using the equilibrium concentrations of the species O, O_2, N_2, OH, and H corresponding to the average fuel/air equivalence ratio and burned gas fraction of the mixture and these pressure and temperature profiles, the rate-limited concentration profiles in Fig. 11-7*e* are obtained. Also shown are the NO concentrations that would correspond to chemical equilibrium at these conditions. The rate-controlled concentrations rise from the residual gas NO concentration, lagging the equilibrium levels, then cross the equilibrium levels and "freeze" well above the equilibrium values corresponding to exhaust conditions. Depending on details of engine operating conditions, the rate-limited concentrations may or may not come close to equilibrium levels at peak cylinder pressure and gas temperature. Also, the amount of decomposition from peak NO levels which occurs during expansion depends on engine conditions as well as whether the mixture element burned early or late.[7]

Once the NO chemistry has frozen during the early part of the expansion stroke, integration over all elements will give the final average NO concentration in the cylinder which equals the exhaust concentration. Thus, if {NO} is the local mass fraction of NO, then the average exhaust NO mass fraction is given by

$$\{\overline{\mathrm{NO}}\} = \int_0^1 \{\mathrm{NO}\}_f \, dx_b \tag{11.16}$$

where $\{\mathrm{NO}\}_f$ is the final frozen NO mass fraction in the element of charge which burned when the mass fraction burned was x_b. Note that $\{\mathrm{NO}\} = [\mathrm{NO}]M_{\mathrm{NO}}/\rho$, where $M_{\mathrm{NO}} = 30$, the molecular weight of NO. The average exhaust concentration of NO as a mole fraction is given by

$$\tilde{x}_{\mathrm{NOav}} = \{\overline{\mathrm{NO}}\} \frac{M_{\mathrm{exh}}}{M_{\mathrm{NO}}} \tag{11.17}$$

and the exhaust concentration in ppm is $\tilde{x}_{\mathrm{NOav}} \times 10^6$. The earlier burning fractions of the charge contribute much more to the exhausted NO than do later burning fractions of the charge: frozen NO concentrations in these early-burning elements can be an order of magnitude higher than concentrations in late-burning elements. In the absence of vigorous bulk gas motion, the highest NO concentrations occur nearest the spark plug.

Substantial experimental evidence supports this description of NO formation in spark-ignition engines. The NO concentration gradient across the burned gas in the engine cylinder, due to the temperature gradient, has been demonstrated using gas sampling techniques[8,9] and using measurements of the chemiluminescent radiation from the reaction $\mathrm{NO} + \mathrm{O} \rightarrow \mathrm{NO}_2 + h\nu$ to determine the local NO concentration. Figure 11-8 shows NO concentration data as a function of crank angle, taken by Lavoie[10] through two different windows in the cylinder head of a specially constructed L-head engine where each window was a different distance from the spark plug. The stars indicate the estimated initial NO concentration that results from mixing of the residual gas with the fresh charge, at the

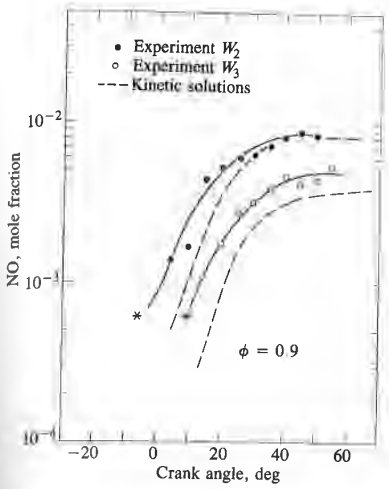

FIGURE 11-8
Spectroscopically measured NO concentrations through two windows W_3 and W_2 in special L-head SI engine (W_2 is closer to spark than W_3). The asterisks mark estimated initial conditions and flame arrival times. The dashed lines are calculated rate-limited concentrations for parts of charge burning at these flame arrival times with zero initial NO concentration.[10]

time of arrival of the flame at each window. The observed NO mole fractions rise smoothly from these initial values and then freeze about one-third of the way through the expansion process. NO levels observed at window W_2, closest to the spark plug, were substantially higher than those observed at window W_3. The dashed lines show calculated NO concentrations obtained using the NO formation kinetic model with an "unmixed" thermodynamic analysis for elements that burned at the time of flame arrival at each window. Since the calculated values started from zero NO concentration at the flame front (and not the diluted residual gas NO level indicated by the star), the calculations initially fall below the data. However, the difference between the two measurement locations and the frozen levels are predicted with reasonable accuracy. Thus, the rate-limited formation process, freezing of NO chemistry during expansion, and the existence of NO concentration gradients across the combustion chamber have all been observed.

The most important engine variables that affect NO emissions are the fuel/air equivalence ratio, the burned gas fraction of the *in-cylinder* unburned mixture, and spark timing. The burned gas fraction depends on the amount of diluent such as recycled exhaust gas (EGR) used for NO_x emissions control, as well as the residual gas fraction. Fuel properties will affect burned gas conditions; the effect of normal variations in gasoline properties is modest, however. The effect of variations in these parameters can be explained with the NO formation mechanism described above: changes in the time history of temperature and oxygen concentration in the burned gases during the combustion process and early part of the expansion stroke are the important factors.[11]

EQUIVALENCE RATIO. Figure 11-9 shows the effect of variations in the fuel/air equivalence ratio on NO emissions. Maximum burned gas temperatures occur at

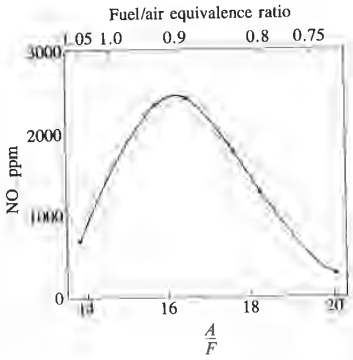

FIGURE 11-9
Variation of exhaust NO concentration with A/F and fuel/air equivalence ratio. Spark-ignition engine, 1600 rev/min, η_v = 50 percent, MBT timing.[12]

$\phi \approx 1.1$; however, at this equivalence ratio oxygen concentrations are low. As the mixture is enriched, burned gas temperatures fall. As the mixture is leaned out, increasing oxygen concentration initially offsets the falling gas temperatures and NO emissions peak at $\phi \approx 0.9$. Detailed predictions of NO concentrations in the burned gases suggest that the concentration versus time histories under fuel-lean conditions are different in character from those for fuel-rich conditions. In lean mixtures NO concentrations freeze early in the expansion process and little NO decomposition occurs. In rich mixtures, substantial NO decomposition occurs from the peak concentrations present when the cylinder pressure is a maximum. Thus in lean mixtures, gas conditions at the time of peak pressure are especially significant.[7]

BURNED GAS FRACTION. The unburned mixture in the cylinder contains fuel vapor, air, and burned gases. The burned gases are residual gas from the previous cycle and any exhaust gas recycled to the intake for NO_x emissions control. The residual gas fraction is influenced by load, valve timing (especially the extent of valve overlap), and, to a lesser degree, by speed, air/fuel ratio, and compression ratio as described in Sec. 6.4. The burned gases act as a diluent in the unburned mixture; the absolute temperature reached after combustion varies inversely with the burned gas mass fraction. Hence increasing the burned gas fraction reduces NO emissions levels. However, it also reduces the combustion rate and, therefore, makes stable combustion more difficult to achieve (see Secs. 9.3 and 9.4).

Figure 11-10 shows the effect of increasing the burned gas fraction by recycling exhaust gases to the intake system just below the throttle plate. Substantial reductions in NO concentrations are achieved with 15 to 25 percent EGR, which is about the maximum amount of EGR the engine will tolerate under normal part-throttle conditions. Of course, increasing the EGR at fixed engine load and speed increases the inlet manifold pressure, while fuel flow and air flow remain approximately constant.

The primary effect of the burned gas diluent in the unburned mixture on the NO formation process is that it reduces flame temperatures by increasing the

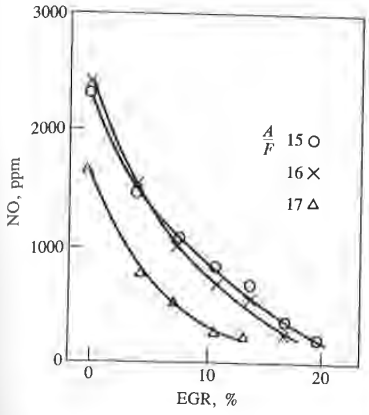

FIGURE 11-10
Variation of exhaust NO concentration with percent recycled exhaust gas (EGR). Spark-ignition engine, 1600 rev/min, $\eta_v = 50$ percent, MBT timing.[12]

NO concentration with A/F and
atio. Spark-ignition engine, 1600
nt, MBT timing.[12]

ncentrations are low. As the
the mixture is leaned out,
alling gas temperatures and
of NO concentrations in the
me histories under fuel-lean
fuel-rich conditions. In lean
nsion process and little NO
NO decomposition occurs
der pressure is a maximum.
peak pressure are especially

n the cylinder contains fuel
sidual gas from the previous
NO_x emissions control. The
ing (especially the extent of
/fuel ratio, and compression
is a diluent in the unburned
bustion varies inversely with
burned gas fraction reduces
nbustion rate and, therefore,
e Secs. 9.3 and 9.4).
burned gas fraction by recy-
he throttle plate. Substantial
5 to 25 percent EGR, which
will tolerate under normal
GR at fixed engine load and
el flow and air flow remain

the unburned mixture on the
peratures by increasing the

heat capacity of the cylinder charge, per unit mass of fuel. Figure 11-11 shows the effect of different diluent gases added to the engine intake flow, in a single-cylinder engine operated at constant speed, fuel flow, and air flow.[13] The data in Fig. 11-11*a* show that equal volume percentages of the different diluents produce different reductions in NO emissions. The same data when plotted against diluent heat capacity (diluent mass flow rate × specific heat, c_p) collapse to a single

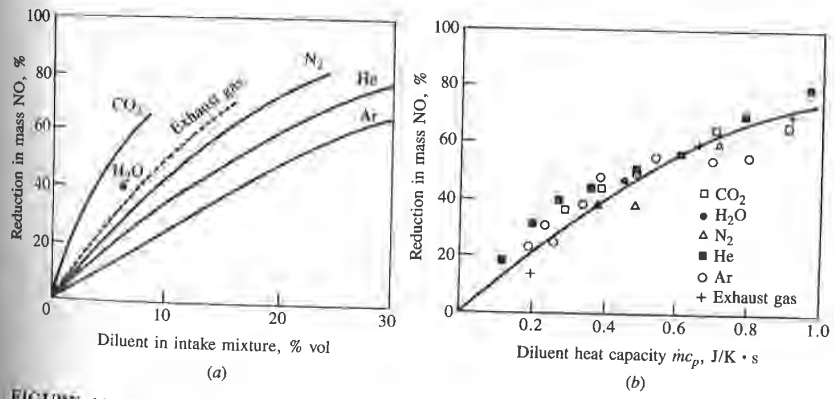

FIGURE 11-11
(*a*) Percentage reduction in mass NO emissions with various diluents. (*b*) Correlation of NO reduction with diluent heat capacity. Spark-ignition engine operated at 1600 rev/min, constant brake load (intake pressure ~0.5 atm), with MBT spark timing.[13]

curve.† A similiar study where the burned gas fraction in the unburned charge was varied by changing the valve overlap, compression ratio, and EGR, separately, showed that, under more realistic engine operating conditions, it is the heat capacity of the total diluent mass in the in-cylinder mixture that is important. Whether the diluent mass is changed by varying the valve overlap, EGR, or even the compression ratio is not important.[14]

EXCESS AIR AND EGR. Because of the above, it is possible to correlate the influence of engine operating variables (such as air/fuel ratio, engine speed, and load) and design variables (such as valve timing and compression ratio) on NO emissions with two parameters which define the in-cylinder mixture composition: the fuel/air equivalence ratio (often the air/fuel ratio is used instead) and the gas/fuel ratio. The gas/fuel ratio (G/F) is given by

$$\frac{G}{F} = \frac{\text{total mass in cylinder}}{\text{fuel mass in cylinder}} = \frac{A}{F}\left(1 + \frac{x_b}{1 - x_b}\right) \tag{11.18}$$

where x_b is the burned gas fraction [Eq. (4.3)]. These together define the relative proportions of fuel, air, and burned gases in the in-cylinder mixture, and hence

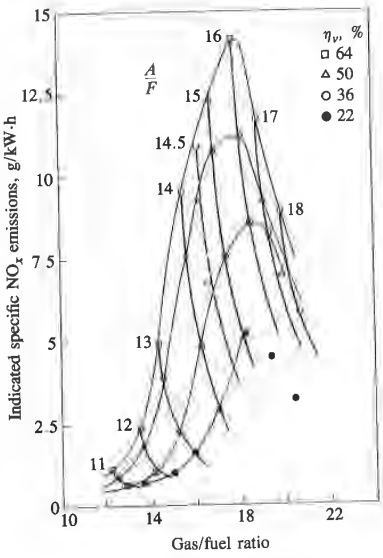

FIGURE 11-12
Correlation between gas/fuel ratio (G/F) and indicated specific NO_x emissions at various air/fuel ratios (A/F) and volumetric efficiencies (η_v). Spark-ignition engine operated at 1400 rev/min with spark timing retarded to give 0.95 of maximum brake torque.[15]

† Some of the scatter in Fig. 11-11 is due to the fact that the residual gas fraction is slightly different for each diluent.

will correlate NO emissions.† Figure 11-12 shows the correlation of specific NO emissions, from a four-cylinder engine, over a wide range of engine operating conditions with the air/fuel ratio and gas/fuel ratio. Lines of constant air/fuel ratio and volumetric efficiency are shown; the direction of increasing dilution with residual gas and EGR at constant air/fuel ratio is to the right. Excessive dilution results in poor combustion quality, partial burning, and, eventually, misfire (see Sec. 9.4.3). Lowest NO emissions consistent with good fuel consumption (avoiding the use of rich mixtures) are obtained with a stoichiometric mixture, with as much dilution as the engine will tolerate without excessive deterioration in combustion quality.[15]

Comparisons between predictions made with the NO formation model (described at the beginning of this section) and experimental data show good agreement with normal amounts of dilution.[16] With extreme dilution, at NO levels of about 100 ppm or less, the NO formed within the flame reaction zone cannot, apparently, be neglected. Within the flame, the concentrations of radicals such as O, OH, and H can be substantially in excess of equilibrium levels, resulting in much higher formation rates within the flame than in the postflame gases. It is believed that the mechanism [reactions (11.1) to (11.3)] and the formation rate equation (11.6) are valid. However, neglecting flame-front-formed NO is no longer an appropriate assumption.[17]

SPARK TIMING. Spark timing significantly affects NO emission levels. Advancing the timing so that combustion occurs earlier in the cycle increases the peak cylinder pressure (because more fuel is burned before TC and the peak pressure moves closer to TC where the cylinder volume is smaller); retarding the timing decreases the peak cylinder pressure (because more of the fuel burns after TC). Higher peak cylinder pressures result in higher peak burned gas temperatures, and hence higher NO formation rates. For lower peak cylinder pressures, lower NO formation rates result. Figure 11-13 shows typical NO emission data for a spark-ignition engine as a function of spark timing. NO emission levels steadily decrease as spark timing is retarded from MBT timing and moved closer to TC. Since exact determination of MBT timing is difficult (and not critical for fuel consumption and power where the variation with timing around MBT is modest), there is always considerable uncertainty in NO emissions at MBT timing. Often, therefore, an alternative reference timing is used, where spark is retarded from MBT timing to the point where torque is decreased by 1 or 2 percent from the maximum value. Great care with spark timing is necessary to obtain accurate NO emissions measurements under MBT-timing operating conditions.

† Spark timing also affects NO emissions, as discussed next. The above discussion relates to engines run with timing at MBT or with torque at a fixed percentage of (and close to) the maximum.

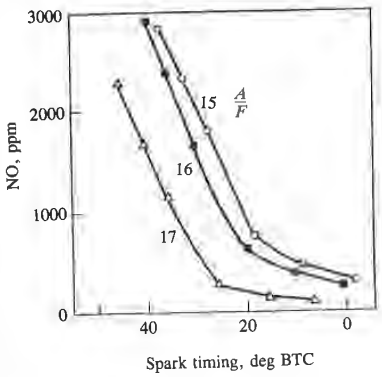

FIGURE 11-13
Variation of exhaust NO concentration with spark retard. 1600 rev/min, $\eta_v = 50$ percent; left-hand end of curve corresponds to MBT timing for each A/F.[12]

11.2.4 NO_x Formation in Compression-Ignition Engines

The kinetic mechanisms for NO and NO_2 formation described in Secs. 11.2.1 and 11.2.2 and the assumptions made regarding equilibration of species in the C—O—H system apply to diesels as well as to spark-ignition engines. The critical difference, of course, is that injection of fuel into the cylinder occurs just before combustion starts, and that nonuniform burned gas temperature and composition result from this nonuniform fuel distribution during combustion. The fuel-air mixing and combustion processes are extremely complex. During the "premixed" or uncontrolled diesel combustion phase immediately following the ignition delay, fuel-air mixture with a spread in composition about stoichiometric burns due to spontaneous ignition and flame propagation. During the mixing controlled combustion phase, the burning mixture is likely to be closer to stoichiometric (the flame structure is that of a turbulent, though unsteady, diffusion flame). However, throughout the combustion process mixing between already burned gases, air, and lean and rich unburned fuel vapor–air mixture occurs, changing the composition of any gas elements that burned at a particular equivalence ratio. In addition to these composition (and hence temperature) changes due to mixing, temperature changes due to compression and expansion occur as the cylinder pressure rises and falls.

The discussion in Sec. 11.2.1 showed that the critical equivalence ratio for NO formation in high-temperature high-pressure burned gases typical of engines is close to stoichiometric. Figure 11-4 is relevant here: it shows the initial NO formation rate in combustion products formed by burning a mixture of a typical hydrocarbon fuel with air (initially at 700 K, at a constant pressure of 15 atm). NO formation rates are within a factor of 2 of the maximum value for $0.85 \lesssim \phi \lesssim 1.1$

The critical time period is when burned gas temperatures are at a maximum i.e., between the start of combustion and shortly after the occurrence of peak cylinder pressure. Mixture which burns early in the combustion process

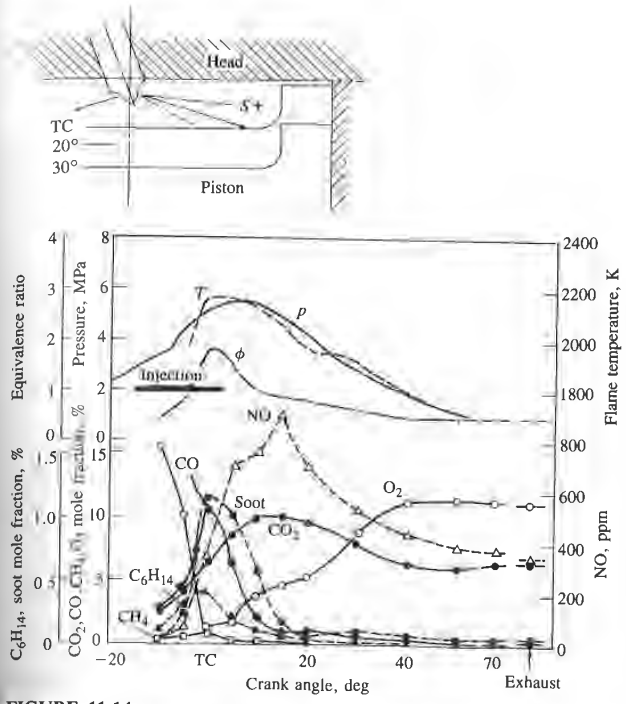

FIGURE 11-14
Concentrations of soot, NO, and other combustion product species measured at outer edge of bowl-in-piston combustion chamber (location *S*) of quiescent DI diesel with rapid sampling valve. Cylinder gas pressure p, mean temperature T, and local equivalence ratio ϕ shown. Bore = 95 mm, stroke = 110 mm, r_c = 14.6. Four-hole nozzle with hole diameter = 0.2 mm.[18]

is especially important since it is compressed to a higher temperature, increasing the NO formation rate, as combustion proceeds and cylinder pressure increases. After the time of peak pressure, burned gas temperatures decrease as the cylinder gases expand. The decreasing temperature due to expansion *and* due to mixing of high-temperature gas with air or cooler burned gas freezes the NO chemistry. This second effect (which occurs only in the diesel) means that freezing occurs more rapidly in the diesel than in the spark-ignition engine, and much less decomposition of the NO occurs.

The above description is supported by the NO concentration data obtained from experiments where gas was sampled from within the cylinder of normally operating diesel engines with special gas-sampling valves and analyzed. Figure 11-14 shows time histories of major species concentrations, through the combustion process, determined with a rapid-acting sampling valve (1 ms open time) in a quiescent *direct-injection diesel* engine. Concentrations at different positions in the combustion chamber were obtained; the sample valve location for the Fig.

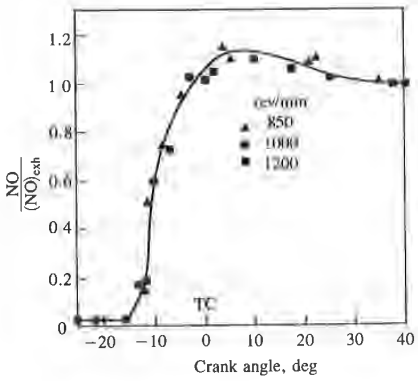

FIGURE 11-15
Ratio of cylinder-average NO concentration at given crank angle (determined from cylinder-dumping experiments) to exhaust NO concentration. DI diesel, equivalence ratio = 0.6, injection timing at 27° BTC.[19]

11-14 data is shown. Local NO concentrations rise from the residual gas value following the start of combustion, to a peak at the point where the local burned gas equivalence ratio changes from rich to lean (where the CO_2 concentration has its maximum value). As the local burned gas equivalence ratio becomes leaner due to mixing with excess air, NO concentrations decrease since formation becomes much slower as dilution occurs. At the time of peak NO concentrations within the bowl (15° ATC), most of the bowl region was filled with flame. The total amount of NO within the cylinder of this type of direct-injection diesel during the NO formation process has also been measured.[19] At a predetermined time in one cycle, once steady-state warmed-up engine operation had been achieved, the contents of the cylinder were dumped into an evacuated tank by rapidly cutting open a diaphragm which had previously sealed off the tank system. Figure 11-15 shows how the ratio of the average cylinder NO concentration divided by the exhaust concentration varies during the combustion process. NO concentrations reach a maximum shortly after the time of peak pressure. There is a modest amount of NO decomposition. Variations in engine speed have little effect on the shape of this curve. The 20 crank angle degrees after the start of combustion is the critical time period.

Results from similar cylinder-dumping experiments where injection timing and load (defined by the overall equivalence ratio) were varied also showed that almost all of the NO forms within the 20° following the start of combustion. As injection timing is retarded, so the combustion process is retarded; NO formation occurs later, and concentrations are lower since peak temperatures are lower. The effect of the overall equivalence ratio on NO_x concentrations is shown in Fig. 11-16. At high load, with higher peak pressures, and hence temperatures, and larger regions of close-to-stoichiometric burned gas, NO levels increase. Both NO and NO_x concentrations were measured; NO_2 is 10 to 20 percent of total NO_x. Though NO levels decrease with a decreasing overall equivalence ratio, they do so much less rapidly than do spark-ignition engine NO emissions (see Fig. 11-9) due to the nonuniform fuel distribution in the diesel. Though the

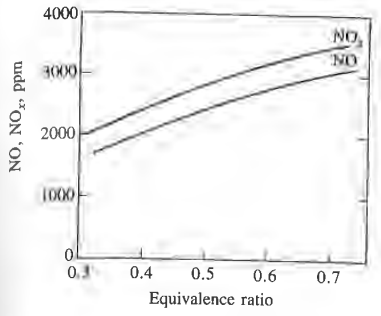

FIGURE 11-16
Exhaust NO_x and NO concentrations as a function of overall equivalence ratio or engine load. DI diesel, 1000 rev/min, injection timing at 27° BTC.[19]

amount of fuel injected decreases proportionally as the overall equivalence ratio is decreased, much of the fuel still burns close to stoichiometric. Thus NO emissions should be roughly proportional to the mass of fuel injected (provided burned gas pressures and temperatures do not change greatly).

Similar gas-sampling studies have been done with *indirect-injection* diesel engines. Modeling studies suggest that most of the NO forms within the prechamber and is then transported into the main chamber where the reactions freeze as rapid mixing with air occurs. However, the prechamber, except at light load, operates rich overall so some additional NO can form as the rich combustion products are diluted through the stoichiometric composition.[20] Figure 11-17 shows local NO concentrations and equivalence ratios as a function of crank angle determined with a rapid-acting sampling valve at different locations

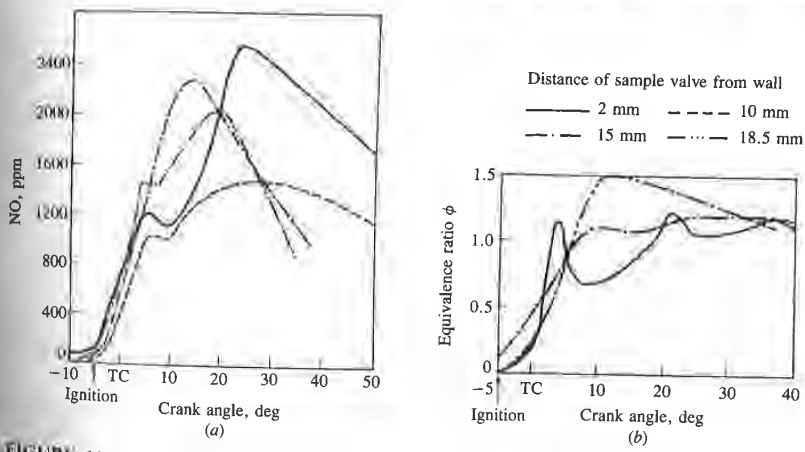

FIGURE 11-17
(*a*) NO concentrations measured with rapid sampling valve and (*b*) calculated equivalence ratios at different distances from the wall in swirl chamber of IDI diesel engine, as function of crank angle. Engine speed = 1000 rev/min, injection at 13° BTC, ignition at 5° BTC.[21]

within the prechamber of a Comet swirl chamber IDI engine.[21] The gas mixture rapidly becomes stoichiometric or fuel-rich. Composition nonuniformities across the prechamber are substantial. Peak NO concentrations, as expected, correspond approximately to locally stoichiometric regions. Because the mixture remains fuel-rich in the prechamber as the burned gases expand (after the time of peak pressure which occurs between 6 and 10° ATC), substantial NO decomposition within the prechamber can occur. However, by this time much of the gas (and NO) in the prechamber has been transferred to the main chamber where freezing of the NO chemistry will occur. Cylinder-gas dumping experiments, where both main chamber and prechamber gases were dumped and quenched, confirm this description. Cylinder average NO concentrations, determined by rapidly opening a diaphram which separated the engine cylinder from an evacuated tank at predetermined points in the cycle of an otherwise normally operated IDI engine, rise rapidly once combustion starts, until the NO chemistry is effectively frozen at about 15° ATC. Little net NO decomposition occurs.[12] Heat-release-rate diagrams obtained from pressure data analysis for the same IDI engine indicate that combustion is only about one-half complete at the time the NO formation process ceases.

Diluents added to the intake air (such as recycled exhaust) are effective at reducing the NO formation rate, and therefore NO_x exhaust emissions. As with spark-ignition engines, the effect is primarily one of reducing the burned gas temperature for a given mass of fuel and oxygen burned. Figure 11-18 shows the effect of dilution of the intake air with N_2, CO_2, and exhaust gas on NO_x exhaust levels.[23] The heat capacity of CO_2 (per mole) at the temperatures relevant to diesel combustion is about twice that of N_2. That of exhaust gas is slightly higher than that of N_2. Therefore these data show that the effect is primarily one of reduced burned gas temperatures. Note that the composition of the exhaust gas of a diesel varies with load. At idle, there is little CO_2 and H_2O, and the composition does not differ much from that of air. At high load the heat

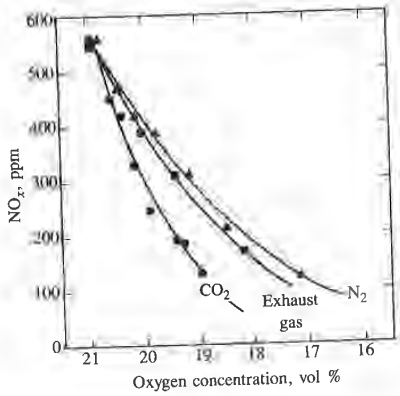

FIGURE 11-18
Effect of reduction in oxygen concentration by different diluents (exhaust gas, CO_2, N_2) on NO_x emissions in DI diesel. Bore = 140 mm, stroke = 152 mm, $r_c = 14.3$. Speed = 1300 rev/min, fuel rate = 142 mm^3/stroke, injection timing at 4° BTC.[23]

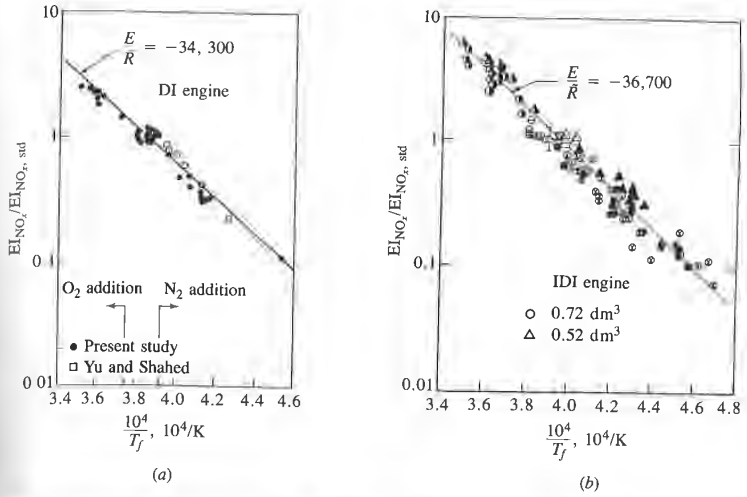

FIGURE 11-19
Correlation of NO_x emissions index EI_{NO_x} for a wide range of operating conditions with reciprocal of stoichiometric mixture flame temperature for: (*a*) DI engines; (*b*) IDI engines. Flame temperatures varied by addition of different diluents and oxygen.[25,26] Values of EI_{NO_x} normalized with value at standard conditions.

capacity increases as the concentrations of CO_2 and H_2O are substantially higher. Similar studies in an *indirect-injection* engine show comparable trends. Addition of diluents [exhaust gas (EGR) and nitrogen] reduce peak flame temperatures and NO_x emissions; also, addition of oxygen (which corresponds to a *reduction* in diluent fraction) increases flame temperatures and therefore increases NO_x emissions.[24]

Confirmation that NO forms in the close-to-stoichiometric burned gas regions and the magnitude of the stoichiometric burned gas temperature controls NO_x emissions is given by the following. Plee *et al.*[25,26] have shown that the effects of changes in intake gas composition (with EGR, nitrogen, argon, and oxygen addition) and temperature on NO_x emissions can be correlated by

$$EI_{NO_x} = \text{constant} \times \exp\left(\frac{E}{\tilde{R}T_f}\right) \tag{11.19}$$

T_f(kelvin) is the stoichiometric adiabatic flame temperature (evaluated at a suitable reference point: fuel-air mixture at top-center pressure and air temperature) and E is an overall activation energy. Figure 11-19 shows EI_{NO_x} for a range of intake air compositions and temperatures, and two DI and two IDI engines for several loads and speeds, normalized by the engine NO_x level obtained for standard air, plotted on a log scale against the reciprocal of the stoichiometric adiabatic flame at TC conditions. A single value of $E/\tilde{R}$ correlates the data over two

orders of magnitude. There is, of course, some scatter since the model used is overly simple, and load, speed, and other engine design and operating parameters affect the process. The overriding importance of the burned gas temperature of close-to-stoichiometric mixture is clear, however.

11.3 CARBON MONOXIDE

Carbon monoxide (CO) emissions from internal combustion engines are controlled primarily by the fuel/air equivalence ratio. Figure 11-20 shows CO levels in the exhaust of a conventional spark-ignition engine for several different fuel compositions.[27] When the data are plotted against the relative air/fuel ratio or the equivalence ratio, they are correlated by a single curve. For fuel-rich mixtures CO concentrations in the exhaust increase steadily with increasing equivalence ratio, as the amount of excess fuel increases. For fuel-lean mixtures, CO concentrations in the exhaust vary little with equivalence ratio and are of order 10^{-3} mole fraction.

Since spark-ignition engines often operate close to stoichiometric at part load and fuel rich at full load (see Sec. 7.1), CO emissions are significant and must be controlled. Diesels, however, always operate well on the lean side of stoichiometric; CO emissions from diesels are low enough to be unimportant, therefore, and will not be discussed further.

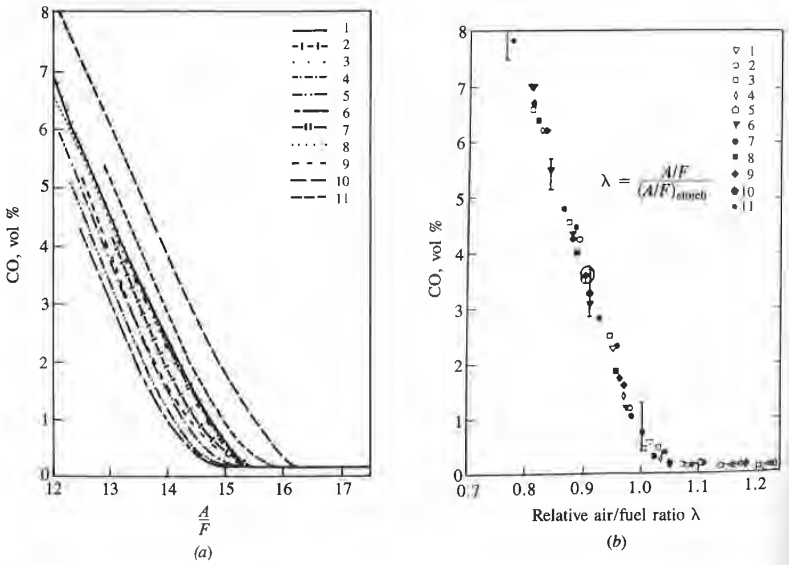

FIGURE 11-20
Variation of SI engine CO emissions with eleven fuels of different H/C ratio: (*a*) with air/fuel ratio; (*b*) with relative air/fuel ratio λ.[27]

atter since the model used is
sign and operating parameters
the burned gas temperature

combustion engines are con-
Figure 11-20 shows CO levels
ıgine for several different fuel
ɜt the relative air/fuel ratio or
e curve. For fuel-rich mixtures
ly with increasing equivalence
uel-lean mixtures, CO concen-
e ratio and are of order 10^{-3}

:lose to stoichiometric at part
ssions are significant and must
:ll on the lean side of stoichio-
ı to be unimportant, therefore,

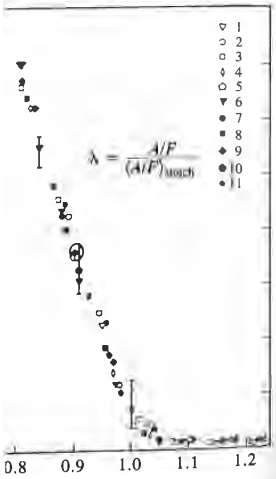

(b)

ɜnt H/C ratio: (*a*) with air/fuel ratio; (*b*)

The levels of CO observed in spark-ignition engine exhaust gases are lower than the maximum values measured within the combustion chamber, but are significantly higher than equilibrium values for the exhaust conditions. Thus the processes which govern CO exhaust levels are kinetically controlled. In premixed hydrocarbon-air flames, the CO concentration increases rapidly in the flame zone to a maximum value, which is larger than the equilibrium value for adiabatic combustion of the fuel-air mixture. CO formation is one of the principal reaction steps in the hydrocarbon combustion mechanism, which may be summarized by[1]

$$RH \rightarrow R \rightarrow RO_2 \rightarrow RCHO \rightarrow RCO \rightarrow CO \tag{11.20}$$

where R stands for the hydrocarbon radical. The CO formed in the combustion process via this path is then oxidized to CO_2 at a slower rate. The principal CO oxidation reaction in hydrocarbon-air flames is

$$CO + OH = CO_2 + H \tag{11.21}$$

The rate constant for this reaction is[1]

$$k_{CO}^{+} = 6.76 \times 10^{10} \exp\left(\frac{T}{1102}\right) \quad \text{cm}^3/\text{gmol} \tag{11.22}$$

It is generally assumed that in the postflame combustion products in a spark-ignition engine, at conditions close to peak cycle temperatures (2800 K) and pressures (15 to 40 atm), the carbon-oxygen-hydrogen system is equilibrated. Thus CO concentrations in the immediate postflame burned gases are close to equilibrium. However, as the burned gases cool during the expansion and exhaust strokes, depending on the temperature and cooling rate, the CO oxidation process [reaction (11.21)] may not remain locally equilibrated.

Newhall carried out a series of kinetic calculations for an engine expansion stroke assuming the burned gas at the time of peak cylinder pressure was uniform and in equilibrium.[28] Of the reactions important to CO chemistry, only three-body radical-recombination reactions such as

$$H + H + M = H_2 + M \tag{11.23}$$

$$H + OH + M = H_2O + M \tag{11.24}$$

$$H + O_2 + M = HO_2 + M \tag{11.25}$$

were found to be rate controlling. The bimolecular exchange reactions and the CO oxidation reaction (11.21) were sufficiently fast to be continuously equilibrated. Only during the later stages of the expansion stroke was the CO concentration predicted to depart from equilibrium, as shown in Fig. 11-21. Using this technique to predict average CO levels at the end of expansion over a range of equivalence ratios (rich to lean), Newhall obtained a good match to experimental data (see Fig. 11-22). The kinetically controlled aspects of the CO emissions mechanism have thus been confirmed.

These calculations showed that a partial equilibrium amongst the bimolecular exchange reactions occurred *a posteriori*. Analyses based explicitly on this partial equilibrium assumption (which are considerably simpler) have been

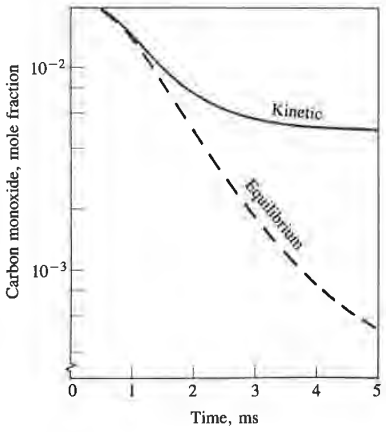

FIGURE 11-21
Results of kinetic calculations of CO concentrations during expansion stroke following TC combustion in SI engine; stoichiometric mixture.[28]

carried out.[29, 30] The appropriate three-body atom and radical recombination reactions [e.g., (11.23) to (11.25)] were treated as the rate-limiting constraint on the total number of particles or moles per unit volume of burnt gases, i.e.,

$$\left(\frac{1}{V}\right)\frac{dn}{dt} = \sum_{i=1}^{k}(R_i^- - R_i^+) \tag{11.26}$$

V is the volume of the elemental system considered, n is the total number of moles, R_i^+ and R_i^- are the forward and backward rates for reaction i, and k represents the number of three-body recombination reactions included. All other

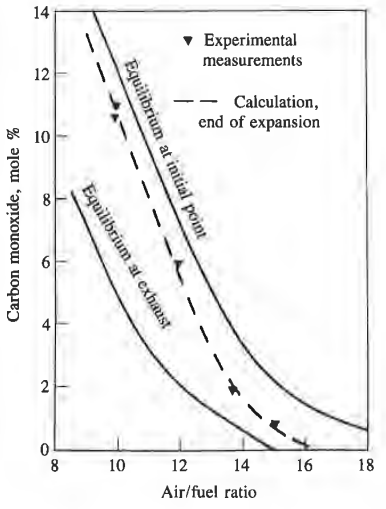

FIGURE 11-22
Predicted CO concentration at end of expansion stroke, compared with measured exhaust concentrations, as function of air/fuel ratio. Equilibrium levels at TC combustion and exhaust conditions also shown.[28]

reactions were assumed to be equilibrated. The studies using this simplified kinetic model have confirmed that at peak cylinder pressures and temperatures, equilibration times for CO are faster than times characteristic of changes in burnt gas conditions due to compression or expansion. Thus the CO concentration rapidly equilibrates in the burnt gases just downstream of the reaction zone following combustion of the hydrocarbon fuel. However, it has already been pointed out in Sec. 9.2.1 that the burnt gases are not uniform in temperature. Also, the blowdown of cylinder pressure to the exhaust manifold level during the exhaust process and the decrease in gas temperature that accompanies it occupies a substantial portion of the cycle—about 60 crank angle degrees. Thus, the temperature- and pressure-time profiles of parts of the charge at different locations throughout the cylinder differ, depending on when these parts of the charge burn and when they exit the cylinder through the exhaust valve and enter the exhaust manifold.

The results of an idealized calculation which illustrate these effects are shown in Fig. 11-23. The CO mole fractions in different elements or parts of the burnt gas mixture are plotted versus crank angle; x_b is the fraction of the total charge which had burned when each element shown burned; z is the mass fraction which had left the cylinder at the time each element left the cylinder. The partial equilibrium calculations show the burned gases are close to equilibrium until about 60 crank angle degrees after top-center. During the exhaust blowdown process after the exhaust valve opens, gas which leaves the cylinder early

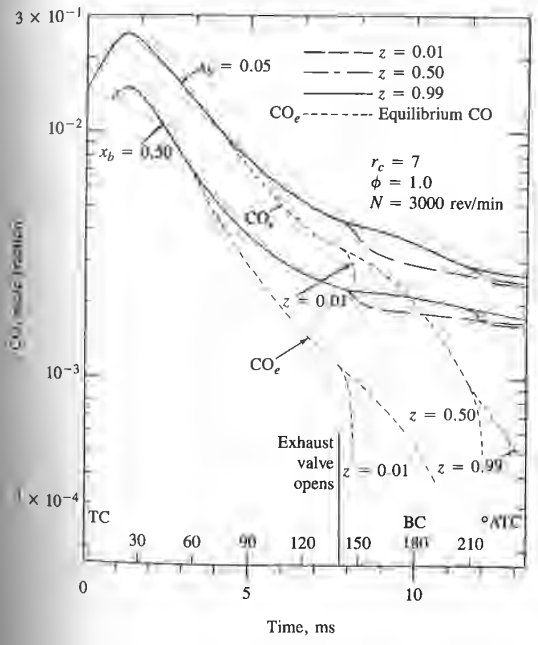

FIGURE 11-23
CO concentrations in selected elements of SI engine cylinder charge, which burn at different times and which exit the cylinder at different times. x_b is mass fraction burned when element burned. z is fraction of gas which has already left cylinder during exhaust process prior to element leaving cylinder. Speed = 3000 rev/min, $r_c = 7$, equivalence ratio = 1.0.[30]

($z \ll 1$) cools more rapidly than gas which leaves late ($z \approx 1$). In these calculations, mixing between gas elements which burn at different times was neglected. It can be seen that a CO gradient exists across the burned gases and that the CO concentration in the exhaust gases is unlikely to be uniform. Experiments with single-cylinder engines support these conclusions that CO is in equilibrium during the combustion process but deviates from equilibrium late in the expansion stroke (e.g., see Refs. 10 and 31).

Conclusions from these detailed studies are as follows. The measured average exhaust CO concentrations for fuel-rich mixtures are close to equilibrium concentrations in the burned gases during the expansion process. For close-to-stoichiometric mixtures, the partial equilibrium CO predictions are in agreement with measurements and are orders of magnitude above CO equilibrium concentrations corresponding to exhaust conditions. For fuel-lean mixtures, measured CO emissions are substantially higher than predictions from any of the models based on kinetically controlled bulk gas phenomena. One possible explanation of this lean-mixture discrepancy is that only partial oxidation to CO may occur of some of the unburned hydrocarbons emerging during expansion and exhaust from crevices in the combustion chamber and from any oil layers or deposits on the chamber walls.

While many questions about details of the CO oxidation mechanisms remain, as a practical matter exhaust emissions are determined by the fuel/air equivalence ratio. The degree of control achieved within the engine to date has come from improving mixture uniformity and leaning-out the intake mixture. In multicylinder engines, because CO increases rapidly as the inlet mixture becomes richer than stoichiometric, cylinder-to-cylinder variations in equivalence ratio about the mean value are important; nonuniform distribution can significantly increase average emissions. Thus improved cylinder-to-cylinder fuel/air ratio distribution has become essential. Also, because it is necessary to enrich the fuel-air mixture when the engine is cold, CO emissions during engine warm-up are much higher than emissions in the fully warmed-up state. Further, in transient engine operation during acceleration and deceleration, control of fuel metering has had to be improved. Additional reductions in CO beyond what can be achieved in the engine are possible with exhaust treatment devices, which are reviewed in Sec. 11.6. Oxidation of CO in the exhaust system without use of special exhaust treatment devices does not occur to any significant degree because the exhaust gas temperature is too low (Fig. 11-23 shows that the CO oxidation reactions effectively freeze as the gas passes through the exhaust valve).

11.4 UNBURNED HYDROCARBON EMISSIONS

11.4.1 Background

Hydrocarbons, or more appropriately organic emissions, are the consequence of incomplete combustion of the hydrocarbon fuel. The level of unburned hydrocarbons (HC) in the exhaust gases is generally specified in terms of the total hydro-

TABLE 11.4
Hydrocarbon composition of spark-ignition engine exhaust (by class)[33]

	Carbon, percent of total HC			
	Paraffins	Olefins	Acetylene	Aromatics
Without catalyst	33	27	8	32
With catalyst	57	15	2	26

carbon concentration expressed in parts per million carbon atoms (C_1).† While total hydrocarbon emission is a useful measure of combustion inefficiency, it is not necessarily a significant index of pollutant emissions. Engine exhaust gases contain a wide variety of hydrocarbon compounds. Table 11.4 shows the average breakdown by class of the hydrocarbons in spark-ignition engine exhaust gases, both with and without a catalytic converter, with gasoline fuel. Some of these hydrocarbons are nearly inert physiologically and are virtually unreactive from the standpoint of photochemical smog. Others are highly reactive in the smog-producing chemistry. (Some hydrocarbons are known carcinogens; see Sec. 11.5.2). Based on their potential for oxidant formation in the photochemical smog chemistry, hydrocarbon compounds are divided into nonreactive and reactive categories. Table 11.5 shows one reactivity scale which has been used to estimate the overall reactivity of exhaust gas hydrocarbon mixtures. Other scales are used for the same purpose.[34] Scales that assign high values for reactivity to the olefins (like Table 11.5), which react most rapidly in the photochemical smog reaction, probably best approximate smog-formation potential near the sources of hydrocarbon pollution. The simplest scale, which divides the HC into two classes—methane and nonmethane hydrocarbons—probably best approximates the end result for all HC emissions. All hydrocarbons except methane react, given enough time. More detailed breakdowns of the composition of spark-ignition and diesel engine exhaust HC are available in the literature.[33, 35]

Fuel composition can significantly influence the composition and magnitude of the organic emissions. Fuels containing high proportions of aromatics and olefins produce relatively higher concentrations of reactive hydrocarbons. However, many of the organic compounds found in the exhaust are not present

† This is because the standard detection instrument, a flame ionization detector (FID), is effectively a carbon atom counter, e.g., one propane molecule generates three times the response generated by one methane molecule. Some data in the literature are presented as ppm propane (C_3), or ppm hexane (C_6); to convert to ppm C_1 multiply by 3 or by 6, respectively. Older measurements of hydrocarbon emissions were made with nondispersive infrared (NDIR) detectors which had different sensitivities for the different hydrocarbon compounds. For gasoline-fueled engines, HC emissions determined by FID analyzers are about twice the levels determined by NDIR analyzers,[32] though this scaling is not exact.

TABLE 11.5
Reactivity of classes of hydrocarbons

Hydrocarbons	Relative reactivity†
C_1–C_4 paraffins Acetylene Benzene	0
C_4 and higher molecular weight paraffins Monoalkyl benzenes *Ortho*- and *para*-dialkyl benzenes Cyclic paraffins	2
Ethylene *Meta*-dialkyl benzenes Aldehydes	5
1-Olefins (except ethylene) Diolefins Tri- and tetraalkyl benzenes	10
Internally bonded olefins	30
Internally bonded olefins with substitution at the double bond Cycloolefins	100

† General Motors Reactivity Scale (0–100). Based on the NO_2 formation rate for the hydrocarbon relative to the NO_2 formation rate for 2,3-dimethyl-2-benzene.[34]

in the fuel, indicating that significant pyrolysis and synthesis occur during the combustion process.

Oxygenates are present in engine exhaust, and are known to participate in the formation of photochemical smog. Some oxygenates are also irritants and odorants. The oxygenates are generally categorized as carbonyls, phenols, and other noncarbonyls. The carbonyls of interest are low molecular weight aldehydes and aliphatic ketones. The volatile aldehydes are eye and respiratory tract irritants. Formaldehyde is a major component ($\lesssim$20 percent of total carbonyls). Carbonyls account for about 10 percent of the HC emissions from diesel passenger car engines, but only a few percent of spark-ignition engine HC emissions. Phenols are odorants and irritants: levels are much lower than aldehyde levels. Other noncarbonyls include methanol, ethanol, nitromethane, methyl formate. Whether these are significant with conventional hydrocarbon fuels is unclear.[35] Use of alcohol fuels increases oxygenate emissions. Both methanol and aldehyde emissions increase substantially above gasoline-fueled levels with methanol-fueled spark-ignition engines.

11.4.2 Flame Quenching and Oxidation Fundamentals

Flame quenching or extinction occurs at the walls of engine combustion chambers. The cool walls of the chamber act as a sink for heat and the active radical species generated within the flame. Quenching of the flame occurs under several different geometrical configurations: the flame may be propagating normal to, parallel to, or at an angle to the wall; the flame may quench at the entrance to a crevice—a thin volume with a narrow entrance to the combustion chamber such as the region between the piston crown and the cylinder wall. When the flame quenches, it leaves a layer or volume of unburned mixture ahead of the flame. (Whether this results in unburned hydrocarbon emissions depends on the extent to which these quench region hydrocarbons can subsequently be oxidized.)

Flame-quenching processes are analyzed by relating the heat release within the flame to the heat loss to the walls under conditions where quenching just occurs. This ratio, a Peclet number (Pe), is approximately constant for any given geometrical configuration. The simplest configuration for study is the two-plate quench process, where the minimum spacing between two parallel plates through which a flame will propagate is determined. The Peclet number for this two-plate configuration is given by:

$$\mathrm{Pe}_2 = \frac{\rho_u S_L c_{p,f}(T_f - T_u)}{k_f(T_f - T_u)/d_{q2}} = \frac{\rho_u S_L c_{p,f} d_{q2}}{k_f} \tag{11.27}$$

which is approximately constant over a wide range of conditions. ρ, S_L, c_p, T, and k are the density, laminar flame speed, specific heat at constant pressure, gas temperature, and thermal conductivity, respectively, with the subscripts u and f referring to unburned and flame conditions. d_{q2} is the two-plate quench distance. The wall temperature and unburned gas temperature are assumed to be equal; this assumption is also appropriate in the engine context since there is ample time during the compression stroke for a thermal boundary layer to build up to a thickness of at least the quench distance.

Lavoie[36] has developed empirical correlations for two-plate quench-distance data for propane-air mixtures; only limited data for liquid hydrocarbon fuels such as isooctane are available. The data in the pressure range 3 to 40 atm are well fitted by

$$\mathrm{Pe}_2 = \frac{9.5}{\phi}\left(\frac{p}{3}\right)^{0.26 \min(1,\, 1/\phi^2)} \tag{11.28}$$

where p is the pressure in atmospheres and ϕ is the fuel/air equivalence ratio. The two-plate quench distance d_{q2} is then obtained from Eq. (11.27) and Prandtl number and viscosity relations for the flame conditions (see Sec. 4.8 or Ref. 36). Thus the minimum size crevice region into which a flame will propagate can be determined.

For the process of a flame front quenching on a single wall, there are many possible geometries. The simplest is where the flame front is parallel to the wall

and approaches it head on. The one-wall quench distance d_{q1}, defined as the position of closest approach of the reaction zone to the wall, scales with flame properties in a similar way to the two-plate quench distance. Thus, a one-wall Peclet number relation can be formed:

$$\mathrm{Pe}_1 = \frac{\rho_u S_L c_{p,u} d_{q1}}{k_u} \approx 8 \tag{11.29}$$

where the subscript u denotes properties evaluated at unburned gas conditions.

Using the wall temperature as representative of the unburned gas temperature (because the thermal boundary-layer thickness is greater than typical quench distances), Lavoie showed that

$$\frac{d_{q1}}{d_{q2}} = \frac{\mathrm{Pe}_1}{\mathrm{Pe}_2} = 0.2 \tag{11.30}$$

is a reasonable fit to the single-wall quench data. Typical two-wall quench distances for spark-ignition engine conditions are 0.2 to 1 mm; these distances represent the minimum crevice size the flame will enter. Single-wall quench distances are, therefore, in the range 0.04 to 0.2 mm.

While a fraction of the fuel hydrocarbons can escape the primary combustion process unburned or only partially reacted, oxidation of some of these hydrocarbons can occur during the expansion and exhaust processes. Hydrocarbon oxidation rates have been determined in a number of different studies and several different empirical correlations of the data in the form of overall reaction rate equations have been proposed. A reasonable fit to the experimental data on unburned HC burnup is the rate expression:[36]

$$\frac{d[\mathrm{HC}]}{dt} = -6.7 \times 10^{15} \exp\left(\frac{-18{,}735}{T}\right) \tilde{x}_{\mathrm{HC}} \tilde{x}_{\mathrm{O}_2} \left(\frac{p}{RT}\right)^2 \tag{11.31}$$

where [ ] denotes concentration in moles per cubic centimeter, $\tilde{x}_{\mathrm{HC}}$ and $\tilde{x}_{\mathrm{O}_2}$ are the mole fractions of HC and O_2, respectively, t is in seconds, T in kelvins, and the density term (p/RT) has units of moles per cubic centimeter. The spread in the data about this equation is substantial, however.

Studies of combustion of premixed fuel-air mixtures at high pressure in closed vessels or bombs have been useful in identifying the mechanisms by which hydrocarbons escape complete combustion. The residual unburned hydrocarbons left in the bomb following a combustion experiment have been shown to come primarily from crevices in the bomb walls. Unburned HC levels were proportional to total crevice volume, and decreased to very low values ($\sim$10 ppm C) as all the crevices were filled with solid material. Thus wall quench hydrocarbons apparently diffuse into the burned gases and oxidize following the quenching event.[37] Analytical studies of the flame quenching process, and postquench diffusion and oxidation with kinetic models of the hydrocarbon oxidation process, are in agreement with these bomb data.[38] Flame quenching can be thought of as a two-stage process. The first step is the extinction of the flame at a short distance from the cold wall, determined by a balance between thermal conduction of heat

from the hot reaction zone to the wall and heat released in the reaction zone by the flame reactions. The second step is the postquench diffusion and oxidation occurring on a time scale of one or a few milliseconds after quenching. The diffusion and oxidation process ultimately reduces the mass of wall quench hydrocarbons to several orders of magnitude below its value at the time of quenching.

Closed-vessel combustion experiments have also been used to show that oil layers on the walls of the bomb cause an increase in residual unburned HC levels after combustion is complete. The additional HC that result in experiments with oil films present are primarily (>95 percent) fuel molecules, and are directly proportional to the amount of oil placed on the walls of the reactor and the solubility of the specific fuel in the oil. These results show that absorption of fuel in the oil occurs prior to ignition. This dissolved fuel is then desorbed into the burned gases well after combustion is complete. Thus fuel absorption into and desorption from any oil layers is a potentially important engine HC mechanism.[39]

11.4.3 HC Emissions from Spark-Ignition Engines

Unburned hydrocarbon levels in the exhaust of a spark-ignition engine under normal operating conditions are typically in the range 1000 to 3000 ppm C_1. This corresponds to between about 1 and $2\frac{1}{2}$ percent of the fuel flow into the engine; the engine combustion efficiency is high. As indicated in Fig. 11-2, HC emissions rise rapidly as the mixture becomes substantially richer than stoichiometric. When combustion quality deteriorates, e.g., with very lean mixtures, HC emissions can rise rapidly due to incomplete combustion or misfire in a fraction of the engine's operating cycles. As outlined in Sec. 11.1, there are several mechanisms that contribute to total HC emissions. Also, any HC escaping the primary combustion process may oxidize in the expansion and exhaust processes. While a complete description of the HC emissions process cannot yet be given, there are sufficient fundamental data available to indicate which mechanisms are likely to be most important, and thus how major engine variables influence HC emission levels.

Four possible HC emissions formation mechanisms for spark-ignition engines (where the fuel-air mixture is essentially premixed) have been proposed: (1) flame quenching at the combustion chamber walls, leaving a layer of unburned fuel-air mixture adjacent to the wall; (2) the filling of crevice volumes with unburned mixture which, since the flame quenches at the crevice entrance, escapes the primary combustion process; (3) absorption of fuel vapor into oil layers on the cylinder wall during intake and compression, followed by desorption of fuel vapor into the cylinder during expansion and exhaust; (4) incomplete combustion in a fraction of the engine's operating cycles (either partial burning or complete misfire), occurring when combustion quality is poor (e.g., during engine transients when A/F, EGR, and spark timing may not be adequately controlled). In addition, as deposits build up on the combustion chamber walls,

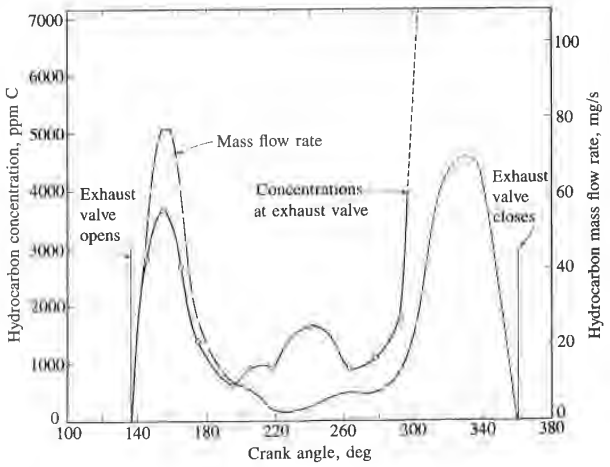

FIGURE 11-24
Variation in HC concentration and HC mass flow rate at the exhaust valve during the exhaust process. SI engine operating at 1200 rev/min and $\phi = 1.2$, unthrottled.[40]

HC emissions increase. Whether the deposits constitute an additional mechanism or merely modify one of the above mechanisms is unclear.

All these processes (except misfire) result in unburned hydrocarbons close to the combustion chamber walls, and not in the bulk of the cylinder gases. Thus, the distribution of HC in the exhaust gases would not be expected to be uniform. Experiments have been done to determine the unburned HC concentration distribution in the exhaust port during the exhaust process to provide insight into the details of the formation mechanisms. Gas concentrations were measured with a rapid-acting sampling valve placed at the exhaust port exit. Figure 11-24 shows results from these time-resolved HC concentration measurements. HC concentrations vary significantly during the exhaust process. Gas which remains in the exhaust port between exhaust pulses has a high HC concentration, so purging techniques where air or nitrogen was bled into the exhaust port were used to displace this high HC gas while the exhaust valve was closed. The high HC concentration in the blowdown exhaust gases is clearly discernible, as is the rapid rise in HC concentration toward the end of the exhaust stroke. The cylinder-exit HC concentrations were then multiplied by the instantaneous exhaust gas mass flow rate to obtain the instantaneous HC mass emission rate from the cylinder throughout the exhaust process, also shown in Fig. 11-24. The unburned HC are exhausted in two peaks of approximately equal mass: the first of these coincides with the exhaust blowdown mass flow pulse (which removes the majority of the *mass* from the cylinder); the second occurs toward the end of the exhaust stroke where HC concentrations are very high and the mass flow rate is relatively low.[40] Other experiments have confirmed these observations.[41] Clearly, mixing of

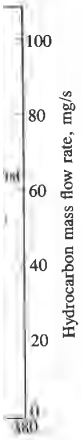

ıe exhaust valve during the exhaust
ttled.[40]

tute an additional mechanism
nclear.
unburned hydrocarbons close
ılk of the cylinder gases. Thus,
ıot be expected to be uniform.
ɔurned HC concentration dis-
ɔrocess to provide insight into
entrations were measured with
t port exit. Figure 11-24 shows
measurements. HC concentra-
ss. Gas which remains in the
HC concentration, so purging
he exhaust port were used to
lve was closed. The high HC
arly discernible, as is the rapid
haust stroke. The cylinder-exit
ıstantaneous exhaust gas mass
mission rate from the cylinder
. 11-24. The unburned HC are
ass: the first of these coincides
ch removes the majority of the
l the end of the exhaust stroke
ass flow rate is relatively low.[43]
vations.[41] Clearly, mixing of

unburned HC with the bulk cylinder gases occurs during expansion and/or the exhaust blowdown process. Then, the final stages of piston motion during the exhaust stroke push most of the remaining fraction of the cylinder mass with its high HC concentration into the exhaust. This would be expected to leave a high concentration of HC in the residual gas in the cylinder. Experiments conducted in which the valve mechanism of a single-cylinder engine was arranged to disengage during operation and trap residual gases in the cylinder confirm this. For one set of typical engine operating conditions, approximately one-third of the hydrocarbons left unburned in an engine combustion event was retained in the cylinder and recycled.[42]

FLAME QUENCHING AT THE WALLS. The existence of quench layers on the cold combustion chamber walls of a spark-ignition engine was shown photographically by Daniel.[43] Photographs of the flame region immediately after flame arrival at the wall through a window in the cylinder head showed a thin nonradiating layer adjacent to the wall. The quench layer thicknesses measured were in the range 0.05 to 0.4 mm (thinnest at high load), in rough agreement with predictions based on experiments in combustion bombs. However, more recent work in bombs and engines indicates that diffusion of hydrocarbons from the quench layer into the burned gases and its subsequent oxidation occur on a time scale of a few milliseconds, at least with smooth clean combustion chamber walls. The constant-volume combustion bomb data which suggested this conclusion and the kinetic calculations which support this explanation of why quench layers are not significant with smooth clean walls have already been described in Sec. 11.4.2. The following evidence shows these conclusions are also valid in an engine.

A special rapid-acting poppet valve was used in a single-cylinder engine to sample the gases from a torus-shaped region, of height of order 0.25 mm and diameter about 6 mm, adjacent to the wall over a 1-ms period. Sampling was repeated every cycle to provide a steady stream of sampled gases for analysis. Figure 11-25 shows the variation in concentrations of HC species through the combustion, expansion, and exhaust processes. The fuel was propane (C_3H_8). The fuel concentration drops rapidly to a low value when the flame arrives at the valve; at the same time, intermediate hydrocarbon product concentrations rise and then fall sharply to values below 1 ppm. Beginning at 60° ATC, all HC concentrations rise and vary somewhat during the remainder of the cycle in a way that depends strongly on engine operating conditions. The observed rapid rise in partial oxidation products immediately after flame arrival is consistent with the flame quenching short of the wall. The presence of CH_2O and CH_3CHO in significant quantities indicates that low-temperature oxidation processes are occurring. However, since all HC product concentrations fall rapidly within 2 ms of flame arrival to very low values, the unburned HC in the quench layer diffuse into the bulk burned gases and oxidize. The increase in HC concentrations later in the cycle results from the sampling of hydrocarbons from sources other than quench layers.[44]

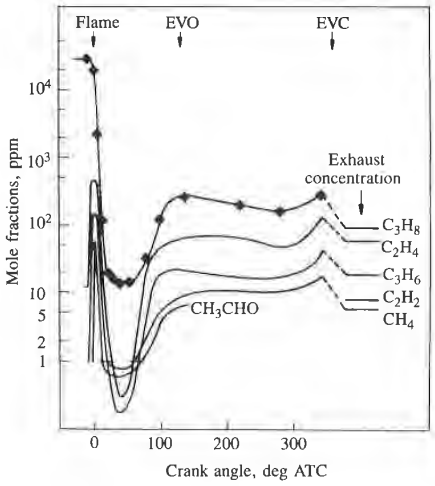

FIGURE 11-25
Concentrations (mole fractions) of selected hydrocarbons adjacent to combustion chamber wall, as a function of crank angle during combustion, expansion, and exhaust processes. Mass sampled with rapid-acting valve held constant at 7.6×10^{-6} g per pulse. Total exhaust HC = 400 ppm C. Engine speed = 1250 rev/min, imep = 380 kPa, equivalence ratio = 0.9, MBT spark timing, no EGR.[44]

Though quench layers on clean smooth combustion chamber walls are not a significant source of unburned hydrocarbons, it has been shown that wall surface finish does affect exhaust HC levels. Comparisons have been made between the standard "rough" as-cast cylinder head surfaces and the same cylinder heads when smoothed. The average exhaust HC concentration decreased by 103 ppm C, or 14 percent; the smoothed surface area was 32 percent of the total combustion chamber surface area.[45] Buildup of deposits on the combustion chamber surfaces also affect HC emission levels, as will be discussed later.

CREVICE HC MECHANISM. The crevices in the combustion chamber walls—small volumes with narrow entrances—into which the flame is unable to penetrate have been shown to be a major source of unburned HC. The largest of these crevice regions is the volumes between the piston, piston rings, and cylinder wall. Other crevice volumes in production engines are the threads around the spark plug, the space around the plug center electrode, crevices around the intake and exhaust valve heads, and the head gasket crevice. Table 8.1 shows the size and relative importance of these crevice regions in one cylinder of a production V-6 engine determined from measurements of cold-engine components. Total crevice volume is a few percent of the clearance volume and the piston and ring pack crevices are the dominant contributor.

The important crevice processes occurring during the engine cycle are the following. As the cylinder pressure rises during compression, unburned mixture is forced into the crevice regions. Since these volumes are thin they have a large surface/volume ratio; the gas flowing into each crevice cools by heat transfer to close to the wall temperature. During combustion, while the pressure continues to rise, unburned mixture continues to flow into the crevice volumes. When the

flame arrives at each crevice, it can either propagate into the crevice and fully or partially burn the fuel and air within the crevice or it can quench at the crevice entrance. Whether the flame quenches depends on crevice entrance geometry, the composition of the unburned mixture, and its thermodynamic state as described in Sec. 11.4.2. After flame arrival and quenching, burned gases will flow into each crevice until the cylinder pressure starts to decrease. Once the crevice gas pressure is higher than the cylinder pressure, gas flows back from each crevice into the cylinder.

The most important of these crevices, the volumes between the piston, piston rings, and cylinder wall, is shown schematically in Fig. 8-27. This crevice consists of a series of volumes, connected by flow restrictions such as the ring side clearance and ring gap whose geometry changes as the ring moves up and down in the ring groove sealing either at the top or bottom ring surface. The gas flow, pressure distribution, and ring motion are therefore coupled, and their behavior during the compression and expansion strokes has already been discussed in Sec. 8.6. During compression and combustion, mass flows *into* the volumes in this total crevice region. Once the cylinder pressure starts to decrease (after about 15° ATC) gas flows out of the top of these crevice regions in Fig. 8-27 into the cylinder at low velocity adjacent to the cylinder wall. The important result is that the fraction of the total cylinder charge (5 to 10 percent) trapped in these regions at the time of peak cylinder pressure escapes the primary combustion process. Most of this gas flows back into the cylinder during the expansion process. Depending on spark plug location in relation to the position of the top ring gap, well above 50 percent of this gas can be unburned fuel-air mixture. Its potential contribution to unburned HC emissions is obvious.

There is substantial evidence to support the above description of crevice HC phenomena and the piston ring crevice region in particular. Visualization studies in a special engine have identified the spark plug crevice outflow, low-velocity gas expansion out of the volume above the first ring after the time of peak pressure, and the jet-like flows through the top ring gap later in the expansion process when the pressure difference across the ring changes sign.[46] Gas sampling from the volume above the top ring, using a rapid-acting sample valve mounted in the piston crown, has shown that the gas composition in this region corresponds to unburned fuel-air mixture until flame arrival at the crevice entrance closest to the sampling valve location. Next, product gases enter the crevice as the cylinder pressure continues to rise. Then, during expansion as gas flows out of this region, the composition of the gas sampled reverts back toward that of the unburned mixture which enters the crevice region earlier.[47]

Direct evidence that the piston and ring crevice regions are a major contributor to exhaust HC emissions comes from experiments where the volume of this crevice region was substantially changed. Wentworth[48] almost completely eliminated this crevice by moving the top piston ring as close to the crown of the piston as possible, and sealing this ring at top and bottom in its groove with O rings. Tests of this sealed ring-orifice design in a production engine showed reductions of between 47 and 74 percent from baseline HC levels over a range of

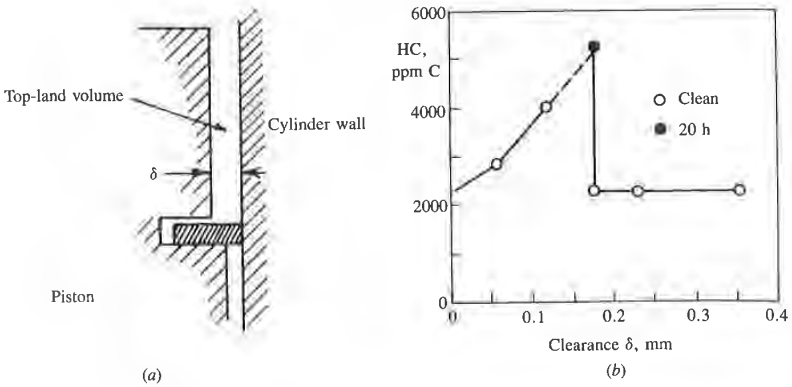

FIGURE 11-26
(*a*) Piston top-land crevice volume. (*b*) Effect of increasing top-land clearance on exhaust hydrocarbon emissions. Unthrottled spark-ignition engine, $r_c = 6$, 885 rev/min, $A/F = 13$, MBT timing.[49]

speeds and loads. Haskell and Legate,[49] in experiments in a single-cylinder CFR engine, steadily increased the piston top-land clearance (see Fig. 11-26*a*) and measured the effect on exhaust HC emissions. Figure 11-26*b* shows the results: HC emissions increase as the top-land clearance increases until the clearance equals about 0.18 mm, when emissions drop to the zero clearance level. This clearance (0.18 mm) is close to the two-plate quench distance estimated from Eq. (11.27). For piston top-land clearances above this value, the flame can enter the crevice and burn up much of the crevice HC.

The relative importance of the different crevices in the combustion chamber walls has been examined by using the cylinder head and piston of a four-cylinder production engine to form two constant-volume reactors or combustion bombs.[50] The cylinder head was sealed with a steel plate across the head gasket plane to make one reactor; the piston and ring pack and cylinder wall, again sealed with a plate at the head gasket plane, formed the second reactor. Each reactor was filled with a propane-air mixture and combustion initiated with a spark discharge across a spark plug; following combustion the burned gases were exhausted, sampled, and analyzed. The crevices were sequentially filled with epoxy or viton rubber, and after filling each crevice, the exhaust HC emission level determined. It was found that the ring pack crevices produced approximately 80 percent of the total scaled HC emissions, the head gasket crevice about 13 percent, and the spark plug threads 5 percent. All other HC sources in these reactors produced less than 2 percent of the total HC. While these numbers cannot be applied directly to an operating engine (the crevice filling and emptying rates in the bomb experiments are substantially different from these rates in an engine), they do underline the importance of the ring pack crevice region.

Blowby is the gas that flows from the combustion chamber, past the piston and into the crankcase. It is forced through any leakage paths afforded by the

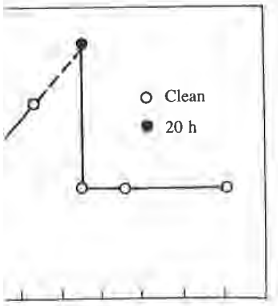

(*b*)

and clearance on exhaust hydrocarbon
n, $A/F = 13$, MBT timing.[49]

ments in a single-cylinder CFR
ance (see Fig. 11-26*a*) and mea-
11-26*b* shows the results: HC
ases until the clearance equals
clearance level. This clearance
ace estimated from Eq. (11.27).
the flame can enter the crevice

ices in the combustion chamber
ad and piston of a four-cylinder
ume reactors or combustion
el plate across the head gasket
pack and cylinder wall, again
rmed the second reactor. Each
ad combustion initiated with a
nbustion the burned gases were
s were sequentially filled with
vice, the exhaust HC emission
ack crevices produced approx-
ssions, the head gasket crevice
ercent. All other HC sources in
total HC. While these numbers
e (the crevice filling and empty-
lly different from these rates in
e ring pack crevice region.
ustion chamber, past the piston
leakage paths afforded by the

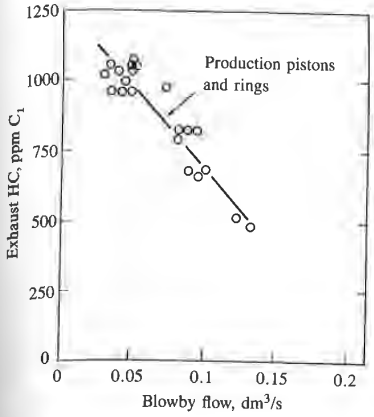

FIGURE 11-27
Effect of increasing crankcase blowby on exhaust hydrocarbon emissions. Production pistons and rings. SI engine at 1200 rev/min, intake manifold pressure 0.6 atm, $A/F = 14.2$.[51]

piston-bore-ring assembly in response to combustion chamber pressure. Blowby of gases from the cylinder to the crankcase removes gas from this crevice region and thereby prevents some of the crevice gases from returning to the cylinder. Crankcase blowby gases used to be vented directly to the atmosphere and constituted a significant source of HC emissions. The crankcase is now vented to the engine intake system, the blowby gases are recycled, and this source of HC emissions is now fully controlled. Blowby at a given speed and load is controlled primarily by the greatest flow resistance in the flow path between the cylinder and the crankcase. This is the smallest of the compression ring ring-gap areas. Figure 8-30 shows how blowby increases linearly with the smallest gap area. Figure 11-27 shows how exhaust HC levels decrease as blowby increases and more crevice HC flows to the crankcase. Crankcase blowby gases represent a direct performance loss. They are a smaller efficiency loss because crankcase gases are now recycled to the engine intake system.

The location of the ring gap in relation to the spark plug also affects HC emission levels. Experiments have shown that HC emissions are highest when the top ring gap is farthest from the spark plug: the gas flowing into the crevice directly above the gap is then unburned mixture for the longest possible time. With the top ring gap closest to the spark plug, HC exhaust levels are lowest because burned gas reaches the gap location at the earliest time in the combustion process. The difference, highest to lowest, was between 9 and 42 percent of the average level for any set of operating conditions, and in most cases was above 20 percent.[51]

The fate of these crevice HC when they flow back into the cylinder during expansion and exhaust is not well understood. Both jet-like flows (e.g., that from the ring gap) and low-velocity creeping flows (e.g., that from the piston top-land crevice) have been observed (see Fig. 8-29). While the former could mix rapidly with the high-temperature bulk burned gases, the latter will enter the cool gases

TABLE 11.6
Amount of gas flowing into and out of crevice regions†

	% mass	ppm C
Total gas in all crevice regions	8.2	
Total gas back to combustion chamber	7.0	
Unburned back to combustion chamber	3.7–7.0‡	5000–9400
Unburned to blowby	0.5–1.2‡	
Total unburned escaping primary combustion	4.2–8.2‡	

† For V-6 engine operating at 2000 rev/min and wide-open throttle.
‡ Depends on spark plug and ring gap location.

in the cylinder wall boundary layer and mix and (probably) burn much more slowly. Hydrocarbon transport and oxidation processes are discussed more fully below.

Table 11.6 presents a summary of estimates of the total mass of gas and mass of unburned mixture in the piston, ring, and cylinder wall crevice region for a typical spark-ignition engine.[46] When compared to exhaust HC levels, it is clear that these crevices are a major source of unburned hydrocarbons.

ABSORPTION AND DESORPTION IN ENGINE OIL. The presence of lubricating oil in the fuel or on the walls of the combustion chamber is known to result in an increase in exhaust hydrocarbon levels. In experiments where exhaust HC concentrations rose irregularly with time, with engine operating conditions nominally constant, it was shown that oil was present on the piston top during these high emission periods. When engine oil was added to the fuel, HC emissions increased, the amount of additional HC in the exhaust increasing with the increasing amount of oil added. The increase in exhaust HC was primarily unreacted fuel (isooctane) and not oil or oil-derived compounds.[51] The increase in HC can be substantial: exhaust HC levels from a clean engine can double or triple when operated on a fuel containing 5 percent lubricating oil over a period of order 10 minutes. (With deposits from leaded-fuel operation present on the combustion chamber walls, however, a much smaller increase in exhaust HC was observed.) It has been proposed that fuel vapor absorption into and desorption from oil layers on the walls of the combustion chamber could explain these phenomena.[49]

The absorption and desorption mechanism would work as follows. The fuel vapor concentration within the cylinder is close to the inlet manifold concentration during intake and compression. Thus, for about one crankshaft revolution, any oil film on the walls will absorb fuel vapor. During the latter part of compression, the fuel vapor pressure is increasing so, by Henry's law, absorption will continue even if the oil was saturated during intake. During combustion the fuel vapor concentration in the bulk gases goes essentially to zero so the absorbed fuel vapor will desorb from the liquid oil film into the gaseous combustion products. Desorption could continue throughout the expansion and exhaust strokes.

Some of the desorbed fuel vapor will mix with the high-temperature combustion products and oxidize. However, desorbed vapor that remains in the cool boundary layer or mixes with the cooler bulk gases late in the cycle may escape full oxidation and contribute to unburned HC emissions.

Experiments, where measured amounts of oil were placed on the piston crown, confirm that oil layers on the combustion chamber surface increase exhaust HC emissions. The exhaust HC levels increased in proportion to the amount of oil added when the engine was fueled with isooctane. Addition of 0.6 cm^3 of oil produced an increase of 1000 ppm C in exhaust HC concentration. Fuel and fuel oxidation species, not oil oxidation products, were responsible for most of this increase. Similar experiments performed with propane fuel showed no increase in exhaust HC emissions when oil was added to the cylinder. The increase in exhaust HC is proportional to the solubility of the fuel in the oil. The exhaust HC levels decreased steadily back to the normal engine HC level before oil addition, over a period of several minutes. At higher coolant temperatures, the increase in HC on oil addition is less, and HC concentrations decreased back to the normal level more quickly. Increasing oil temperature would decrease viscosity, increasing the rate of drainage into the sump. It also changes the solubility and diffusion rate of the fuel in the oil.[52]

At the outer surface of the oil layer, the concentration of fuel vapor dissolved in the oil is given by Henry's law for dilute solutions in equilibrium:

$$\tilde{x}_f = \frac{p_f}{H} \tag{11.32}$$

where $\tilde{x}_f$ is the mole fraction of fuel vapor in the oil, p_f is the partial pressure of fuel vapor in the gas, and H is Henry's constant. If the oil layer is sufficiently thin, and hence diffusion sufficiently rapid, Eq. (11.32) can be used to estimate the mole fraction of the fuel dissolved in the oil. Since $p_f = n_{f,c}\tilde{R}T/V$ (where $n_{f,c}$ is the number of moles of fuel in the cylinder, T is the temperature, and V the cylinder volume) and $x_f = n_{f,o}/(n_{f,o} + n_o) = n_{f,o}/n_o$ for $n_o \gg n_{f,o}$ (where $n_{f,o}$ is the number of moles of fuel dissolved in the oil and n_o is the number of moles of oil),[53] then

$$\frac{n_{f,o}}{n_{f,c}} = \frac{n_o \tilde{R}T}{HV} \tag{11.33}$$

Diffusion is sufficiently rapid for Eq. (11.33) to be valid if the diffusion time constant τ_d is much less than characteristic engine times: i.e.,

$$\tau_d \approx \frac{\delta^2}{D} \ll N^{-1}$$

where δ is the oil layer thickness, D is the diffusion coefficient for fuel vapor in the oil, and N is engine speed. D for a hydrocarbon through a motor oil is of order 10^{-6} cm^2/s at 300 K and of order 10^{-5} cm^2/s at 400 K. Oil film thicknesses on the cylinder wall vary during the operating cycle between about 1 and 10 μm.[54, 55] Thus diffusion times for engine conditions are 10^{-1} to 10^{-3} s; for the thinnest oil layers approximate equilibration would be achieved. A theoretical

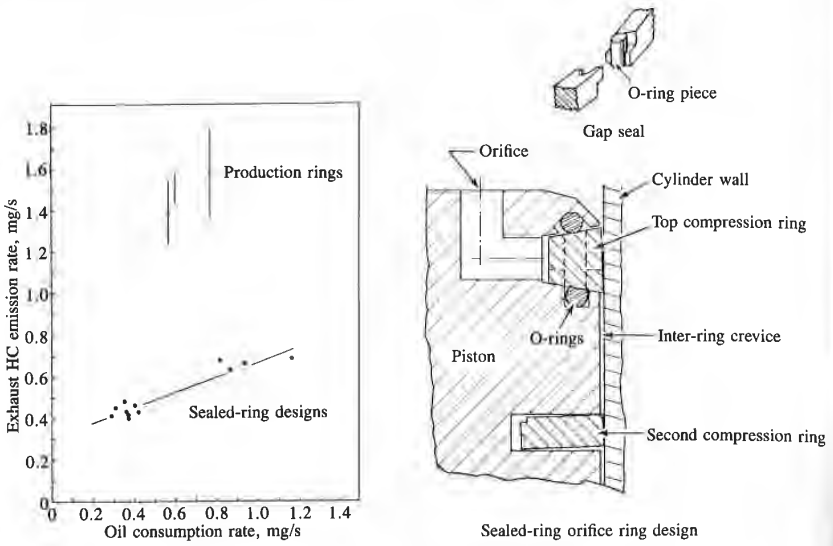

FIGURE 11-28
Correlation between exhaust hydrocarbon emissions and oil consumption rate. Production piston rings and sealed ring–orifice ring designs. SI engine at 1600 rev/min, imep = 422 kPa, equivalence ratio = 0.9, r_c = 8.0, intake pressure = 54 kPa, MBT spark timing.[57]

study of this problem—the one-dimensional cyclic absorption and desorption of a dilute amount of gas in a thin (constant thickness) isothermal liquid layer where diffusion effects are important—has been carried out. It suggests that oil layers on the cylinder wall could be a significant contributor to HC emission levels.[56]

Correlations between engine oil consumption and exhaust HC emissions provide a perspective on the relative importance of oil absorption/desorption and crevice mechanisms. Wentworth measured oil consumption and HC emissions in a spark-ignition engine for a range of piston ring designs.[57] Some of these designs were of the sealed ring–orifice type which effectively eliminates all the crevices between the piston, piston rings, and cylinder, and prevents any significant gas flow into or out of the ring region. HC emissions increase with increasing oil consumption for both production ring designs and the sealed ring–orifice designs, as shown in Fig. 11-28. Extrapolation to zero oil consumption from normal consumption levels shows a reduction in exhaust HC levels, but this decrease is significantly less than the difference in emission levels between the production and the sealed ring–orifice designs which effectively remove the major crevice region. The production piston used had a chamfered top land. The HC emissions for a normal piston top-land design would probably be higher.

POOR COMBUSTION QUALITY. Flame extinction in the bulk gas, before all of the flame front reaches the wall, is a source of HC emissions under certain engine

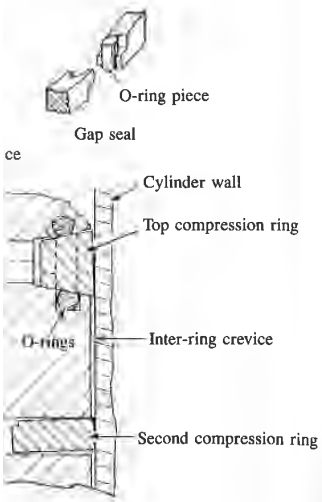

ed-ring orifice ring design

consumption rate. Production piston rev/min, imep = 422 kPa, equivalence ing.[57]

c absorption and desorption of s) isothermal liquid layer where out. It suggests that oil layers ıtor to HC emission levels.[56]

on and exhaust HC emissions f oil absorption/desorption and sumption and HC emissions in lesigns.[57] Some of these designs vely eliminates all the crevices ıd prevents any significant gas ns increase with increasing oil l the sealed ring–orifice designs, consumption from normal con- HC levels, but this decrease is levels between the production vely remove the major crevice ed top land. The HC emissions ly be higher.

ın in the bulk gas, before all of emissions under certain engine

operating conditions. As the cylinder pressure falls during the expansion stroke, the temperature of the unburned mixture ahead of the flame decreases. Thus slows the burning rate [the laminar flame speed decreases so the burning rate in Eq. (9.52) decreases]. If the pressure and temperature fall too rapidly, the flame can be extinguished. This type of bulk quench has been observed in spark-ignition engines; it results in very high HC concentrations for that particular cycle. Engine conditions where bulk quenching is most likely to occur are at idle and light load where engine speed is low and the residual gas fraction is high, with high dilution with excessive EGR or overly lean mixtures, and with substantially retarded combustion. Even if steady-state engine calibrations of A/F, EGR, and spark timing are such that bulk quenching does not occur, under transient engine operation these variables may not be appropriately set to avoid bulk quenching in some engine cycles due to the different dynamic characteristics of the engine subsystems which control these variables.

The existence of zones of stable and unstable engine operation with lean or dilute mixtures has already been discussed (see Sec. 9.4.3). Detailed engine combustion studies have shown that, as mixture composition becomes more dilute (e.g., by increasing EGR) and unburned gas temperature and pressure during combustion become lower, combustion quality (or variability) and engine stability deteriorate. The standard deviation in a parameter such as indicated mean effective pressure (which depends for its magnitude on the proper timing of the start of combustion and on the duration of the combustion process) increases due first to an increase in the number of slower burning cycles, then as conditions worsen to the occurrence of partial burning cycles, and finally to some misfiring cycles. Figure 9-36 showed how unburned hydrocarbon emissions from a spark-ignition engine rise as the EGR rate is increased at constant load and speed, and combustion quality (defined by the ratio of standard deviation in imep to the average imep) deteriorates. Initially the increase in HC is modest and is caused by changes in the other HC emission mechanisms described above. However, when partial burning cycles are detected, HC emissions rise more rapidly due to incomplete combustion of the fuel in the cylinder in these cycles. When misfiring cycles—no combustion—occur the rise in HC becomes more rapid still.

The relative importance of bulk gas quenching in a fraction of the engine's operating cycles due to inadequate combustion quality as a source of HC, compared with the other sources described in this section, has yet to be established. However, one obvious technique for reducing its importance, burning the mixture faster so that combustion is completed before conditions conducive to slow and partial burning exist in the cylinder, does reduce engine exhaust HC emissions. Figure 11-29 shows a comparison of HC emissions from a moderate burn rate engine with HC emissions with a faster burn rate [i.e., with improved combustion quality—lower coefficient of variation in imep, COV_{imep}, Eq. (9.50)], achieved by the use of two spark plugs instead of one.[58] The exhaust measurements show lower HC emissions when significant amounts of EGR are used for NO_x control for the faster, and hence less variable, combustion process. Such evidence suggests that occasional partial burning cycles may occur, even under

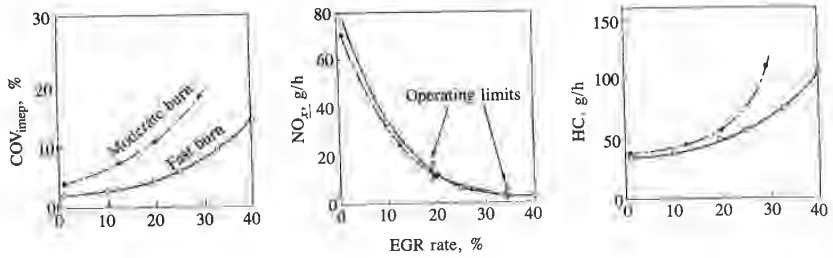

FIGURE 11-29
Effect of increasing burn rate on tolerance to recycled exhaust gas (EGR) and HC and NO_x emissions levels. COV_{imep} defined by Eq. (9.50). SI engine at 1400 rev/min, 324 kPa imep, equivalence ratio = 1.0, MBT timing.[58]

conditions where combustion appears to be "normal," and that this mechanism is important in practice.

EFFECT OF DEPOSITS. Deposit buildup on the combustion chamber walls (which occurs in vehicles over several thousands of miles) is known to increase unburned HC emissions. With leaded gasoline operation, the increase in HC emissions varies between about 7 and 20 percent. The removal of the deposits results typically in a reduction in HC emissions to close to clean engine levels. With unleaded gasoline, while the deposit composition is completely different (carbonaceous rather than lead oxide), the increase in HC emissions with accumulated mileage is comparable. Soft sooty deposits, such as those which accumulate after running the engine on a rich mixture, also cause an increase in HC emissions. Again, when the deposits were removed the emission rate fell about 25 percent to the original level.[59] Studies with simulated deposits (pieces of metal-foam sheet 0.6 mm thick) attached to the cylinder head and piston also showed increases in HC emissions. The increase varied between about 10 and 100 ppm C/cm^2 of simulated deposit area. The effect for a given area of deposit varied with deposit location. Locations close to the exhaust valve, where the flow direction during the exhaust process would be expected to be directly into the exhaust port, showed the highest increase in emissions.[45]

It is believed that absorption and desorption of hydrocarbons by these surface deposits is the mechanism that leads to an increase in emissions. Deposits can also build up in the piston ring crevice regions. A reduction in volume of these crevice regions would decrease HC emissions (and such a decrease has been observed). However, changes in piston-cylinder wall clearance due to deposits can affect the flame-quenching process and could increase emissions.[49]

HYDROCARBON TRANSPORT MECHANISMS. All of the above mechanisms (except misfire) result in high hydrocarbon concentrations adjacent to the combustion chamber walls. While any jet-type flows out of crevices during the expan-

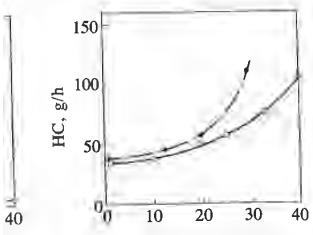

gas (EGR) and HC and NO_x emissions
rev/min, 324 kPa imep, equivalence

mal," and that this mechanism

ne combustion chamber walls
of miles) is known to increase
operation, the increase in HC
t. The removal of the deposits
to close to clean engine levels.
position is completely different
se in HC emissions with accu-
s, such as those which accumu-
also cause an increase in HC
l the emission rate fell about 25
lated deposits (pieces of metal-
r head and piston also showed
ried between about 10 and
ffect for a given area of deposit
ne exhaust valve, where the flow
xpected to be directly into the
ions.[45]
tion of hydrocarbons by these
increase in emissions. Deposits
ions. A reduction in volume of
ns (and such a decrease has been
wall clearance due to deposits
increase emissions.[49]

All of the above mechanisms
entrations adjacent to the com-
out of crevices during the expan-

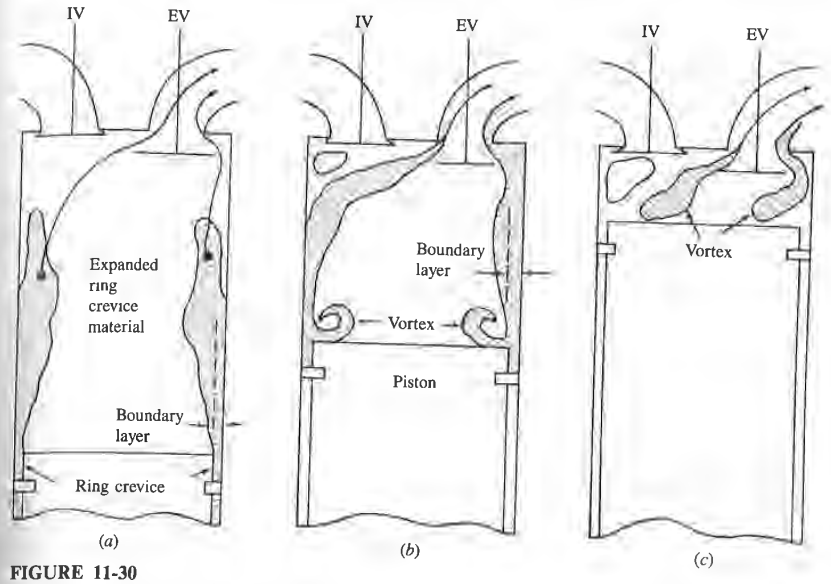

FIGURE 11-30
Schematic of flow processes by which ring crevice HC and HC desorbed from cylinder wall oil film exit the cylinder: (*a*) exhaust blowdown process; (*b*) during exhaust stroke; (*c*) end of exhaust stroke.[60]

sion and exhaust strokes can transport unburned HC into the bulk gases, most of the HC will remain near the wall. Two mechanisms by which gas near the cylinder wall exits the cylinder have been demonstrated. One is entrainment in the vigorous gas flow out of the cylinder which occurs during the exhaust blowdown process. The other is the vortex generated in the piston crown–cylinder wall corner during the exhaust stroke.

Figure 11-30 illustrates these flow processes. In Fig. 11-30*a* the engine cylinder is shown as the exhaust valve opens during the blowdown process. At this time the unburned HC from the ring crevice regions, laid along the wall during expansion (and possibly HC from the oil film on the cylinder wall), is expanding into the cylinder as the cylinder pressure falls. Some of this material will be entrained by the bulk gases in the rapid motion which occurs during exhaust blowdown (see Sec. 6.5). The rapid thinning of the thermal boundary-layer regions on the combustion chamber walls during blowdown, which would result from entrainment of the denser hydrocarbon-containing gas adjacent to the wall, has been observed in schlieren movies taken in a transparent engine.[46] This process, plus entrainment of any HC from the spark plug and head gasket crevices, would contribute to unburned HC in the blowdown gases which contain about half the total HC emissions (see Fig. 11-24). During the exhaust stroke this bulk gas entrainment process will continue, exhausting additional unburned HC, as shown in Fig. 11-30*b*.

The second mechanism starts at the beginning of the exhaust stroke in the piston crown–cylinder wall corner. The piston motion during the exhaust stroke scrapes the boundary-layer gases off the cylinder wall (which contain the remainder of the piston and ring crevice hydrocarbons), rolls them up into a vortex, and pushes them toward the top of the cylinder. This piston crown–cylinder wall corner flow is discussed in Sec. 8.7, and has been observed in transparent engines as well as in water-flow engine analog studies. At the end of the exhaust stroke, the height of this vortex is comparable to the engine clearance height. As shown in Fig. 11-30*c*, a recirculation flow is likely to build up in the upper corner of the cylinder away from the exhaust valve, causing the vortex to detach from the wall and partly sweep out of the cylinder. In the corner nearest the valve, the flow is deflected around the valve, also tending to pull part of the vortex out of the chamber. In this way it is possible for a large part of the vortex, which now contains a substantial fraction of the unburned HC originally located adjacent to the cylinder wall, to leave the cylinder at the end of the exhaust stroke. This vortex flow is thought to be the mechanism that leads to the high HC concentrations measured at the end of the exhaust process, which contributes the other half of the exhausted HC mass (see Fig. 11-24), and to be responsible for the HC concentrations measured in the residual gases being much higher than average exhaust HC levels.[62] This study showed that at close to wide-open-throttle conditions, only about two-thirds of the HC which fail to oxidize inside the cylinder were exhausted, though 95 percent of the gas within the cylinder flows out through the exhaust valve. The residual gas HC concentration was about 11 times the average exhaust level. At part-throttle conditions, where the residual gas fraction is higher, it has been estimated that only about half of the unreacted HC in the cylinder will enter the exhaust.[63]

HYDROCARBON OXIDATION. Unburned hydrocarbons which escape the primary engine combustion process by the mechanisms described above must then survive the expansion and exhaust process without oxidizing if they are to appear in the exhaust. Since the formation mechanisms produce unburned HC at temperatures close to the wall temperature, mixing with bulk burned gas must take place first to raise the HC temperature to the point where reaction can occur. The sequence of processes which links the source mechanisms to hydrocarbons at the exhaust exit is illustrated in Fig. 11-31; it involves mixing and oxidation in both the cylinder and the exhaust system.

There is considerable evidence that substantial oxidation does occur. The oxidation of unburned HC in the quench layers formed on the combustion chamber walls on a time scale of order 1 ms after the flame is extinguished has already been discussed. Because the quench layers are thin, diffusion of HC into the bulk burned gas is rapid. Because the burned gases are still at a high temperature, oxidation then occurs quickly. Measurements of in-cylinder HC concentrations by gas sampling prior to exhaust valve opening show levels about 1.5 to 2 times the average exhaust level.[44, 63] The exhaust unburned HC are a mixture of fuel hydrocarbon compounds and pyrolysis and partial oxidation pro-

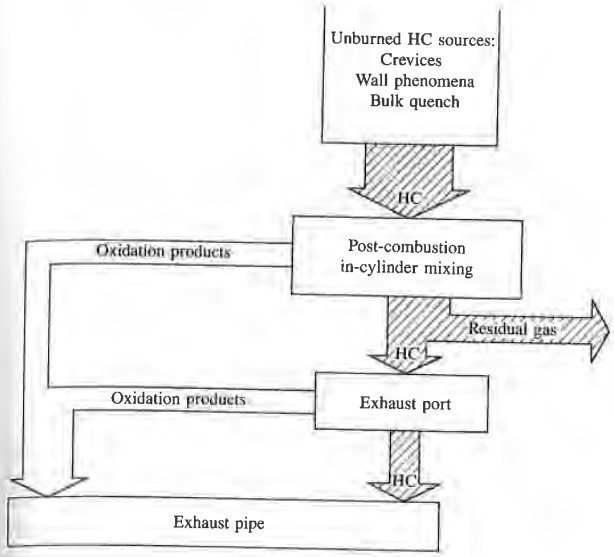

FIGURE 11-31
Schematic of complete SI engine HC formation and oxidation mechanism within the cylinder and exhaust system.[62]

ducts. While the relative proportion of fuel compared to reaction product hydrocarbon compounds varies substantially with engine operating conditions, an average value for passenger car vehicle exhausts is that fuel compounds comprise 40 percent of the total HC. Though partially reacted HC are produced in the flame-quenching process, these are closest to the high-temperature burned gases and are likely to mix and burn rapidly. That such a large fraction of the exhaust HC are reaction products indicates that substantial postformation HC reactions are occurring. There is direct evidence that HC oxidation in the exhaust system occurs.[64] Since in-cylinder gas temperatures are higher, it is likely that mixing of unburned HC with the bulk cylinder gases limits the amount of oxidation rather than the reaction kinetics directly.

Overall empirically based expressions for the rate of oxidation of hydrocarbons of the form of Eq. (11.31) have been developed and used to examine in-cylinder and exhaust burnup. A characteristic time τ_{HC} for this burnup process can be defined:

$$\frac{1}{\tau_{HC}} = \frac{1}{[HC]} \frac{d[HC]}{dt} \tag{11.34}$$

Using an expression similar to Eq. (11.31) for $d[HC]/dt$, Weiss and Keck[63] have shown that any HC mixing with the burned gases in the cylinder prior to exhaust

blowdown will oxidize. The in-cylinder gas temperature prior to blowdown generally exceeds 1250 K; the characteristic reaction time τ_{HC} is then less than 1 ms. During blowdown the temperature falls rapidly to values typically less than 1000 K; τ_{HC} is then greater than about 50 ms. An experimental study of HC exiting from a simulated crevice volume has shown that complete HC oxidation only occurs when the cylinder gas temperature is above 1400 K.[65] Thus a large fraction of the HC leaving crevice regions or oil layers during the exhaust process can be expected to survive with little further oxidation. Gas-sampling data show little decrease in in-cylinder HC concentrations during the exhaust stroke, thus supporting this conclusion.[44, 63] Overall, probably about half of the unburned HC formed by the source mechanisms described above will oxidize within the engine cylinder (the exact amount cannot yet be predicted with any accuracy; it is likely to depend on engine design and operating conditions[61]).

As shown schematically in Fig. 11-31, oxidation of HC in the exhaust system can occur. Often this is enhanced by air addition into the port region to ensure that adequate oxygen for burnup is available. However, since the gas temperature steadily decreases as the exhaust gases flow through the exhaust port and manifold, the potential for HC burnup rapidly diminishes. To oxidize the hydrocarbons in the gas phase, a residence time of order 50 ms or longer at temperatures in excess of 600°C are required. To oxidize carbon monoxide temperatures in excess of 700°C are required. Average exhaust gas temperatures at the cylinder exit (at the exhaust valve plane) are about 800°C; average gas temperatures at the exhaust port exit are about 600°C.† Figure 6-21 shows an example of the measured cylinder pressure, measured gas temperature at the exhaust port exit, and estimated mass flow rate into the port and gas temperature in the cylinder, during the exhaust process at a part-throttle operating condition. Port residence time and gas temperatures vary significantly through the process. Precise values of these variables obviously depend on engine operating conditions. It is apparent that only in the exhaust port and upstream end of the manifold can any significant gas-phase HC oxidation occur.

The importance of exhaust gas temperature to exhaust system emissions burnup is illustrated by the results shown in Fig. 11-32.[66] The exhaust system of a four-cylinder engine was modified by installing a section of heated and insulated pipe to maintain the exhaust gas temperature constant in the absence of any HC or CO burnup. The exhaust temperature entering this test section was varied by adjusting the engine operating conditions. The figure shows CO and HC concentrations as functions of residence time in the exhaust test section (or effectively as a function of distance from the engine). T_e is the entering gas temperature. The exhaust composition was fuel lean with 3 percent O_2 in the burned

† Note that there is a significant variation in the temperature of the exhaust gases throughout the exhaust process. The gas exhausted first is about 100 K hotter than the gas exhausted at the end of the process (see Sec. 6.5).

re prior to blowdown gen-
τ_{HC} is then less than 1 ms.
values typically less than
experimental study of HC
ıat complete HC oxidation
›ve 1400 K.[65] Thus a large
during the exhaust process
n. Gas-sampling data show
ıg the exhaust stroke, thus
bout half of the unburned
ove will oxidize within the
licted with any accuracy; it
.ditions[61]).
ion of HC in the exhaust
tion into the port region to
However, since the gas tem-
v through the exhaust port
diminishes. To oxidize the
: order 50 ms or longer at
dize carbon monoxide tem-
:xhaust gas temperatures at
ut 800°C; average gas tem-
C.† Figure 6-21 shows an
:ed gas temperature at the
he port and gas temperature
:hrottle operating condition.
icantly through the process.
on engine operating condi-
i upstream end of the mani-
r.
o exhaust system emissions
32.[66] The exhaust system of
section of heated and insu-
: constant in the absence of
ntering this test section was
. The figure shows CO and
the exhaust test section (or
). T_e is the entering gas tem-
ı 3 percent O_2 in the burned

f the exhaust gases throughout the
ıan the gas exhausted at the end of

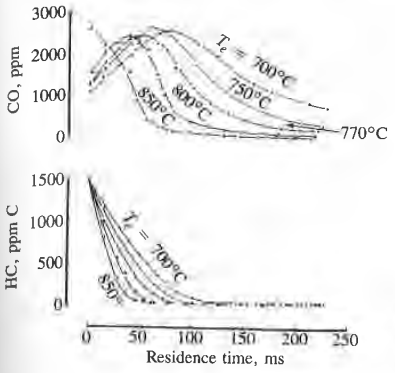

FIGURE 11-32
Effect of exhaust gas temperature on HC and CO burnup in the exhaust. SI engine at 1600 rev/min, engine air flow = 7.7 dm³/s, lean mixture with 3% O_2 and 13% (CO + CO_2) in exhaust.[66]

gas stream. HC oxidation starts immediately (for $T \gtrsim 600$°C), the rate of oxidation increasing rapidly with increasing temperature. Under fuel-lean conditions, incomplete HC oxidation can result in an increase in CO levels. CO oxidation commences later, when the gas temperature rises above the entering value due to heat released by the already occurring HC oxidation. The further heat released by CO oxidation accelerates the CO burnup process. These data underline the importance of the exhaust port heat-transfer and mixing processes. Both mixing between the hotter blowdown gases (with their lower HC concentration) and the cooler end-of-exhaust gases (with their higher HC concentration) and mixing between burned exhaust gas and secondary air are important.

Engine experiments where the exhaust gas reactions were quenched by timed injection of cold carbon dioxide at selected locations within the exhaust port have shown that significant reductions in HC concentration in the port can occur. Parallel modeling studies of the HC burnup process (based on instantaneous mass flow rate, estimated exhaust gas temperature, and an overall hydrocarbon reaction-rate expression), which predicted closely comparable magnitudes and trends, indicated that gas temperature and port residence time are the critical variables. The percent of unburned HC exiting the cylinder which reacted in the exhaust system (with most of the reaction occurring in the port) varied between a few and 40 percent. Engine operating conditions that gave highest exhaust temperatures (stoichiometric operation, higher speeds, retarded spark timing, lower compression ratio) and longest residence times (lighter load) gave relatively higher percent reductions. Air injection at the exhaust valve-stem base, phased to coincide with the exhaust process, showed that for stoichiometric and slightly rich conditions secondary air flow rates up to 30 percent of the exhaust flow substantially increased the degree of burnup. The timing of the secondary air flow relative to the exhaust flow and the location of the air injection point in the port are known to be critical.[64]

Reductions in exhaust port heat losses through the use of larger port cross-sectional areas (to reduce flow velocity and surface area per unit volume), inser-

tion of port liners to provide higher port wall temperatures, and attention to port design details to minimize hot exhaust gas impingement on the walls are known to increase the degree of reaction occurring in the port.

SUMMARY. It will be apparent from the above that the HC emissions formation process in spark-ignition engines is extremely complex and that there are several paths by which a small but important amount of the fuel escapes combustion. It is appropriate here to summarize the overall structure of the spark-ignition engine hydrocarbon emission problem and identify the key factors and engine variables that influence the different parts of that problem. Table 11.7 provides such a summary. The total process is divided into four sequential steps: (1) the formation of unburned hydrocarbon emissions; (2) the oxidation of a fraction of these HC emissions within the cylinder, following mixing with the bulk gases; (3) the flow of a fraction of the unoxidized HC from the cylinder into the exhaust; (4) the oxidation in the exhaust system of a fraction of the HC that exit the cylinder. The detailed processes and the design and operating variables that influence each of these steps in a significant way are listed.

The four separate formation mechanisms identified in step 1 have substantial, though as yet incomplete, evidence behind them. They are listed in the most likely order of importance. Each has been extensively described in this section. It is through each of these mechanisms that fuel or fuel-air mixture escapes the primary combustion process. That fuel must then survive the expansion and exhaust processes and pass through the exhaust system without oxidation if it is to end up in the atmosphere as HC emissions. The rate of mixing of these unburned HC with the hot bulk cylinder gases, the temperature and composition of the gases with which these HC mix, and the subsequent temperature-time and composition-time histories of the mixture will govern the amount of in-cylinder oxidation that occurs. The distribution of these HC around the combustion chamber is nonuniform (and changes with time); they are concentrated close to the walls of the chamber. The fraction of these HC that will exit the chamber during the exhaust process will depend on the details of the in-cylinder flow patterns that take them through the exhaust valve. Overall, the magnitude of the residual fraction will be one major factor; the residual gas is known to be much richer in HC than the average exhaust. In particular, the flow patterns in the cylinder toward the end of the exhaust stroke as the gas scraped off the cylinder wall by the piston moves toward the exhaust valve will be important. Finally, a fraction of the unburned HC which leave the cylinder through the exhaust valve will burn up within the exhaust system. Gas-phase oxidation in the exhaust ports and hotter parts of the exhaust manifold is significant. The amount depends on the gas temperature, composition, and residence time. If catalysts or a thermal reactor are included in the exhaust system, very substantial additional reduction in HC emission levels can occur. These devices and their operating characteristics are described in Sec. 11.6.

TABLE 11.7
Critical factors and engine variables in HC emissions mechanisms

1. *Formation of HC*
   - (*a*) Crevices
     - (1) Crevice volume
     - (2) Crevice location (relative to spark plug)
     - (3) Load
     - (4) Crevice wall temperature
     - (5) Mixture composition†
   - (*b*) Oil layers
     - (1) Oil consumption
     - (2) Wall temperature
     - (3) Speed
   - (*c*) Incomplete combustion
     - (1) Burn rate and variability
     - (2) Mixture composition†
     - (3) Load
     - (4) Spark timing‡
   - (*d*) Combustion chamber walls
     - (1) Deposits
     - (2) Wall roughness
2. *In-cylinder mixing and oxidation*
   - (*a*) Mixing rate with bulk gas
     - (1) Speed
     - (2) Swirl ratio
     - (3) Combustion chamber shape
   - (*b*) Bulk gas temperature during expansion and exhaust
     - (1) Speed
     - (2) Spark timing‡
     - (3) Mixture composition†
     - (4) Compression ratio
     - (5) Heat losses to walls
   - (*c*) Bulk gas oxygen concentration
     - (1) Equivalence ratio
   - (*d*) Wall temperature
     - (1) Important if HC source near wall
     - (2) For crevices: importance depends on geometry
3. *Fraction HC flowing out of cylinder*
   - (*a*) Residual fraction
     - (1) Load
     - (2) Exhaust pressure
     - (3) Valve overlap
     - (4) Compression ratio
     - (5) Speed
   - (*b*) In-cylinder flow during exhaust stroke
     - (1) Valve overlap
     - (2) Exhaust valve size and location
     - (3) Combustion chamber shape
     - (4) Compression ratio
     - (5) Speed
4. *Oxidation in exhaust system*
   - (*a*) Exhaust gas temperature
     - (1) Speed
     - (2) Spark timing‡
     - (3) Mixture composition†
     - (4) Compression ratio
     - (5) Secondary air flow
     - (6) Heat losses in cylinder and exhaust
   - (*b*) Oxygen concentration
     - (1) Equivalence ratio
     - (2) Secondary air flow and addition point
   - (*c*) Residence time
     - (1) Speed
     - (2) Load
     - (3) Volume of critical exhaust system component
   - (*d*) Exhaust reactor§
     - (1) Oxidation catalyst
     - (2) Three-way catalyst
     - (3) Thermal reactor

† Fuel/air equivalence ratio and burned gas fraction (residual plus recycled exhaust gas).
‡ Relative to MBT timing.
§ Of at least as great an importance as engine details if present in total emission control system. See Sec. 11.6

11.4.4 Hydrocarbon Emission Mechanisms in Diesel Engines

BACKGROUND. Diesel fuel contains hydrocarbon compounds with higher boiling points, and hence higher molecular weights, than gasoline. Also, substantial pyrolysis of fuel compounds occurs within the fuel sprays during the diesel combustion process. Thus, the composition of the unburned and partially oxidized hydrocarbons in the diesel exhaust is much more complex than in the spark-ignition engine and extends over a larger molecular size range. Gaseous hydrocarbon emissions from diesels are measured using a hot particulate filter (at 190°C) and a heated flame ionization detector. Thus the HC constituents vary from methane to the heaviest hydrocarbons which remain in the vapor phase in the heated sampling line (which is also maintained at about 190°C). Any hydrocarbons heavier than this are therefore condensed and, with the solid-phase soot, are filtered from the exhaust gas stream upstream of the detector. The particulate emission measurement procedure measures a portion of total engine hydrocarbon emissions also. Particulates are collected by filtering from a diluted exhaust gas stream at a temperature of 52°C or less. Those hydrocarbons that condense at or below this temperature are absorbed onto the soot. They are the extractable fraction of the particulate: i.e., that fraction which can be removed by a powerful solvent, typically between about 15 and 45 percent of the total particulate mass. This section discusses gaseous hydrocarbon emissions; particulate emissions—soot and extractable material—are discussed in Sec. 11.5.

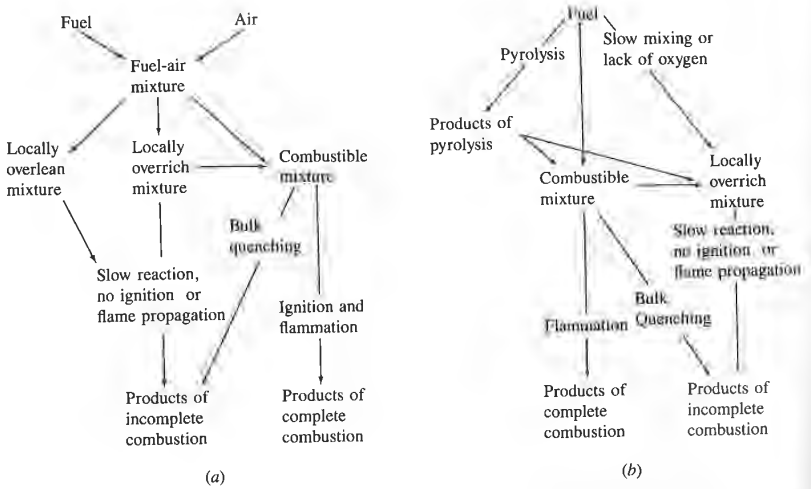

FIGURE 11-33
Schematic representation of diesel hydrocarbon formation mechanisms: (*a*) for fuel injected during delay period; (*b*) for fuel injected while combustion is occurring.[23]

bon compounds with higher
s, than gasoline. Also, substan-
ıe fuel sprays during the diesel
ıe unburned and partially oxi-
ch more complex than in the
molecular size range. Gaseous
using a hot particulate filter (at
Thus the HC constituents vary
h remain in the vapor phase in
:d at about 190°C). Any hydro-
l and, with the solid-phase soot,
of the detector. The particulate
ırtion of total engine hydrocar-
filtering from a diluted exhaust
ɔse hydrocarbons that condense
he soot. They are the extractable
h can be removed by a powerful
ɛnt of the total particulate mass.
ıissions; particulate emissions—
ec. 11.5.

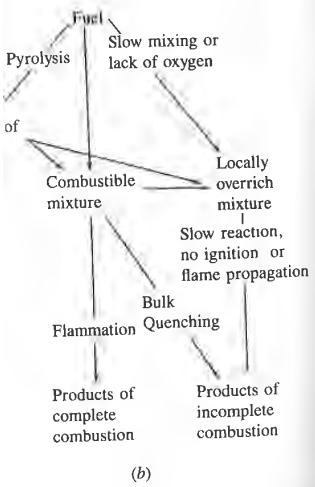

(*b*)

ı mechanisms: (*a*) for fuel injected during
ring.[23]

The complex heterogeneous nature of diesel combustion, where fuel evaporation, fuel-air and burned-unburned gas mixing, and combustion can occur simultaneously, has been discussed extensively in Chap. 10. As a result of this complexity, there are many processes that could contribute to diesel engine hydrocarbon emissions. In Chap. 10 the diesel's compression-ignition combustion process was divided into four stages: (1) the ignition delay which is the time between the start of injection and ignition; (2) the premixed or rapid combustion phase, during which the fuel that has mixed to within combustible limits during the delay period burns; (3) the mixing controlled combustion phase, during which the rate of burning depends on the rate of fuel-air mixing to within the combustible limits; (4) the late combustion phase where heat release continues at a low rate governed by the mixing of residual combustibles with excess oxygen and the kinetics of the oxidation process. There are two primary paths by which fuel can escape this normal combustion process unburned: the fuel-air mixture can become too lean to autoignite or to support a propagating flame at the conditions prevailing inside the combustion chamber, or, during the primary combustion process, the fuel-air mixture may be too rich to ignite or support a flame. This fuel can then be consumed only by slower thermal oxidation reactions later in the expansion process after mixing with additional air. Thus, hydrocarbons remain unconsumed due to incomplete mixing or to quenching of the oxidation process.†

Figure 11-33 shows schematically how these processes can produce incomplete combustion products. Fuel injected during the ignition delay (Fig. 11-33*a*) will mix with air to produce a wide range of equivalence ratios. Some of this fuel will have mixed rapidly to equivalence ratios lower than the lean limit of combustion (locally overlean mixture), some will be within the combustible range, and some will have mixed more slowly and be too rich to burn (locally overrich mixture). The overlean mixture will not autoignite or support a propagating flame at conditions prevailing inside the combustion chamber (though some of this mixture may burn later if it mixes with high-temperature burned products early in the expansion stroke). In the "premixed" combustible mixture, ignition occurs where the local conditions are most favorable for autoignition. Unless quenched by thermal boundary layers or rapid mixing with air, subsequent autoignition or flame fronts propagating from the ignition sites consume the combustible mixture. Complete combustion of overrich mixture depends on further mixing with air or lean already-burned gases within the time available before rapid expansion and cooling occurs. Of all these possible mechanisms, the overlean mixture path is believed to be the most important.[23]

For the fuel injected after the ignition delay period is over (Fig. 11-33*b*), rapid oxidation of fuel or the products of fuel pyrolysis, as these mix with air,

† Note that under normal engine operating conditions, the combustion inefficiency is less than 2 percent; see Sec. 4.9.4 and Fig. 3-9.

results in complete combustion. Slow mixing of fuel and pyrolysis products with air, resulting in overrich mixture or quenching of the combustion reactions, can result in incomplete combustion products, pyrolysis products, and unburned fuel being present in the exhaust.[23]

Hydrocarbon emission levels from diesels vary widely with operating conditions, and different HC formation mechanisms are likely to be most important at different operating modes. Engine idling and light-load operation produce significantly higher hydrocarbon emissions than full-load operation. However, when the engine is overfueled, HC emissions increase very substantially. As will be explained more fully below, overmixing (overleaning) is an important source of HC, especially under light-load operation. Undermixing, resulting in overrich mixture during the combustion period, is the mechanism by which some of the fuel remaining in the injector nozzle sac volume escapes combustion, and is also the cause of very high HC emissions during overfueling. Wall temperatures affect HC emissions, suggesting that wall quenching is important, and under especially adverse conditions very high cyclic variability in the combustion process can cause an increase in HC due to partial burning and misfiring cycles.

OVERLEANING. As soon as fuel injection into the cylinder commences, a distribution in the fuel/air equivalence ratio across the fuel sprays develops. The amount of fuel that is mixed leaner than the lean combustion limit ($\phi_L \sim 0.3$) increases rapidly with time.[23] Figure 11-34 illustrates this equivalence ratio distribution in the fuel spray at the time of ignition. In a swirling flow, ignition occurs in the slightly lean-of-stoichiometric region downstream of the spray core

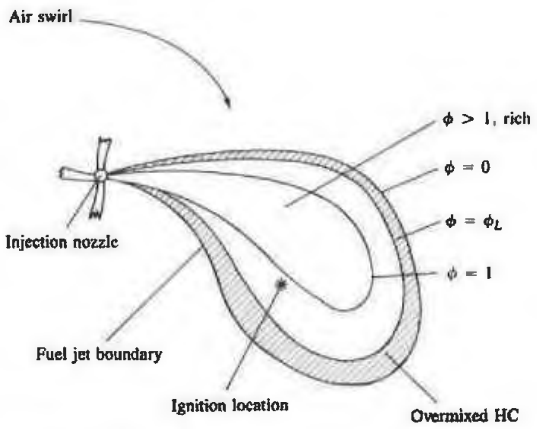

FIGURE 11-34
Schematic of diesel engine fuel spray showing equivalence ratio (ϕ) contours at time of ignition. ϕ_L = equivalence ratio at lean combustion limit (≈ 0.3). Shaded region contains fuel mixed leaner than ϕ_L.[67]

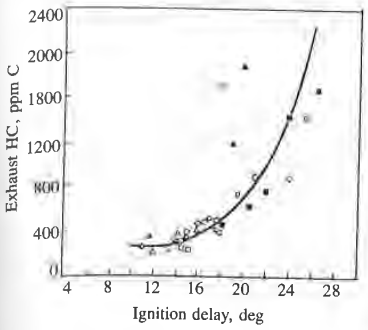

FIGURE 11-35
Correlation of exhaust HC concentration with duration of ignition delay for DI diesel engine. Various fuels, engine loads, injection timings, boost pressures, at 2800 rev/min.[67]

where the fuel which has spent most time within the combustible limits is located. However, the fuel close to the spray boundary has already mixed beyond the lean limit of combustion and will not autoignite or sustain a fast reaction front. This mixture can only oxidize by relatively slow thermal-oxidation reactions which will be incomplete. Within this region, unburned fuel, fuel decomposition products, and partial oxidation products (aldehydes and other oxygenates) will exist; some of these will escape the cylinder without being burned. The magnitude of the unburned HC from these overlean regions will depend on the amount of fuel injected during the ignition delay, the mixing rate with air during this period, and the extent to which prevailing cylinder conditions are conducive to autoignition. A correlation of unburned HC emissions with the length of the ignition delay would be expected. The data in Fig. 11-35 from a direct-injection naturally aspirated engine show that a good correlation between these variables exists. As the delay period increases beyond its minimum value (due to changes in engine operating conditions), HC emissions increase at an increasing rate.[67] Thus, overleaning of fuel injected during the ignition delay period is a significant source of hydrocarbon emissions, especially under conditions where the ignition delay is long.

UNDERMIXING. Two sources of fuel which enter the cylinder during combustion and which result in HC emissions due to slow or under mixing with air have been identified. One is fuel that leaves the injector nozzle at low velocity, often late in the combustion process. The most important source here is the nozzle sac volume, though secondary injections can increase HC emissions if the problem is severe. The second source is the excess fuel that enters the cylinder under overfueling conditions.

At the end of the fuel-injection process, the injector sac volume (the small volume left in the tip of the injector after the needle seats) is left filled with fuel. As the combustion and expansion processes proceed, this fuel is heated and vaporizes, and enters the cylinder at low velocity through the nozzle holes. This fuel vapor (and perhaps large drops of fuel also) will mix relatively slowly with air

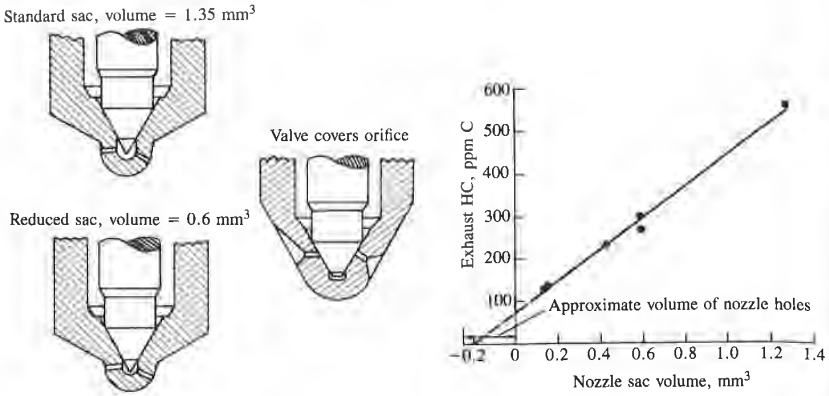

FIGURE 11-36
Effect of nozzle sac volume on exhaust HC concentration, DI diesel engine, at minimum ignition delay. V_d = 1 dm³/cylinder, 1700–2800 rev/min.[67]

and may escape the primary combustion process. Figure 11-36 shows HC emissions at the minimum ignition delay for a direct-injection diesel engine as a function of sac volume, along with drawings of some of the injector nozzles used. The correlation between HC emissions (under conditions when the overleaning mechanism is least significant) and sac volume is striking. The extrapolation to zero HC emissions suggests that the fuel in the nozzle holes also contributes. Not all the fuel in the sac volume is exhausted as unburned hydrocarbons. For example, in Fig. 11-36 a volume of 1 mm³ gives 350 ppm C_1 while 1 mm³ of fuel would give 1660 ppm C_1. The sac volume may not be fully filled with fuel. Also, the higher-boiling-point fractions of the fuel may remain in the nozzle. Significant oxidation may also occur. In indirect-injection engines, similar trends have been observed, but the HC emission levels at short ignition delay conditions are substantially lower. The sac volume in current production nozzles helps to equalize the fuel pressures immediately upstream of the nozzle orifices. A small sac volume makes this equalization less complete and exhaust smoke deteriorates. The contribution of sac and hole volumes to exhaust HC can be reduced to below 0.75 g/kW · h for a 1 dm³ per cylinder displacement DI engine.[67]

In DI engines, exhaust smoke limits the full-load equivalence ratio to about 0.7. Under transient conditions as the engine goes through an acceleration process, overfueling can occur. Even though the overall equivalence ratio may remain lean, locally overrich conditions may exist through the expansion stroke and into the exhaust process. Figure 11-37 shows the effect of increasing the amount of fuel injected at constant speed, with the injection timing adjusted to keep the ignition delay at its minimum value (when HC emissions from overleaning are lowest). HC emissions are unaffected by an increasing equivalence ratio until a critical value of about 0.9 is reached when levels increase dramatically. A

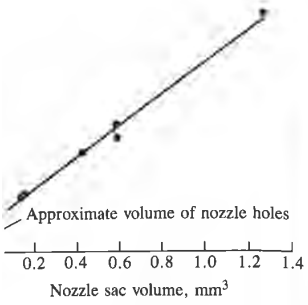

l diesel engine, at minimum ignition

Figure 11-36 shows HC emis-
ection diesel engine as a func-
the injector nozzles used. The
itions when the overleaning
striking. The extrapolation to
zle holes also contributes. Not
unburned hydrocarbons. For
) ppm C_1 while 1 mm³ of fuel
t be fully filled with fuel. Also,
main in the nozzle. Significant
gines, similar trends have been
tion delay conditions are sub-
ction nozzles helps to equalize
zle orifices. A small sac volume
smoke deteriorates. The con-
an be reduced to below 0.75 g/
gine.[67]
oad equivalence ratio to about
goes through an acceleration
overall equivalence ratio may
through the expansion stroke
/s the effect of increasing the
ie injection timing adjusted to
1 HC emissions from overlean-
n increasing equivalence ratio
levels increase dramatically λ

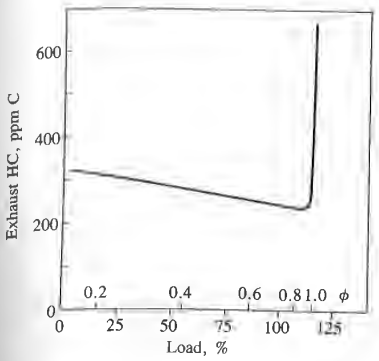

FIGURE 11-37
Effect of overfueling on exhaust HC concentration. DI diesel engine, speed = 1700 rev/min, injection timing at full-load 15° BTC.[67]

similar trend exists for IDI engines.[67] This mechanism is not significant under normal operating conditions, but can contribute HC emissions under acceleration conditions if overfueling occurs. However, it produces less HC than does overleaning at light load and idle.[23]

QUENCHING AND MISFIRE. Hydrocarbon emissions have been shown to be sensitive to oil and coolant temperature: when these temperatures were increased from 40 to 90°C in a DI diesel, HC emissions decreased by 30 percent. Since ignition delay was maintained constant, overmixing phenomena should remain approximately constant. Thus, wall quenching of the flame may also be a significant source of HC, depending on the degree of spray impingement on the combustion chamber walls.

While cycle-by-cycle variation in the combustion process in diesel engines is generally much less than in spark-ignition engines, it can become significant under adverse conditions such as low compression temperatures and pressures and retarded injection timings. Substantial variations, cycle-by-cycle, in HC emissions are thought to result. In the limit, if misfire (no combustion) occurs in a fraction of the operating cycles, then engine HC emissions rise as the percentage of misfires increases. However, complete misfires in a well-designed and adequately controlled engine are unlikely to occur over the normal operating range.[23]

SUMMARY. There are two major causes of HC emissions in diesel engines under normal operating conditions: (1) fuel mixed to leaner than the lean combustion limit during the delay period; (2) undermixing of fuel which leaves the fuel injector nozzle at low velocity, late in the combustion process. At light load and idle, overmixing is especially important, particularly in engines of relatively small cylinder size at high speed. In IDI engines, the contribution from fuel in the nozzle sac volume is less important than with DI engines. However, other sources of low velocity and late fuel injection such as secondary injection can be significant.

11.5 PARTICULATE EMISSIONS

11.5.1 Spark-Ignition Engine Particulates

There are three classes of spark-ignition engine particulate emissions: lead, organic particulates (including soot), and sulfates.

Significant sulfate emissions can occur with oxidation-catalyst equipped engines. Unleaded gasoline contains 150 to 600 ppm by weight sulfur, which is oxidized within the engine cylinder to sulfur dioxide, SO_2. This SO_2 can be oxidized by the exhaust catalyst to SO_3 which combines with water at ambient temperatures to form a sulfuric acid aerosol. Levels of sulfate emissions depend on the fuel sulfur content, the operating conditions of the engine, and the details of the catalyst system used. Typical average automobile sulfate emission rates are 20 mg/km or less.[68]

For automobile engines operated with regular and premium leaded gasolines (which contain about 0.15 g Pb/liter or dm^3) the particulate emission rates are typically 100 to 150 mg/km. This particulate is dominated by lead compounds: 25 to 60 percent of the emitted mass is lead.[69] The particulate emission rates are considerably higher when the engine is cold, following start-up. The exhaust temperature has a significant effect on emission levels. The particle size distribution with leaded fuel is about 80 percent by mass below 2 μm diameter and about 40 percent below 0.2 μm diameter. Most of these particles are presumed to form and grow in the exhaust system due to vapor phase condensation enhanced by coagulation. Some of the particles are emitted directly, without settling. Some of the particles either form or are deposited on the walls where agglomeration may occur. Many of these are removed when the exhaust flow rate is suddenly increased, and these particles together with rust and scale account for the increase in mass and size of particles emitted during acceleration. Only a fraction (between 10 and 50 percent) of the lead consumed in the fuel is exhausted, the remainder being deposited within the engine and exhaust system.

Use of unleaded gasoline reduces particulate emissions to about 20 mg/km in automobiles without catalysts. This particulate is primarily soluble (condensed) organic material. Soot emissions (black smoke) can result from combustion of overly rich mixtures. In properly adjusted spark-ignition engines, soot in the exhaust is not a significant problem.

11.5.2 Characteristics of Diesel Particulates

MEASUREMENT TECHNIQUES. Diesel particulates consist principally of combustion generated carbonaceous material (soot) on which some organic compounds have become absorbed. Most particulate material results from incomplete combustion of fuel hydrocarbons; some is contributed by the lubricating oil. The emission rates are typically 0.2 to 0.6 g/km for light-duty diesels in an automobile. In larger direct-injection engines, particulate emission rates are 0.5 to 1.5 g/brake kW · h. The composition of the particulate material depends on the conditions in the engine exhaust and particulate collection system. At tem-

peratures above 500°C, the individual particles are principally clusters of many small spheres or spherules of carbon (with a small amount of hydrogen) with individual spherule diameters of about 15 to 30 nm. As temperatures decrease below 500°C, the particles become coated with adsorbed and condensed high molecular weight organic compounds which include: unburned hydrocarbons, oxygenated hydrocarbons (ketones, esters, ethers, organic acids), and polynuclear aromatic hydrocarbons. The condensed material also includes inorganic species such as sulfur dioxide, nitrogen dioxide, and sulfuric acid (sulfates).

The objective of most particulate measurement techniques is to determine the amount of particulate being emitted to the atmosphere. Techniques for particulate measurement and characterization range from simple smoke meter opacity readings to analyses using dilution tunnels. Most techniques require lengthy sample-collection periods because the emission rate of individual species is usually low. The physical conditions under which particulate measurements are made are critical because the emitted species are unstable and may be altered through loss to surfaces, change in size distribution (through collisions), and chemical interactions among other species in the exhaust at any time during the measurement process (including sampling, storage, or examination). The most basic information is normally obtained on a mass basis: for example, grams per kilometer for a vehicle, grams per kilowatt-hour for an engine, grams per kilogram of fuel or milligrams per cubic meter of exhaust (at standard conditions). Smoke meters measure the relative quantity of light that passes through the exhaust or the relative reflectance of particulate collected on filter paper. They do not measure mass directly. They are used to determine visible smoke emissions and provide an approximate indication of mass emission levels. Visible smoke from heavy-duty diesels at high load is regulated. In the standard mass emission measurement procedure, dilution tunnels are used to simulate the physical and chemical processes the particulate emissions undergo in the atmosphere. In the dilution tunnel, the raw exhaust gases are diluted with ambient air to a temperature of 52°C or less, and a sample stream from the diluted exhaust is filtered to remove the particulate material.

PARTICULATE COMPOSITION AND STRUCTURE. The structure of diesel particulate material is apparent from the photomicrographs shown in Fig. 11-38 of particulates collected from the exhaust of an IDI diesel engine. The samples are seen to consist of collections of primary particles (spherules) agglomerated into aggregates (hereafter called particles). Individual particles range in appearance from clusters of spherules to chains of spherules. Clusters may contain as many as 4000 spherules. Occasional liquid hydrocarbon and sulfate droplets have been identified. The spherules are combustion generated soot particles which vary in diameter between 10 and 80 nm, although most are in the 15 to 30 nm range. Figure 11-39 shows a typical distribution of spherule size (solid line) determined by sizing and counting images in the photomicrographs. The number-mean diameter ($=\sum N_i d_i/N$) is 28 nm. The volume contribution of these

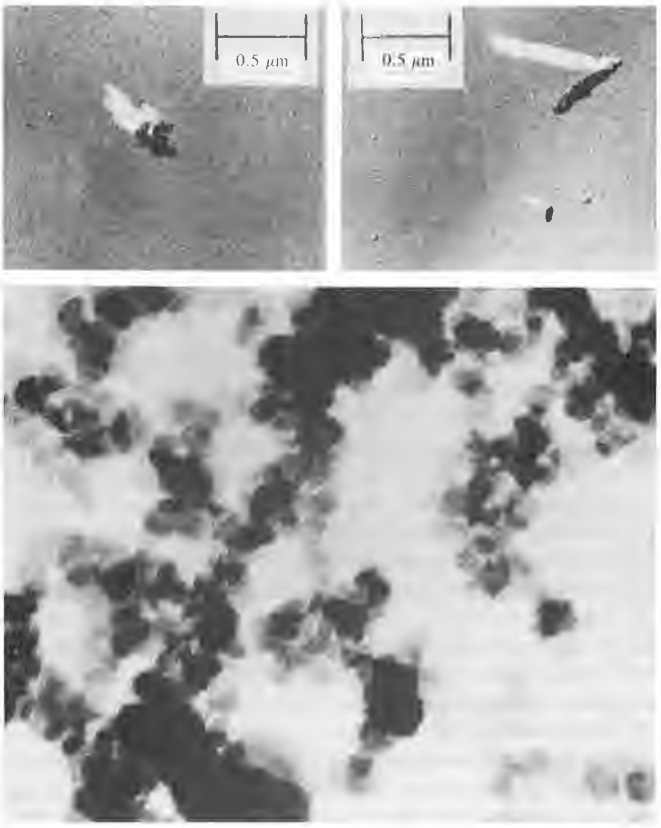

FIGURE 11-38
Photomicrographs of diesel particulates: cluster (upper left), chain (upper right), and collection from filter (bottom).[70]

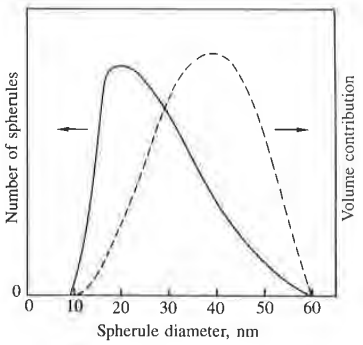

FIGURE 11-39
Typical distributions of spherule diameter and volume.[70]

chain (upper right), and collection from

39
ributions of spherule diameter and

TABLE 11.8
Chemical composition of particular matter[70]

	Idle	48 km/h
Extractable composition	$C_{23}H_{29}O_{4.7}N_{0.21}$	$C_{24}H_{30}O_{2.6}N_{0.18}$
H/C	1.26	1.63
Dry soot composition	$CH_{0.27}O_{0.22}N_{0.01}$	$CH_{0.21}O_{0.15}N_{0.01}$
H/C	0.27	0.21

spherules is shown as the dashed curve in Fig. 11-39. The volume-mean diameter, $(\sum N_i d_i^3/N)^{1/3}$, is 31 nm.

Determination of the *particle* size distribution with a similar technique involves assigning a single dimension to a complex and irregular aggregate, and introduces uncertainties arising from only having two-dimensional images of particles available. Other approaches based on inertial impactors and electrical aerosol analysers have been used. Some of the data suggest that the particle size distribution is bimodal. The smaller-size range is thought to be liquid hydrocarbon drops and/or individual spherules characterized by number-mean diameters of 10 to 20 nm; the larger-size range is thought to be the particles of agglomerated spherules characterized by number-mean diameters of 100 to 150 nm. However, other particulate samples have not shown a bimodal distribution: volume-mean diameters ranged from 50 to 220 nm with no notable trend with either speed or load.[70]

The exhaust particulate is usually partitioned with an extraction solvent into a soluble fraction and a dry-soot fraction. Two commonly used solvents are dichloromethane and a benzene-ethanol mixture. Typically 15 to 30 mass percent is extractable, though the range of observations is much larger ($\sim$10 to 90 percent). Thermogravimetric analysis (weighing the sample as it is heated) produces comparable results. Typical average chemical compositions of the two particulate fractions are given in Table 11.8. Dry soot has a much lower H/C ratio than the extractable material. Although most of the particulate emissions are formed through incomplete combustion of fuel hydrocarbons, engine oil may also contribute significantly. The number-average molecular weight of the extractable material shown in Table 11.8 ranged from about 360 to 400 for a variety of engine conditions. This fell between the average molecular weight of the fuel (199) and that of the lubricating oil (443 when fresh and 489 when aged).[70] Radioactive tracer studies in a light-duty IDI diesel have shown that the oil was the origin of between 2 to 25 percent by mass of the total particulate and 16 to 80 percent of the extractable organic portion, the greatest percentages being measured at the highest engine speed studied (3000 rev/min). All of the oil contribution appeared in the extractable material. The contributions from the different individual compounds in the fuel have also been studied. All the compounds tested—paraffins,

FIGURE 11-40
Lattice-imaging micrograph of a diesel particulate.[72]

olefins, and aromatics—contributed to the particulate emissions; as a group, aromatics were the greatest contributors. Eighty percent of the carbon-14 used to tag individual fuel compounds was found in the *insoluble* fraction and 20 percent in the *soluble* particulate fraction.[71]

In addition to the elements listed in Table 11.8, trace amounts of sulfur, zinc, phosphorus, calcium, iron, silicon, and chromium have been found in particulates. Sulfur and traces of calcium, iron, silicon, and chromium are found in diesel fuel; zinc, phosphorus, and calcium compounds are frequently used in lubricating oil additives.[70]

A lattice image of a diesel particle is shown in Fig. 11-40; it suggests a concentric lamellate structure arranged around the center of each spherule. This arrangement of concentric lamellas is similar to the structure of carbon black. This is not surprising; the environment in which diesel soot is produced is similar to that in which oil furnace blacks are made. The carbon atoms are bonded together in hexagonal face-centered arrays in planes, commonly referred to as platelets. As illustrated in Fig. 11-41, the mean layer spacing is 0.355 nm (only slightly larger than graphite). Platelets are arranged in layers to form crystallites. Typically, there are 2 to 5 platelets per crystallite, and on the order of 10^3 crys-

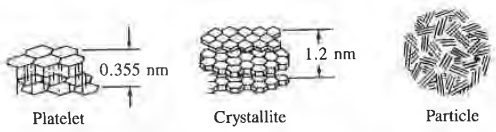

FIGURE 11-41
Substructure of carbon particle.[73]

rticulate emissions; as a group, aro-
percent of the carbon-14 used to tag
insoluble fraction and 20 percent in

'able 11.8, trace amounts of sulfur,
:hromium have been found in parti-
ilicon, and chromium are found in
compounds are frequently used in

shown in Fig. 11-40; it suggests a
nd the center of each spherule. This
r to the structure of carbon black.
ich diesel soot is produced is similar
de. The carbon atoms are bonded
n planes, commonly referred to as
ean layer spacing is 0.355 nm (only
ranged in layers to form crystallites.
allite, and on the order of 10^3 crys-

FIGURE 11-41
le Substructure of carbon particle.[73]

tallites per spherule. The crystallites are arranged with their planes more or less parallel to the particle surface. This structure of unordered layers is called turbostatic. The spherules, 10 to 50 nm in diameter, are fused together to form particles as shown in Fig. 11-40. A single spherule contains 10^5 to 10^6 carbon atoms.[70, 73]

A surface area of about 200 m^2/g has been measured for diesel soot. A smooth-surfaced 30-nm diameter sphere with a density of 2 g/cm^3 would have a surface/mass ratio of 100 m^2/g, so the measured value is about twice the superficial area. Approximating a particle of agglomerated spherules by a single sphere of 200 nm diameter gives a surface/mass ratio of 15 m^2/g.[70] These data and estimates of superficial area per unit mass indicate that diesel soot has low porosity.

SOLUBLE FRACTION COMPONENTS. The extractable organic fraction of diesel particulate emissions includes compounds that may cause health and environmental hazards. Thus chemical and biological characterization of the soluble organic fraction are important. Both soxhlet and sonification methods are used to extract the organic fraction from particulate samples. Because the particulates are mixtures of polar and nonpolar components, full extraction requires different solvents; any one solvent is a compromise. Methylene chloride is the most commonly used extractant, however. Since a complex mixture of organic compounds is associated with diesel particulates, a preliminary fractionation scheme is used to group similar types of compounds before final separation and identification. The scheme most frequently used results in seven fractions generally labeled as: basics, acidics, paraffins, aromatics, transitionals, oxygenates, and ether insolubles. Table 11.9 indicates the types of components in each fraction and the approximate proportions. The biological activity of the soluble organic fraction and its subfractions is most commonly assessed with the Ames *Salmonella*/microsomal test. With this test, a quantitative dose-response curve showing the mutagenicity of a sample compound is obtained. The Ames test uses a mutant strain of *Salmonella typhimurium* that is incapable of producing histidine. Mutagenicity is defined as the ability of a tested compound to revert—back-mutate—this bacterium to its wild state, where it regains its ability to produce histidine.[15]

11.5.3 Particulate Distribution within the Cylinder

Measurements have been made of the particulate distribution within the combustion chamber of operating diesel engines. The results provide valuable information on the particulate formation and oxidation processes and how these relate to the fuel distribution and heat-release development within the combustion chamber. Techniques used to obtain particulate concentration data include: use of rapid-acting poppet or needle valves which draw a small gas sample from the cylinder at a specific location and time for analysis (e.g., Refs. 21

TABLE 11-9
Components of the soluble organic fraction[35]

Fraction	Components of fraction	Percent of total
Acidic	Aromatic or aliphatic Acidic functional groups Phenolic and carboxylic acids	3–15
Basic	Aromatic or aliphatic Basic functional groups Amines	<1–2
Paraffin	Aliphatics, normal and branched Numerous isomers From unburned fuel and/or lubricant	34–65
Aromatic	From unburned fuel, partial combustion, and recombination of combustion products; from lubricants Single ring compounds Polynuclear aromatics	3–14
Oxygenated	Polar functional groups but not acidic or basic Aldehydes, ketones, or alcohols Aromatic phenols and quinones	7–15
Transitional	Aliphatic and aromatic Carbonyl functional groups Ketones, aldehydes, esters, ethers	1–6
Insoluble	Aliphatic and aromatic Hydroxyl and carbonyl groups High molecular weight organic species Inorganic compounds Glass fibers from filters	6–25

and 74), optical absorption techniques (e.g., Refs. 75 and 76), and cylinder dumping where the cylinder contents are rapidly emptied into an evacuated tank at a preset time in the cycle (e.g., Ref. 77). Both DI and IDI engines have been studied. Of course, concentration data taken at specific locations in the cylinder during the engine cycle are not necessarily representative of the cylinder contents in general; nor do they represent the time history of a given mass of gas. The fuel distribution, mixing, and heat-release patterns in the cylinder are highly nonuniform during the soot-formation process, and the details of gas motion in the vicinity of the sampling location as the piston changes position are usually unknown.

In direct-injection diesel engines, the highest particulate concentrations are found in the core region of each fuel spray where local average equivalence ratios are very rich (see Secs. 10.5.6 and 10.7.2). Soot concentrations rise rapidly soon after combustion starts. Figure 11-42 shows a set of sample-valve soot-concentration data from a large (30.5-cm bore, 38.1-cm stroke), quiescent, direct-

	Percent of total
	3–15
	<1–2
	34–65
ı, and ts; from	3–14
or basic	7–15
	1–6
	6–25

., Refs. 75 and 76), and cylinder dly emptied into an evacuated tank oth DI and IDI engines have been at specific locations in the cylinder presentative of the cylinder contents ory of a given mass of gas. The fuel s in the cylinder are highly nonunif the details of gas motion in the ston changes position are usually

ghest particulate concentrations are ere local average equivalence ratios ot concentrations rise rapidly soon ows a set of sample-valve soot- e, 38.1-cm stroke), quiescent, direct-

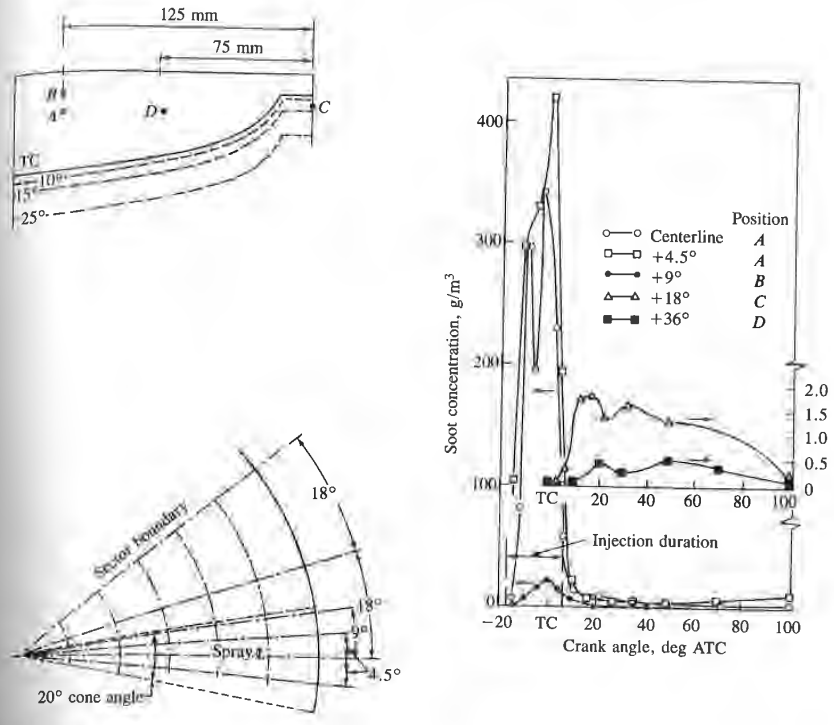

FIGURE 11-42
Particulate concentrations, in g/m³ at standard temperature and pressure, in various regions of the fuel spray as a function of crank angle in quiescent DI diesel engine, measured with rapid sampling valve. Different sample valve locations in combustion chamber and spray indicated on left. Cylinder bore = 30.5 cm, stroke = 38.1 cm, r_v = 12.9, engine speed = 500 rev/min, bmep = 827 kPa.[74]

injection diesel engine which illustrates these points.[74] The particulate concentrations on the fuel spray axis close to the injector orifice are remarkably high (~200 to 400 g/m³ at standard temperature and pressure). This corresponds to a large fraction of the fuel carbon in the extremely rich fuel vapor core being sampled as particulate (as soot and condensed HC species). Such high particulate fractions of the local fuel carbon (~50 percent) have also been found in the very fuel rich cores of high-pressure liquid-fueled turbulent diffusion flames. Pyrolysis of the fuel is therefore an important source of soot. These very high local soot concentrations decrease rapidly once fuel injection ceases and the rich core mixes to leaner equivalence ratios. Soot concentrations in the spray close to the piston bowl outer radius and at the cylinder wall rise later, are an order of magnitude less, and decay more slowly. Away from the fuel spray core, soot concentrations

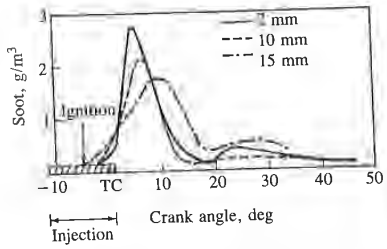

FIGURE 11-43
Particulate concentrations at various distances from wall of prechamber in swirl-chamber IDI diesel engine, measured with rapid sampling valve. Engine speed = 1000 rev/min, injection at 12° BTC, ignition at 5° BTC.[24]

decrease rapidly with increasing distance from the centerline. A useful comparison with these soot concentrations is the fuel concentration in a *stoichiometric* mixture, about 75 g fuel/m^3. Approximate estimates of the mean soot concentration inside the cylinder through the combustion process suggests that almost all (over 90 percent) of the soot formed is oxidized prior to exhaust. Similar results have been obtained in a small direct-injection engine with swirl.[78, 79] Peak soot concentrations in the outer regions of the fuel spray were comparable (~10 g/m^3). Measurements were not made in the spray core near the injector orifice; however, based on the equivalence ratio results in Fig. 10-46, soot concentrations would be expected to be lower due to the more rapid mixing with air that occurs with swirl.

Similar data are available from sampling in the prechamber of an IDI swirl chamber engine.[24] Figure 11-43 shows soot concentrations 2, 10, and 15 mm from the wall of the prechamber. Equivalence ratio distributions from this study have already been shown in Fig. 11-17. Concentrations peak 5 to 10° ATC at levels ~2 g/m^3; these are substantially lower than DI engine peak soot concentrations (presumably due to the more rapid mixing of fuel and air in the IDI engine). Concentrations in the prechamber at these locations then decrease substantially.

A better indication of average concentrations within the cylinder is given by total cylinder sampling experiments. Measurements of the total number of soot particles and soot volume fraction through the combustion process have been made in an IDI passenger car diesel. The contents of the engine cylinder, at a preselected point in the cycle, were rapidly expelled through a blowdown port, diluted, and collected in a sample bag. Figure 11-44 shows one set of results. Particles first appear shortly after the start of combustion (4 to 5° ATC). The number density rises to a maximum at 20° ATC and then falls rapidly as a result of particle coagulation and, possibly, oxidation. The exhaust particulate number density is less than one-tenth of the peak value. The volume fraction soot data (soot mass concentration is proportional to volume fraction) show a much flatter maximum earlier in the combustion process and a decrease (due to oxidation) from 20 to 40° ATC to about one-third of the peak value. Oxidation apparently ceases at about 40° ATC at these conditions.

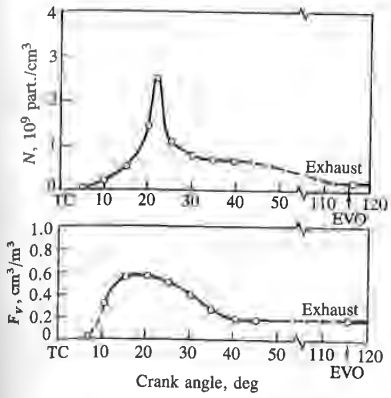

FIGURE 11-44
Cylinder-average particle-number density N and particle-volume fraction F_v, as a function of crank angle in IDI diesel engine determined from cylinder-dumping experiments. 1000 rev/min, $\phi = 0.32$, injection starts at 3.5° BTC. Gas volumes at standard temperature and pressure.[77]

11.5.4 Soot Formation Fundamentals

The soot particles, whose characteristics have been described in the above two sections, form primarily from the carbon in the diesel fuel. Thus, the formation process starts with a fuel molecule containing 12 to 22 carbon atoms and an H/C ratio of about 2, and ends up with particles typically a few hundred nanometers in diameter, composed of spherules 20 to 30 nm in diameter each containing some 10^5 carbon atoms and having an H/C ratio of about 0.1. Most of the information available on the fundamentals of soot formation in combustion comes from studies in simple premixed and diffusion flames, stirred reactors, shock tubes, and constant-volume combustion bombs. A recent review[80] summarizes the extensive literature available from such studies. Also, the production of carbon black requires a high yield of soot from pyrolysis of a hydrocarbon feedstock, and the literature from that field has much to contribute (see Ref. 81). However, the characteristics of diesel combustion which make it unsuitable for more fundamental studies—the high gas temperatures and pressures, complex fuel composition, dominance of turbulent mixing, the unsteady nature of the process, and the three-dimensional geometry—also make it difficult to interpret fundamental ideas regarding soot formation in the diesel context. There is much about the soot formation process in diesel engines, therefore, that is poorly and incompletely understood.

Soot formation takes place in the diesel combustion environment at temperatures between about 1000 and 2800 K, at pressures of 50 to 100 atm, and with sufficient air *overall* to burn fully all the fuel. The time available for the formation of solid soot particles from a fraction of the fuel is in the order of milliseconds. The resulting aerosol—dispersed solid phase particles in a gas—can be characterized by the total amount of condensed phase (often expressed as the soot volume fraction, F_v, the volume of soot/total volume), the number of soot particles per unit volume (N), and the size of the particles (e.g., average diameter d). F_v, N, and d are mutually dependent [e.g., for spherical particles $F_v =$

$(\pi/6)Nd^3$], and any two of these variables characterize the system. It is most convenient to consider N and F_V as the independent variables since they each relate to the "almost-separate" stages of soot particle generation (the source of N) and soot particle growth (the source of F_V).

These stages can be summarized as follows:[80]

1. Particle formation, where the first condensed phase material arises from the fuel molecules via their oxidation and/or pyrolysis products. These products typically include various unsaturated hydrocarbons, particularly acetylene and its higher analogues ($C_{2n}H_2$), and polycyclic aromatic hydrocarbons (PAH). These two types of molecules are considered the most likely precursors of soot in flames. The condensation reactions of gas-phase species such as these lead to the appearance of the first recognizable soot particles (often called nuclei). These first particles are very small ($d < 2$ nm) and the formation of large numbers of them involve negligible soot loading in the region of their formation.
2. Particle growth, which includes both surface growth, coagulation, and aggregation. Surface growth, by which the bulk of the solid-phase material is generated, involves the attachment of gas-phase species to the surface of particles and their incorporation into the particulate phase. Figure 11–45, where the log of the molecular weight of a species is plotted against its hydrogen mole fraction $\tilde{x}_H$, illustrates some important points about this process. Starting with a fuel molecule of $\tilde{x}_H \gtrsim 0.5$ it is apparent that neither purely polyacetylene chain

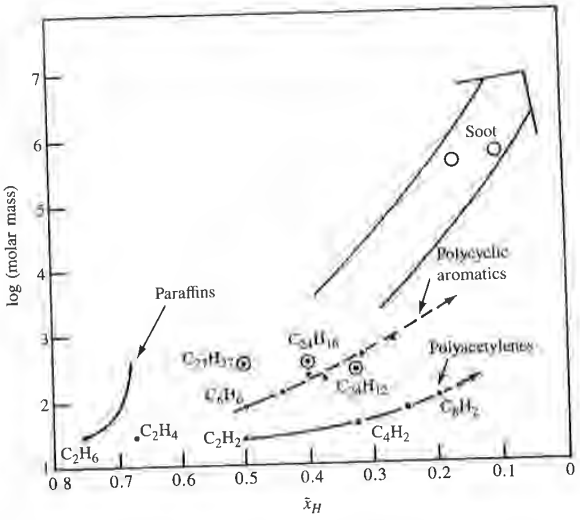

FIGURE 11-45
Paths to soot formation on plot of species molecular weight M versus hydrogen mole fraction $\tilde{x}_H$.[80]

growth nor purely PAH growth would lead to soot particles which have $\tilde{x}_H$ in the range 0.1 to 0.2. What is required is condensation of species with the right hydrogen content, or condensation of species with higher hydrogen content followed by dehydrogenation, or a combination of both these processes. Obviously some polyacetylenes and some PAH can satisfy these requirements, as can saturated platelets (e.g., $C_{27}H_{27}$; see Sec. 11.5.2). Surface growth reactions lead to an increase in the amount of soot (F_V) but the number of particles (N) remains unchanged. The opposite is true for growth by coagulation, where the particles collide and coalesce, which decreases N with F_V constant. Once surface growth stops, continued aggregation of particles into chains and clusters can occur.

These stages of particle generation and growth constitute the soot formation process. At each stage in the process oxidation can occur where soot or soot precursors are burned in the presence of oxidizing species to form gaseous products such as CO and CO_2. The eventual emission of soot from the engine will depend on the balance between these processes of formation and burnout. The emitted soot is then subject to a further mass addition process as the exhaust gases cool and are diluted with air. Adsorption into the soot particle surface and condensation to form new particles of hydrocarbon species in the exhaust gases occurs in the exhaust system and in the dilution tunnel which simulates what happens in the atmosphere. Figure 11-46 illustrates the relationship between these processes.[70] Although they are illustrated as discrete processes, there is some overlap, and they may occur concurrently in a given elemental mixture region within the diesel combustion chamber. Of course, due also to the nonhomogeneous nature of the mixture and the duration of fuel injection and its overlap with combustion, at any given time different processes are in progress in different regions or packets of fluid. The fundamentals of each of these processes will now be reviewed.

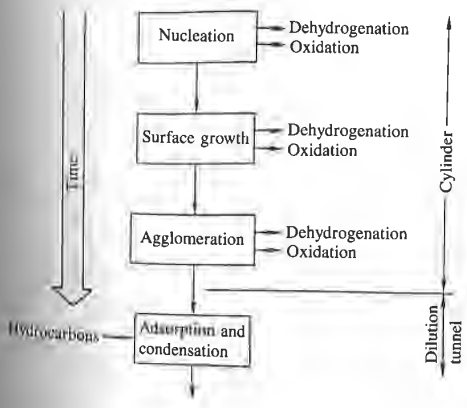

FIGURE 11-46
Processes leading to net production of diesel particulates.[70]

SOOT PARTICLE FORMATION. Empirically, it has been found useful to define the composition of the fuel-oxidizer mixture at the onset of soot formation in flames by the carbon/oxygen ratio. Equilibrium considerations indicate that soot formation should occur when, in

$$C_m H_n + yO_2 \rightarrow 2_y CO + \frac{n}{2} H_2 + (m - 2y)C_S \tag{11.35}$$

m becomes larger than $2y$: i.e., the C/O ratio exceeds unity. The corresponding fuel/air equivalence ratio is given by

$$\phi = 2\left(\frac{C}{O}\right)(1 + \delta) \tag{11.36}$$

where $\delta = n/(4m)$; ϕ is 3 for (C/O) = 1, with $n/m = 2$. The experimentally observed critical C/O ratios are less than unity, however, varying with fuel composition and details of the experimental setup from about 0.5 to 0.8. The critical C/O ratio for soot formation increases with increasing temperature but is only weakly dependent on pressure. Beyond the carbon formation limit, the yield of soot increases rapidly with increasing C/O ratio and is strongly enhanced by increasing pressure.[80]

It is obvious that soot formation is a nonequilibrium process. Yet despite decades of study, the precise details of the chemistry leading to the establishment of soot nuclei still elude investigators. Several different theories have been advanced to explain the pyrolysis process—the extensive decomposition and atomic rearrangement of the fuel molecules—that culminates in nucleation. Reviews of these theories can be found in Refs. 73, 80, and 81. Often-cited mechanisms are thermal cracking that results in fragmentation of fuel molecules into smaller ones, condensation reactions and polymerization that result in larger molecules, and dehydrogenation that lowers the H/C ratio of the hydrocarbons destined to become soot. Three different paths to the production of soot appear to exist, depending on the formation temperature. At the lowest temperatures ($\lesssim$1700 K) only aromatics or highly unsaturated aliphatic compounds of high molecular weight are very effective in forming solid carbon through pyrolysis. At intermediate temperatures typical of diffusion flames ($\gtrsim$1800 K), all normally used hydrocarbon fuels produce soot if burned at sufficiently rich stoichiometry, but appear to do so by following a different path. At very high temperatures, above the range of interest for diesel combustion, a third nucleation process seems likely that involves carbon vapor.[70]

A simple mechanistic model for nucleation in the low and intermediate temperature ranges which has considerable experimental support for its basic features has been advanced by Graham et al.[82] It is illustrated in Fig. 11-47. At low temperatures, an aromatic hydrocarbon can produce soot via a relatively fast direct route that involves condensation of the aromatic rings into a graphitelike structure. Above about 1800 K, however, a slower, less-direct route is favored that entails ring breakup into smaller hydrocarbon fragments. These fragments then polymerize to form larger unsaturated molecules that ultimately produce

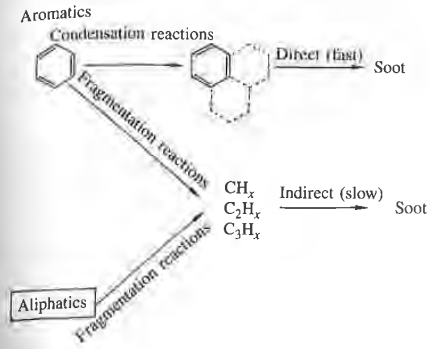

FIGURE 11-47
Mechanistic model for formation of soot from aromatic and aliphatic hydrocarbon compounds.[70]

soot nuclei. Aliphatic molecules can only follow this latter less-direct route. Experimental measurements in flames suggest that polyunsaturated hydrocarbon compounds are involved in nucleation, and acetylenes and polyacetylenes have been detected that decrease in concentration as the mass of carbon formed increases. Such observations fit the indirect path in Fig. 11-47. Results of studies of pyrolysis of benzene between 1300 and 1700 K support a physical condensation mechanism for the low-temperature path. This mechanism begins with the transformation of the initial hydrocarbon into macromolecules by a gas-phase reaction. The partial pressure of these macromolecules grows until supersaturation becomes sufficient to force their condensation into liquid microdroplets. These become nuclei, and subsequently formed gaseous macromolecules then contribute to nuclei growth.[70]

SOOT PARTICLE GROWTH. Nucleation produces a large number of very small particles with an insignificant soot loading. The bulk of the solid-phase material is generated by surface growth, which involves the gas-phase deposition of hydrocarbon intermediates on the surfaces of the spherules that develop from the nuclei. A qualitative description of the changes that occur as a function of time in a premixed flame during nucleation and surface growth is shown in Fig. 11-48. The soot fraction F_V, in units of soot volume per unit volume of gas, is related to the number density N and the volume-mean diameter of the soot particles by

$$F_V = \frac{\pi}{6} N d^3 \tag{11.37}$$

d is the actual diameter of the spherules, or the diameter of a sphere of equivalent volume to an agglomerated particle. The rate of change of particle number density with time t can be written

$$\frac{dN}{dt} = \dot{N}_n - \dot{N}_a \tag{11.38}$$

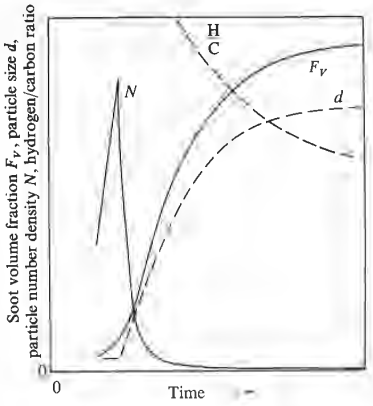

FIGURE 11-48
Variation in soot volume fraction F_V, particle number density N, particle size d, and soot hydrogen/carbon ratio with time in a flame.[70]

where $\dot{N}_n$ is the rate at which fresh nuclei appear and $\dot{N}_a$ is the rate of agglomeration of spherules or particles that collide and stick. At the peak of the N curve, $\dot{N}_n = \dot{N}_a$. To the left of the peak, $\dot{N}_n > \dot{N}_a$, the particle diameter remains essentially constant at the minimum detectable diameter and the (small) rise in soot volume is dominated by nucleation. To the right of the peak in the N curve, $\dot{N}_a > \dot{N}_n$. The number of agglomerating collisions is high because of the high number density; at the same time nucleation ends because there is enough dispersed surface area for gaseous deposition of hydrocarbon intermediates so the probability of generating new nuclei falls to zero. With nucleation halted slightly to the right of the N curve peak, all the subsequent increase in soot volume fraction (the majority) stems from surface growth. To the right of the N curve peak, the number density falls in the case illustrated by three orders of magnitude. This is the result of agglomeration, which is responsible for a portion of the increase in particle diameter. Agglomeration does not contribute to the rise in soot volume fraction, F_V. Surface growth that takes place on nuclei and on spherules is responsible for forming the concentric shells (somewhat distorted and warped) that constitute the outer portions of spherules and which are distinct from the less-organized spherule center (see Figs. 11-40 and 11-41). Surface growth on agglomerated particles may partly fill in the crevices at the junctures of adjoining spherules to provide the nodular structure evident in Fig. 11-40.[70]

Once particles have formed, interparticle collisions can lead to agglomeration, thereby decreasing the number of particles and increasing their size. Three types of agglomeration have been identified in soot formation. During the early stages of particle growth, collision of two spherical particles may result in their *coagulation* into a single spheroid. This is easy to visualize in hydrocarbon pyrolysis where the beginnings of a soot particle may have the viscosity of a tarry liquid.[70] Also, when the individual particles are small, rapid surface growth will quickly restore the original spherical shape.[78] This process occurs up to diameters of about 10 nm. On the other hand, if spherules have solidified before colli-

sion and surface growth rates have diminished, the resulting particles resemble a cluster in which the original spherules retain much of their individual identity. After surface growth essentially ceases, continued coalescence of the soot particles results in the formation of chainlike structures of discrete spherules. This suggests electrostatic forces are significant. Positive charge measured on these particle chains is claimed to be the cause of their chainlike structure.[70, 73] This latter coalescence once surface growth ceases is termed *aggregation.*

It has been shown experimentally that during coagulation the rate of decrease of particle number density was proportional to the product of a coagulation coefficient and the square of the number density:

$$-\frac{dN}{dt} = KN^2 \tag{11.39}$$

This is the Smoluchowski equation for coagulation of a liquid colloid. Based on brownian motion, this equation is applicable when the Knudsen number (ratio of mean free path to particle diameter) exceeds 10. K depends on such factors as particle size and shape, size distribution, and the temperature, pressure, and density of the gas. Equation (11.39) has been used to predict coagulation rates in low-pressure sooting flames.[73, 80] It has also been modified so that it applies where the particle size and mean free path are comparable by using a more complex expression for K (see Ref. 83). These studies show that under conditions approximating those in engine flames, the fraction of the initial number density N_0 remaining at time t is given approximately by

$$\frac{N}{N_0} \approx (KN_0 t)^{-1} \tag{11.40}$$

Thus as t increases, N/N_0 decreases rapidly Although these coagulation calculations are simplistic (in that many of the assumptions made are not strictly valid since soot particles are not initially distributed homogeneously in the combustion space, they are not monodisperse, and surface growth and oxidation may be taking place during agglomeration), an overall conclusion is that the rate of coagulation of spherules and particles to larger particles is very sensitive to number density. Thus the number of particles decreases rapidly with advancing crank angle in the diesel engine during the early part of the expansion process (see Fig. 11-44) and agglomeration is essentially complete well before the exhaust valve opens.

Throughout the soot formation process in a flame, the H/C ratio of the hydrocarbons formed in the pyrolysis and nucleation process and of the soot particles continually decreases. The H/C ratio decreases from a value of about 2, typical of common fuels, to of order 1 in the youngest soot particles that can be sampled, and then to 0.2 to 0.3 once surface growth has ceased in the fully agglomerated soot.[80] The latter stages of this process are indicated in Fig. 11-48. The addition of mass to the soot particles occurs by reaction with gas-phase molecules. The reacting gas-phase hydrocarbons appear to be principally acetylenes, with larger polymers adding faster than the smaller Small polyacetylenes

11-48
in soot volume fraction F_V, particle density N, particle size d, and soot /carbon ratio with time in a flame.[70]

ear and $\dot{N}_a$ is the rate of agglomer-
stick. At the peak of the N curve,
ıe particle diameter remains essen-
ımeter and the (small) rise in soot
right of the peak in the N curve,
isions is high because of the high
ends because there is enough dis-
hydrocarbon intermediates so the
:ro. With nucleation halted slightly
bsequent increase in soot volume
›wth. To the right of the N curve
ıstrated by three orders of magni-
ı is responsible for a portion of the
does not contribute to the rise in
ıat takes place on nuclei and on
ıtric shells (somewhat distorted and
f spherules and which are distinct
: Figs. 11-40 and 11-41). Surface
fill in the crevices at the junctures
ıtructure evident in Fig. 11-40.[70]
e collisions can lead to agglomer-
:les and increasing their size. Three
n soot formation. During the early
ıerical particles may result in their
to visualize in hydrocarbon pyrol-
may have the viscosity of a tarry
.re small, rapid surface growth will
[3] This process occurs up to diam-
›herules have solidified before colli-

undergo further polymerization in the gas phase, presumably by the same mechanism leading to nucleation. As a result of preferential addition of the larger polymers, the H/C ratio of the particles decreases toward its steady-state value. Thus most of the polyacetylenes added must be of very high molecular weight or dehydrogenation must also take place.[73, 80]

11.5.5 Soot Oxidation

In the overall soot formation process, shown schematically in Fig. 11-46, oxidation of soot at the precursor, nuclei, and particle stages can occur. The engine cylinder soot-concentration data reviewed in Sec. 11.5.3 indicate that a large fraction of the soot formed is oxidized within the cylinder before the exhaust process commences. In the discussion of diesel combustion movies in Sec. 10.3.1, dark brown regions were observed in the color photographs (see color plate, Fig. 10-4); these were interpreted as soot particle clouds, and were seen to be surrounded by a diffusion flame which appeared white from the luminosity of the high-temperature soot particles consumed in this flame. As air mixed with this soot-rich region, the white flame eradicated the dark soot clouds as the particles were burned up.

In general, the rate of heterogeneous reactions such as the oxidation of soot depends on the diffusion of reactants to and products from the surface as well as the kinetics of the reaction. For particles less than about 1 μm diameter, diffusional resistance is minimal. The soot oxidation process in the diesel cylinder is kinetically controlled, therefore, since particle sizes are smaller than this limit. There are many species in or near the flame that could oxidize soot: examples are O_2, O, OH, CO_2, and H_2O. Recent reviews of soot formation[70, 73, 80] have concluded that at high oxygen partial pressures, soot oxidation can be correlated with a semiempirical formula based on pyrographite oxidation studies. For fuel-rich and close-to-stoichiometric combustion products, however, oxidation by OH has been shown to be more important than O_2 attack, at least at atmospheric pressure.

It is argued on the basis of structural similarities that the rates of oxidation of soot and of pyrographites should be the same. This is a significant simplification. It has proved difficult to follow the oxidation of soot aerosols in flames, and if care is taken to avoid diffusional resistance, studies of bulk samples of pyrographite can then be used as a basis for understanding soot oxidation. The semiempirical formula of Nagle and Strickland-Constable has been shown[84] to correlate pyrographite oxidation for oxygen partial pressures $p_{O_2} < 1$ atm and temperatures between 1100 and 2500 K. This formula is based on the concept that there are two types of sites on the carbon surface available for O_2 attack. For the more reactive type A sites, the oxidation rate is controlled by the fraction of sites not covered by surface oxides (and therefore is of mixed order, between 0 and 1 in p_{O_2}). Type B sites are less reactive, and react at a rate which is first order in p_{O_2}. A thermal rearrangement of A sites into B sites is also allowed (with rate constant k_T). A steady-state analysis of this mechanism gives a surface mass oxi-

TABLE 11.10
Rate constants for Nagle and Strickland-Constable soot oxidation mechanism[84]

Rate constant	Units
$k_A = 20 \exp(-15{,}100/T)$	g/cm² · s · atm
$k_B = 4.46 \times 10^{-3} \exp(-7640/T)$	g/cm² · s · atm
$k_T = 1.51 \times 10^{5} \exp(-48{,}800/T)$	g/cm² · s
$k_Z = 21.3 \exp(2060/T)$	atm^{-1}

dation rate w (g C/cm² · s):

$$\frac{w}{12} = \left(\frac{k_A p_{O_2}}{1 + k_Z p_{O_2}}\right) x + k_B p_{O_2}(1 - x) \tag{11.41}$$

where x is the fraction of the surface occupied by type A sites and is given by

$$x = \left(1 + \frac{k_T}{p_{O_2} k_B}\right)^{-1} \tag{11.42}$$

The empirical rate constants determined by Nagle and Strickland-Constable for this model are listed in Table 11.10. According to this mechanism, the reaction is first order at low oxygen partial pressures, but approaches zero order at higher pressures. At a given oxygen pressure, the rate initially increases exponentially with temperature (equivalent activation energy is k_A/k_Z or 34,100 cal/mol). Beyond a certain temperature the rate decreases as the thermal rearrangement favors formation of less reactive B sites. When, at sufficiently high temperature, the surface is completely covered with B sites, the rate is first order in oxygen partial pressure and increases again with temperature.[80]

Park and Appleton[84] have compared this formula with oxidation rate data obtained from pyrographite samples, carbon black particles, and with the available flame soot oxidation data. Figure 11-49 shows both the soot oxidation rate predicted by Eqs. (11.41) and (11.42) as a function of temperature and oxygen partial pressure, and the above-mentioned data. The formula correlates the data shown to within a factor of 2. Under diesel engine conditions, the O_2 partial pressure can be high (~several atmospheres), as can the temperatures of close-to-stoichiometric mixtures ($\lesssim$2800 K).

Equations (11.41) and (11.42) have been used to estimate the amount of soot that can be oxidized in a typical IDI diesel engine. It was assumed that soot was present in stoichiometric combustion products at selected times in the cycle and that mixing with air leaned out the burned gas mixture at different rates until the overall fuel/air equivalence ratio was reached. The surface recession rate during this process was computed. Figure 11-50 shows sample results at an engine speed of 1600 rev/min and an overall cylinder equivalence ratio of 0.58. Fast, intermediate, and slow mixing occurred in 30, 70, and 140°, respectively. The surface recession rate rises to a maximum as p_{O_2} increases and then decreases as the

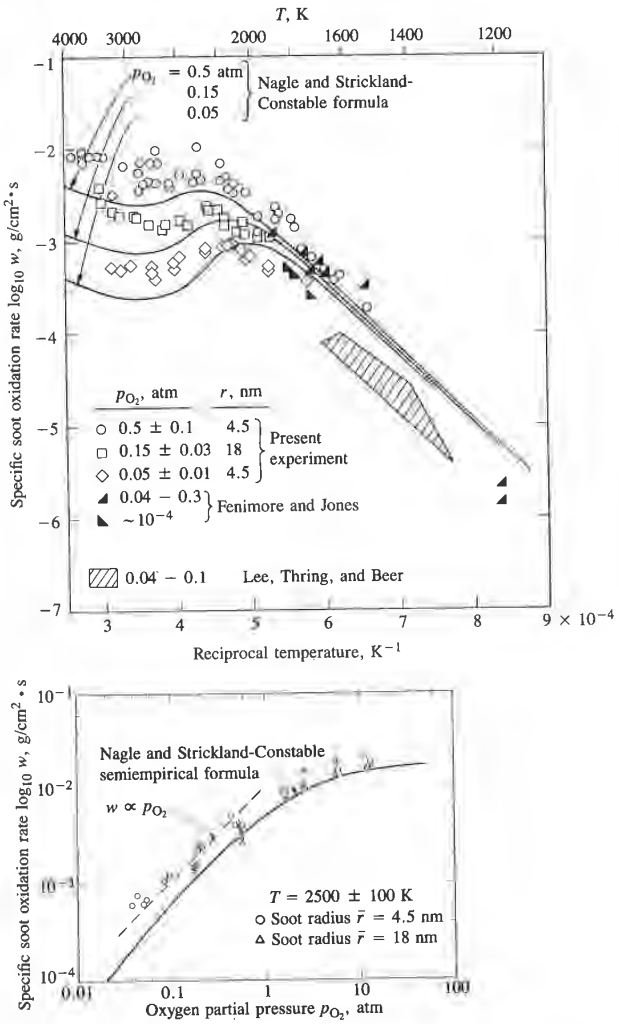

FIGURE 11-49
Specific soot oxidation rate measurements and predictions as a function of temperature and oxygen partial pressure.[84]

falling gas temperature more than offsets the increasing oxygen concentration. While the shape of the recession rate versus time curves depends on the mixing rate, the total amount of carbon burned (the area under each curve in Fig. 11-50*b*) is about the same (0.1 μg/mm²). However, the point in the cycle at which the soot-containing burned gas mixture passes through stoichiometric is much

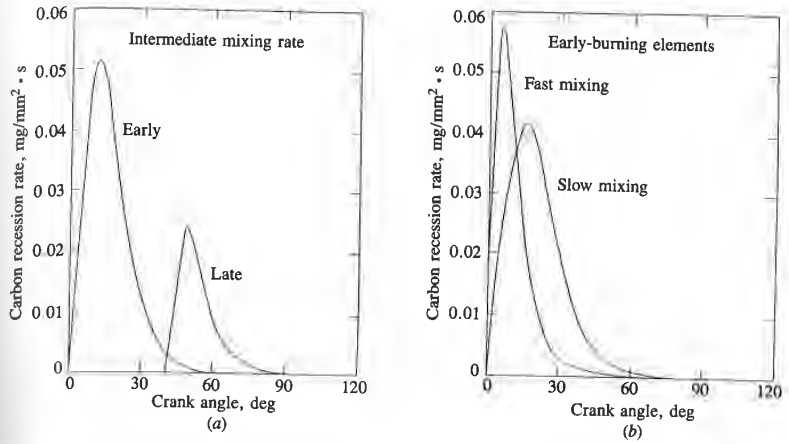

FIGURE 11-50
Soot particle burnup rate in diesel combustion environment: (*a*) in early- and late-burned fuel-air elements with intermediate mixing rate; (*b*) for fast and slow mixing for early-burning elements.[83]

more important. For the late mixing element shown (mixing lean of stoichiometric at 40° ATC), the total carbon mass oxidized is only 40 percent of that for the early mixing calculation. This is due primarily to the decreasing gas temperatures as the expansion stroke proceeds, and not the longer time available for burnup.[83]

For a spherical particle, the mass burning rate w (g/cm^2 · s) can be converted to a surface recession rate using

$$\frac{dr}{dt} = \frac{-w}{\rho}$$

where ρ is the density (≈ 2 g/cm^3). The integrated values of $w(t)$ when divided by ρ then give the maximum radius of a soot particle that can be burned up. Integrated values of 0.1 μg/mm^2 (estimated for TC start of burnup) correspond to a radius of about 50 nm or diameter of 100 nm. Individual spherule diameters are about 30 nm, so soot which mixes with air early in the expansion stroke is likely to be fully burned. Thus the soot present in the exhaust would be expected to come from regions which mix with air too late for the oxidation rate to be sufficient for particle burnup.

Agglomeration will have an indirect influence on the amount of soot oxidized through its effect on surface area. In the limiting case of a spherical cluster, n monodisperse spherules ($10 \lesssim n \lesssim 100$) can be imagined as compacted into a single solid sphere of equal volume. Alternatively, the same n spherules can be imagined compacted into a cylinder of diameter equal to that of the original spherules. Since oxidative attack is essentially an exterior surface phenomenon, the surface/volume ratio is the appropriate measure of the effect of particle shape on soot mass burnup rate. It can be shown that the surface/volume ratios for the

single sphere, cylinder, and individual spherule are in the ratio $n^{-1/3}$, $\frac{2}{3}$, and 1, respectively. Thus agglomeration will decrease the relative oxidation rate. In the limit spherical clusters are less desirable than a chain; the larger the cluster the bigger the relative reduction in surface area. However, the densely packed spherule limit does not appear to be approached in practice. A specific surface area, of about 200 m^2/g for diesel soot, has been measured.[85] A smooth-surfaced 30-nm diameter spherule with a 2-g/cm^3 density has a surface/mass ratio of 100 m^2/g; the measured value is about twice this value, indicating low porosity and an agglomerate structure which is loosely rather than densely packed.[83]

Equation (11.41) shows a maximum recession rate in combustion products corresponding to a fuel/air equivalence ratio of about 0.9. Recent evidence shows that in an atmospheric pressure environment with rich and close-to-stoichiometric combustion products where O_2 mole fractions are low, oxidation by OH radical attack is much more significant than oxidation by O or O_2. The OH radical may be important in oxidizing soot in the flame zone under close-to-stoichiometric conditions.

11.5.6 Adsorption and Condensation

The final process in the particulate formation sequence illustrated in Fig. 11-46 is adsorption and condensation of hydrocarbons. This occurs primarily after the cylinder gases have been exhausted from the engine, as these exhaust gases are diluted with air. In the standard particulate mass emission measurement process this occurs in a dilution tunnel which simulates approximately the actual atmospheric dilution process. A diluted exhaust gas sample is filtered to remove the particulate. After equilibrating the collection filter at controlled conditions to remove water vapor, the particulate mass is obtained by weighing. In the prescribed EPA procedure, the filter temperature must not exceed 52°C. For a given exhaust gas temperature, the filter (and sample) temperature depends on the dilution ratio, as shown in Fig. 11-51.

The effect of the dilution ratio (and the dependent sample temperature) on collected particulate mass is shown in Fig. 11-52 for a standard dilution tunnel,

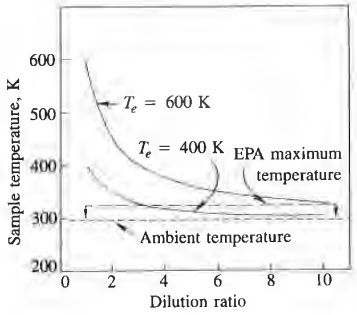

FIGURE 11-51
Effect of exhaust gas dilution ratio on the temperature of the collected particulate sample as a function of engine exhaust temperature T_e.[70]

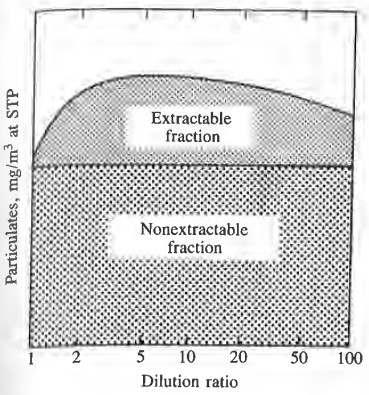

FIGURE 11-52
Typical effect of dilution ratio on particulate mass emission and its partitioning between extractable and nonextractable fractions.[70]

where the total sample is partitioned into extractable and nonextractable fractions. The nonextractable fraction is the carbonaceous soot generated during combustion and is not affected by the dilution process. With no dilution (dilution ratio of unity) the difference between the total and nonextractable mass is small; the bulk of the extractable fraction is acquired after the exhaust gas is mixed with dilution air. Extensive studies of this dilution process have shown that both adsorption and condensation occur. Adsorption involves the adherence of molecules of unburned hydrocarbons to the surfaces of the soot particles by chemical or physical (van der Waals) forces. This depends on the fraction of the available particle surface area occupied by hydrocarbons and on the partial pressure of the gaseous hydrocarbons that drives the adsorption process. As the dilution ratio increases from unity, the effect of decreasing temperature on the number of active sites dominates and, as shown in Fig. 11-52, the extractable fraction increases. At high dilution ratios, the sample temperature becomes insensitive to the dilution ratio (see Fig. 11-51) but the decreasing hydrocarbon partial pressure causes the extractable mass to fall again. Condensation will occur whenever the vapor pressure of the gaseous hydrocarbon exceeds its saturated vapor pressure. Increasing dilution decreases hydrocarbon concentrations and hence vapor pressure. However, the associated reduction in temperature does reduce the saturation pressure. High exhaust concentrations of hydrocarbons are the conditions where condensation is likely to be most significant, and the hydrocarbons most likely to condense are those of low volatility. Sources of low-volatility hydrocarbons are the high-boiling-point end of the fuel, unburned hydrocarbons that have been pyrolyzed but not consumed in the combustion process, and the lubricating oil.[70]

Experiments with a passenger car IDI diesel, where the oil was tagged with a radioactive tracer, have shown that the oil can contribute from 2 to 25 percent of the total particulate mass, with the greatest contribution occurring at high speed. On average, over half of the extractable mass was traceable to the oil. All the material traceable to the oil was found in the extractable fraction, indicating that the oil did not participate in the combustion process. However, the oil is not

always a significant contributer: in another engine, fuel was the dominant source of extractable material.[70, 71]

11.6 EXHAUST GAS TREATMENT

11.6.1 Available Options

Our discussion so far has focused on *engine* emissions. Further reductions in emissions can be obtained by removing pollutants from the exhaust gases in the engine exhaust system. Devices developed to achieve this result include catalytic converters (oxidizing catalysts for HC and CO, reducing catalysts for NO_x, and three-way catalysts for all three pollutants), thermal reactors (for HC and CO), and traps or filters for particulates.

The temperature of exhaust gas in a spark-ignition engine can vary from 300 to 400°C during idle to about 900°C at high-power operation. The most common range is 400 to 600°C. Spark-ignition engines usually operate at fuel/air equivalence ratios between about 0.9 and 1.2 (see Sec. 7.1). The exhaust gas may therefore contain modest amounts of oxygen (when lean) or more substantial amounts of CO (when rich). In contrast, diesel engines, where load is controlled by the amount of fuel injected, always operate lean. The exhaust gas therefore contains substantial oxygen and is at a lower temperature (200 to 500°C). Removal of gaseous pollutants from the exhaust gases after they leave the engine cylinder can be either thermal or catalytic. In order to oxidize the hydrocarbons in the gas phase without a catalyst, a residence time of order or greater than 50 ms and temperatures in excess of 600°C are required. To oxidize CO, temperatures in excess of 700°C are required. Temperatures high enough for some homogeneous thermal oxidation can be obtained by spark retard (with some loss in efficiency) and insulation of the exhaust ports and manifold. The residence time can be increased by increasing the exhaust manifold volume to form a *thermal reactor* (see Sec. 11.6.3). However, this approach has limited application.

Catalytic oxidation of CO and hydrocarbons in the exhaust can be achieved at temperatures as low as 250°C. Thus effective removal of these pollutants occurs over a much wider range of exhaust temperatures than can be achieved with thermal oxidation. The only satisfactory method known for the removal of NO from exhaust gas involves catalytic processes. Removal of NO by catalytic oxidation to NO_2 requires temperatures <400°C (from equilibrium considerations) and subsequent removal of the NO_2 produced. Catalytic reaction of NO with added ammonia NH_3 is not practical because of the transient variations in NO produced in the engine. Reduction of NO by CO, hydrocarbons, or H_2 in the exhaust to produce N_2 is the preferred catalytic process. It is only feasible in spark-ignition engine exhausts. Use of catalysts in spark-ignition engines for CO, HC, and NO removal has become widespread. Catalysts are discussed in Sec. 11.6.2.

Particulates in the exhaust gas stream can be removed by a trap. Due to the small particle size involved, some type of filter is the most effective trapping

method. The accumulation of mass within the trap and the increase in exhaust manifold pressure during trap operation are major development problems. Diesel particulates, once trapped, can be burned up either by initiating oxidation within the trap with an external heat source or by using a trap which contains catalytically active material. The operation of particulate traps is reviewed briefly in Sec. 11.6.4.

11.6.2 Catalytic Converters

The catalytic converters used in spark-ignition engines consist of an active catalytic material in a specially designed metal casing which directs the exhaust gas flow through the catalyst bed. The active material employed for CO and HC oxidation or NO reduction (normally noble metals, though base metals oxides can be used) must be distributed over a large surface area so that the mass-transfer characteristics between the gas phase and the active catalyst surface are sufficient to allow close to 100 percent conversion with high catalytic activity. The two configurations commonly used are shown in Fig. 11-53. One system employs a ceramic honeycomb structure or monolith held in a metal can in the exhaust stream. The active (noble metal) catalyst material is impregnated into a highly porous alumina washcoat about 20 μm thick that is applied to the passageway walls. The typical monolith has square-cross-section passageways with inside dimensions of ~1 mm separated by thin (0.15 to 0.3 mm) porous walls. The number of passageways per square centimeter varies between about 30 and 60. The washcoat, 5 to 15 percent of the weight of the monolith, has a surface area of 100 to 200 m^2/g. The other converter design uses a bed of spherical ceramic pellets to provide a large surface area in contact with the flow. With pellet catalysts, the noble metal catalyst is impregnated into the highly porous surface of the spherical alumina pellets (typically 3 mm diameter) to a depth of about 250 μm. The pellet material is chosen to have good crush and abrasion resistance after exposure to temperatures of order 1000°C. The gas flow is directed down through the bed as shown to provide a large flow area and low pressure drop. The gas flow is turbulent which results in high mass-transfer rates; in the monolith catalyst passageways, it is laminar.

OXIDATION CATALYSTS. The function of an oxidation catalyst is to oxidize CO and hydrocarbons to CO_2 and water in an exhaust gas stream which typically contains ~12 percent CO_2 and H_2O, 100 to 2000 ppm NO, ~20 ppm SO_2, 1 to 5 percent O_2, 0.2 to 5 percent CO, and 1000 to 6000 ppm C_1 HC, often with small amounts of lead and phosphorus. About half the hydrocarbons emitted by the SI engine are unburned fuel compounds. The saturated hydrocarbons (which comprise some 20 to 30 percent) are the most difficult to oxidize. The ease of oxidation increases with increasing molecular weight. Sufficient oxygen must be present to oxidize the CO and HC. This may be supplied by the engine itself

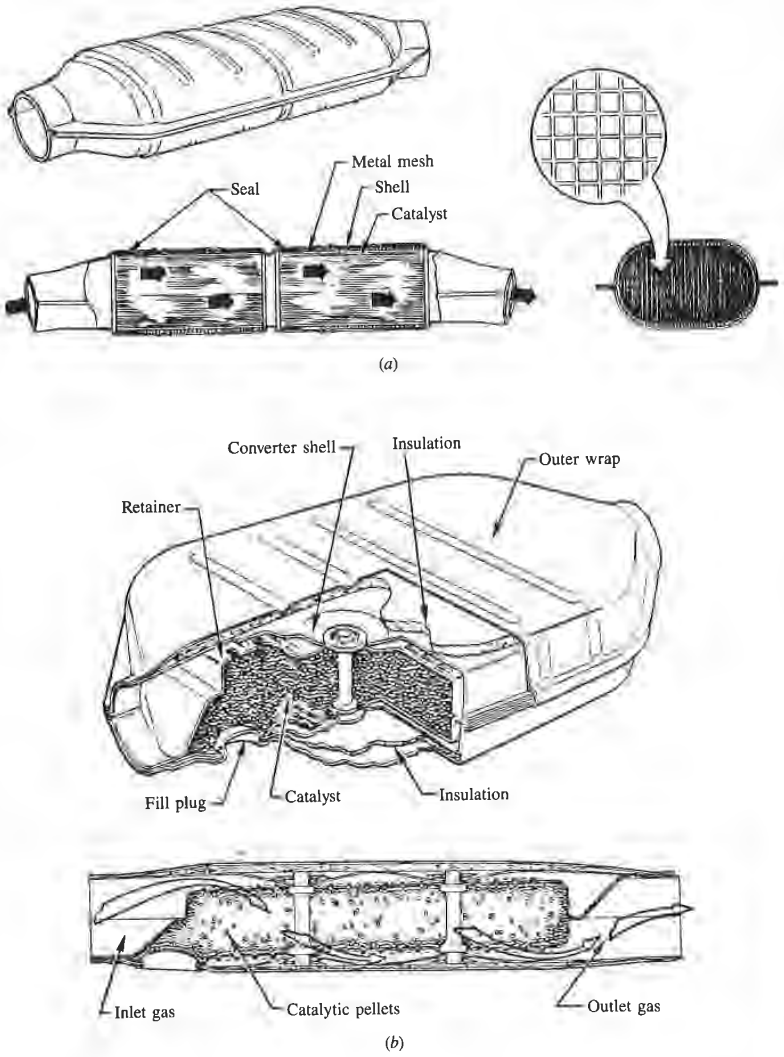

FIGURE 11-53
Catalytic converters for spark-ignition engine emission control: (*a*) monolith design; (*b*) pelletized design.[62]

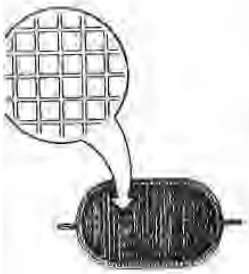

Outer wrap

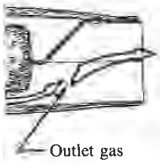

Outlet gas

(*a*) monolith design; (*b*) pelletized

running lean of stoichiometric or with a pump that introduces air into the exhaust ports just downstream of the valve. Venturi air addition into the exhaust port using the pressure pulsations generated by the exhaust process can also be used to add the required air.

Because of their high intrinsic activity, noble metals are most suitable as the catalytic material. They show higher specific activity for HC oxidation, are more thermally resistant to loss of low-temperature activity, and are much less deactivated by the sulfur in the fuel than base metal oxides. A mixture of platinum (Pt) and palladium (Pd) is most commonly used. For the oxidation of CO, olefins, and methane, the specific activity of Pd is higher than that of Pt. For the oxidation of aromatic compounds, Pt and Pd have similar activity. For oxidation of paraffin hydrocarbons (with molecular size greater than C_3), Pt is more active than Pd. Pure noble metals sinter rapidly in the 500 to 900°C temperature range experienced by exhaust catalysts. Since catalytic behavior is manifested exclusively by surface atoms, the noble metals are dispersed as finely as possible on an inert support such as γ-A_2O_3 which prevents particle-to-particle metal contact and suppresses sintering. The particle size of the noble metal particles in a fresh catalyst is less than 50 nm. This can increase to ~100 nm when the catalyst is exposed to the high temperatures of the exhaust in vehicle operation. Typical noble metal concentrations in a commercial honeycomb catalyst are between 1 and 2 g/dm^3 of honeycomb volume, with Pt/Pd = 2 on a weight basis. As a rough rule of thumb, the ceramic honeycomb volume required is about half the engine displaced volume. This gives a space velocity through the converter (volume flow rate of exhaust divided by converter volume) over the normal engine operating range of 5 to 30 per second.[68]

The *conversion efficiency* of a catalyst is the ratio of the rate of mass removal in the catalyst of the particular constituent of interest to the mass flow rate of that constituent into the catalyst; e.g., for HC,

$$\eta_{cat} = \frac{\dot{m}_{HC,\,in} - \dot{m}_{HC,\,out}}{\dot{m}_{HC,\,in}} = 1 - \frac{\dot{m}_{HC,\,out}}{\dot{m}_{HC,\,in}} \tag{11.43}$$

The variation of conversion efficiency of a typical oxidizing catalytic converter with temperature is shown in Fig. 11-54. At high enough temperatures, the steady-state conversion efficiencies of a new oxidation catalyst are typically 98 to 99 percent for CO and 95 percent or above for HC. However, the catalyst is ineffective until its temperature has risen above 250 to 300°C. The term *light-off temperature* is often used to describe the temperature at which the catalyst becomes more than 50 percent effective.

The above numbers apply to fresh noble metal oxidation catalysts; as catalysts spend time in service their effectiveness deteriorates. Catalysis involves the adsorption of the reactants onto surface sites of high activity, followed by chemical reaction, then desorption of the products. Catalyst degradation involves both the deactivation of these sites by catalyst poisons and a reduction in the effective area of these sites through sintering. Poisoning affects both the warm-up and

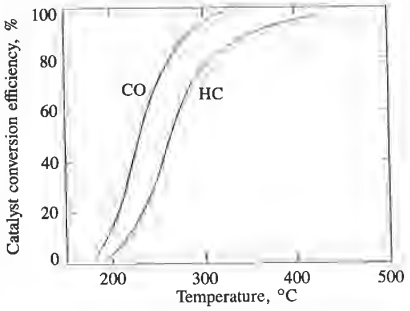

FIGURE 11-54
Conversion efficiency for CO and HC as a function of temperature for typical oxidizing catalytic converter.[62]

steady-state performance of the catalyst. When poisoning occurs, catalytic activity is impeded through prolonged contact with interfering elements that either physically block the active sites or interact chemically with the active material. The lead in fuel antiknock agents and the phosphorus in oil additives are the most important poisons. Though lead antiknock agents are not added to the gasoline used with catalyst-equipped vehicles, this "unleaded" fuel can be contaminated with small amounts ($\sim$10 mg Pb/dm^3) from the fuel distribution system. Between 10 and 30 percent of the lead in the fuel ends up on the catalyst. Its effect on catalyst conversion efficiency depends on the amount of lead on the catalyst, as shown in Fig. 11-55. Lead depresses the catalytic oxidation of HC to a greater extent than oxidation of CO. The oxidation activity of saturated hydrocarbons is particularly depressed. The extent of the poisoning that results from traces of critical elements in the fuel and oil depends on which elements are present and the amounts absorbed, as well as the composition of the catalyst and its operating conditions (especially its temperature).[63] Sintering is promoted by exposure of the catalyst to high operating temperatures. It involves the migration and agglomeration of sites, thus decreasing their active surface area. Sintering slows warm-up but has minimal effect on the steady-state conversion efficiency.

The oxidation kinetics of CO over Pt and Pd noble metal catalysts can be described by

$$\frac{d[\mathrm{CO}]}{dt} = \frac{K_1 p_{\mathrm{CO}} p_{\mathrm{O_2}}}{(1 + K_2 p_{\mathrm{CO}} + K_3 p_{\mathrm{HC}})^2 (1 + K_4 p_{\mathrm{NO}}^n)} \tag{11.44}$$

where K_1 to K_4 and n are constants at any given temperature, and p_{CO}, $p_{\mathrm{O_2}}$, p_{HC}, and p_{NO} are the partial pressures of carbon monoxide, oxygen, hydrocarbons, and nitric oxide, respectively. A similar relationship can be written for the olefinic and aromatic HC oxidation rate (these being the most reactive hydrocarbons). These relationships incorporate the fact that the rates of CO and HC oxidation are inhibited by high CO and reactive HC concentrations, and that NO concentrations in the range 0 to 1000 ppm strongly inhibit oxidation also. The oxidation rate of paraffin hydrocarbons varies with the first power of the HC partial pres-

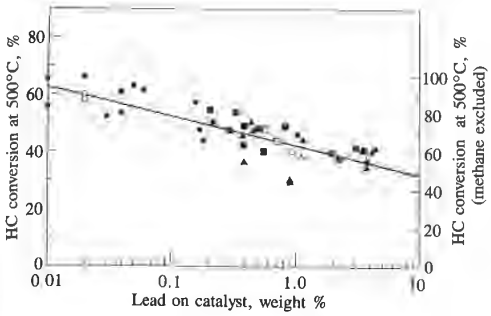

FIGURE 11-55
HC conversion efficiency as a function of lead concentration on catalyst. Total HC conversion on left; nonmethane HC conversion on right. 0.001–0.013 g Pb/dm^3 in fuel.[68]

sure, is inhibited by CO, olefins, and NO, and increases as the O_2 partial pressure is decreased to near-stoichiometric values.[68]

It will be apparent from the above that two extremely important considerations for successful use of catalysts for automotive applications are the test procedure that is used to measure emissions and the methods used to determine if the catalyst has the required durability. The U.S. Federal Test Procedure requires that the vehicle under test be at a temperature of 16 to 30°C for 12 hours prior to the test and that emissions are measured from the time the ignition key is turned on until the test has ended. In spark-ignition engines the mixture fed into the engine during start-up is enriched substantially (carburetors have a choke to accomplish this; additional fuel is injected with port or manifold fuel injection). The rationale is that if sufficient fuel is added to the inlet air, enough will evaporate to start the engine. However, until the rest of the fuel is consumed, the engine then runs rich and emits high concentrations of CO and HC. The catalyst is cold at this time, and until it warms up, these emissions will pass through without reaction. It is important that the catalyst be brought to its light-off temperature as quickly as possible (preferably in less than 60 s) and that mixture enrichment during start-up be held to a minimum. Thus catalysts should have low thermal inertia for rapid warm-up and low light-off temperatures for CO and HC, so they become effective quickly. The closer they are placed to the engine the faster they will reach light-off. However, they will then experience higher temperatures when fully warmed up and so be more susceptible to thermal degradation. While it is not too difficult to prepare catalysts that are highly effective when fresh, it is much more difficult to maintain effectiveness over extended mileage (50,000 miles) in which the catalyst is exposed to high temperatures and catalyst poisons. These can degrade both cold-start and warmed-up performance. Also, catalyst durability is affected by engine durability. Any engine malfunction that will expose the catalyst to excessive amounts of unburned fuel (such as ignition failure, misfire with too lean a mixture, or excessively rich operation) will severely overheat the catalyst.

Oxidation-catalyst-equipped vehicles may emit sulfuric acid aerosol. Unleaded gasoline contains 150 to 600 ppm by weight of S, which leaves the

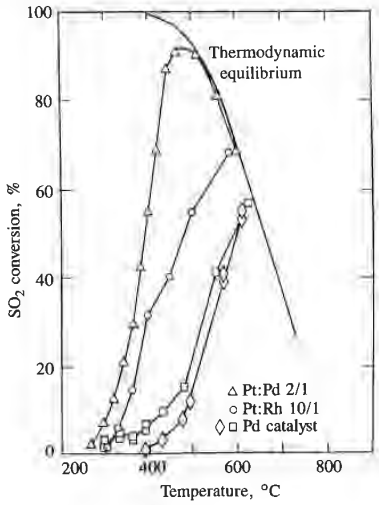

FIGURE 11-56
SO_2 conversion to SO_3 as a function of temperature with 5% O_2 concentration and no reducing gases present. Space velocity (volume flow per unit volume) $\sim 10\ s^{-1}$. Results for Pt–Pd, Pt–Rh, and Pd catalysts.[68]

combustion chamber as SO_2. This SO_2 can be oxidized by the catalyst to SO_3 which combines with water at ambient conditions to form an H_2SO_4 aerosol. The SO_3 can be chemisorbed on the alumina catalyst surface; when large pellet beds are used, considerable storage of SO_3 at temperatures $<500°C$ can occur. At higher catalyst temperatures, this stored SO_3 is emitted as an SO_3–SO_2 mixture. SO_3 production can be controlled by lowering or raising the catalyst temperature. Figure 11-56 shows that at low temperatures SO_3 production is kinetically limited; at high temperatures SO_3 production is thermodynamically limited. Palladium and rhodium produce less SO_3 than Pt and have comparable HC and CO catalytic activity. By decreasing oxygen concentrations leaving the catalyst to ~ 1 percent, SO_3 production can be substantially reduced.[68]

NO CATALYSIS. NO is removed by reduction using the CO, hydrocarbons, and H_2 in the exhaust. The reactions are shown in Table 11.11. No catalyst is available for the decomposition of NO to O_2 and N_2 (thermodynamically favored at exhaust temperatures) which is sufficiently active for use in engine exhausts. NO reduction can be carried out under rich conditions where there is an excess of reducing species over oxidizing species. The catalyst used under these conditions is referred to as an *NO reduction catalyst*. Such a system requires a follow-up oxidation catalyst, together with addition of air from an air pump before the oxidation catalyst, to remove the remaining CO and hydrocarbons. Such a two-bed system can remove all three pollutants (NO, CO, and HC) from the exhaust. However, the rich operation necessary for NO reduction results in a fuel consumption penalty and constrains the performance of the NO catalyst since a fraction of the NO removed is converted to ammonia NH_3 rather than N_2. NH_3

TABLE 11.11
Possible NO reactions under reducing conditions[68]

1.	$NO + CO \rightarrow \frac{1}{2}N_2 + CO_2$
2.	$2NO + 5CO + 3H_2O \rightarrow 2NH_3 + 5CO_2$
3.	$2NO + CO \rightarrow N_2O + CO_2$
4.	$NO + H_2 \rightarrow \frac{1}{2}N_2 + H_2O$
5.	$2NO + 5H_2 \rightarrow 2NH_3 + 2H_2O$
6.	$2NO + H_2 \rightarrow N_2O + H_2O$

Reactions 3 and 6 occur at 200°C, which is below that usually found in auto exhausts.

formation under rich operation in the first bed must be small in this two-bed system because the second (oxidation) catalyst readily oxidizes NH_3 back to NO. Reduction of NO by CO or H_2 can be accomplished by base metal catalysts (e.g., CuO, NiO) in the temperature range 350 to 600°C. However, these catalyst materials are deactivated by sulfur and have shown limited thermal stability when used in vehicle exhausts. Alumina-supported noble metal catalysts reduce NO with CO–H_2 mixtures. Their NO-reduction activity is in the order Ru > Rh > Pd > Pt. Ruthenium (Ru) and rhodium (Rh) produce considerably less NH_3 than Pd or Pt under slightly rich conditions. While these properties make ruthenium a desirable NO catalyst, it forms volatile oxides under oxidizing conditions which results in loss of ruthenium from the alumina support.[68]

THREE-WAY CATALYSTS. If an engine is operated at all times with an air/fuel ratio at or close to stoichiometric, then both NO reduction and CO and HC oxidation can be done in a single catalyst bed. The catalyst effectively brings the exhaust gas composition to a near-equilibrium state at these exhaust conditions; i.e., a composition of CO_2, H_2O, and N_2. Enough reducing gases will be present to reduce NO and enough O_2 to oxidize the CO and hydrocarbons. Such a catalyst is called a *three-way catalyst* since it removes all three pollutants simultaneously. Figure 11-57 shows the conversion efficiency for NO, CO, and HC as a function of the air/fuel ratio. There is a narrow range of air/fuel ratios near stoichiometric in which high conversion efficiencies for all three pollutants are achieved. The width of this window is narrow, about 0.1 air/fuel ratios (7×10^{-3} in equivalence ratio units) for catalyst with high mileage use, and depends on catalyst formulation and engine operating conditions.

This window is sufficiently narrow to be beyond the control capabilities of an ordinary carburetor, though it can sometimes be achieved with sophisticated carburetors and fuel-injection systems. Thus closed-loop control of equivalence ratio has been introduced. An oxygen sensor in the exhaust is used to indicate whether the engine is operating on the rich or lean side of stoichiometric, and provide a signal for adjusting the fuel system to achieve the desired air-fuel mixture (see Sec. 7.4). Holding the equivalence ratio precisely on the chosen near-

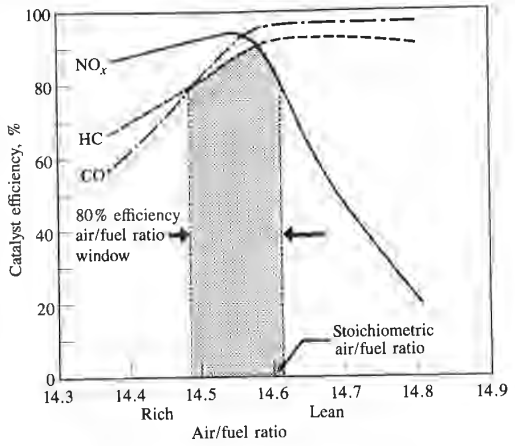

FIGURE 11-57
Conversion efficiency for NO, CO, and HC for a three-way catalyst as a function of exhaust gas air/fuel ratio.[68]

stoichiometric value is not a practical expectation of such a feedback system, and the equivalence ratio oscillates around the set point in an approximately periodic manner as the fuel flow is varied. Experimental data show that there is a considerable widening of the air/fuel ratio window where all three pollutants are effectively removed, with cyclic variation of the fuel flow. The maximum conversion in the middle of the window is reduced, however, from its value when there are no fluctuations. The effect of fluctuations depends on the frequency; frequencies of about 0.5 to 1 hertz are most effective and the usable window (at lower conversion efficiencies) can be broadened to about 1 air/fuel ratio. Some of the benefits of fluctuations in equivalence or air/fuel ratios are available even without any deliberate attempt to produce such variations with closed-loop feedback. Open-loop systems exhibit variations in the air/fuel ratio during normal vehicle operation.

Because of these cyclic variations in exhaust gas composition about a set point close to stoichiometric, it is desirable that the catalyst be able to reduce NO when a slight excess of oxygen is present (on the lean side) and remove CO and HC when there is a slight deficiency of oxygen (on the rich side). Rhodium is the principal ingredient used in commercial catalysts to remove NO. It is very active for NO reduction, is much less inhibited by CO and sulfur compounds, and produces less NH_3 than Pt. To remove NO under slightly lean-of-stoichiometric conditions, the catalyst must react the CO, H_2, or HC with NO rather than with O_2, as the exhaust gas passes through the catalyst bed. Rhodium shows some NO reduction activity slightly lean of stoichiometric. On the rich side, the three-way catalyst window is determined by hydrocarbon and CO removal. Platinum is most commonly used for HC and CO oxidation; it has good activity under stoichiometric and slightly lean conditions. When sufficient rhodium is present, the participation of Pt in NO removal is minimal. In the rich

regime, the three-way catalyst consumes all the oxygen that is present in the exhaust, and as a consequence removes an equivalent amount of CO, H_2, and hydrocarbons; it is thought that the H_2 is removed first. In addition, the water-gas shift reaction

$$CO + H_2O = H_2 + CO_2$$

and the steam-reforming reaction

$$\text{Hydrocarbon} + H_2O \rightarrow CO, CO_2, H_2$$

can consume CO and HC. The exhaust contains an H_2/CO ratio of about $\frac{1}{3}$ (see Sec. 4.9.1), where the equilibrium ratio at 500°C is about 4. Considerable CO removal can be expected if the water-gas shift equilibrium is approached. Platinum is active in promoting this equilibrium. For large molecular weight paraffin hydrocarbons, and for olefins and aromatic hydrocarbons, the equilibrium for the steam-reforming reactions lies to the right. This reaction can therefore lead to considerable hydrocarbon removal. Rhodium is particularly active in the steam-reforming reaction; platinum is also active.[68]

The conversions of NO, CO, and hydrocarbons in a three-way catalyst operated with cyclical variations in equivalence ratio are larger than estimates based on summation of steady-state values during the cycle. At least part of the improved performance is thought to be due to the ability of the catalyst to undergo reduction-oxidation reactions. Such a catalyst component is usually referred to as an oxygen-storage component. In its oxidized state it can provide oxygen for CO and hydrocarbon oxidation in a rich exhaust gas environment, and in the process be reduced. When the exhaust cycles to lean conditions, this reduced component can react with O_2 or NO (which removes NO directly or indirectly by reducing the O_2 concentration). The oxidized component can then oxidize CO and HC in the next rich cycle, etc. Components such as ReO_2 or CeO_2 which exhibit this "redox" behavior can be included in three-way catalyst formulations. Commercial three-way catalysts contain platinum and rhodium (the ratio Pt/Rh varying substantially in the range 2 to 17) with some A_2O_3, NiO, and CeO_2. Alumina is the preferred support material.[68]

11.6.3 Thermal Reactors

In Secs. 11.3 and 11.4.2 it was explained that oxidation of CO and HC occurred during the expansion and exhaust processes in the cylinder of a conventional spark-ignition engine and, under certain circumstances, in the exhaust system. Oxidation after passage through the exhaust port can be enhanced with a *thermal reactor*—an enlarged exhaust manifold that bolts directly onto the cylinder head. Its function is to promote rapid mixing of the hot exhaust gases with any secondary air injected into the exhaust port (required with fuel-rich engine operation to produce a net oxidizing atmosphere), to remove nonuniformities in temperature and composition in the exhaust gases, and to retain the gases at a high enough

FIGURE 11-57
Conversion efficiency for NO, CO, and HC for a three-way catalyst as a function of exhaust gas air/fuel ratio.[68]

of such a feedback system, and
t in an approximately periodic
lata show that there is a con-
where all three pollutants are
el flow. The maximum conver-
ver, from its value when there
epends on the frequency; fre-
ve and the usable window (at
about 1 air/fuel ratio. Some of
/fuel ratios are available even
riations with closed-loop feed-
e air/fuel ratio during normal

t gas composition about a set
the catalyst be able to reduce
the lean side) and remove CO
(on the rich side). Rhodium is
ysts to remove NO. It is very
by CO and sulfur compounds,
NO under slightly lean-of-
the CO, H_2, or HC with NO
ses through the catalyst bed.
htly lean of stoichiometric. On
termined by hydrocarbon and
r HC and CO oxidation; it has
an conditions. When sufficient
removal is minimal. In the rich

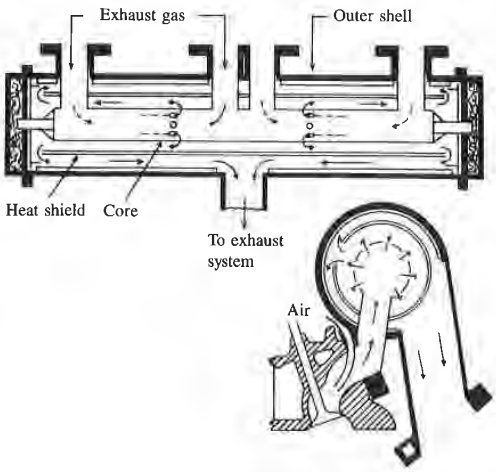

FIGURE 11-58
Schematic of exhaust thermal reactor for HC and CO oxidation.

temperature for sufficient time to oxidize much of the HC and CO which exits the cylinder. An example of a thermal reactor design is shown in Fig. 11-58.

The temperature levels typically required for bulk gas oxidation of HC and CO in a reactor are about 600 and 700°C, respectively. Note that they are considerably higher than those required for equivalent conversion in a catalytic converter and that higher temperatures are required for CO oxidation than for HC oxidation. The exhaust gas temperature in the manifold of a conventional engine is not sufficient to achieve any substantial reduction in engine exhaust port emissions. To achieve greater reductions, the reactor must be designed to reduce heat losses and increase residence time. In addition, to achieve rapid warm-up after engine start, a low thermal inertia reactor is desirable. Typically, a thin steel liner acts as the core of the reactor inside a cast-iron outer casing; with suitably arranged flow paths, this construction holds heat losses to a minimum by thermally isolating the core.

The effectiveness of the reactor depends on its operating temperature, the availability of excess oxygen mixed throughout the reacting gases, and the reactor volume. The operating temperature depends on the reactor inlet gas temperature, heat losses, and the amount of HC, CO, and H_2 burned up in the reactor. This latter factor is important: 1.5 percent CO removal results in a 220 K temperature rise. As a consequence, reactors with fuel-rich cylinder exhaust gas and secondary air give greater fractional reductions in HC and CO emissions than reactors with fuel-lean cylinder exhaust (which do not require any secondary air). As has already been explained, a higher core gas temperature is required to burn up the same fraction of CO which enters the reactor as of HC which enters. For lean engine exhaust gas, where the reactor core gas temperatures are a hundred degrees K lower than under fuel-rich operation, substan-

tial reductions in CO emissions are difficult to achieve. For very lean operation, HC burnup becomes marginal.

A practical limitation to reactor effectiveness with fuel-rich engine operation is mixing of secondary air and engine exhaust gases in the exhaust port and the reactor core. The secondary air flow with a conventional air pump is effectively shut off by the exhaust blowdown process, and virtually no oxidation occurs in the exhaust port because the air and exhaust gases are segregated. Mixing in the reactor itself is promoted by suitably arranging the reactor inlet and exit ports and by using baffles. In systems with conventional secondary air pumps, maximum reductions in CO and HC occur with 10 to 20 percent excess air in the mixture. However, even with very high reactor core gas temperatures, 100 percent HC and CO oxidation is not achieved due to incomplete mixing. Improved control of secondary air flow has been shown to increase significantly CO emissions burnup.

FIGURE 11-58
Schematic of exhaust thermal reactor for HC and CO oxidation.

f the HC and CO which exits
n is shown in Fig. 11-58.
bulk gas oxidation of HC and
tively. Note that they are con-
t conversion in a catalytic con-
or CO oxidation than for HC
ifold of a conventional engine
n in engine exhaust port emis-
ust be designed to reduce heat
achieve rapid warm-up after
ble. Typically, a thin steel liner
n outer casing; with suitably
losses to a minimum by ther-

its operating temperature, the
the reacting gases, and the
ls on the reactor inlet gas tem-
O, and H_2 burned up in the
ent CO removal results in a
actors with fuel-rich cylinder
nal reductions in HC and CO
aust (which do not require any
higher core gas temperature is
ch enters the reactor as of HC
re the reactor core gas tem-
er fuel-rich operation, substan-

11.6.4 Particulate Traps

An exhaust treatment technology that substantially reduces diesel engine particulate emissions is the trap oxidizer. A temperature-tolerant filter or trap removes the particulate material from the exhaust gas; the filter is then "cleaned off" by oxidizing the accumulated particulates. This technology is difficult to implement because: (1) the filter, even when clean, increases the pressure in the exhaust system; (2) this pressure increase steadily rises as the filter collects particulate matter; (3) under normal diesel engine operating conditions the collected particulate matter will not ignite and oxidize; (4) once ignition of the particulate occurs, the burnup process must be carefully controlled to prevent excessively high temperatures and trap damage or destruction. Trap oxidizers have been put into production for light-duty automobile diesel engines. Their use with heavy-duty diesel engines poses more difficult problems due to higher particulate loading and lower exhaust temperatures.

Types of particulate filters include: ceramic monoliths, alumina-coated wire mesh, ceramic foam, ceramic fiber mat, woven silica-fiber rope wound on a porous tube. Each of these has different inherent pressure loss and filtering efficiency. Regeneration of the trap by burning up the filtered particulate material can be accomplished by raising its temperature to the ignition point while providing oxygen-containing exhaust gas to support combustion and carry away the heat released. Diesel particulate matter ignites at about 500 to 600°C. This is above the normal temperature of diesel exhaust so either the exhaust gas flowing through the trap during regeneration must be heated (positive regeneration) or ignition must be made to occur at a lower temperature with catalytic materials on the trap or added to the fuel (catalytic regeneration). Catalytic coatings on the trap reduce the ignition temperature by up to 200°C.

Figure 11-59 shows a ceramic-coated trap oxidizer mounted on the exhaust system of a turbocharged IDI diesel engine. The trap is a ceramic honeycomb with half the cells closed at the inlet end and the other half of the cells closed at

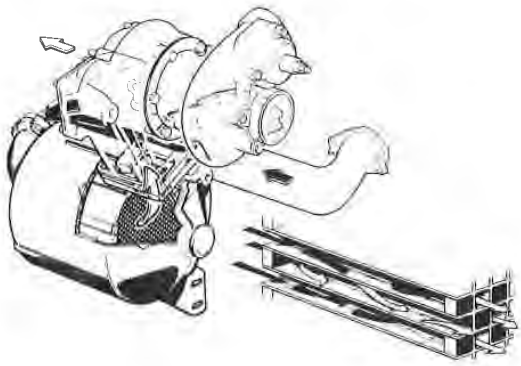

FIGURE 11-59
Catalytic ceramic-monolith particulate trap oxidizer mounted on exhaust of turbocharged automobile diesel engine.[86]

the exit end. Thus the particulate laden exhaust is forced to flow through the porous ceramic cell walls. The outside of the honeycomb is insulated and the trap is mounted close to the engine to maintain as high a trap temperature as possible. The pressure drop across the unloaded trap increases from 0.02 atm at 1000 rev/min to 0.15 atm at the maximum engine speed of 4500 rev/min. As the trap loads up, the pressure drop increases, requiring more fuel to be injected to compensate for the loss in power. This leads to higher exhaust temperature which eventually results in catalytic ignition of the particulate. The particulate oxidation rate depends on the trap temperature. With suitable trap location and design, the regeneration process is largely self-regulating. The particulate emissions from the engine are reduced by 70 percent or more.[86]

PROBLEMS

11.1. Figure 11-2 shows concentrations of NO, CO, and HC in a spark-ignition engine exhaust as a function of fuel/air equivalence ratio. Assume the concentration scale is parts per million. Explain the trends shown as the mixture is first made richer and then leaner than stoichiometric.

11.2. Figure 11-2 is for a spark-ignition engine. Construct a similar qualitative graph of NO, CO, and HC concentrations versus equivalence ratio for a direct-injection four-stroke cycle diesel engine.

11.3. A spark-ignition engine driving a car uses, on average, 120 grams of gasoline per mile traveled. The average emissions from the engine (upstream of the catalyst) are 1.5, 2, and 20 grams per mile of NO_x (as NO_2), HC, and CO, respectively. The engine operates with a stoichiometric gasoline-air mixture. Find the average concentrations in parts per million of NO_x, HC (as ppm C_1), and CO in the engine exhaust.

11.4. Calculate the average combustion inefficiency corresponding to the spark-ignition engine emissions levels given in Prob. 11.3. Include any hydrogen you estimate would be present in the exhaust stream.

11.5. A three-way catalytic converter is used with the spark-ignition engine in Prob. 11.3. For 10 percent of the driving time, the catalyst is cold and ineffective, and does not reduce the engine's emissions. For 90 percent of the time, the catalyst is hot and has conversion efficiencies as given in Fig. 11-57. Estimate the average *vehicle* emissions of NO_x, HC, and CO in grams per mile.

11.6. Figure 15-11 shows the variation in NO and HC emissions as concentrations (ppm) in the exhaust of a spark-ignition engine as a function of speed and load. Convert these data to graphs of indicated specific NO and HC emissions (g/kW · h) versus speed and imep. Assume η_v (based on atmospheric air density) = imep (kPa) $\times 10^{-3}$.

11.7. Use the data in Fig. 11-44 to estimate:

(*a*) The exhaust particulate emissions as a fraction of the maximum particulate loading during the cycle.

(*b*) The maximum measured soot loading and the exhaust soot loading as fractions of the fuel carbon.

(*c*) The equivalent sphere size of each soot particle at the number density peak (22° ATC) and in the exhaust.

Assume a particulate density of 2 g/cm^3. Note that the gas volumes in Fig. 11-44 are determined at standard temperature and pressure.

11.8. Explain the following emissions trends. Highest marks will be given for succinct summaries of the *important* technical issues.

(*a*) Nitric oxide (NO) emissions from diesels and spark-ignition engines as the equivalence ratio is varied show significantly different behavior (see Figs. 11-9 and 11-16). Redraw these graphs on the same plot and explain the different trends for these two types of engines as ϕ decreases on the lean side of stoichiometric.

(*b*) Recirculation of a fraction of the exhaust gases to the intake is used to control engine nitric oxide emissions at part load. Exhaust gas recycle is usually more effective with spark-ignition engines than with diesels, as shown in Fig. P11-8. Explain why these trends are different.

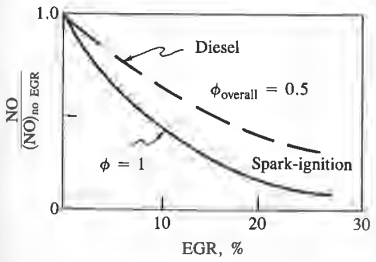

FIGURE P11-8

(*c*) Brake specific particulate emissions from diesels are a major problem. Particulate emissions from conventional spark-ignition engines are negligible. Briefly explain why the particulate emission levels from these two types of engines are so different in magnitude.

FIGURE 11-59
Catalytic ceramic-monolith particulate trap oxidizer mounted on exhaust of turbocharged automobile diesel engine.[86]

is forced to flow through the
/comb is insulated and the trap
a trap temperature as possible.
reases from 0.02 atm at 1000
d of 4500 rev/min. As the trap
ore fuel to be injected to com-
ıer exhaust temperature which
iculate. The particulate oxida-
th suitable trap location and
gulating. The particulate emis-
more.[86]

.nd HC in a spark-ignition engine
o. Assume the concentration scale
ıs the mixture is first made richer

ruct a similar qualitative graph of
alence ratio for a direct-injection

ıverage, 120 grams of gasoline per
ıgine (upstream of the catalyst) are
,), HC, and CO, respectively. The
ir mixture. Find the average con-
s ppm C_1), and CO in the engine

ɔrresponding to the spark-ignition
clude any hydrogen you estimate

(*d*) Diesels have low carbon monoxide (CO) emissions. Spark-ignition engine CO emissions when *averaged* over a typical urban automobile trip (cold engine start, warm-up, cruise, idle, acceleration, etc.) are substantial and require a catalyst for effective control. Explain this difference in average CO emissions (upstream of any catalyst) from these two types of engines.

11.9. The following questions refer to an engine with these geometric and operating characteristics (see Fig. 11-26*a*): $\phi = 1.0$; compression ratio = 8 : 1; bore = 100 mm; stroke = 100 mm; piston diameter above top ring = 99.4 mm; distance from piston crown top to top ring = 9.52 mm; volumetric efficiency = 0.8; temperature in cylinder at the start of compression = 333 K; pressure in cylinder at start of compression = 1 atm; mixture temperature before entering cylinder = 30°C; brake specific fuel consumption = 300 g/kW · h.

A substantial fraction of spark-ignition engine hydrocarbon emissions comes from the crevice between the piston crown and cylinder wall. Gas is forced into this crevice as the cylinder pressure increases and flows out of this crevice as the cylinder pressure decreases. The gas in the crevice can be assumed to be at the wall temperature, 400 K. The gas pushed into the crevice ahead of the flame is unburned mixture; the gas pushed in behind the flame is burned mixture. About two-thirds of the crevice gas is unburned. The maximum cylinder pressure is 3 MPa.

(*a*) Calculate the mass fraction of the cylinder gas which is in the crevice between the piston and cylinder wall and above the first piston ring, at the time of peak pressure.

(*b*) Assuming that half of the unburned fuel in this region is oxidized within the cylinder and a further one-third is oxidized in the exhaust port, calculate the engine HC emissions from this source in parts per million (ppm C_1) by volume.

(*c*) Calculate the ratio of brake specific hydrocarbon emissions to brake specific fuel consumption.

(*d*) Calculate the brake specific hydrocarbon emissions in grams of HC per kilowatt-hour.

11.10. Nitric oxide, NO, forms via reactions (11.1) to (11.3). Reaction (11.1) is "slow" and reactions (11.2) and (11.3) are "fast," so the initial rate of formation of NO is given by Eq. (11.8):

$$\frac{d[\mathrm{NO}]}{dt} = 2k_1^+[\mathrm{N_2}]_e[\mathrm{O}]_e$$

where [ ] denote concentrations in gram-moles per cubic centimeter, k_1^+ is the rate constant for reaction (11.1), and the factor of 2 enters because the N atom formed in (11.1) immediately reacts via (11.2) or (11.3) to give an additional NO molecule:

$$k_1^+ = 7.6 \times 10^{13} \exp\left(\frac{-38{,}000}{T}\right) \qquad \mathrm{cm^3/gmol \cdot s}$$

where T is in kelvin.

Using the equilibrium composition data provided for mole fraction atomic oxygen (O), molecular nitrogen (N_2), and nitric oxide (NO):

(*a*) Plot the formation rate of NO as a function of the equivalence ratio at 3000 K and 5.5 MPa, and as a function of temperature for a stoichiometric mixture at 5.5 MPa.

(*b*) Estimate approximately the time taken to reach equilibrium NO levels at $\phi = 1$, 2750 K and 3000 K, 5.5 MPa.

(*c*) If the stoichiometric mixture inducted into the engine reaches 3000 K and 5.5 MPa after combustion, in the absence of any exhaust gas recirculation, calculate the percentage of the exhaust that must be recycled to the intake (at the initial intake temperature) to reduce the NO formation rate by a factor of 4 (assume the final pressure 5.5 MPa stays the same; of course, the final temperature decreases as the exhaust gas is recycled).

$p = 5.5$ MPa

		Mole fraction	
ϕ	T(K)	O	N_2
0.9	3000	2.1×10^{-3}	0.73
1.0	3000	1.5×10^{-3}	0.73
1.1	3000	1×10^{-3}	0.73

$\phi = 1.0$, $p = 5.5$ MPa

	Mole fraction		
T(K)	O	N_2	NO
2500	6×10^{-5}	0.73	—
2750	5×10^{-4}	0.73	4×10^{-3}
3000	1.5×10^{-3}	0.73	8×10^{-3}

REFERENCES

1. Bowman, C. T.: "Kinetics of Pollutant Formation and Destruction in Combustion," *Prog. Energy Combust. Sci.*, vol. 1, pp. 33–45, 1975.
2. Lavoie, G. A., Heywood, J. B., and Keck, J. C.: "Experimental and Theoretical Investigation of Nitric Oxide Formation in Internal Combustion Engines," *Combust. Sci. Technol.*, vol. 1, pp. 313–326, 1970.
3. Heywood, J. B., Fay, J. A., and Linden, L. H.: "Jet Aircraft Air Pollutant Production and Dispersion," *AIAA J.*, vol. 9, no. 5, pp. 841–850, 1971.
4. Newhall, H. K., and Shahed, S. M.: "Kinetics of Nitric Oxide Formation in High-Pressure Flames," in *Proceedings of Thirteenth International Symposium on Combustion*, pp. 381–390, The Combustion Institute, 1971.
5. Hilliard, J. C., and Wheeler, R. W.: "Nitrogen Dioxide in Engine Exhaust," SAE paper 790691, *SAE Trans.*, vol. 88, 1979.
6. Merryman, E. L., and Levy, A.: "Nitrogen Oxide Formation in Flames: The Roles of NO_2 and Fuel Nitrogen," in *Proceedings of Fifteenth International Symposium on Combustion*, p. 1073, The Combustion Institute, 1975.
7. Komiyama, K., and Heywood, J. B.: "Predicting NO_x Emissions and Effects of Exhaust Gas Recirculation in Spark-Ignition Engines," SAE paper 730475, *SAE Trans.*, vol. 82, 1973.
8. Alperstein, M., and Bradow, R. L.: "Exhaust Emissions Related to Engine Combustion Reactions," SAE paper 660781, *SAE Trans.*, vol. 75, 1966.
9. Starkman, E. S., Stewart, H. E., and Zvonow, V. A.: "Investigation into Formation and Modification of Exhaust Emission Precursors," SAE paper 690020, 1969.
10. Lavoie, G. A.: "Spectroscopic Measurement of Nitric Oxide in Spark-Ignition Engines," *Combust. Flame*, vol. 15, pp. 97–108, 1970.
11. Blumberg, P., and Kummer, J. K.: "Prediction of NO Formation in Spark-Ignition Engines—An Analysis of Methods of Control," *Combust. Sci. Technol.*, vol. 4, pp. 73–96, 1971.
12. Sakai, Y., Miyazaki, H., and Mukai, K.: "The Effect of Combustion Chamber Shape on Nitrogen Oxides," SAE paper 730154, 1973.
13. Quader, A. A.: "Why Intake Charge Dilution Decreases Nitric Oxide Emission from Spark Ignition Engines," SAE paper 710009, *SAE Trans.*, vol. 80, 1971.

14. Benson, J. D., and Stebar, R. F.: "Effects of Charge Dilution on Nitric Oxide Emission from a Single-Cylinder Engine," SAE paper 710008, *SAE Trans.*, vol. 80, 1971.
15. Toda, T., Nohira, H., and Kobashi, K.: "Evaluation of Burned Gas Ratio (BGR) as a Predominant Factor to NO_x," SAE paper 760765, *SAE Trans.*, vol. 85, 1976.
16. Lavoie, G. A., and Blumberg, P. N.: "A Fundamental Model for Predicting Fuel Consumption, NO_x and HC Emissions of the Conventional Spark-Ignited Engine," *Combust. Sci. Technol.*, vol. 21, pp. 225–258, 1980.
17. Lavoie, G. A., and Blumberg, P. N.: "Measurements of NO Emissions from a Stratified Charge Engine: Comparison of Theory and Experiment," *Combust. Sci. Technol.*, vol. 8, p. 25, 1973.
18. Aoyagi, Y., Kamimoto, T., Matsui, Y., and Matsuoka, S.: "A Gas Sampling Study on the Formation Processes of Soot and NO in a DI Diesel Engine," SAE paper 800254, SAE Trans., vol. 89, 1980.
19. Vioculescu, I. A., and Borman, G. L.: "An Experimental Study of Diesel Engine Cylinder-Averaged NO_x Histories," SAE paper 780228, *SAE Trans.*, vol. 87, 1978.
20. Mansouri, S. H., Heywood, J. B., and Radhakrishnan, K.: "Divided-Chamber Diesel Engine, Part I: Cycle-Simulation Which Predicts Performance and Emissions," SAE paper 820273, *SAE Trans.*, vol. 91, 1982.
21. Duggal, V. K., Priede, T., and Khan, I. M.: "A Study of Pollutant Formation within the Combustion Space of a Diesel Engine," SAE paper 780227, *SAE Trans.*, vol. 87, 1978.
22. Liu, X., and Kittelson, D. B.: "Total Cylinder Sampling from a Diesel Engine (Part II)," SAE paper 820360, 1982.
23. Yu, R. C., and Shahed, S. M.: "Effects of Injection Timing and Exhaust Gas Recirculation on Emissions from a D.I. Diesel Engine," SAE paper 811234, *SAE Trans.*, vol. 90, 1981.
24. Plee, S. L., Myers, J. P., and Ahmed, T.: "Flame Temperature Correlation for the Effects of Exhaust Gas Recirculation on Diesel Particulate and NO_x Emissions," SAE paper 811195, *SAE Trans.*, vol. 90, 1981.
25. Plee, S. L., Ahmad, T., and Myers, J. P.: "Diesel NO_x Emissions—A Simple Correlation Technique for Intake Air Effects," in *Proceedings of Nineteenth International Symposium on Combustion*, pp. 1495–1502, The Combustion Institute, Pittsburgh, 1983.
26. Ahmad, T., and Plee, S. L.: "Application of Flame Temperature Correlations to Emissions from a Direct-Injection Diesel Engine," SAE paper 831734, *SAE Trans.*, vol. 92, 1983.
27. Harrington, J. A., and Shishu, R. C.: "A Single-Cylinder Engine Study of the Effects of Fuel Type, Fuel Stoichiometry, and Hydrogen-to-Carbon Ratio and CO, NO, and HC Exhaust Emissions," SAE paper 730476, 1973.
28. Newhall, H. K.: "Kinetics of Engine-Generated Nitrogen Oxides and Carbon Monoxide," in *Proceedings of Twelfth International Symposium on Combustion*, pp. 603–613, Mono of Maryland, 1968.
29. Keck, J. C., and Gillespie, D.: "Rate-Controlled Partial-Equilibrium Method for Treating Reacting Gas Mixtures," *Combust. Flame*, vol. 17, pp. 237–241, 1971.
30. Delichatsios, M. M.: "The Kinetics of CO Emissions from an Internal Combustion Engine," S.M. Thesis, Department of Mechanical Engineering, MIT, June 1972.
31. Johnson, G. L., Caretto, L. S., and Starkman, E. S.: "The Kinetics of CO Oxidation in Reciprocating Engines," paper presented at the Western States Section, The Combustion Institute, Spring Meeting, April 1970.
32. Jackson, M. W.: "Analysis for Exhaust Gas Hydrocarbons—Nondispersive Infrared Versus Flame-Ionization," *J. Air Pollution Control Ass.*, vol. 16, p. 697–702, 1966.
33. Jackson, M. W.: "Effect of Catalytic Emission Control on Exhaust Hydrocarbon Composition and Reactivity," SAE paper 780624, *SAE Trans.*, vol. 87, 1978.
34. Patterson, D. J., and Henein, N. A.: *Emissions from Combustion Engines and Their Control*, Ann Arbor Science Publishers, Ann Arbor, Michigan, 1972.
35. "Diesel Technology, Impacts of Diesel-Powered Light-Duty Vehicles," report of the Technology Panel of the Diesel Impacts Study Committee, National Research Council, National Academy Press, Washington, D.C., 1982.
36. Lavoie, G. A.: "Correlations of Combustion Data for S.I. Engine Calculations—Laminar Flame

Speed, Quench Distance and Global Reaction Rates," SAE paper 780229, *SAE Trans.*, vol. 87, 1978.

37. Adamczyk, A. A., Kaiser, E. W., Cavolowsky, J. A., and Lavoie, G. A.: "An Experimental Study of Hydrocarbon Emissions from Closed Vessel Explosions," in *Proceedings of Eighteenth International Symposium on Combustion*, pp. 1695–1702, The Combustion Institute, 1981.
38. Westbrook, C. K., Adamczyk, A. A., and Lavoie, G. A.: "A Number Study of Laminar Wall Quenching," *Combust. Flame*, vol. 40, pp. 81–91, 1981.
39. Kaiser, E. W., Adamczyk, A. A., and Lavoie, G. A.: "The Effect of Oil Layers on the Hydrocarbon Emissions Generated During Closed Vessel Combustion," in *Proceedings of Eighteenth International Symposium on Combustion*, pp. 1881–1890, The Combustion Institute, 1981.
40. Tabaczynski, R. J., Heywood, J. B., and Keck, J. C.: "Time-Resolved Measurements of Hydrocarbon Mass Flow Rate in the Exhaust of a Spark-Ignition Engine," SAE paper 720112, *SAE Trans.*, vol. 81, 1972.
41. Ekchian, A., Heywood, J. B., and Rife, J. M.: "Time Resolved Measurements of the Exhaust from a Jet Ignition Prechamber Stratified Charge Engine," SAE paper 770043, *SAE Trans.*, vol. 86, 1977.
42. Daniel, W. A., and Wentworth, J. T.: "Exhaust Gas Hydrocarbons—Genesis and Exodus," SAE paper 486B, March 1962; also SAE Technical Progress Series, vol. 6, p. 192, 1964.
43. Daniel, W. A.: "Flame Quenching at the Walls of an Internal Combustion Engine," in *Proceedings of Sixth International Symposium on Combustion*, p. 886, Reinhold, New York, 1957.
44. LoRusso, J. A., Lavoie, G. A., and Kaiser, E. W.: "An Electrohydraulic Gas Sampling Valve with Application to Hydrocarbon Emissions Studies," SAE paper 800045, *SAE Trans.*, vol. 89, 1980.
45. Wentworth, J. T.: "More on Origins of Exhaust Hydrocarbons—Effects of Zero Oil Consumption, Deposit Location, and Surface Roughness," SAE paper 720939, *SAE Trans.*, vol. 81, 1972.
46. Namazian, M., and Heywood, J. B.: "Flow in the Piston-Cylinder-Ring Crevices of a Spark-Ignition Engine: Effect on Hydrocarbon Emissions, Efficiency and Power," SAE paper 820088, *SAE Trans.*, vol. 91, 1982.
47. Furuhama, S., and Tateishi, Y.: "Gases in Piston Top-Land Space of Gasoline Engine," *Trans. SAEJ*, no. 4, 1972.
48. Wentworth, J. T.: "The Piston Crevice Volume Effect on Exhaust Hydrocarbon Emission," *Combust. Sci. Technol.*, vol. 4, pp. 97–100, 1971.
49. Haskell, W. W., and Legate, C. E.: "Exhaust Hydrocarbon Emissions from Gasoline Engines—Surface Phenomena," SAE paper 720255, 1972.
50. Adamczyk, A. A., Kaiser, E. W., and Lavoie, G. A.: "A Combustion Bomb Study of the Hydrocarbon Emissions from Engine Crevices," *Combust. Sci. Technol.*, vol. 33, pp. 261–277, 1983.
51. Wentworth, J. T.: "Piston and Ring Variables Affect Exhaust Hydrocarbon Emissions," SAE paper 680109, *SAE Trans.*, vol. 77, 1968.
52. Kaiser, E. W., LoRusso, J. A., Lavoie, G. A., and Adamczyk, A. A.: "The Effect of Oil Layers on the Hydrocarbon Emissions from Spark-Ignited Engines," *Combust. Sci. Technol.*, vol. 28, pp. 69–73, 1982.
53. Kaiser, E. W., Adamczyk, A. A., and Lavoie, G. A.: "The Effect of Oil Layers on the Hydrocarbon Emissions Generated during Closed Vessel Combustion," in *Proceedings of Eighteenth International Symposium on Combustion*, pp. 1881–1890, The Combustion Institute, 1981.
54. McGeehan, J. A.: "A Literature Review of the Effects of Piston and Ring Friction and Lubricating Oil Viscosity on Fuel Economy," SAE paper 780673, *SAE Trans.*, vol. 87, 1978.
55. Shin, K., Tateishi, Y., and Furuhama, S.: "Measurement of Oil-Film-Thickness between Piston Ring and Cylinder," SAE paper 830068, *SAE Trans.*, vol. 92, 1983.
56. Carrier, G. F., Fendell, F. E., and Feldman, P. S.: "Cyclic Absorption/Desorption of Gas in a Liquid Wall Film," *Combust. Sci. Technol.*, vol. 25, pp. 9–19, 1981.
57. Wentworth, J. T.: "Effects of Top Compression Ring Profile on Oil Consumption and Blowby with the Sealed Ring Orifice Design," SAE paper 820089, 1982.
58. Kuroda, H., Nakajima, Y., Sugihara, K., Takagi, Y., and Muranaka, S.: "The Fast Burn with Heavy EGR, New Approach for Low NO_x and Improved Fuel Economy," SAE paper 780006, *SAE Trans.*, vol. 87, 1978.

59. Jackson, M. W., Wiese, W. M., and Wentworth, J. T.: "The Influence of Air-Fuel Ratio, Spark Timing, and Combustion Chamber Deposits on Exhaust Hydrocarbon Emissions," SAE paper 486A, in *Vehicle Emissions*, vol. TP-6, SAE, 1962.
60. Lavoie, G. A., Lorusso, J. A., and Adamczyk, A. A.: "Hydrocarbon Emissions Modeling for Spark Ignition Engines," in J. N. Mattavi and C. A. Amann (eds.), *Combustion Modeling in Reciprocating Engines*, pp. 409–445, Plenum Press, 1978.
61. Daniel, W. A.: "Why Engine Variables Affect Exhaust Hydrocarbon Emission," SAE paper 700108, *SAE Trans.*, vol. 79, 1970.
62. Amann, C. A.: "Control of the Homogeneous-Charge Passenger-Car Engine—Defining the Problem," SAE paper 801440, 1980.
63. Weiss, P., and Keck, J. C.: "Fast Sampling Valve Measurements of Hydrocarbons in the Cylinder of a CFR Engine," SAE paper 810149, *SAE Trans.*, vol. 90, 1981.
64. Caton, J. A., Heywood, J. B., and Mendillo, J. V.: "Hydrocarbon Oxidation in a Spark Ignition Engine Exhaust Port," *Combust. Sci. Technol.*, vol. 37, nos. 3 and 4, pp. 153–169, 1984.
65. Green, R. M., Smith, J. R., and Medina, S. C.: "Optical Measurement of Hydrocarbons Emitted from a Simulated Crevice Volume in an Engine," SAE paper 840378, *SAE Trans.*, vol. 93, 1984.
66. Nakagawa, Y., Etoh, Y., and Maruyama, R.: "A Fundamental Analysis of HC and CO Oxidation Reaction in the Exhaust System," *JSAE Rev.*, no. 1, pp. 98–106, 1978.
67. Greeves, G., Khan, I. M., Wang, C. H. T., and Fenne, I.: "Origins of Hydrocarbon Emissions from Diesel Engines," SAE paper 770259, *SAE Trans.*, vol. 86, 1977.
68. Kummer, J. T.: "Catalysts for Automobile Emission Control," *Prog. Energy Combust. Sci.*, vol. 6, pp. 177–199, 1981.
69. Cadle, S. H., Nebel, G. J., and Williams, R. L.: "Measurements of Unregulated Emissions from General Motors' Light-Duty Vehicles," SAE paper 790694, *SAE Trans.*, vol. 88, 1979.
70. Amann, C. A., and Siegla, D. C.: "Diesel Particulates—What They Are and Why," *Aerosol Sci. Technol.*, vol. 1, pp. 73–101, 1982.
71. Mayer, W. J., Lechman, D. C., and Hilden, D. L.: "The Contribution of Engine Oil to Diesel Exhaust Particulate Emissions," SAE paper 800256, *SAE Trans.*, vol. 89, 1980.
72. Lahaye, J., and Prado, G.: "Morphology and Internal Structure of Soot and Carbon Blacks," in D. C. Siegla and G. W. Smith (eds.), *Particulate Carbon Formation during Combustion*, pp. 33–55, Plenum Press, 1981.
73. Smith, O. I.: "Fundamentals of Soot Formation in Flames with Application to Diesel Engine Particulate Emissions," *Prog. Energy Combust. Sci.*, vol. 7, pp. 275–291, 1981.
74. Whitehouse, N. D., Clough, E., and Uhunmwangho, S. O.: "The Development of Some Gaseous Products during Diesel Engine Combustion," SAE paper 800028, 1980.
75. Greeves, G., and Meehan, J. O.: "Measurement of Instantaneous Soot Concentration in a Diesel Combustion Chamber," paper C88/75, in *Combustion in Engines*, pp. 73–82, Institution of Mechanical Engineers, 1975.
76. Chang, Y. J., Kobayashi, H., Matsuzawa, K., and Kamimoto, T.: "A Photographic Study of Soot Formation and Combustion in a Diesel Flame with a Rapid Compression Machine," Proceedings of International Symposium on *Diagnostics and Modeling of Combustion in Reciprocating Engines*, COMODIA 85, pp. 149–157, Tokyo, Japan, September 4–6, 1985.
77. Du, C. J., and Kittelson, D. B.: "Total Cylinder Sampling from a Diesel Engine: Part III—Particle Measurements," SAE paper 830243, *SAE Trans.*, vol. 92, 1983.
78. Aoyagi, Y., Kamimoto, T., Matsui, Y., and Matsuoka, S.: "A Gas Sampling Study on the Formation Processes of Soot and NO in a DI Diesel Engine," SAE paper 800254, *SAE Trans.*, vol. 89, 1980.
79. Matsui, Y., Kamimoto, T., and Matsuoka, S.: "Formation and Oxidation Processes of Soot Particles in a D.I. Diesel Engine—An Experimental Study Via the Two-Color Method," SAE paper 820464, *SAE Trans.*, vol. 91, 1982.
80. Haynes, B. S., and Wagner, H. G.: "Soot Formation," *Prog. Energy Combust. Sci.*, vol. 7, pp. 229–273, 1981.
81. Lahaye, J., and Prado, G.: "Mechanisms of Carbon Black Formation," in P. L. Walker and P. A.

Thrower (eds.), *Chemistry and Physics of Carbon*, vol. 14, pp. 168–294, Marcel Dekker, New York, 1978.

82. Graham, S. C., Homer, J. B., and Rosenfeld, J. L. J.: "The Formation and Coagulation of Soot Aerosols Generated by the Pyrolysis of Aromatic Hydrocarbons," *Proc. R. Soc. Lond.*, vol. A344, pp. 259–285, 1975.
83. Amann, C. A., Stivender, D. L., Plee, S. L., and MacDonald, J. S.: "Some Rudiments of Diesel Particulate Emissions," SAE paper 800251, *SAE Trans.*, vol. 89, 1980.
84. Park, C., and Appleton, J. P.: "Shock-Tube Measurements of Soot Oxidation Rates," *Combust. Flame*, vol. 20, pp. 369–379, 1973.
85. Otto, K., Sieg, M. H., Zinbo, M., and Bartosiewicz, L.: "The Oxidation of Soot Deposits from Diesel Engines," SAE paper 800336, *SAE Trans.*, vol. 89, 1980.
86. Abthoff, J., Schuster, H., Langer, H., and Loose, G.: "The Regenerable Trap Oxidizer—An Emission Control Technique for Diesel Engines," SAE paper 850015, 1985.

:owicz, J. K.: "KIVA: A Computer with Chemical Reactions and Fuel oratory, Los Alamos, New Mexico,

Watkins, A. P.: "Multidimensional Charge Engine: A Progress Report,"

Fuel-Air Mixing and Combustion in ., vol. 91, 1982.
is of Engine Combustion: Compari- 982.
for Spark Ignition Engines," SAE

ng of Knocking Combustion in SI

of Diesel Ignition," paper 87-FE-2, ice, Dallas, February 1987.

CHAPTER 15

ENGINE OPERATING CHARACTERISTICS

This chapter reviews the operating characteristics of the common types of spark-ignition and compression-ignition engines. The performance, efficiency, and emissions of these engines, and the effect of changes in major design and operating variables, are related to the more fundamental material on engine combustion, thermodynamics, fluid flow, heat transfer, and friction developed in earlier chapters. The intent is to provide data on, and an explanation of, actual engine operating characteristics.

15.1 ENGINE PERFORMANCE PARAMETERS

The practical engine performance parameters of interest are power, torque, and specific fuel consumption. Power and torque depend on an engine's displaced volume. In Chap. 2 a set of normalized or dimensionless performance and emissions parameters were defined to eliminate the effects of engine size. Power, torque, and fuel consumption were expressed in terms of these parameters (Sec. 2.14) and the significance of these parameters over an engine's load and speed range was discussed (Sec. 2.15). Using these normalized parameters, the effect of engine size can be made explicit. The power P can be expressed as:

$$P = \text{mep}\ A_p \bar{S}_p/4 \quad \text{(four-stroke cycle)}$$
$$P = \text{mep}\ A_p \bar{S}_p/2 \quad \text{(two-stroke cycle)} \qquad (15.1)$$

The torque T is given by

$$\begin{aligned} T &= \text{mep } V_d/(4\pi) \qquad \text{(four-stroke cycle)} \\ T &= \text{mep } V_d/(2\pi) \qquad \text{(two-stroke cycle)} \end{aligned} \tag{15.2}$$

Thus for well-designed engines, where the maximum values of mean effective pressure and piston speed are either flow limited (in naturally aspirated engines) or stress limited (in turbocharged engines), power is proportional to piston area and torque to displaced volume. Mean effective pressure can be expressed as

$$\text{mep} = \eta_f \eta_v Q_{\text{HV}} \rho_{a,i} \left(\frac{F}{A}\right) \tag{15.3}$$

for four-stroke cycle engines [Eq. (2.41)], and as

$$\text{mep} = \eta_f \eta_{tr} \Lambda Q_{\text{HV}} \rho_{a,i} \left(\frac{F}{A}\right) \tag{15.4}$$

for two-stroke cycle engines [Eqs. (2.19), (2.38), and (6.25)]. The importance of high fuel conversion efficiency, breathing capacity, and inlet air density is clear. Specific fuel consumption is related to fuel conversion efficiency by Eq. (2.24):

$$\text{sfc} = \frac{1}{\eta_f Q_{\text{HV}}} \tag{15.5}$$

These parameters have both brake and indicated values (see Secs. 2.3, 2.4, and 2.5). The difference between these two quantities is the engine's friction (and pumping) requirements and their ratio is the mechanical efficiency η_m.

The relative importance of these parameters varies over an engine's operating speed and load range. The maximum or normal rated brake power (see Sec. 2.1) and the quantities such as bmep derived from it (see Sec. 2.7) define an engine's full potential. The maximum brake torque (and bmep derived from it), over the full speed range, indicates the ability of the designer to obtain a high air flow through the engine over the full speed range and use that air effectively. Then over the whole operating range, and most especially those parts of that range where the engine will operate for long periods of time, engine fuel consumption and efficiency, and engine emissions are important. Since the operating and emissions characteristics of spark-ignition and compression-ignition engines are substantially different, each engine type is dealt with separately.

15.2 INDICATED AND BRAKE POWER AND MEP

The wide-open-throttle operating characteristics of a production spark-ignition automotive engine are shown in Fig. 15-1. The power shown is the gross power for the basic engine; this includes only the built-in engine accessories.[2] The maximum net power for the fully equipped engine with the complete intake and exhaust system and full cooling system is about 14 percent lower. The indicated

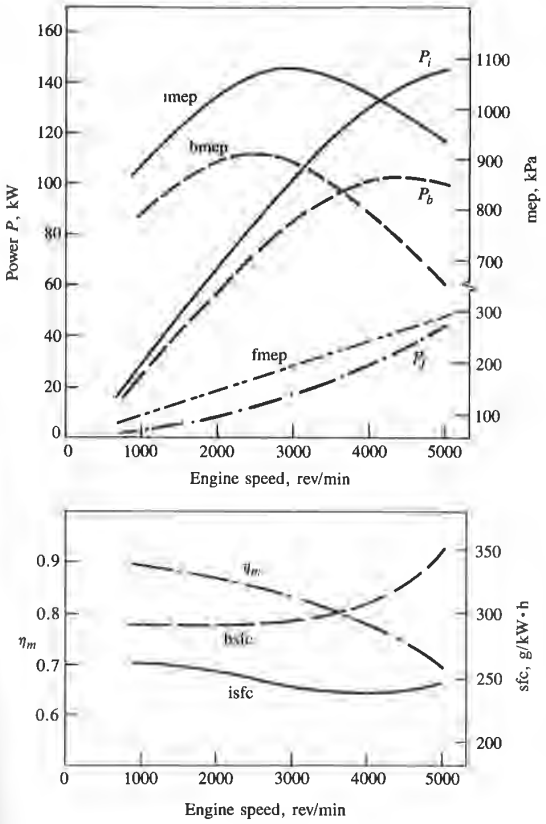

FIGURE 15-1
Gross indicated, brake, and friction power (P_i, P_b, P_f), indicated, brake, and friction mean effective pressure, indicated and brake specific fuel consumption, and mechanical efficiency for 3.8-dm^3 six-cylinder automotive spark-ignition engine at wide-open throttle. Bore = 96.8 mm, stroke = 86 mm, $r_c = 8.6$.[1]

power was obtained by adding the friction power to the brake power; it is the average rate of work transfer from the gases in the engine cylinders to the pistons during the compression and expansion strokes of the engine cycle (see Sec. 2.4). The indicated mean effective pressure shows a maximum in the engine's mid-speed range, just below 3000 rev/min. The shape of the indicated power curve follows from the imep curve. Since the full-load indicated specific fuel consumption (and hence indicated fuel conversion efficiency) varies little over the full speed range, this variation of full-load imep and power with speed is primarily due to the variation in volumetric efficiency, η_v [see Eq. (15.3)]. Since friction mean effective pressure increases almost linearly with increasing speed, friction

FIGURE 15-2
Gross indicated and brake power (P_i, P_b), mean effective pressure (imep, bmep), and specific fuel consumption (isfc, bsfc) for: (*a*) 8.4-dm^3 six-cylinder naturally aspirated direct-injection diesel engine; bore = 115 mm, stroke = 135 mm, $r_c = 16$;[3] (*b*) 1.8-dm^3 four-cylinder naturally aspirated indirect-injection swirl-chamber diesel engine; bore = 84 mm, stroke = 82 mm, $r_c = 22$.[4]

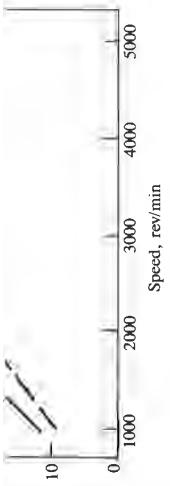

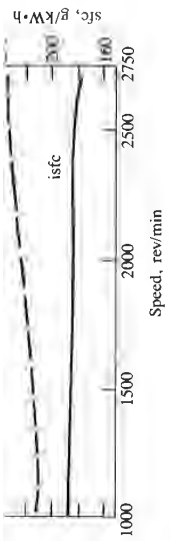

FIGURE 15-2
Gross indicated and brake power (P_i, P_b), mean effective pressure (imep, bmep), and specific fuel consumption (isfc, bsfc) for: (*a*) 8.4-dm^3 six-cylinder naturally aspirated direct-injection diesel engine: bore = 115 mm, stroke = 135 mm, $r_c = 16$;[3] (*b*) 1.8-dm^3 four-cylinder naturally aspirated indirect-injection swirl-chamber diesel engine: bore = 84 mm, stroke = 82 mm, $r_c = 22$.[4]

power will increase more rapidly. Hence mechanical efficiency decreases with increasing speed from a maximum of about 0.9 at low speed to 0.7 at 5000 rev/min. Thus bmep peaks at a lower speed than imep. The brake power shows a maximum at about 4300 rev/min; increases in speed above this value result in a decrease in P_b. The indicated fuel conversion efficiency increases by about 10 percent from 0.31 to 0.34 over the speed range 1000 to 4000 rev/min. This is primarily due to the decreasing importance of heat transfer per cycle with increasing speed.

At part load at fixed throttle position, these parameters behave similarly; however, at higher speeds torque and mean effective pressure decrease more rapidly with increasing speed than at full load. The throttle chokes the flow at lower and lower speeds as the throttle open area is reduced, increasingly limiting the air flow (see Fig. 7-22). The pumping component of total friction also increases as the engine is throttled, decreasing mechanical efficiency (see Figs. 13-9 and 13-10).

Figure 15-2 shows full-load indicated and brake power and mean effective pressure for naturally aspirated DI and IDI compression-ignition engines. Except at high engine speeds, brake torque and mep vary only modestly with engine speed since the intake system of the diesel can have larger flow areas than the intake of SI engines with their intake-system fuel transport requirements. The part-load torque and bmep characteristics (at fixed amount of fuel injected per cycle) have a similar shape to the full-load characteristics in Fig. 15-2. The decrease in torque and bmep with increasing engine speed is due primarily to the increase in friction mep with speed (see Figs. 13-7, 13-11, and 13-12). Decreasing engine heat transfer per cycle and decreasing air-flow rate, as speed increases, have modest additional impacts.

15.3 OPERATING VARIABLES THAT AFFECT SI ENGINE PERFORMANCE, EFFICIENCY, AND EMISSIONS

The major operating variables that affect spark-ignition engine performance, efficiency, and emissions at any given load and speed are: spark timing, fuel/air or air/fuel ratio relative to the stoichiometric ratio, and fraction of the exhaust gases that are recycled for NO_x emission control. Load is, of course, varied by varying the inlet manifold pressure. The effect of these variables will now be reviewed.

15.3.1 Spark Timing

Figure 9-3 and the accompanying text explain how variations in spark timing relative to top-center affected the pressure development in the SI engine cylinder. If combustion starts too early in the cycle, the work transfer from the piston to the gases in the cylinder at the end of the compression stroke is too large; if combustion starts too late, the peak cylinder pressure is reduced and the expan-

sion stroke work transfer from the gas to the piston decreases. There exists a particular spark timing which gives maximum engine torque at fixed speed, and mixture composition and flow rate. It is referred to as MBT—maximum brake torque—timing. This timing also gives maximum brake power and minimum brake specific fuel consumption. Figure 15-3*a* shows the effect of spark advance variations on wide-open-throttle brake torque at selected speeds between 1200 and 4200 rev/min for a production eight-cylinder engine. At each speed, as spark is advanced from an initially retarded setting, torque rises to a maximum and then decreases. MBT timing depends on speed; as speed increases the spark must be advanced to maintain optimum timing because the duration of the combustion process in crank angle degrees increases. Optimum spark timing also depends on load. As load and intake manifold pressure are decreased, the spark timing must be further advanced to maintain optimum engine performance.

The maximum in each brake torque curve in Fig. 15-3*a* is quite flat. Thus accurate determination of MBT timing is difficult, but is important because NO and HC emissions vary significantly with spark timing. In practice, to permit a more precise definition of spark timing, the spark is often retarded to give a 1 or 2 percent reduction in torque from the maximum value.

In Fig. 15-3*a* the mixture composition and flow rate were held constant at each engine speed. If the mixture flow rate is adjusted to maintain constant brake

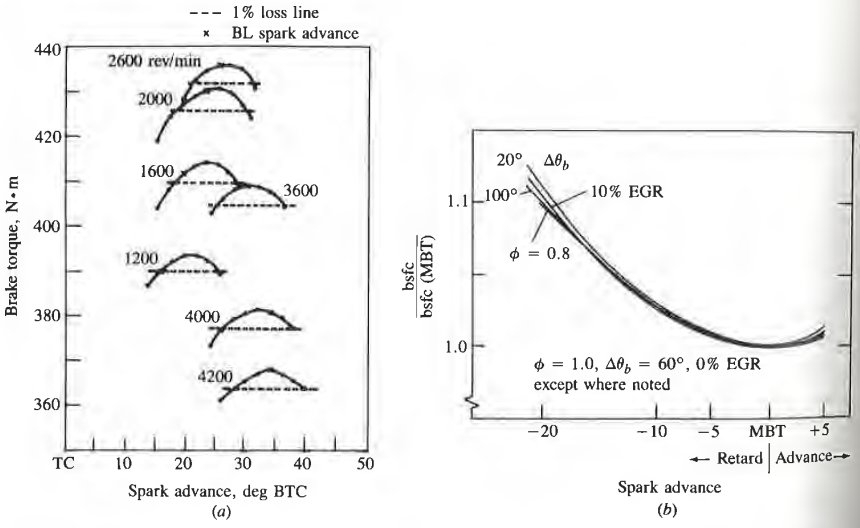

FIGURE 15-3
(*a*) Variation in brake torque with spark advance, eight-cylinder automotive spark-ignition engine at wide-open throttle, at engine speeds from 1200 to 4200 rev/min. 1 percent torque loss from MBT and spark advance for borderline knock are shown.[5] (*b*) Predicted variation in brake specific fuel consumption (normalized by MBT value) with spark retard at several different part-load engine conditions.[6, 7]

torque, the effect of spark timing variations on fuel consumption at constant engine load can be evaluated. Figure 15-3*b* shows results obtained with a computer simulation of the engine operating cycle.[6, 7] The curves for several different part-load operating conditions and burn durations (from fast to slow) have been normalized and fall essentially on top of each other. Five degrees of retard in spark timing have only a modest effect on fuel consumption; for 10 to 20° retard, the impact is much more significant.

Spark timing affects peak cylinder pressure and therefore peak unburned and burned gas temperatures (see Sec. 9.2.1). Retarding spark timing from the optimum reduces these variables. Retarded timing is sometimes used therefore for NO_x emission control (see Fig. 11-13 and accompanying text) and to avoid knock (see Sec. 9.6.1). The exhaust temperature is also affected by spark timing. Retarding timing from MBT increases exhaust temperature; both engine efficiency and heat loss to the combustion chamber walls (see Fig. 12-27) are decreased. Retarded timing is sometimes used to reduce hydrocarbon emissions by increasing the fraction oxidized during expansion and exhaust due to the higher burned gas temperatures that result (see Sec. 11.4.3). Retarded timing may be used at engine idle to bring the ignition point closer to TC where conditions for avoiding misfire are more favorable.

15.3.2 Mixture Composition

The unburned mixture in the engine cylinder consists of fuel (normally vaporized), air, and burned gases. The burned gas fraction is the residual gas plus any recycled exhaust used for NO control. Mixture composition during combustion is most critical, since this determines the development of the combustion process which governs the engine's operating characteristics. While substantial efforts are made to produce a uniform mixture within the cylinder, some nonuniformities remain (see Sec. 9.4.2). In a given cylinder, cycle-by-cycle variations in average charge composition exist. Also, within each cylinder in a given engine cycle, the fuel, air, EGR, and residual gas are not completely mixed, and composition nonuniformities across the charge may be significant.† These together produce variations in composition at the spark plug location (the critical region since the early stages of flame development influence the rest of the combustion process) which can be of order ± 10 percent peak-to-peak (see Fig. 9-34). In addition, in multicylinder engines, the average air, fuel, and EGR flow rates to each cylinder are not identical. Typical cylinder-to-cylinder variations have standard deviations of ±5 percent of the mean for air flow rate and fuel flow rate (giving a

† This aspect of mixture nonuniformity is least well defined. Mixing of the fresh mixture (fuel, air, and EGR) with residual gas is likely to be incomplete (see Fig. 14-36), especially at light load when the residual gas fraction is highest. With intake-port fuel-injection systems, there is evidence of incomplete fuel-air mixing due to the fact that the air flow and fuel flow processes are not in phase.[9] When the engine is cold, fuel distribution within the cylinder is known to be nonuniform.

ı decreases. There exists a
torque at fixed speed, and
as MBT—maximum brake
rake power and minimum
the effect of spark advance
ected speeds between 1200
ne. At each speed, as spark
rises to a maximum and
ed increases the spark must
the duration of the com-
ptimum spark timing also
re are decreased, the spark
engine performance.
ig. 15-3*a* is quite flat. Thus
t is important because NO
ıg. In practice, to permit a
ften retarded to give a 1 or
rate were held constant at
to maintain constant brake

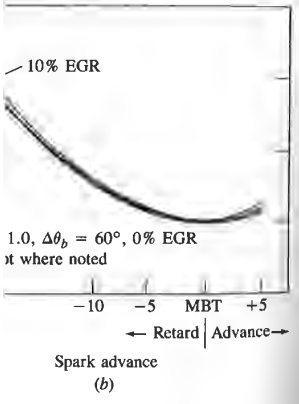

tomotive spark-ignition engine at
ercent torque loss from MBT and
iation in brake specific fuel con-
different part-load engine condi-

±7 percent variation in the air/fuel ratio) for steady-state engine operation. EGR cylinder-to-cylinder flow rates may have higher variability. Under unsteady engine operating conditions all these variations can be higher.

It is necessary to consider the effect of mixture composition changes on engine operating and emissions characteristics in two regimes: (1) wide-open throttle (WOT) or full load and (2) part throttle or load. At WOT, the engine air flow is the maximum that the engine will induct.† Fuel flow can be varied, but air flow is set by engine design variables and speed. At part throttle, air flow, fuel flow, and EGR flow can be varied. Evaluation of mixture composition changes at part load should be done at fixed (brake) load and speed, i.e., under conditions where the engine provides the desired torque level at the specified speed. To maintain torque (or load or bmep) constant as mixture composition is varied normally requires changes in throttle setting (and if EGR is varied, changes in EGR flow-control valve setting). This distinction between part-load comparisons at specified torque or bmep, rather than at constant throttle settings (which gives essentially constant air flow), is important because the pumping work component of engine friction will vary at constant engine load as mixture composition changes. At constant throttle setting and speed, the pumping work remains essentially unchanged.

AIR/FUEL OR EQUIVALENCE RATIO CHANGES. Mixture composition effects are usually discussed in terms of the air/fuel ratio (or fuel/air ratio) because in engine tests, the air and fuel flow rates to the engine can be measured directly and because the fuel metering system is designed to provide the appropriate fuel flow for the actual air flow at each speed and load. However, the relative proportions of fuel and air can be stated more generally in terms of the fuel/air equivalence ratio ϕ [the actual fuel/air ratio normalized by dividing by the stoichiometric fuel/air ratio, see Eq. (3.8)] or the relative air/fuel ratio λ [see Eq. (3.9)]. The combustion characteristics of fuel-air mixtures and the properties of combustion products, which govern engine performance, efficiency, and emissions, correlate best for a wide range of fuels relative to the stoichiometric mixture proportions. Where appropriate, therefore, the equivalence ratio will be used as the defining parameter. Equation (7.1) converts the air/fuel ratio with gasoline to the equivalence ratio.

The theoretical basis for understanding the effect of changes in the equivalence ratio is the fuel-air cycle results in Figs. 5-9 and 5-10, where the indicated fuel conversion efficiency and mean effective pressure are shown as a function of the fuel/air equivalence ratio, ϕ. The mean effective pressure peaks slightly rich of stoichiometric, between $\phi = 1$ and 1.1. Due to dissociation at the high temperatures following combustion, molecular oxygen is present in the burned gases under stoichiometric conditions, so some additional fuel can be added and par-

† EGR is normally zero at WOT, since maximum torque is usually desired.

tially burned. This increases the temperature and the number of moles of the burned gases in the cylinder. These effects increase the pressure to give increased power and mep. Fuel conversion efficiency decreases approximately as $1/\phi$, as the mixture is richened above stoichiometric ($\phi > 1$) due to the decreasing combustion efficiency associated with the richening mixture.

For mixtures lean of stoichiometric, the theoretical fuel conversion efficiency increases linearly as ϕ decreases below 1.0. Combustion of mixtures leaner than stoichiometric produces products at lower temperature, and with less dissociation of the triatomic molecules CO_2 and H_2O. Thus the *fraction* of the chemical energy of the fuel which is released as sensible energy near TC is greater; hence a greater *fraction* of the fuel's energy is transferred as work to the piston during expansion, and the fraction of the fuel's available energy rejected to the exhaust system decreases (see Sec. 5.7). There is a discontinuity in the fuel conversion efficiency and imep curves at the stoichiometric point; the burned gas composition is substantially different on the rich and the lean sides of $\phi = 1$.

Figure 15-4 shows gross indicated specific fuel consumption data for a six-cylinder spark-ignition engine at wide-open throttle and 1200 rev/min,[9] and values of gross indicated mean effective pressure and fuel conversion efficiency derived from the isfc data. In these engine tests, the fuel-air mixture was prepared in two different ways: (1) with the normal carburetor and (2) with a heated vaporizing tank to ensure intake-mixture uniformity. Shapes of the practical efficiency curves and the theoretical curves in Fig. 5-9 differ. Cylinder-to-cylinder air/fuel ratio maldistribution prevents the carbureted engine operating leaner than $\phi \approx 0.85$ ($A/F \approx 17$) without misfire under these conditions. While use of a fuel vaporizing and mixing tank essentially removes this maldistribution and extends the lean misfire limit, $\eta_{f,i}$ does not continue to increase as ϕ decreases. The reasons for this are that cycle-to-cycle pressure fluctuations and the total dura-

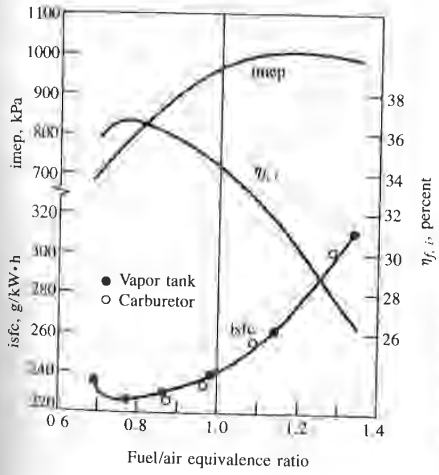

FIGURE 15-4
Effect of the fuel/air equivalence ratio variations on indicated mean effective pressure, specific fuel consumption, and fuel conversion efficiency of six-cylinder spark-ignition engine at wide-open throttle and 1200 rev/min. Data for standard carbureted engine, and engine equipped with vapor tank which extends the lean operating limit, are shown.[9]

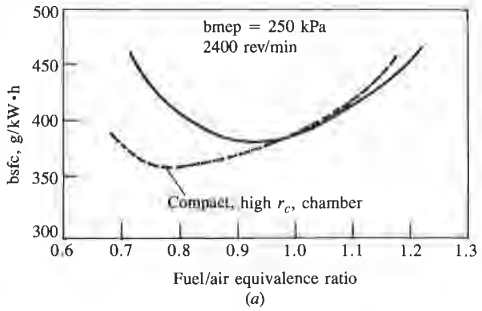

(*a*)

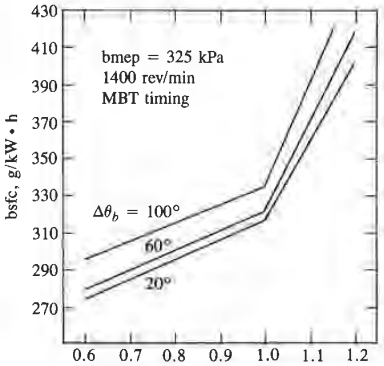

(*b*)

FIGURE 15-5
Effect of combustion chamber design and burn rate on spark-ignition engine brake specific fuel consumption. (*a*) 1.6-dm^3 four-cylinder engine with conventional combustion chamber and 1.5-dm^3 four-cylinder engine with compact fast-burning high-compression-ratio chamber beneath the exhaust valve with $r_c = 13$, both at bmep of 250 kPa and 2400 rev/min.[10] (*b*) Predictions from thermodynamic-based computer simulation of engine cycle for 5.7-dm^3 eight-cylinder engine at bmep of 325 kPa and 1400 rev/min with MBT spark timing.[6]

tion of the burning process increase as the mixture becomes leaner: both these factors degrade engine efficiency. Since the spark advance is set for the average cycle, increasing cycle-to-cycle dispersion produces increasing imep (and hence $\eta_{f,i}$) losses in "nonaverage" cycles due to nonoptimum timing. The lengthening burn duration directly decreases efficiency, even in the absence of cyclic variations.

Engine fuel consumption and efficiency well lean of stoichiometric depend strongly on the engine combustion chamber design. Figure 15-5 shows two sets of engine bsfc data, for a conventional combustion chamber and a compact high-compression-ratio chamber, at constant load and speed (250 kPa bmep and 2400 rev/min) as a function of equivalence ratio. Also shown are bsfc results obtained from a thermodynamic-based computer cycle simulation of the spark-ignition engine operating cycle (at 325 kPa bmep and 1400 rev/min).[6] Though the load and speed are different, the behavior of the data and predictions for rich mixtures, $\phi > 1$, are comparable. On the lean side of stoichiometric, however, fuel consumption depends on the combustion characteristics of the chamber. The faster-burning compact high-compression-ratio chamber shows decreasing bsfc

until the lengthening burn duration and larger cycle-by-cycle variations cause bsfc to increase. For the slower-burning conventional chamber, this deterioration in combustion starts to occur almost immediately on the lean side of stoichiometric, and fuel consumption worsens for $\phi \leq 0.9$.

Thus the equivalence ratio for optimum fuel consumption at a given load depends on the details of chamber design (including compression ratio) and mixture preparation quality. It also varies for a given chamber over the part-throttle load and speed range. For lighter loads and lower speeds it is closer to stoichiometric since the residual gas fraction is higher and combustion quality is poorer with greater dilution and at lower speeds.

At part load, as the air/fuel ratio is varied at constant brake load, the pumping work varies, and this also contributes to the brake specific fuel consumption and efficiency variation with equivalence ratio. Figure 15-6 shows the gross and net indicated fuel conversion efficiencies and brake efficiency as a function of equivalence ratio at a part-throttle constant load and speed point (325 kPa bmep and 1400 rev/min), calculated using a thermodynamic-based computer simulation of the engine's operating cycle. The difference between the net and gross indicated curves illustrates the magnitude of the effect of the pumping work changes. Part-throttle comparisons of different operating conditions should be done at constant brake load (torque or bmep) and speed; the task the engine is required to perform is then the same. At constant bmep and speed, the mechanical rubbing friction is essentially fixed; thus *net* imep is constant (and *gross* imep will vary if the pumping mep varies).

Note that all the engine data show a smooth transition between the rich and lean characteristics at the stoichiometric point, whereas the calculated sfc and

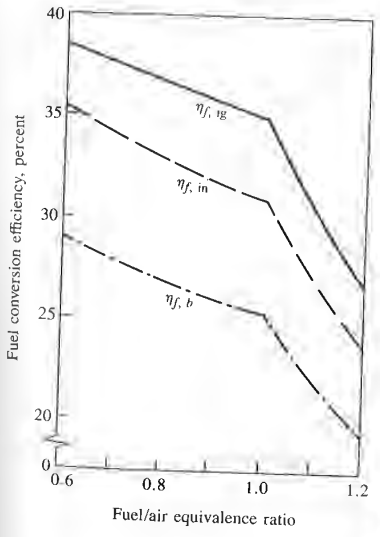

FIGURE 15-6
Gross and net indicated, and brake, fuel conversion efficiencies predicted by thermodynamic-based cycle simulation at constant part-load bmep (325 kPa) and speed (1400 rev/min) for a fixed burn duration (0–100 percent, 60° CA).[6]

JRE 15-5
of combustion chamber design burn rate on spark-ignition engine specific fuel consumption. (*a*) n^3 four-cylinder engine with conal combustion chamber and n^3 four-cylinder engine with act fast-burning high-compression-chamber beneath the exhaust valve $r_c = 13$, both at bmep of 250 kPa 400 rev/min.[10] (*b*) Predictions from iodynamic-based computer simula- of engine cycle for 5.7-dm³ eight- ler engine at bmep of 325 kPa and rev/min with MBT spark timing.[6]

becomes leaner: both these lvance is set for the average increasing imep (and hence ium timing. The lengthening the absence of cyclic varia-

an of stoichiometric depend Figure 15-5 shows two sets hamber and a compact high- speed (250 kPa bmep and Also shown are bsfc results cle simulation of the spark- and 1400 rev/min).[6] Though data and predictions for rich stoichiometric, however, fuel ristics of the chamber. The mber shows decreasing bsfc

efficiency characteristics show a discontinuity in slope. The difference is due to cylinder-to-cylinder and cycle-by-cycle mixture composition variations[7] and to cycle-by-cycle cylinder pressure variations which exist (though to a lesser extent) even in the absence of these mixture variations. Averaging over these variations smooths out the theoretical discontinuity in slope at $\phi = 1.0$.

The equivalence ratio requirements of a spark-ignition engine over the full load and speed range can now be explained from the point of view of performance and efficiency. However, since emissions depend on ϕ also, emission control requirements may dictate a different engine calibration, as will be discussed later. The mixture requirements in the induction system are usually discussed in relation to *steady* and *transient* engine operation. Steady operation includes operation at a given speed and load over several engine cycles with a warmed-up engine. Transient operation includes engine starting, engine warm-up to steady-state temperatures, and changing rapidly from one engine load and speed to another. The mixture requirements of the engine as defined by the composition of the combustible mixture at the time of ignition, while they vary somewhat with speed and load, are essentially the same for all these operating modes.† However, the methods used to prepare the mixture prior to entry to the cylinder must be modified in the transient modes when liquid fuels are used, to allow for variations in the liquid fuel flow and fuel evaporation rate in the intake manifold as the air flow varies and as the manifold and inlet port pressure and temperature change. The transient fuel metering requirements for adequate mixture preparation are discussed in Chap. 7.

At all load points at a given speed, the ideal equivalence ratio is that which gives minimum brake specific fuel consumption at the required load. However, once wide-open-throttle air flow has been reached, increases in power can only be obtained by increasing the fuel flow rate. The equivalence ratio requirements for optimum-efficiency steady-state engine operation can be summarized on a plot of equivalence ratio versus percent of maximum air flow at any given speed. A typical plot was shown in Fig. 7-1. For part-throttle operation, unless dictated otherwise by emission control requirements, the equivalence ratio is set close to the equivalence ratio for minimum fuel consumption consistent with avoiding partial burning or misfire in one or more cylinders. At very light load the best bsfc mixture is richer to compensate for slower flame speeds at lower mixture density and increased residual fraction. As wide-open throttle is approached, the mixture is richened to obtain maximum power.

The exhaust gas temperature varies with the equivalence ratio. The exhaust gas temperature also varies continuously as the gas leaves the engine cylinder and flows through the exhaust port and the manifold and pipe (see Sec. 6.5), so an appropriate definition of an average exhaust gas temperature should be used

† Except during start-up and cold engine operation, when a substantial part of the fuel within the cylinder can be in the liquid phase.

in quantifying this variation. However, time-averaged thermocouple measurements from specific locations in the exhaust system can provide useful information on trends. Figure 14-10 shows examples of predictions of the enthalpy-averaged exhaust gas temperature at the exhaust port exit as a function of equivalence ratio compared with time-averaged measurements. The enthalpy-averaged temperature is defined by Eq. (6.19). These are typically 50 to 100 K higher than time-averaged measurements. The exhaust temperature peaks at the stoichiometric point and decreases as the mixture is richened and leaned on either side.

The fuel/air equivalence ratio is an important parameter controlling spark-ignition engine emissions. The critical factors affecting emissions, that are governed by the equivalence ratio, are the oxygen concentration and the temperature of the burned gases. Excess oxygen is available in the burned gases lean of stoichiometric. The maximum burned gas temperatures occur slightly rich of stoichiometric at the start of the expansion stroke, and at the stoichiometric composition at the end of expansion and during the exhaust process. Figure 11-2 illustrates the general trends in emissions with equivalence ratio which have already been discussed.

Figure 15-7 shows the effect of variations in fuel/air equivalence ratio on NO_x and HC emissions and fuel consumption when a special fuel vapor generator was used to produce a uniform fuel-air mixture. As explained in Sec. 11.2.3, the formation rate of NO depends on the gas temperature and oxygen concentration. While maximum burned gas temperatures occur at $\phi \approx 1.1$, at this equiva-

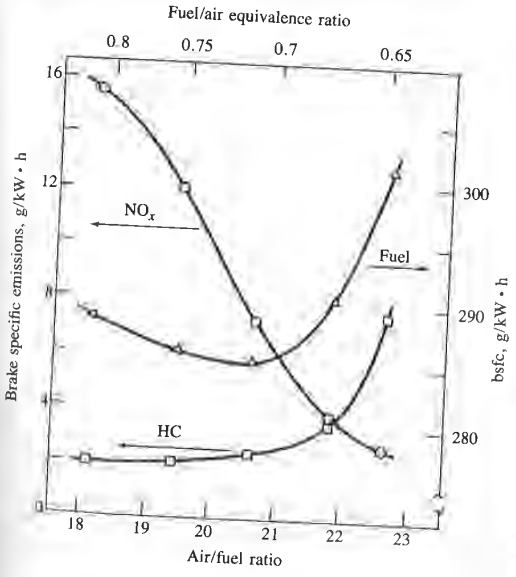

FIGURE 15-7
Variation of brake specific HC and NO_x emissions and fuel consumption with (A/F) and fuel/air equivalence ratio, 5.7-dm³ eight-cylinder spark-ignition engine at 385 kPa bmep and 1400 rev/min with uniform vaporized fuel-air mixture.[11]

lence ratio oxygen concentrations are low. As the mixture is leaned out, increasing oxygen concentration initially offsets the falling gas temperatures and NO emissions peak at $\phi \approx 0.9$. Then, decreasing temperatures dominate and NO emissions decrease to low levels.

Figure 15-7 also shows the effect of variations in equivalence ratio for lean mixtures on unburned hydrocarbon emissions. For rich mixtures, Fig. 11-2 shows that emissions are high. This is primarily due to the lack of oxygen for afterburning of any unburned hydrocarbons that escape the primary combustion process, within the cylinder and the exhaust system. HC emissions decrease as the stoichiometric point is approached: increasing oxygen concentration and increasing expansion and exhaust stroke temperatures result in increasing HC burnup. For moderately lean mixtures, HC emission levels vary little with equivalence ratio. Decreasing fuel concentration and increasing oxygen concentration essentially offset the effect of decreasing bulk gas temperatures. As the lean operating limit of the engine is approached, combustion quality deteriorates significantly and HC emissions start to rise again due to the occurrence of occasional partial-burning cycles. For still leaner mixtures, HC emissions rise more rapidly due to the increasing frequency of partial-burning cycles, and even the occurrence of completely misfiring cycles (see Sec. 9.4.3). The equivalence ratio at which partial-burning and misfiring cycles just start to appear depends on details of the engine combustion and fuel preparation systems, as well as the load and speed point.

The effect of equivalence ratio variations on CO emissions has already been explained in Sec. 11.3 (see Fig. 11-20). For rich mixtures, CO levels are high because complete oxidation of the fuel carbon to CO_2 is not possible due to insufficient oxygen. For lean mixtures, CO levels are approximately constant at a low level of about 0.5 percent or less.

Figure 15-7 indicates that if an engine can be designed and operated so that its stable operating limit under the appropriate part-load conditions is sufficiently lean, excellent fuel consumption and substantial control of engine NO, HC, and CO emissions can be achieved. Such an approach requires good control of mixture preparation and a fast-burning combustion chamber design (see Sec. 15.4.1). However, this lean-engine approach is not compatible with the three-way catalyst system (see Sec. 11.6.2) which, with close-to-stoichiometric mixtures, achieves substantial additional reductions in NO, HC, and CO emissions.

EXHAUST GAS RECYCLE. Exhaust gas recycle (EGR) is the principal technique used for control of SI engine NO_x emissions (see Sec. 11.2.3). A fraction of the exhaust gases are recycled through a control valve from the exhaust to the engine intake system. The recycled exhaust gas is usually mixed with the fresh fuel-air mixture just below the throttle valve. EGR acts, at part load, as an additional diluent in the unburned gas mixture, thereby reducing the peak burned gas temperatures and NO formation rates. Note that it is the total burned gas fraction in the unburned mixture in the cylinder that acts as a diluent. These burned gases are comprised of both residual gas from the previous cycle and exhaust gas

recycled to the intake. As described in Sec. 6.4, the residual gas fraction is influenced by load and valve timing (especially the extent of valve overlap) and, to a lesser degree, by the air/fuel ratio and compression ratio. The total burned gas mass fraction is given by Eq. (4.3). Since the burned gases dilute the unburned mixture, the absolute temperature reached after combustion varies inversely with the burned gas mass fraction. Hence increasing the burned gas fraction reduces the rate of formation of NO emissions.

Figure 11-10 shows the effect on NO emissions of increasing the burned gas fraction by recycling exhaust gases to the intake system. Substantial reductions in NO concentrations are achieved with 10 to 25 percent EGR. However, EGR also reduces the combustion rate which makes stable combustion more difficult to achieve (see Sec. 9.4.3 and Fig. 9-36). The amount of EGR a particular combustion chamber design will tolerate depends on its combustion characteristics, the speed and load, and the equivalence ratio. EGR percentages in the 15 to 30 range are about the maximum amount of EGR a spark-ignition engine will tolerate under normal part-throttle conditions. Faster-burning engines will tolerate more EGR than slower-burning engines. Because of the decrease in burn rate and increase in cycle-by-cycle combustion variations, hydrocarbon emissions increase with increasing EGR, as shown in Fig. 11-29. At first the increase in HC is modest and is due primarily to decreased HC burnup due to lower expansion and exhaust stroke temperatures. The HC increase becomes more rapid as slow combustion, partial burning, and even misfire, in turn, occur with increasing frequency. EGR has no significant effect on engine CO emissions.

The effect of exhaust gas recycle on engine performance and efficiency, for mixtures with $\phi \leq 1.0$, is similar to the addition of excess air. Both EGR and excess air dilute the unburned mixture. In practice since EGR is only used at part-throttle conditions, $\phi \leq 1.0$ is the region of interest. Because three-way catalysts are now used where NO_x emission constraints are severe, greatest attention has focused on dilution with EGR at $\phi \approx 1.0$. Figure 15-8 shows the effect of increasing EGR on bsfc and enthalpy-mean exhaust temperature [defined by Eq. (6.19)] at constant bmep, predicted using a thermodynamic-based computer simulation of the engine's operating cycle. Predictions made for different burn durations are shown, at MBT timing for a stoichiometric mixture. At constant burn duration, bsfc and exhaust temperature decrease with increasing EGR. Only for very long combustion processes is the burn rate especially significant. This improvement in fuel consumption with increasing EGR is due to three factors: (1) reduced pumping work as EGR is increased at constant brake load (fuel and air flows remain almost constant; hence intake pressure increases); (2) reduced heat loss to the walls because the burned gas temperature is decreased significantly; and (3) a reduction in the degree of dissociation in the high-temperature burned gases which allows more of the fuel's chemical energy to be converted to sensible energy near TC. The first two of these are comparable in magnitude and each is about twice as important as the third.[12]

Figure 15-9 shows experimental bsfc versus EGR data for two combustion chambers: a combustion chamber with a moderate burning rate and a faster-

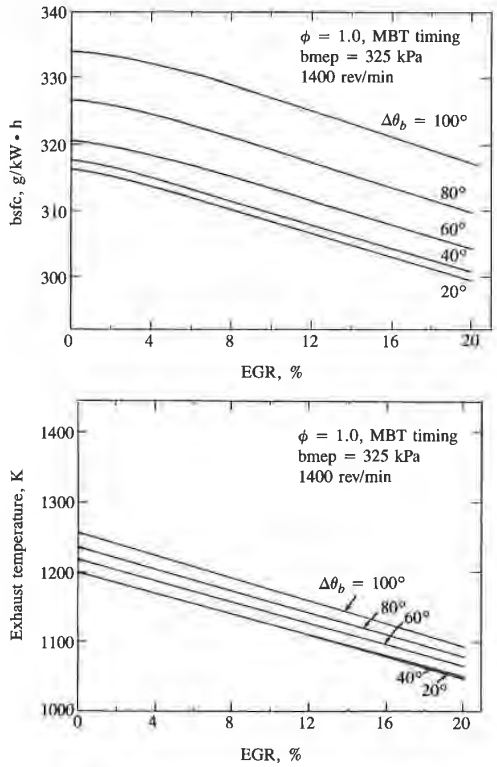

FIGURE 15-8
Effect of recycled exhaust on brake specific fuel consumption and exhaust temperature at constant bmep and speed, stoichiometric mixture, and various burn durations (0–100 percent). Predictions from thermodynamic-based cycle simulation.[6]

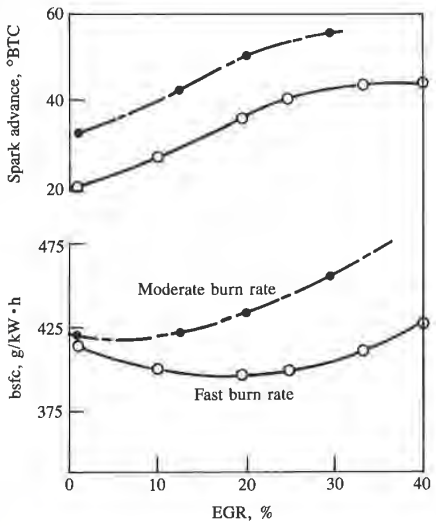

FIGURE 15-9
Brake specific fuel consumption and MBT spark advance as a function of percent recycled exhaust, for four-cylinder spark-ignition engine with a moderate burn rate combustion chamber and a fast burn rate combustion chamber. 1400 rev/min, 324 kPa bmep, equivalence ratio 1.0.[12]

burning chamber with open geometry and with induction-generated swirl. Though addition of EGR lengthens both the flame development and propagation processes (as indicated by the increasing MBT spark advance requirement with increasing EGR), the faster-burning chamber follows the anticipated pattern of significant bsfc reductions until, at about 20 percent EGR, the combustion quality deteriorates. For the slower-burning combustion chamber, the tolerance to dilution with EGR is much less.

15.3.3 Load and Speed

One common way to present the operating characteristics of an internal combustion engine over its full load and speed range is to plot brake specific fuel consumption contours on a graph of brake mean effective pressure versus engine speed. Operation of the engine coupled to a dynamometer on a test stand, over its load and speed range, generates the torque and fuel flow-rate data from which such a *performance map* is derived. Equation (2.20) relates bmep to torque, and bsfc values are obtained from Eq. (2.22) at each operating point. Figure 15-10 shows an example of such a performance map for a four-cylinder spark-ignition engine. The upper envelope of the map is the wide-open-throttle performance curve. Points below this curve define the part-load operating characteristics. While details differ from one engine to another, the overall shapes of these maps for spark-ignition engines are remarkably similar. When mean piston speed S_p is used instead of crankshaft speed for the abscissa, the quantitative similarity of such maps over a wide range of engine sizes is more apparent.

Maximum bmep occurs in the mid-speed range; the minimum bsfc island is located at a slightly lower speed and at part load. These map characteristics can be understood in terms of variations in volumetric efficiency η_v, gross indicated fuel conversion efficiency η_{f,i_g} and mechanical efficiency η_m as A/F, EGR (if used), and the importance of heat losses and friction change, via Eqs. (15.3) and (15.5).

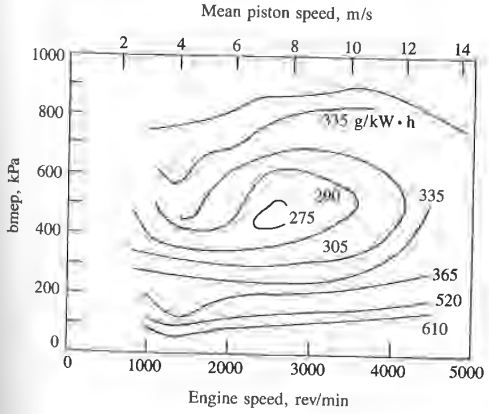

FIGURE 15-10
Performance map for 2-dm³ four-cylinder fast-burn spark-ignition engine showing contours of constant bsfc in grams per kilowatt-hour.[13]

GURE 15-8
ect of recycled exhaust on brake ecific fuel consumption and exhaust mperature at constant bmep and ed, stoichiometric mixture, and ious burn durations (0–100 cent). Predictions from thermo-namic-based cycle simulation.[6]

15-9
ecific fuel consumption and MBT vance as a function of percent recy-ust, for four-cylinder spark-ignition with a moderate burn rate com-chamber and a fast burn rate com-chamber. 1400 rev/min, 324 kPa uivalence ratio 1.0.[12]

The maximum bmep curve reflects the variation with speed of η_v, the decrease of η_m as $\bar{S}_p$ increases, and the increase of $\eta_{f,\text{ig}}$ as $\bar{S}_p$ increases due to decreasing importance of heat transfer per cycle. The bsfc contours have the following explanation. Starting at the minimum bsfc point, increasing speed at constant load increases bsfc due primarily to the increasing friction mep at higher speeds (which decreases η_m). While $\eta_{f,\text{ig}}$ increases as speed increases, friction increases dominate. Decreasing speed at constant load increases bsfc due primarily to the increasing importance of heat transfer per cycle (which decreases $\eta_{f,\text{ig}}$). Friction decreases, increasing η_m, but this is secondary. Any mixture enrichment required to maintain a sufficiently repeatable combustion process at low engine speeds (see Fig. 7-1) contributes too. Increasing load at constant speed from the minimum bsfc point increases bsfc due to the mixture enrichment required to increase torque as the engine becomes increasingly air-flow limited. Decreasing load at constant speed increases bsfc due to the increased magnitude of friction (due to increased pumping work), the increased relative importance of friction, and increasing importance of heat transfer (which decreases $\eta_{f,\text{ig}}$).

The effects of speed and load variations on NO and HC emissions are shown in Fig. 15-11.[14] NO concentrations increase moderately with increasing speed at constant load. At lower loads, the proportional increase in NO is greater

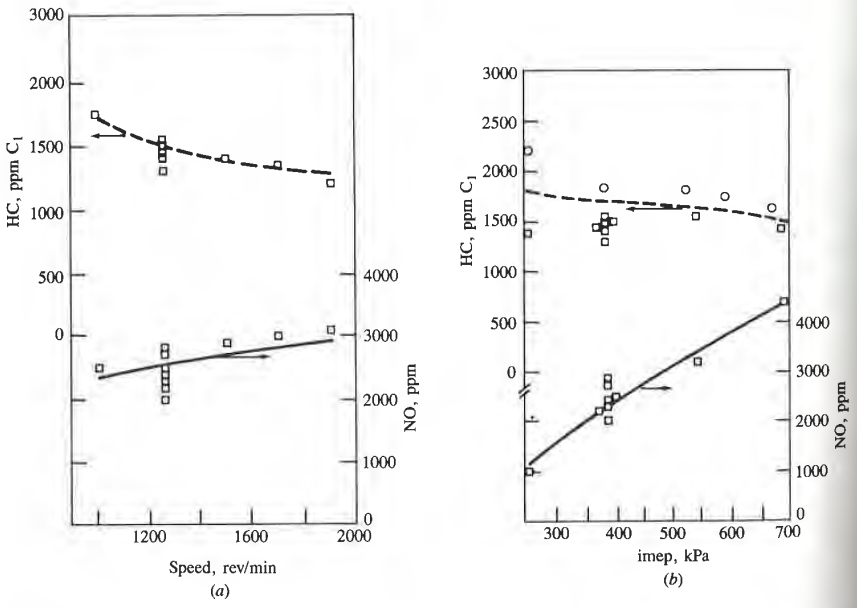

FIGURE 15-11
Variation in spark-ignition engine HC and NO_x emissions with (*a*) engine speed at 379 kPa imep and (*b*) load (or imep) at 1250 rev/min. Equivalence ratio = 0.9, MBT spark timing, $r_c = 7$.[14]

ith speed of η_v, the decrease of
$\bar{S}_p$ increases due to decreasing
itours have the following expla-
easing speed at constant load
on mep at higher speeds (which
ses, friction increases dominate.
due primarily to the increasing
reases $\eta_{f,ig}$). Friction decreases,
enrichment required to main-
at low engine speeds (see Fig.
speed from the minimum bsfc
t required to increase torque as
l. Decreasing load at constant
ide of friction (due to increased
ace of friction, and increasing

on NO and HC emissions are
ase moderately with increasing
tional increase in NO is greater

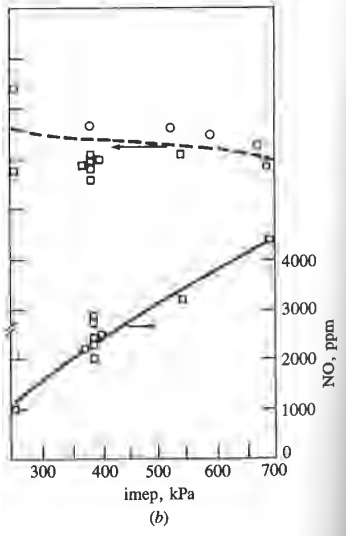

th (*a*) engine speed at 379 kPa imep and
BT spark timing, $r_c = 7$.[14]

than at higher loads.[6] The residual gas fraction decreases as speed increases, this effect being greater at lower inlet manifold pressures (lighter loads) (see Fig. 6-19). Also, the relative importance of heat transfer per cycle is less as speed increases (see Fig. 12-25), which would also be expected to increase NO concentration. With increasing load (at constant speed), NO concentrations also increase. Again, as inlet manifold pressure and load increase, the residual gas fraction decreases (Fig. 6-19); also, the relative importance of heat transfer per cycle decreases with increasing load (Fig. 12-25).

The hydrocarbon concentration trends with speed and load changes are the opposite of the NO concentration trends. As indicated in Table 11.7, speed and load are likely to affect several of the HC formation mechanisms, the in-cylinder mixing of unburned hydrocarbons which escape combustion with the bulk gases, and the fraction of the in-cylinder HC which escape into the exhaust. However, not enough is yet known about the details of these processes to make these dependencies explicit. If oxygen is available, oxidation of unburned hydrocarbons both within the cylinder and in the exhaust system will be significantly enhanced by increases in speed since the expansion stroke and exhaust process gas temperatures increase substantially, due to the reduced significance of heat transfer per cycle with increasing speed. This more than offsets the reduced residence time in the cylinder and in the exhaust. Measurements of the percent HC reacted in the exhaust port as a function of engine speed show the same proportional reduction in the exhaust emissions data in Fig. 15-11.[15] The rationale for the variation with load is less clear. As load increases at constant speed, expansion and exhaust stroke temperatures increase, and the in-cylinder oxidation rate, if oxygen is available, will increase. However, as the exhaust gas flow rate increases, the residence time in critical sections of the exhaust system decreases and a reduction in exhaust port HC oxidation occurs.[16] The net trend is for HC concentration to decrease modestly as load is increased.

15.3.4 Compression Ratio

The ideal cycle analysis of Chap. 5 showed that indicated fuel conversion efficiency increased continuously with compression ratio according to Eq. (5.31). With $\gamma = 1.3$, this relation also matches closely the fuel-air cycle predictions with $\phi \approx 1.0$. However, in an actual engine other processes which influence engine performance and efficiency vary with changes in compression ratio: namely, combustion rate and stability, heat transfer, and friction. Over the load and speed range, the relative impact that these processes have on power and efficiency varies also. Hence, the applicability of Eq. (5.31) is open to question. Also, while the geometric compression ratio (ratio of maximum to minimum cylinder volume) is well defined, the actual compression and expansion processes in engines depend on valve timing details and the importance of flow through the valves while they are opening or closing (which depends on engine speed). Of course, our ability to increase the compression ratio is limited by the octane quality of available fuels and knock (see Sec. 9.6.1).

Only a few studies have examined the effect of compression ratio on spark-ignition engine performance and efficiency over a wide range of compression ratios. Figure 15-12 shows results obtained at wide-open throttle at 2000 rev/min with a series of eight-cylinder 5.3-dm^3 displacement engines, from the most extensive of these studies.[17] Gross-indicated and brake fuel conversion efficiencies and mean effective pressures are shown. Indicated mep was obtained by adding motoring friction mep to brake mep. The mep data were obtained with (A/F) and spark timing adjusted to give maximum torque; for the efficiency data, (A/F) and spark timing were adjusted to give maximum efficiency. The mechanical efficiency remained essentially constant at 0.89 over the full compression ratio range. The volumetric efficiency was also constant at 0.825. Both $\eta_{f,\text{ig}}$ and mep show a maximum at a compression ratio of about 17; for higher compression ratios efficiency and mep decrease slightly. This trend was explained as being due to increasing surface/volume ratio and slower combustion, and is also due to the increasing importance of crevice volumes: at the higher compression ratios studied the combustion chamber height became very small.

To assess more broadly the effect of compression ratio variations on fuel conversion efficiency, several data sets have been normalized and compared in Fig. 15-13 which shows the ratio of fuel conversion efficiency at the given compression ratio divided by the efficiency at $r_c = 8$, for wide-open-throttle engine operation. The agreement for $r_c \leq 14$ is good. Over the compression ratio range that is accessible to SI engines with available fuels ($r_c \leq 12$), fuel conversion efficiency increases by about 3 percent per unit of compression ratio increase. Note, of course, that engine power increases by about the same amount.

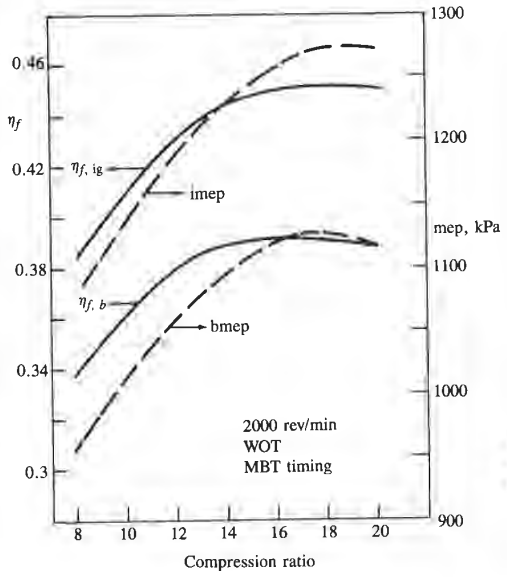

FIGURE 15-12
Effect of compression ratio on indicated mean effective pressure and fuel conversion efficiency. 5.3-dm^3 eight-cylinder spark-ignition engine at 2000 rev/min and wide-open throttle. Equivalence ratio and spark timing adjusted for maximum torque for mep data; adjusted for minimum fuel consumption for efficiency data.[17]

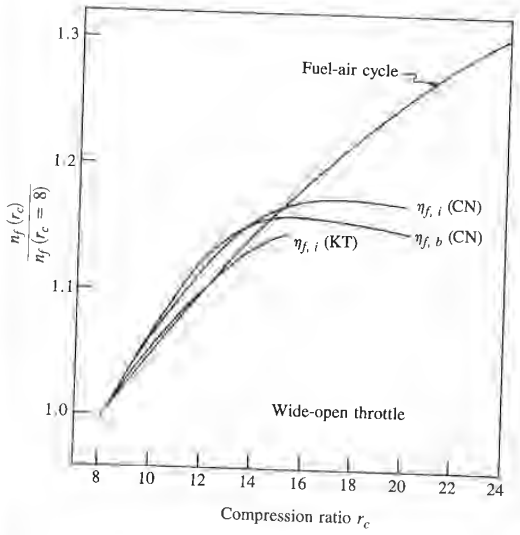

FIGURE 15-13
Relative fuel conversion efficiency improvement with increasing compression ratio, spark-ignition engines at wide-open throttle: CN,[17] KT.[18]

A similar comparison of the effect of compression ratio increases on efficiency at part load is shown in Fig. 15-14.[19] The figure shows brake fuel conversion efficiency data from engines of different cylinder volume. Both the compression ratio for maximum efficiency and the maximum efficiency depend on cylinder size. The wide-open-throttle and road-load data (top two curves[17]) confirm that the increase in efficiency with an increase in the compression ratio at part load apparently depends on the details of engine operation to a significant degree also. For the important compression ratio range of 9 to 11, the relative

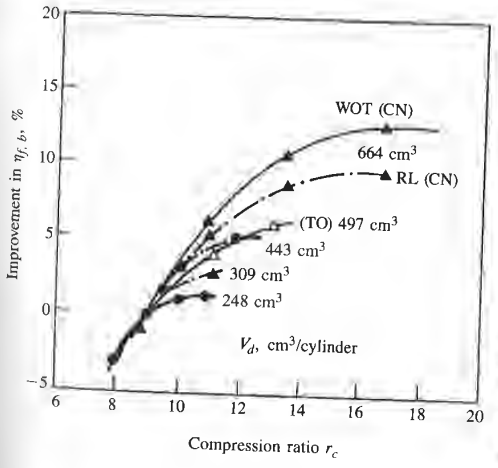

FIGURE 15-14
Relative brake fuel conversion efficiency improvement with increasing compression ratio of spark-ignition engines of different displaced volume per cylinder at part throttle (except top curve at WOT).[19] RL road load. CN,[17] TO.[10]

ompression ratio on spark-
wide range of compression
pen throttle at 2000 rev/min
ngines, from the most exten-
l conversion efficiencies and
was obtained by adding
ere obtained with (A/F) and
ne efficiency data, (A/F) and
y. The mechanical efficiency
mpression ratio range. The
oth $\eta_{f,ig}$ and mep show a
higher compression ratios
explained as being due to
ion, and is also due to the
higher compression ratios
small.
ion ratio variations on fuel
ormalized and compared in
efficiency at the given com-
r wide-open-throttle engine
the compression ratio range
$_c \leq 12$), fuel conversion effi-
ression ratio increase. Note,
me amount.

URE 15-12
ct of compression ratio on indi-
d mean effective pressure and fuel
version efficiency. 5.3-dm³ eight-
nder spark-ignition engine at 2000
/min and wide-open throttle.
uivalence ratio and spark timing
usted for maximum torque for mep
a; adjusted for minimum fuel con-
mption for efficiency data.[17]

efficiency improvement is between 1 and 3 percent per unit of compression ratio increase, depending on cylinder size and operating conditions.

The exhaust temperature decreases as compression ratio and efficiency increase until the compression ratio corresponding to maximum efficiency is reached. It has also been shown that heat losses to the combustion chamber walls, as a fraction of the fuel's chemical energy, also decrease as the compression ratio and efficiency both increase.[17]

The effect of compression ratio changes on NO emissions is small. Some studies show a modest increase in specific NO emissions as the compression ratio increases at constant load and speed; other studies show a slight decrease. Increasing the compression ratio increases exhaust hydrocarbon emissions. Several trends could contribute: increased importance of crevice volumes at high r_c; lower gas temperatures during the latter part of the expansion stroke, thus producing less HC oxidation in the cylinder; decreasing residual gas fraction, thus increasing the fraction of in-cylinder HC exhausted; lower exhaust temperatures, hence less oxidation in the exhaust system.

15.4 SI ENGINE COMBUSTION CHAMBER DESIGN

15.4.1 Design Objectives and Options

There has always been extensive debate over the optimum SI engine combustion chamber design. There are a large number of options for cylinder head and piston crown shape, spark plug location, size and number of valves, and intake port design.[20] Debate revolves around issues such as chamber compactness, surface/volume ratio, flame travel length, and use of swirl and squish types of mixture motion. Figure 15-15 shows examples of several common types of combustion chamber shapes. Over the past few years a consensus has developed which favors faster-burning combustion-chamber designs. A chamber design where the fuel burning process takes place faster, i.e., occupies a shorter crank angle interval at a given engine speed, produces a more robust and repeatable combustion pattern that provides emission control and efficiency gains simultaneously. A faster-burning chamber with its shorter burn time permits operation with substantially higher amounts of EGR, or with very lean mixtures, within the normal constraints of engine smoothness and response. Thus greater emissions control within the engine can be achieved, and at part load at this higher level of dilution a faster-burning chamber shows an improvement in fuel consumption due to the reduced pumping work, reduced heat transfer (due to lower burned gas temperatures), and reduced amount of dissociation in the burned gases.[22]

The major combustion chamber design objectives which relate to engine performance and emissions are: (1) a fast combustion process, with low cycle-by-cycle variability, over the full engine operating range; (2) a high volumetric efficiency at wide-open throttle, (3) minimum heat loss to the combustion chamber walls; (4) a low fuel octane requirement.

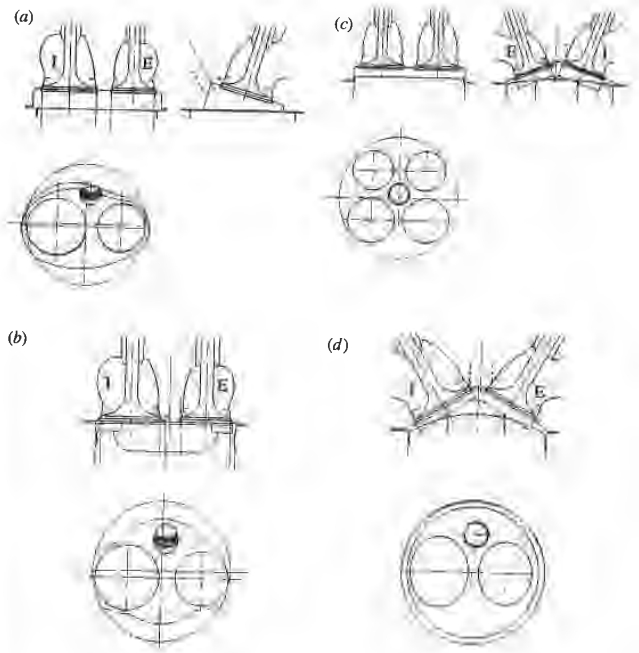

FIGURE 15-15
Examples of common spark-ignition engine combustion chamber shapes: (*a*) bathtub and wedge: (*b*) bowl-in-piston; (*c*) four-valve pent roof; (*d*) hemispherical.[21]

Many methods for producing a "fast burn" have been proposed. These include ways of making the combustion chamber shape more compact, moving the spark plug to a more central location within the chamber, using two plugs, and increasing in-cylinder gas motion by creating swirl during the induction process or during the latter stages of compression.

A faster combustion process relative to more moderate burn rate engines does result in a direct engine efficiency gain, other factors being equal. The magnitude of this direct gain is relatively modest. Experimental studies of the effect of an increase in burn rate from moderate to fast at constant engine load, speed, and mixture composition show that this effect is a few percent at most.[23] Computer simulations of the engine operating cycle confirm these experimental observations: while a decrease in total burn duration from 100 to 60° (slow to moderate burn) does result in a 4 percent decrease in bsfc, a decrease in burn duration from 60 to 20° gives only a further 1.5 percent bsfc decrease.[6]

Of greater importance is the fact that the faster burn process is more robust and results in the engine being able to operate satisfactorily with much more EGR, or much leaner, without a large deterioration in combustion quality. Faster

burning chamber designs exhibit much less cycle-by-cycle variability. This ability to operate with greater dilution at part load while maintaining a short burn duration and low cycle-by-cycle variability, permits much greater control of NO_x within the engine with 20 or more percent EGR without any substantial increase in HC emissions (see Fig. 11-29), or permits very lean operation. In both cases the efficiency gain relative to moderate burn rate engines, *which must operate with less dilution*, is sizeable.[24]

High volumetric efficiency is required to obtain the highest possible power density. The shape of the cylinder head affects the size of valves that can be incorporated into the design. Effective valve open area, which depends on valve diameter and lift, directly affects volumetric efficiency. Swirl is used in many modern chamber designs to speed up the burning process and achieve greater combustion stability. Induction-generated swirl appears to be a particularly stable in-cylinder flow. Swirl results in higher turbulence inside the chamber during combustion, thus increasing the rate of flame development and propagation. Generating swirl during the intake process decreases volumetric efficiency.

Heat transfer to the combustion chamber walls has a significant impact on engine efficiency. It is affected by cylinder head and piston crown surface area, by the magnitude of in-cylinder gas velocities during combustion and expansion, by the gas temperatures and the wall temperatures. The heat-transfer implications of a combustion chamber should be included in the design process.

Knock effectively limits the maximum compression ratio that can be used in any combustion chamber; it therefore has a direct impact on efficiency. Knock is affected by all the factors discussed above. It is the hardest of all the constraints to incorporate into the design process because of its obvious complexity.

Knowledge of the fundamentals of spark-ignition engine combustion, in-cylinder gas motion, and heat transfer has developed to the point where a rational procedure for evaluating these factors for optimum combustion chamber development and design can be defined. The next two sections develop such a procedure.

15.4.2 Factors That Control Combustion

Our understanding of the structure of the spark-ignition engine flame as it develops and propagates across the combustion chamber (see Secs. 9.3 and 9.4) allows us to relate the physical and chemical factors that control this process to the relevant engine design and operating parameters. The following factors affect the flame development and propagation processes:

1. *Geometry.* Combustion chamber shape and spark plug location.
2. *Flow field characteristics.* Mean velocity, turbulence intensity, and characteristic turbulence length scale in the unburned mixture during combustion.
3. *Unburned mixture composition and state.* Fuel, equivalence ratio, burned gas fraction, mixture pressure and temperature.

Geometry primarily affects combustion through the flame front surface area. It has a lesser effect on combustion development through its influence on in-cylinder motion. Geometric calculations (see Sec. 14.4.2), based solely on the assumption that the front surface of the flame can be modeled as a portion of a sphere centered at the spark plug, provide data on flame front area and the volume behind the flame front surface (the enflamed volume), contained within the combustion chamber at the appropriate flame radii and piston positions.

Flame area varies significantly from one chamber shape to another for a given enflamed volume. In the example shown in Fig. 14-7, the bowl-in-piston chamber gives flame surface areas 30 to 45 percent larger than those for the disc chamber under equivalent conditions around top-center. Hemispherical and open or clamshell chambers showed gains of about 30 percent relative to the equivalent disc configuration. For a given chamber shape, flame area depends even more significantly on plug location. Figure 14-7 shows that shifting the plug from a side to a center location for the bowl-in-piston chamber increased the peak flame area by 150 percent. For hemispherical and open chambers, the increases for a similar shift in plug location were 75 and 90 percent, respectively.[25]

Maps of flame area as a function of radius at different crank angle locations indicate the following pattern. For chamber geometries with side ignition, as flame radius increases, the flame area first rises slowly, then remains approximately constant, and then decreases slowly to zero. In contrast, chambers with central ignition show, as flame radius increases, a rise in flame area to a peak during the major part of the flame travel followed by a rapid decrease as the flame encounters the chamber walls. Moving the plug location toward the center of the chamber produces a larger increase in flame front area than does making the chamber shape more compact (though this has a positive impact too).

The effect of chamber geometry on burn rate has been examined using thermodynamic-based engine cycle simulations with various types of combustion model (e.g., the type developed by Keck and coworkers, see Sec. 14.4.2). Figure 15-16 shows results from one such study.[25] The combustion characteristics of ten different chamber geometries were compared at fixed part-load engine operating conditions. The flame development and propagation phases were separated into 0 to 10 and 10 to 90 percent mass fraction burned times. These were then normalized by the equivalent burn times of the slowest burning chamber—the disc with side ignition. Chamber geometry has the greatest impact on the 10 to 90 percent burn time; its effect on 0 to 10 percent time is significant but substantially smaller. Total burn times can be reduced by between 20 to 30 percent by optimizing spark plug location—comparing worst to best location for each chamber shape. Comparing worst and best chamber shapes, total burn time with fixed plug location can be reduced by about 10 percent.

Increased turbulence in the unburned mixture at the time of combustion increases the burning rate. Turbulence is usually increased by generating swirl during the induction process (see Sec. 8.3.2 and below). Cycle simulation studies[25] indicate that both the duration of the early stage of the burning process and of the main stage decrease when the turbulent velocity at the start of com-

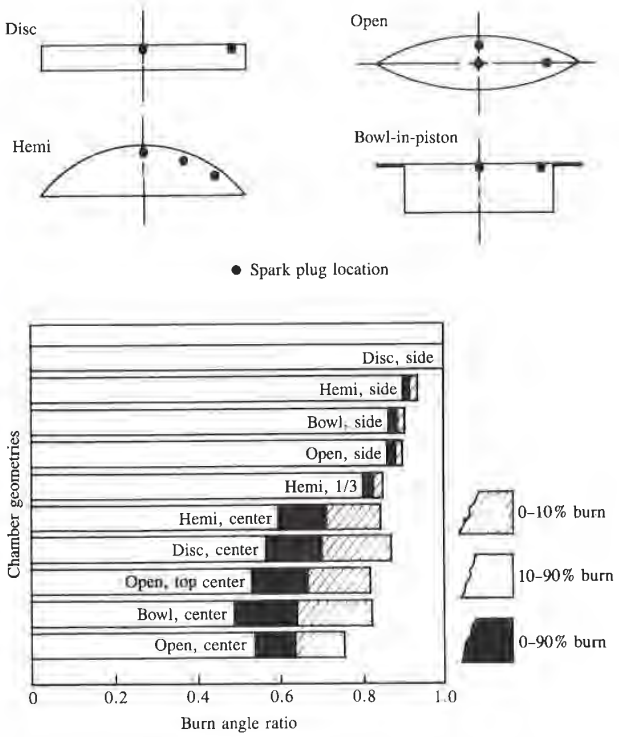

FIGURE 15-16
Comparison of burn angles (0–10 percent burned, 10–90 percent burned, 0–90 percent burned; see Fig. 9-13) for ten different spark-ignition engine combustion chamber geometries and spark plug locations. Burn angles are normalized by angles for slowest burning chamber: disc with side plug.[26]

bustion is increased. The faster combustion process comes primarily from the higher turbulence intensity; however, the decreased characteristic turbulence scale that accompanies the increased turbulence is also significant since it results in a shorter characteristic burning time [see Eq. (14.39) and the accompanying text]. It is important to note that the fuel conversion efficiency of higher-turbulence chambers at the same operating conditions can be lower than for normal chambers, despite the faster burn rates, due to the higher heat transfer that accompanies the higher in-cylinder velocities. For example, predictions based on the combustion model defined by Eqs. (14.33) to (14.35), where the characteristic mixture speed u_7 was increased by a factor of two, showed that the 0 to 10 percent and 10 to 90 percent burn durations decreased by about one-third. However, the indicated fuel conversion efficiency decreased by about 6 percent due to the predicted 15 percent increase in heat transfer.[25]

Mixture composition and state affect the burn rate through the dependence

of laminar flame speed on temperature, pressure, fuel/air equivalence ratio, and burned gas fraction (residual gas and EGR): see Sec. 9.3.3 and Eqs. (14.33) to (14.35). Table 15.1 compares the burn durations for a stoichiometric mixture, a lean mixture with $\phi = 0.8$, and a stoichiometric mixture with 20 percent EGR. The values of the laminar flame speed at the time of spark are also given (conditions at spark as well as composition are different in each case). The longer burn durations of the more dilute mixtures are clear. Note that EGR as a diluent has a much more deleterious effect on combustion than does air at these approximately equal levels of dilution.

All the above-described factors—flame geometry, fluid motion, and mixture composition—can vary cycle-by-cycle, and therefore contribute to combustion variability (see Sec. 9.4). Cyclic differences in gas motion in the vicinity of the spark plug result in differences in motion of the flame kernel during its early stages of development. Differences in turbulence result in differences in the rates at which the initially smooth surface of the flame kernel becomes wrinkled and convoluted by the flow. Different initial flame center motions change the geometrical interaction of the flame front with the combustion chamber walls later in the flame propagation process. Differences in the amount of fuel, air, and EGR which enter each cylinder cycle-by-cycle, the nonuniformity in composition of the entering charge, and any incomplete mixing of that entering charge with the residual gases in the cylinder also contribute to combustion variability. These composition nonuniformities lead to differences in the early stages of flame development. The variations in the amounts of fuel, air, and EGR that enter each cylinder cycle-by-cycle and in the uniformity of that mixture are factors within the direct control of the engine designer.

A fast combustion process reduces cyclic combustion variability for the following reasons. With a faster burn, optimum spark timing is closer to top-center: mixture temperature and pressure at the time of spark are higher, so the laminar flame speed at the start of combustion is greater. This, combined with the higher turbulence of most fast-burn concepts, results in faster flame kernel development.

TABLE 15.1
Effect of excess air and recycled exhaust on burn duration

ϕ	EGR, %	θ_s, degree	Burn durations, degree		S_L at θ_s, cm/s
			0–10%	10–90%	
1.0	0	340	22	17	75
0.8	0	336	26	21	52
1.0	20	324	31	28	23

400 cm³ per cylinder displaced volume, 80 mm bore, 8.5 compression ratio, disc chamber, center plug location 1500 rev/min, stoichiometric operation, θ_s = spark timing (MBT), inlet pressure 0.5 atm, inlet temperature 350 K, S_L = laminar flame speed.[26]

More rapid initial flame growth results in less variation in flame center motion during the critical flame-development phase. The resulting geometric variations in the flame front/chamber wall interaction are therefore reduced; this decreases the variations in burn rate that result from these geometric variations. Also, the faster burning process ends earlier in the expansion stroke. Thus the problem of occasional slow burning cycles, partial burning cycles, and eventually misfire, which occurs with dilute mixtures under normal burning conditions due to quenching of the combustion process as gas temperatures fall during expansion, is largely avoided (see Sec. 9.4.3).

15.4.3 Factors That Control Performance

VOLUMETRIC EFFICIENCY. Combustion chamber shape affects volumetric efficiency through its constraints on maximum valve size and through the degree of swirl (if any) that the chamber and port designs produce to achieve the desired combustion characteristics. To obtain maximum performance and to reduce pumping losses, the size of the valve heads should be as large as practical; the valve sizes that can be accommodated depend on cylinder head layout. Table 6.1 lists the typical maximum valve sizes that can be accommodated into several common chamber shapes (see Fig. 15-15). The approximate mean piston speed at maximum power is a measure of the maximum air flow that each engine design can pump. Note that of the two-valve configurations, the designs with inclined valve stems permit substantially greater maximum air flow. The four-valve pent-roof design, which also has inclined valve stems, is the best of those listed since it accommodates the largest valve and port areas (there are other four-valve head designs which are comparable).

Swirl can be generated during the intake process through suitable port, valve, and head design. It requires either that the flow through the intake valve be directed tangentially into the cylinder so that gas flows through one side of the valve opening preferentially (e.g., through the use of masks to restrict flow at the mask location or through the use of a tangentially directed port or a flow deflector in the port just upstream of the valve), or requires the use of a helical intake port that imparts an angular velocity to the flow before it enters the cylinder. In either case the inlet flow enters the cylinder with higher velocity than it would have in the absence of swirl; hence the pressure drop across the valve is increased, and maximum air flow through the cylinder is reduced. Well-designed helical swirl-generating ports (see Sec. 8.3.2) appear to be the best way to create swirl. However, geometric and production constraints often prevent the incorporation of such ports into the cylinder head design, and other swirl-generating methods must be used. The engine maximum-power penalty associated with generating significant swirl is of order 5 to 10 per cent.

Since swirl is only required at part-throttle operation when enhancement of the burn rate is most critical and is not usually required at full throttle when the flow restriction penalty is most significant, induction systems with a separate passage for the part-throttle air flow, where only this separate passage generates

swirl, are an attractive option. However, the gains in volumetric efficiency are offset by a higher cost due to the additional complexity in port and manifold of the double passage and the individual throttle valves required in each port for flow control.

Swirl can be *intensified* during compression with bowl-in-piston combustion chambers by decreasing the moment of inertia of the in-cylinder charge as the piston moves toward top-center, and thereby increasing its angular velocity (see Sec. 8.3.3). An advantage here is that the swirl level generated during induction is less than would be required without the compression-produced radially inward motion of the charge. This approach can be used with combustion chamber designs that are axisymmetric and compact. Swirl can also be *generated* by squish motion toward the end of compression with a suitable design of chamber. The advantage of this approach is that there is no induction-stroke swirl-generating volumetric efficiency penalty. However, the cylinder head geometries proposed to date for either intensifying or generating swirl have vertical valve stems, and hence have smaller valve sizes which in themselves restrict air flow. Also, the cylinder head geometry required to generate swirl during compression has a larger surface area than more open chamber designs and, therefore, has significantly higher heat losses.

The impact of conventional radially inward squish motion (see Sec. 8.4) on in-cylinder turbulence, and hence combustion, is unclear. Chambers with significant squish are also more compact; for this reason alone they would be faster burning.

HEAT TRANSFER. The convective engine heat transfer to the combustion chamber walls is described by equations of the form of (12.2): e.g., Eq. (12.21). The heat-transfer coefficient is usually correlated by expressions of the form of Eq. (12.3), which relate the Nusselt, Reynolds, and Prandtl numbers (see Sec. 12.4). Thus combustion chamber surface area, and especially the surface area in contact with the burned gases, is important. Gas velocity is also important; it influences the heat-transfer rate through the Reynolds number. Various characteristic velocities have been used in the Reynolds number to scale heat transfer: mean piston speed, mean in-cylinder gas velocity, turbulence intensity, either individually or in combination. Both of these variables, area and velocity, are affected by combustion chamber design.

Studies of engine performance using thermodynamic-based simulations of the engine's operating cycle (see Sec. 14.4) provide data that indicate the importance of changes in heat transfer. At part-throttle operating conditions, such simulation calculations show that a 10 percent change in combustion chamber heat losses results in a change of between 2 and 5 percent in brake specific fuel consumption; an average fuel consumption change of about one-third the magnitude of the heat-transfer change (and of opposite sign) is an appropriate rule of thumb.[35, 27] At wide-open throttle, the effect on mean effective pressure is comparable: a 10 percent change in heat transfer results in about a 3 percent change in bmep.

This impact of heat transfer on engine efficiency and performance underlines the importance of combustion chamber details that affect heat transfer. For the chamber shapes shown in Fig. 15-16, the total heat losses as a fraction of the fuel's energy, at fixed engine speed and intake conditions, were also calculated. Both chamber shape and spark plug details affect heat losses since together these govern the surface area of the hot burned gases in contact with the walls. The open and hemispherical chambers had least heat transfer. Geometries such as the bowl-in-piston, which obviously have a higher surface area, had about 10 percent higher heat transfer. The effect of shifting the plug from a side to center location depended on chamber shape. Open and bowl-in-piston chambers showed little change; the hemispherical chamber showed a 4 percent reduction. Given a general chamber shape choice, the details of the actual design are important also; it is easy to add substantial surface area with piston cutouts, plug bosses, and cylinder head masking or squish regions which will deteriorate chamber performance to a measurable degree.

Higher in-cylinder velocities affect heat-transfer rates through the Reynolds number term in the heat-transfer coefficient correlation. Swirl- and squish-generated flows increase in-cylinder gas velocities and will, therefore, increase heat-transfer rates.

15.4.4 Chamber Octane Requirement

Knock limits an engine's compression ratio, and hence its performance and efficiency. The more fundamental aspects of knock were reviewed in Sec. 9.6. Knock occurs when the end-gas autoignites prior to its being burned up by the normal flame-propagation process. The tendency to knock depends on engine design and operating variables which influence end-gas temperature, pressure, and time spent at high values of these two properties before flame arrival.

The presence or absence of knock in an engine depends primarily on the antiknock quality of the fuel, which is defined by the fuel's *octane number* (see Sec. 9.6.3). It determines whether or not a fuel will knock in a given engine under given operating conditions: the higher the octane number, the higher the resistance to knock. The *octane number requirement* of an engine is defined as the minimum fuel octane number that will resist knock throughout its speed and load range. The following factors affect an engine's octane requirement: (1) composition of the fuel; (2) chamber geometry and size; (3) charge motion; (4) spark-advance curve; (5) inlet air, intake manifold, and water jacket temperatures; (6) carburetor or fuel-injector air-fuel ratio calibration; (7) the ambient conditions—pressure, temperature, and relative humidity—during the requirement determination.

The following illustrates the interaction between fuel factors and engine operating variables. Figure 15-17 shows the relation between spark advance, torque, and speed in an engine operating at wide-open throttle. The dashed lines, determined with a fuel of sufficiently high octane rating to avoid knock, show MBT timing as a function of speed, along with the spark-advance limits for con-

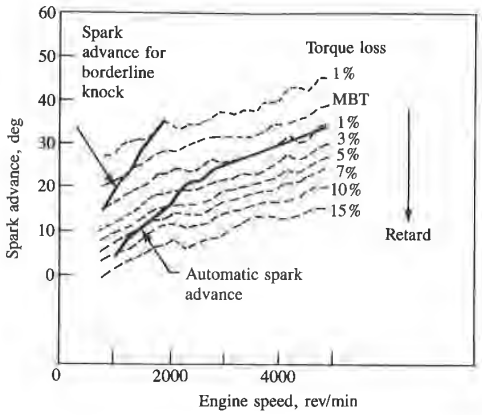

FIGURE 15-17
Relation between spark advance, speed, and torque loss, for spark-ignition engine at wide-open throttle, showing knock limit for specific gasoline and typical spark-advance schedule that avoids knock problems.[28]

stant specified percentage torque reductions. The upper solid line traces the spark advance for borderline knock with a particular commercial gasoline. To avoid knock with this fuel, the spark advance must be set to lose one percent of engine torque at 800 rev/min, with the torque loss diminishing to zero at 1200 rev/min. Above that speed this particular fuel allows operation at MBT timing without knocking. The lower solid curve represents a typical spark-advance schedule at WOT. It lies below the borderline knock advance (and results in a significant torque loss) for the following reasons. One is that different commercial gasolines with the same research octane number can respond differently to variations in engine operating conditions. Calibrating the engine (i.e., specifying the schedules for spark advance, A/F, and EGR) must be done with sufficient margin of conservatism to avoid objectionable knock with the normal range of commercial gasolines over the full operating conditions of the engine. A second reason is engine-to-engine production variability despite the close dimensional tolerances of modern production engineering. For example, the effective compression pressure in each cylinder of a multicylinder engine is not identical, due to geometric and ring-pack behavior differences. The cylinder with the highest compression pressure is most knock-prone. Allowing for corresponding effects of cylinder-to-cylinder variations in A/F, EGR rates, and spark timing, it is obvious that for a given operating condition in a multicylinder engine, one cylinder is more likely to knock than the others. It is that cylinder which limits the spark advance.† A third reason for the discrepancy between actual spark-advance calibration and the knock limit for a given engine and fuel is the octane requirement increase associated with the buildup of deposits on the combustion chamber walls over extended mileage (see Sec. 9.6.3).

† There is no assurance that the same cylinder will be the principal offender in all engines of the same model, nor in a given engine at all operating conditions.

In the example shown above, it was the problem of knock at low engine speed which required the spark advance calibration to be retarded. Whether low-, medium-, or high-speed knock is the limiting factor in a particular engine depends on the sensitivity of the fuel, on engine design features, and especially upon the engine's spark-advance requirements for MBT. The knock-limited spark advance determined from road octane rating tests will vary with engine speed and fuel sensitivity, as shown in Fig. 15-18. Low sensitivity fuels will tolerate more severe engine operating conditions and vice versa. Figure 15-18*b*, *c*, and *d* shows a typical engine spark-advance characteristic superposed on the knock-limited spark-advance plot. Depending on the fuel sensitivity and shape of the spark-advance curve, the knock region may occur at low, medium, or high speed (or not at all).

It will be apparent from the above discussion that defining the effect of combustion chamber geometry on knock can only be done in an approximate fashion. The importance of fuel composition details, differences in engine design, the variability between engines of the same type, and the effect of deposits all make the quantification of trends as chamber design is varied extremely difficult. One of the most important chamber variables is the compression ratio. Figure 15-19 shows the relationship between the octane requirement and compression ratio for a number of combustion chambers. The octane requirement was defined as the research octane number of the fuel required to operate the engine at WOT with the weakest mixture for maximum power with borderline

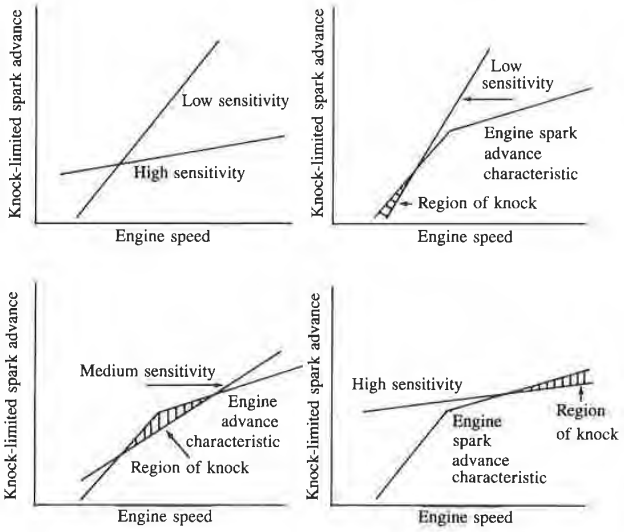

FIGURE 15-18
Diagrams showing knock-limited spark-advance curves for fuels of different sensitivity and how these can give low-, medium-, and high-speed knock in the same engine.[29]

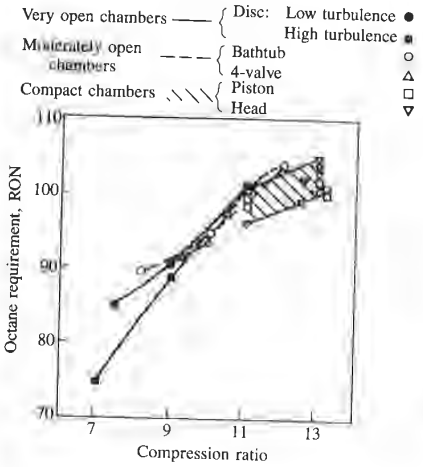

FIGURE 15-19
Octane requirement (gasoline research octane number), at wide-open throttle and MBT timing, to avoid knock as a function of compression ratio for various combustion chamber designs.[10]

(or light) knock coinciding with MBT timing at the given speed. As is well known, the octane requirement increases with increasing compression ratio; there are, however, differences in the octane requirement between different types of chamber at the same compression ratio. The chambers studied were disc-shaped chambers, bathtub and four-valve (open chambers with squish) and compact high compression ratio chambers (bowl or cup-type chambers in the piston crown or in the cylinder head around one of the valves). In the 9 to 11 compression ratio range there are only modest differences between the chambers studied. At higher compression ratios, 11 to 13, the compact chambers show a lower octane requirement which gives them a 1 to 2 compression ratio advantage over the more open chambers. This advantage for the compact (and high-turbulence) chambers comes largely from the increased heat-transfer rates in these chambers. Whether the higher turbulence is generated during intake or at the end of the compression stroke, it increases the heat transfer from the end-gas, reducing its temperature and therefore its propensity to knock. However, this higher heat transfer also reduces engine power and efficiency, so the benefits of the compression ratio advantage are reduced. There is some increase in the knock-limited compression ratio with a given fuel as burn time is decreased by using one, two, three, and then four spark plugs simultaneously, with a given chamber geometry, but the effect is much smaller than the differences suggested by Fig. 15-19.[23]

Spark plug location within the chamber is an important factor affecting octane requirement. More centrally located plug positions shorten the flame travel path to the cylinder walls and decrease the time between spark discharge and flame arrival at the end-gas location. This decreases the octane requirement. The position of the spark plug in relation to the exhaust valve is also important: it is advantageous to burn the unburned mixture which has been heated by contact with the hot exhaust valve early in the combustion process.

TABLE 15.2
Engine conditions affecting octane number requirement

Octane number requirement tends to go *up* when:	Octane number requirement tends to go *down* when:
1. Ignition timing is advanced.	1. Ignition timing is retarded.
2. Air density rises due to supercharging or a larger throttle opening or higher barometric pressure.	2. Engine is operated at higher altitudes or smaller throttle opening or lower barometric pressure.
3. Humidity or moisture content of the air decreases.	3. Humidity of the air increases.
4. Inlet air temperature is increased.	4. Inlet air temperature is decreased.
5. Coolant temperature is raised.	5. Fuel/air ratio is richer or leaner than that producing maximum knock.
6. Antifreeze (glycol) engine coolant is used.	6. Exhaust gas recycle system operates at part throttle.
7. Engine load is increased.	7. Engine load is reduced.

Operating variables that affect the temperature or pressure time histories of the end-gas during combustion or the basic autoignition characteristics of the unburned fuel, air, residual mixture will also affect the engine's octane requirement. The most important additional variables which increase or decrease octane requirement in a consistent manner are listed in Table 15.2. Relative spark

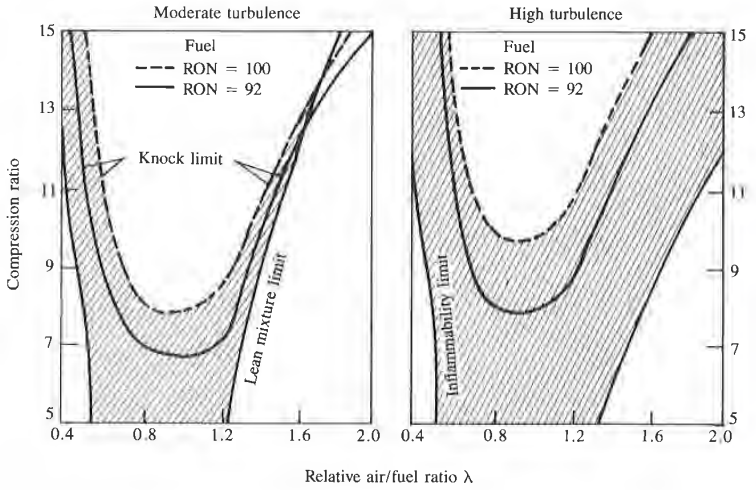

FIGURE 15-20
Knock limits and lean engine operating limits as function of compression ratio and relative air/fuel ratio λ ($\lambda = 1/\phi$) for moderate and high-turbulence engine combustion chambers.[32]

advance has a major impact on knock; since it is also easy to adjust, it is the engine variable most commonly used to control knock. Studies show that typically 0.5 to 1.0 RON reduction is achieved per degree of retard.[30] Atmospheric conditions—pressure, temperature, and humidity—all affect the octane number requirement.[31]

The fuel/air equivalence ratio affects the octane requirement of an engine. The highest requirement is for slightly rich mixtures; increasing richness and leanness about this point decrease the octane requirement substantially. Figure 15-20 shows the knock-limited compression ratio as a function of the relative air/fuel ratio ($\lambda = 1/\phi$; $\lambda > 1$ for lean mixtures) for conventional and high-turbulence chambers, for two fuels with different octane ratings. Substantially higher compression ratios can be used with lean mixtures, especially with the high-turbulence chamber which extends the lean limit. The coolant temperature affects the octane requirement. Higher coolant temperature increases the inlet mixture temperature, and reduces heat losses from the end-gas to a modest degree.

15.4.5 Chamber Optimization Strategy

The discussion in the previous sections suggests that the following sequence of steps in a combustion chamber development process is most logical. First should come the selection of the best chamber geometry. Geometric optimization can result in substantial benefits and carries no significant penalties. Chamber geometry involves cylinder head and piston crown shape, and plug location. Open chambers such as the hemispherical or pent-roof cylinder head, and clam-shell, with near central plug location, give close to the maximum flame front surface area (and hence a faster burn), have the lowest chamber surface area in contact with the burned gases (and therefore the lowest heat transfer), and have inclined valves which give high volumetric efficiency. Spark plug location close to the center of the chamber is especially important in obtaining a fast burn rate. More compact chamber shapes than the open chambers listed above, such as the bowl-in-piston or chamber-in-head designs, do produce a somewhat faster burn, but with lower volumetric efficiency and higher heat losses.

Following this first step, two problem areas may remain: the chamber may have a higher octane requirement than is desired and the burn rate may not be fast enough to absorb the high dilution required at part load to meet the emissions and fuel consumption goals.

Positioning the spark plug as close to the center as possible will have reduced the octane requirement for that particular chamber shape. Depending on chamber design details, some squish area could be introduced. However, the perceived octane advantage of chamber designs which contain substantial squish is offset, at least in part, by their higher heat losses. A unit compression ratio increase results in a 3 percent or less increase in efficiency at part load. However, if the measures required to increase the compression ratio from, say, 9 to 10 resulted in a 10 percent increase in heat transfer, engine efficiency would not improve.

The next step should be to reduce the cyclic variability in the combustion process to the maximum extent feasible, by improving the uniformity of the intake fuel, air, and EGR mixture. Delivery of equal amounts of each of these constituents to each cylinder, provision for good mixing between constituents in the intake manifold and port, and accurate control of mixture composition during engine transients are all especially important. Also important is achieving closely similar flow patterns within each engine cylinder during intake so as to obtain equal burn rates in all cylinders. Attention to these intake process and mixture preparation details will always improve engine operation and carries no performance penalties.

However, the burn rate may still not be fast enough, especially during the critical early stages of flame development, and cyclic variability may still be too high to meet the engine's performance goals. Then higher turbulence levels during combustion must be achieved. This is usually best done by creating swirl during the induction process. The appropriate method for introducing swirl will depend on any geometric manufacturing constraints and cost issues. With no geometric constraints, use of helical swirl-generating ports or a divided intake-port system with valves to control the flow at light load are likely to have the lowest power penalties. It is especially important that only the minimum additional turbulence required to achieve the performance objectives be added at this stage. Higher than necessary gas velocities within the cylinder result in excessive heat losses and low volumetric efficiency.

In summary, to meet the objectives of a fast, repeatable, and robust combustion process with high volumetric efficiency, low heat transfer, and acceptable octane requirement, combustion chamber development should proceed through the following steps.

1. Optimize the chamber geometry within the design constraints for the maximum flame front area, minimum burned gas/chamber wall contact area, and largest valve size.
2. Obtain additional reductions in the cyclic combustion variability by improving mixture distribution and uniformity and by creating flow patterns into each cylinder that are essentially identical.
3. Achieve any additional improvement in burn rate and cyclic variability required to meet objectives by increasing turbulence to the minimum extent. This is usually best done by creating swirl during the induction process.

15.5 VARIABLES THAT AFFECT CI ENGINE PERFORMANCE, EFFICIENCY, AND EMISSIONS

15.5.1 Load and Speed

The performance of a naturally aspirated DI heavy-duty truck diesel engine and a small IDI engine at full load over the engine speed range have already been

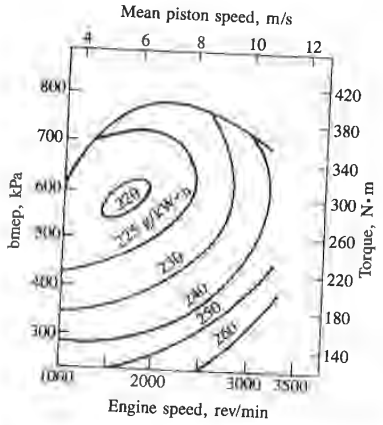

FIGURE 15-21
Performance map for 6.54-dm³ eight-cylinder air-cooled naturally aspirated medium-swirl DI diesel engine. Contours of constant bsfc in grams per kilowatt-hour shown. Bore = 102 mm, stroke = 100 mm, $r_c = 18$. Multihole fuel nozzle.[33]

discussed in Sec. 15.2. Here we examine the part-load behavior of various types of naturally aspirated diesel engines.

As with SI engines (see Sec. 15.3.3), performance maps where bsfc contours are plotted on a graph of bmep versus engine speed are commonly used to describe the effects of load and speed variations. Figure 15-21 shows the performance map for an air-cooled four-stroke cycle medium-swirl naturally aspirated DI diesel (similar to the engine in Fig. 1-23). Maximum rated power for this 6.54-dm³ displacement engine at 3200 rev/min is 119 kW, maximum bmep at 2000 rev/min is 784 kPa, and minimum bsfc (at 1600 rev/min and 580 kPa bmep) is 220 g/kW · h, which corresponds to a brake fuel conversion efficiency of 38.5 percent. The gross indicated fuel conversion efficiency would be about 48 percent.

Figure 15-22 shows the performance map for a small high-swirl DI diesel which uses the M.A.N. combustion system with a single fuel jet sprayed tangentially into the swirling air flow. Due to the higher speed and higher swirl than the

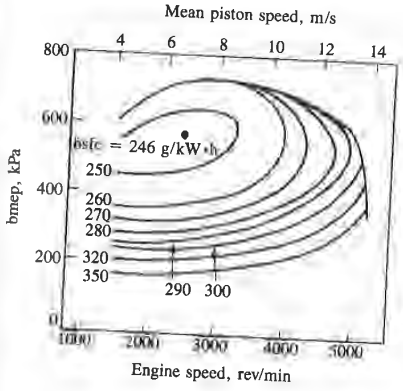

FIGURE 15-22
Performance map for 1.47-dm³ four-cylinder naturally aspirated DI diesel engine with high-swirl single-hole-nozzle M.A.N. combustion system. Contours of constant bsfc in grams per kilowatt-hour shown. Bore = 76.5 mm, stroke = 80 mm, $r_c = 18.5$.[34]

larger DI engine in Fig. 15-21, the maximum bmep is slightly lower. The best bsfc is about 10 percent higher largely due to higher friction mep, but in part due to higher heat losses resulting from the less favorable surface/volume ratio of the smaller bore engine and higher swirl, and lower heat-release rate of the M.A.N. system. Note that the maximum mean piston speed for this engine, 13.3 m/s at 5000 rev/min, is comparable to that of the larger medium-swirl engine in Fig. 15-21 (10.7 m/s).

Figure 15-23 gives the performance characteristics of an automotive naturally aspirated swirl-chamber IDI diesel engine. Maximum bmep values are usually higher than those of equivalent size DI engines because without the need to generate swirl during the intake process, the intake port and valve are less restrictive and volumetric efficiency is higher, and because the IDI engine can be run at lower A/F without smoking. The best bsfc values are usually some 15 percent higher than values typical of equivalent DI engines. The best brake fuel conversion efficiency of the engine of Fig. 15-23 is 32.5 percent.

Comparisons between naturally aspirated DI and IDI diesel engines of closely comparable design and size indicate that the DI engine is always more efficient, though the benefit varies with load. At full load, differences of up to 20 percent in bsfc have been noted, especially in engines with larger displacement per cylinder. At part load, the gain is less—of order 10 percent. Comparisons should be made at equal emission levels, a task that is difficult to accomplish in practice. Emission control with the DI engine is more difficult, so this constraint reduces the benefit somewhat. Figure 15-24 shows a breakdown of the indicated efficiency differences between the two systems. At full load ($A/F = 18$ to 20) the IDI suffers a penalty of about 15 to 17 percent due in large part to the retarded timing of the IDI combustion process and its long, late-burning, heat-release profile. At light load, about 300 kPa bmep ($A/F = 50$), these combustion effects are small and the indicated efficiency penalty of the IDI (around 5 to 7 percent) is due to the higher heat losses associated with the larger surface area and high-velocity flow through the connecting nozzle of the divided-chamber geometry and due to the pumping pressure loss between the main and auxiliary chambers.[36]

Note that all these diesel engine performance maps are similar in general

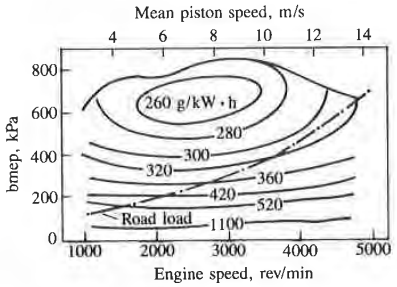

FIGURE 15-23
Performance map for 1.987-dm^3 five-cylinder naturally aspirated IDI swirl-chamber diesel engine. Contours of constant bsfc in grams per kilowatt-hour shown. Bore = 76.5 mm, stroke = 86.4 mm, $r_c = 23$.[35]

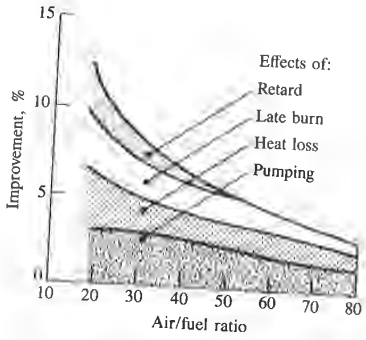

FIGURE 15-24
Factors which improve the indicated efficiency of naturally aspirated small DI diesel combustion systems relative to IDI swirl-chamber combustion system, as a function of A/F at load.[38]

shape and when plotted against S_p are quantitatively comparable. The increase in bsfc from the minimum value with increasing speed at constant load is due to the increase in friction mep, partly offset by the effect of decreasing importance of heat losses per cycle on efficiency. The increase in bsfc with decreasing load at constant speed is dominated by the decreasing mechanical efficiency as bmep is reduced. The indicated fuel conversion efficiency increase as the fuel/air equivalence ratio is decreased partly offsets this. The trends in bsfc when increasing load at constant speed and increasing speed at constant load from the minimum are more modest. They are the net results of (1) the increase in mechanical efficiency and decrease in indicated fuel conversion efficiency as the load increases and (2) decreasing indicated efficiency due to increasing importance of heat losses and increasing mechanical efficiency as the speed decreases. The enrichment of the mixture at high load and low speed of spark-ignition engines is, of course, absent.

Figure 15-25 shows the effect of load on NO_x and HC emissions for naturally aspirated DI and IDI diesel engines. For the DI engine NO_x concentrations rise steadily as the fuel/air ratio increases with increasing bmep at constant injection timing. The increasing quantity of fuel injected per cycle results in an increasing amount of close-to-stoichiometric combustion products near the peak pressure and temperature (see Sec. 11.2.4). The IDI engine shows a similiar trend except that, at high load, NO_x concentrations level off. These characteristics do not change substantially with engine speed. The IDI engine shows significantly lower HC emissions than the DI engine. The high HC at idle and light load are thought to result from fuel mixing to too lean an equivalence ratio. If diesel engines are overfueled at high load, HC emissions then rise rapidly. These HC mechanisms are described in Sec. 11.4.4. Injection timing affects NO_x and HC emissions significantly, as discussed in Sec. 15.5.2 below.

Figure 15-26 shows smoke and particulate mass emissions from a naturally aspirated IDI engine. Rapidly increasing black smoke at very high load limits the maximum bmep that a diesel engine can produce. On a specific emission basis [Eq. (2.36)], the particulates typically show a U-shaped behavior due to the predominance of hydrocarbons in their composition at light load and of carbon at high load.[38]

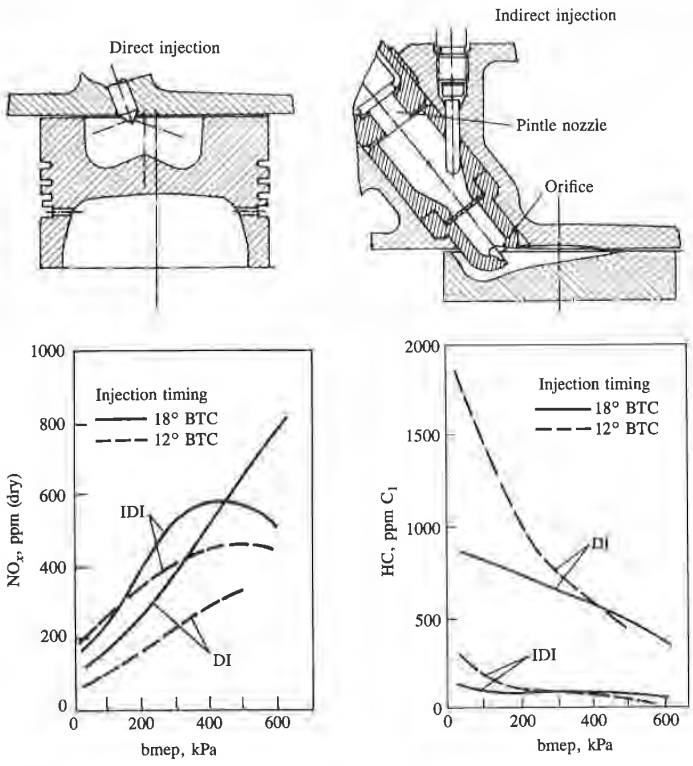

FIGURE 15-25
Effect of load on naturally aspirated diesel engine NO_x and HC emissions at rated speed, with two injection timings. Direct-injection and indirect-injection (prechamber) combustion systems. Six-cylinder, 5.9-dm^3 displaced volume, engine. DI: $r_c = 17$, rated speed = 2800 rev/min; IDI: $r_c = 16.7$, rated speed = 3000 rev/min.[37]

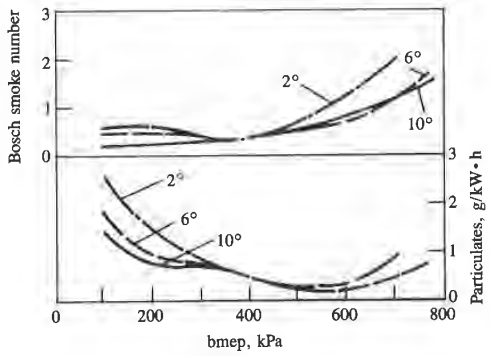

FIGURE 15-26
Smoke (Bosch smoke number) and particulate mass emissions (in grams per kilowatt-hour) as a function of load and injection timing for six-cylinder 3.7-dm^3 IDI swirl-chamber diesel engine at 1600 rev/min (no EGR).[38]

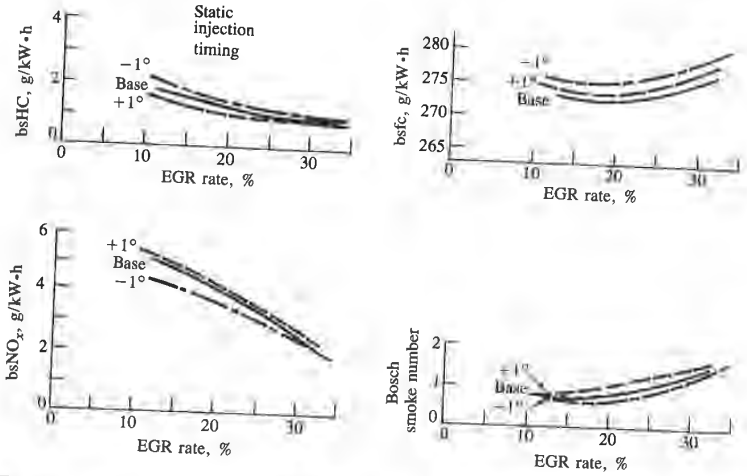

FIGURE 15-27
Brake specific HC, NO_x and fuel consumption, and smoke emissions, as a function of percent recycled exhaust for 2.4-dm^3 four-cylinder high-swirl DI diesel engine at 1250 rev/min and 255 kPa bmep.[39]

Recycled exhaust gas, at part load, can be used to reduce diesel engine NO_x emissions. Note that since diesel engines operate with the air flow unthrottled, at part load the CO_2 and H_2O concentrations in exhaust gas are low; they are essentially proportional to the fuel/air ratio. Because of this, high EGR levels are required for significant reductions in NO_x emissions. Figure 11-18 shows how NO_x concentrations decrease as a DI diesel engine inlet air flow is diluted at a constant fueling rate. The dilution is expressed in terms of oxygen concentration in the mixture after dilution. Figure 15-27 shows how the EGR affects specific NO_x and HC, fuel consumption, and smoke for a small high-swirl DI diesel engine at typical automobile engine part-load conditions. Effective reduction of $bsNO_x$ is achieved and modest reductions in bsHC, with only a slight increase in bsfc. However, smoke increased as the EGR rate increased.[39]

15.5.2 Fuel-Injection Parameters

Fuel-injection timing essentially controls the crank angle at which combustion starts. While the state of the air into which the fuel is injected changes as injection timing is varied, and thus ignition delay will vary, these effects are predictable (see Sec. 10.6.4). The fuel-injection rate, fuel nozzle design (including number of holes), and fuel-injection pressure all affect the characteristics of the diesel fuel spray and its mixing with air in the combustion chamber.

Figure 15-28 shows the effect on performance and emissions of varying injection timing, in (*a*) a medium-swirl DI diesel engine and (*b*) an IDI engine. At fixed speed and constant fuel delivery per cycle, the DI engine shows an optimum

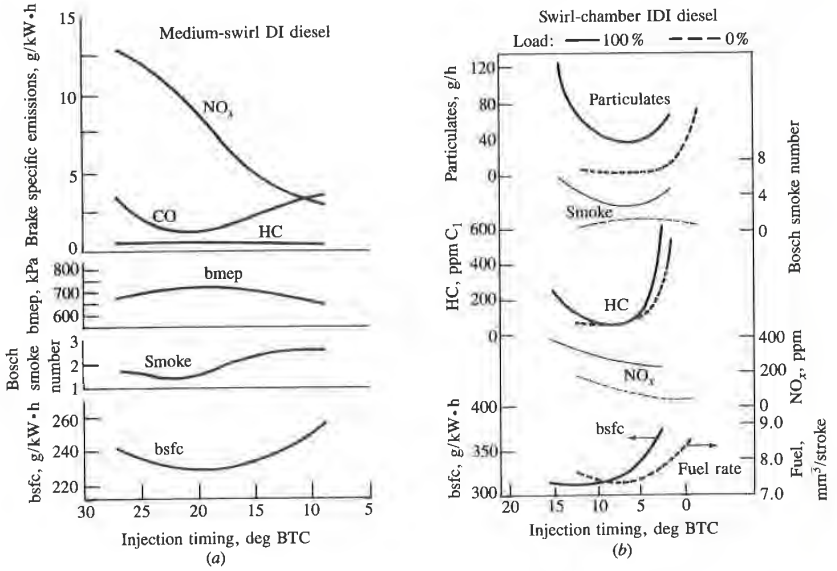

FIGURE 15-28
Effect of start-of-injection timing on diesel engine performance and emissions. (*a*) Medium-swirl DI diesel engine with deep combustion bowl and four-hole injection nozzle, 2600 rev/min, fuel delivery 75 mm^3/cycle, fuel/air equivalence ratio 0.69.[37] (*b*) Swirl-chamber IDI engine, 2500 rev/min, 0 and 100 percent load.[40]

bsfc and bmep at a specific start of injection for a given injection duration.† The IDI engine experiments are at fixed bmep; here, bsfc at full load and fueling rate at idle show a minimum at specific injection timings. Injection timing which is more advanced than this optimum results in combustion starting too early before TC; injection retarded from this optimum results in combustion starting too late.

Injection timing variations have a strong effect on NO_x emissions for DI engines: the effect is significant but less for IDI engines. Retarded injection is commonly used to help control NO_x emissions. It gives substantial reductions, initially with only modest bsfc penalty. For the DI engine, at high load, specific HC emissions are low and vary only modestly with injection timing. At lighter loads, HC emissions are higher and increase as injection becomes significantly retarded from optimum. This trend is especially pronounced at idle. For IDI diesel engines HC emissions show the same trends but are much lower in magnitude than DI engine HC emissions.[41] Figure 15-25 supports this discussion.[37]

† This optimum injection timing gives maximum brake torque, though the designation MBT timing is less commonly used with diesels than with SI engines.

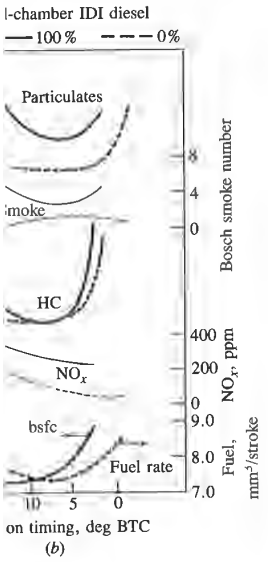

emissions. (*a*) Medium-swirl DI
zzle, 2600 rev/min, fuel delivery
engine, 2500 rev/min, 0 and 100

ı injection duration.† The
full load and fueling rate
Injection timing which is
n starting too early before
ıbustion starting too late.
ɔn NO_x emissions for DI
ıes. Retarded injection is
es substantial reductions,
ɡine, at high load, specific
ıjection timing. At lighter
ion becomes significantly
ıounced at idle. For IDI
are much lower in magni-
ɔorts this discussion.[37]

ıgh the designation MBT timing

Retarding timing generally increases smoke, though trends vary significantly between different types and designs of diesel engine. Mass particulate emissions increase as injection is retarded.

The injection rate depends on the fuel-injector nozzle area and injection pressure. Higher injection rates result in higher fuel-air mixing rates, and hence higher heat-release rates (see Sec. 10.7.3). For a given amount of fuel injected per cylinder per cycle, as the injection rate is increased the optimum injection timing moves closer to TC. The effects of injection rate and timing on bsfc in a naturally aspirated DI diesel engine are shown in Fig. 15-29. The higher heat-release rates and shorter overall combustion process that result from the increased injection rate decrease the minimum bsfc at optimum injection timing; however, a limit to these benefits is eventually reached.

Increasing the injection rate increases NO_x emissions and decreases smoke or particulate emissions. The controlling physical process is the rate of fuel-air mixing in the combustion chamber so, at constant fuel injected per cylinder per cycle, both increased injection pressure at fixed nozzle orifice area (which reduces injection duration) and reduced nozzle area at fixed injection duration produce these trends.[42]

The engine designer's goal is obviously to achieve the best bsfc possible

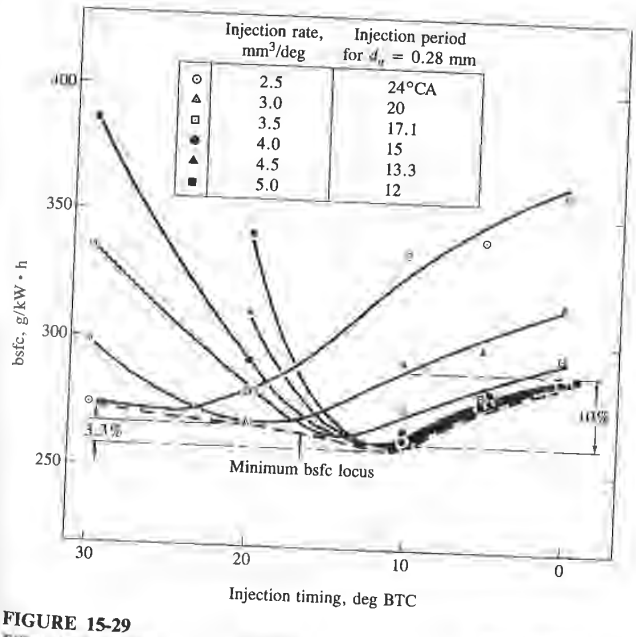

FIGURE 15-29
Effect of injection timing and injection rate on bsfc for 0.97-dm³ single-cylinder naturally aspirated DI diesel engine with swirl. 2000 rev/min, 60 mm³ per stroke fueling rate.[42]

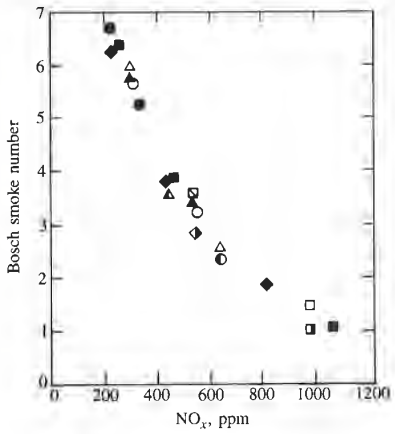

FIGURE 15-30
Tradeoff between NO_x and smoke emissions for quiescient single-cylinder DI diesel engine with bore = 140 mm, stroke = 152 mm, $r_c = 14.3$, eight-hole injector nozzle. Various speeds, fueling rates, injection timings, injection pressures, % EGR; constant $A/F = 25$.[43]

with emission levels low enough to satisfy the constraints imposed by emission standards. The variations of bsfc, NO_x, and particulate emissions described above involve tradeoffs that make achieving this goal especially difficult. One well-established tradeoff is between bsfc and $bsNO_x$. Injection retard from optimum injection timing decreases $bsNO_x$ at the expense of an increase in bsfc. A second important tradeoff is that between NO_x and particulate emissions, illustrated for a DI diesel engine in Fig. 15-30. Smoke is plotted versus NO_x for a range of speeds, loads (fuel per cycle), injection timings, injection pressures, and EGR rates. The air/fuel ratio was maintained constant at 25 ($\phi = 0.58$). The figure indicates that for a well-optimized DI diesel engine, the smoke nitric oxide tradeoff is relatively independent of engine speed, injection rate, injection timing, and amount of EGR. A given reduction in one of these pollutants through changing any one of these variables results in a given increase in the other pollutant. This tradeoff exists for essentially all types of diesel engine, though the magnitude depends on engine details.

15.5.3 Air Swirl and Bowl-in-Piston Design

Increasing amounts of air swirl within the cylinder (see Sec. 8.3) are used in direct-injection diesel engines, as engine size decreases and maximum engine speed increases, to achieve adequately fast fuel-air mixing rates (see Sec. 10.2.1). In these medium-to-small size engines, use of a bowl-in-piston combustion chamber (Fig. 10-1*b* and *c*) results in substantial swirl amplification at the end of the compression process (Sec. 8.3.3). Here, the impacts of varying air swirl on the performance and emissions characteristics of this type of DI engine are reviewed.

Since air swirl is used to increase the fuel-air mixing rate, one would expect the overall duration of the combustion process to shorten as swirl increases and emissions that depend on the local fuel/air equivalence ratio to be dependent on

swirl level. Figure 15-31 shows the effects of swirl and injection-timing variations on bsfc and emissions of a DI engine of 1.36 dm^3 per cylinder displacement with a toroidal bowl-in-piston chamber (see Fig. 10-3*b*). The swirl ratio [Eq. (8.28)] was varied using shrouded inlet valves with shrouds of different subtended angle (60 to 120°). The injection timing which gives minimum bsfc shifts toward TC as the swirl ratio increases due to the decreasing total combustion duration. The minimum bsfc was achieved with a swirl ratio of 6 to 7; while higher swirl levels continue to increase fuel-air mixing rates, heat transfer increases also and eventually offsets the mixing rate gain. Particulate and CO emissions decrease as swirl increases due to more rapid fuel-air mixing. NO_x emissions increase with increasing swirl. At constant injection timing, however, about half the increase is due to the effect of injection advance relative to the optimum timing and half to the shorter combustion process.[44] Similar trends have been observed as swirl is varied with the M.A.N. single-hole-nozzle diesel combustion system of Fig. 10-1*c*.

In production engines, the various types of port design shown in Fig. 8-13 can be used to generate swirl during the induction process. Of these, the helical ports are most effective at producing relatively uniform high swirl with the minimum loss in volumetric efficiency.

The geometry of the bowl-in-piston combustion chamber governs the extent to which induction-generated swirl is amplified during compression. The flow field in the bowl during fuel injection is also dependent on the interaction between this swirling flow and the squish motion which occurs as the top of the piston crown approaches the cylinder head (see Sec. 8.4). Various types of bowl-in-piston design for multihole fuel nozzle DI engines are shown in Fig. 15-32 (for the M.A.N. single-hole-nozzle system a spherical bowl is used; see Fig. 10-1*c*). More conventional designs (e.g., Fig. 15-32*a*) have the bowl sides essentially parallel to the cylinder liner. Note that it is often necessary to offset the bowl axis from the cylinder axis and the injector nozzle hole locations from the bowl axis.

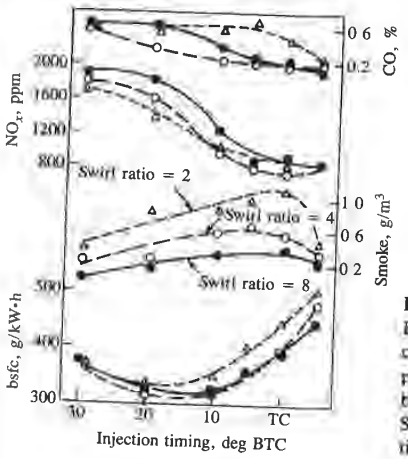

FIGURE 15-31
Effect of air swirl on bsfc and emissions of single-cylinder DI diesel engine with toroidal bowl-in-piston chamber. 1.36-dm^3 displacement, $r_c = 16$; bowl diameter/bore = 0.5, 2000 rev/min, full load. Swirl ratio measured in bowl-in-piston at injection.[44]

NO_x and smoke emissions for linder DI diesel engine with stroke = 152 mm, $r_c = 14.3$, nozzle. Various speeds, fueling nings, injection pressures, % = 25.[43]

nts imposed by emission late emissions described especially difficult. One . Injection retard from ıse of an increase in bsfc. ırticulate emissions, illus- ɔlotted versus NO_x for a , injection pressures, and nt at 25 ($\phi = 0.58$). The ıe, the smoke nitric oxide ion rate, injection timing, ɔollutants through chang- se in the other pollutant. ıe, though the magnitude

see Sec. 8.3) are used in s and maximum engine ng rates (see Sec. 10.2.1). wl-in-piston combustion mplification at the end of f varying air swirl on the DI engine are reviewed. ıg rate, one would expect en as swirl increases and ratio to be dependent on

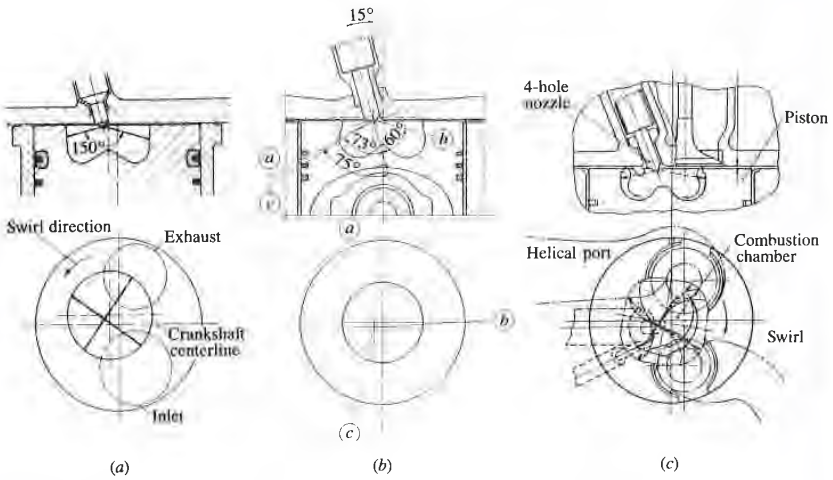

FIGURE 15-32
Various bowl-in-piston chamber designs for DI diesel engines with swirl: (*a*) conventional straight-sided bowl,[37] (*b*) reentrant bowl,[45] (*c*) square reentrant bowl.[46]

due to the geometric constraints imposed by the valves. An alternative design with a reentrant bowl (Fig. 15-32*b*) is sometimes used to promote more rapid fuel-air mixing within the bowl. The squish-swirl interaction with highly reentrant bowl designs differs markedly from the interaction in nonreentrant bowls. Figure 15-33 shows the two different flow patterns set up in a diametral plane. With a conventional bowl, the swirling air entering the bowl flows down to the base of the bowl, then inward and upward in a toroidal motion. In reentrant bowls the swirling air entering the bowl spreads downward and outward into the undercut region, and then divides into a stream rising up the bowl sides and a stream flowing along the bowl base. Reentrant chambers generally produce higher swirl at the end of compression, and maintain a high swirl level further

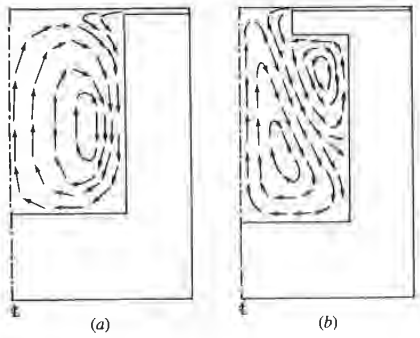

FIGURE 15-33
Flow pattern set up in diametral plane by squish-swirl interaction in (*a*) conventional and (*b*) reentrant bowl-in-piston combustion chambers. ℄ cylinder axis.[47]

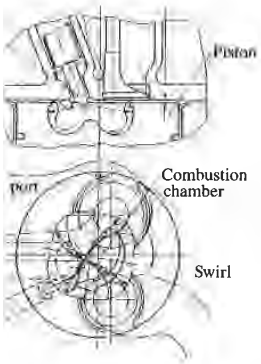

(*c*)

wirl: (*a*) conventional straight-

es. An alternative design
to promote more rapid
action with highly reen-
n in nonreentrant bowls.
up in a diametral plane.
bowl flows down to the
dal motion. In reentrant
ard and outward into the
up the bowl sides and a
nbers generally produce
a high swirl level further

set up in diametral plane
nteraction in (*a*) conventional
ant bowl-in-piston combus-
cylinder axis.[47]

into the expansion stroke.[47] Reentrant chambers usually achieve lower HC and smoke emissions and slightly lower bsfc, especially at retarded injection timings.

Square cavity chambers (see Fig. 15-32*c*) are also used with swirl to achieve low emissions in smaller-size DI diesel engines. The interaction between the swirl and the chamber corners produces additional turbulence which, with fuel injected into the corners as shown, achieves a more uniform mixture within the bowl.

The air flow field within bowl-in-piston combustion chambers when fuel injection occurs is highly complex. Certain generalizations hold: e.g., reducing the bowl diameter at a constant compression ratio increases the swirl levels in the bowl at TC [see Eq. (8.35) and the accompanying text] which decreases smoke and increases NO_x and HC emissions.[37] However, the squish-swirl interaction is difficult to unravel, especially with the off-center bowls often required due to the constraints on injector location caused by the valves. Figure 14-33 gives an example of such a flow. It shows velocity vectors and turbulence intensities in two orthogonal bowl-diametral planes within an off-center reentrant bowl as TC is approached in a small high-swirl DI engine. The off-center bowl location coupled with the swirl-squish interaction cause substantial asymmetry in the flow within the bowl.

15.6 SUPERCHARGED AND TURBOCHARGED ENGINE PERFORMANCE

The equations for power, torque, and mep in Sec. 2.14 show that these engine performance parameters are proportional to the mass of air inducted per cycle. This depends primarily on inlet air density. Thus the performance of an engine of given displacement can be increased by compressing the inlet air prior to entry to the cylinder. Methods for achieving higher inlet air density in the gas exchange processes—mechanical supercharging, turbocharging, and pressure-wave supercharging—are discussed in Sec. 6.8. The arrangements of the various practical supercharging and turbocharging configurations are shown in Fig. 6-37. Figures 1-11, 6-40, 6-43, 6-49, 6-53, and 6-58 show examples of the different devices used to achieve higher inlet air densities. In this section the effects of boosting air density on engine performance are examined. Spark-ignition and compression-ignition engines are dealt with separately. Power boosting via supercharging and/or turbocharging is common in diesel engines: few spark-ignition engines are turbocharged. Knock prevents the full potential of boosting from being realized in the latter type of engine. A more extensive discussion of turbocharged engine operation is provided by Watson and Janota.[48]

15.6.1 Four-Stroke Cycle SI Engines

The bmep of most production spark-ignition engines at wide-open throttle is knock-limited over part of the engine speed range (see Sec. 15.4.4). The compression ratio is usually set at a sufficiently high value so that some spark retard from

MBT timing is needed to avoid knock for the expected range of available fuel octane rating and sensitivity (see Fig. 15-17). The propensity of the end-gas to knock is increased by increases in end-gas temperature and pressure (see Sec. 9.6.2). Hence attempts to boost the output of a given size spark-ignition engine by an inlet air compression device that increases air pressure and temperature will aggravate the knock problem, since end-gas pressure and temperature will increase. However, the potential advantages of power boosting are significant. The higher output for a given displaced volume will decrease engine specific weight and volume (Sec. 2.11). Also, if the power requirements in a specific application (such as an automobile) can be met with either a naturally aspirated SI engine of a certain size or with a *smaller* size engine which is turbocharged to the same maximum power, the smaller turbocharged engine should offer better fuel economy at part load. At a given part-load torque requirement, the mechanical efficiency of the smaller turbocharged engine is higher, and if the gross indicated efficiencies of the engines are the same, the smaller engine will show a brake efficiency benefit. In practice, it proves difficult to realize much of this potential efficiency gain for the reasons described below.

While a naturally aspirated spark-ignition engine may have sufficient margin of safety relative to knock to allow modest inlet-air boost, any substantial air compression prior to cylinder entry will require changes in engine design and/or operating variables to offset the negative impact on knock. The variables which are adjusted to control knock in turbocharged SI engines are: compression ratio, spark retard from optimum, charge air temperature, and fuel/air equivalence ratio.† Figure 15-34 shows how the knock limits depend on charge pressure, temperature, fuel/air equivalence ratio and compression ratio for given octane rating fuels. The difference in boost achievable with the premium and the regular quality gasoline is significant, as expected (Sec. 9.6.3). Charge-air temperature has a strong influence on allowable boost levels; lowering the compressed air temperature prior to entry to the cylinder with a charge-air cooler allows a substantially higher compression ratio to be used at a given boost level, with a corresponding impact on engine efficiency.‡ The boost pressure benefits of the richer mixtures in Fig. 15-34*a* ($\phi = 1.1$ compared with 0.9) are largely due to the cooling effect of the additional fuel on the air charge. For example, Fig. 15-34*b* shows that, with a rich mixture and charge cooling to 60°C, a charge pressure of 1.5 atm can be utilized at optimum spark timing with a compression ratio of 8. Without charge cooling, the same charge pressure can only be used with a compression ratio of 6.[49]

In turbocharged SI engines, the knock limit is usually reached at spark timings retarded from the MBT optimum. Figure 15-35 shows the brake mean

† Valve timing changes are often made too. These are done primarily to improve low-speed torque where turbocharging has a limited impact.

‡ The turbocharged engine in Fig. 1-10 has an intercooler to reduce the inlet charge temperature.

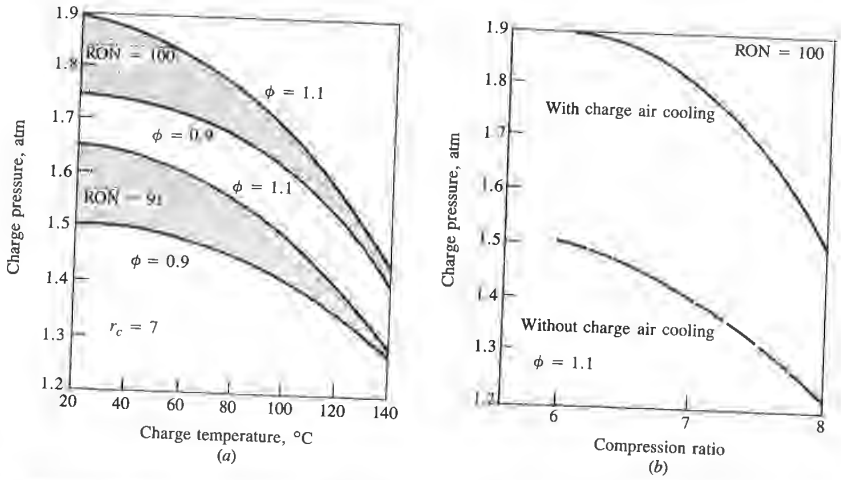

FIGURE 15-34
Dependence of SI engine knock limits on: (a) charge pressure, temperature, and equivalence ratio ϕ, with r_c = 7, 2500 rev/min, MBT timing, 91 and 100 research octane number fuel; (b) charge pressure and compression ratio, without and with (to 60°C) charge air cooling, 2500 rev/min, MBT timing, ϕ = 1.1, 100 RON fuel.[49]

effective pressure achievable at a fixed compression ratio as a function of charge pressure and ignition timing with and without charge-air cooling. Additional retard allows higher boost pressures to be utilized; however, at a constant safety margin from the knock limit, the resulting gains in bmep decrease as retard is increased. To avoid an unnecessary fuel consumption penalty, retarded timing should only be used when the turbocharger does develop a high boost pressure.

The above discussion illustrates why turbocharged spark-ignition engines normally have lower compression ratios than naturally aspirated engines, use substantial mixture enrichment (up to $\phi \approx 1.3$) at high boost to cool the charge, often use an intercooler to reduce the charge-air temperature, and operate with

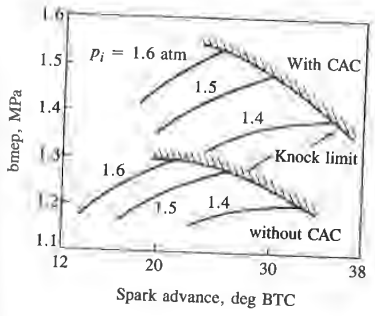

FIGURE 15-35
Brake mean effective pressure and knock limits for turbocharged SI engines as a function of spark advance and inlet pressure p_i (in atmospheres). 2500 rev/min, r_c = 7, ϕ = 1.1, 99 RON fuel, without and with (ΔT = 45°C) charge-air cooling.[49]

retarded timing at high boost pressures. Since compression ratio reductions and retarded ignition timings result in losses in efficiency, and unintended knock with high boost pressures would be especially damaging, precise control of ignition timing is critical. Most turbocharged SI engines now use a knock sensor and ignition-timing control system so that timing can be adjusted continuously to avoid knock without unnecessary retard. The sensor is usually an accelerometer which senses above-normal vibration levels on the cylinder head at the characteristic knock frequency. With a knock sensor, ignition timing can be automatically adjusted in response to changes in fuel octane rating and sensitivity, and ambient conditions.

Turbocharged SI engines where fuel is mixed with the air upstream or downstream of the compressor, using carburetors or fuel-injection systems, have been developed and used. Most modern turbocharged engines use port fuel injection. This provides easier electronic control of fuel flow, avoids filling most of the pressurized manifold volume with fuel-air mixture, and improves the dynamic response of the system by reducing fuel transport delays.

We now consider the performance of actual turbocharged spark-ignition engines. Examples of compressor outlet or boost pressure schedules as a function of speed at wide-open throttle for three turbocharged engines are shown in Fig. 15-36. The essential features of the curves are the same. Below about 1000 engine rev/min the turbocharger achieves negligible boost. Boost pressure then rises with increasing speed to 1.4 to 1.8 atm (absolute pressure) at about 2000 rev/min. Boost pressure then remains essentially constant with increasing engine speed. The rising portion of the curve is largely governed by the relative size of the turbine selected for a given engine. This is usually expressed in terms of the A/R ratio of the turbine—the ratio of the turbine's inlet casing or volute area A to the radius of the centroid of that area. Lower A/R values (smaller-capacity turbines) give a more rapid boost pressure rise with increasing speed; however, they give higher boost pressures at high engine speed, which is undesirable.[48, 50]

Avoidance of knock is the reason why boost must be limited at medium to

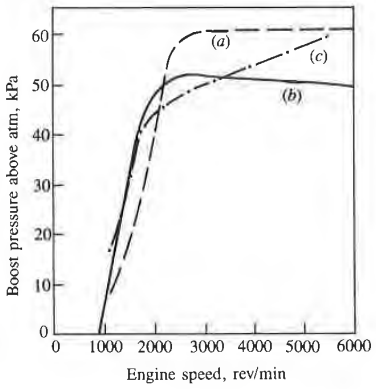

FIGURE 15-36
Boost pressure schedules for three turbocharged spark-ignition engines: (*a*) 3.8-dm^3 V-6 engine, 86.4 mm stroke, $r_c = 8$;[50] (*b*) 2.2-dm^3 four-cylinder engine, 92 mm stroke, $r_c = 8.1$;[51] (*c*) 2.32-dm^3 four-cylinder engine, 80 mm stroke, $r_c = 8.7$.[52] All schedules are wastegate controlled.

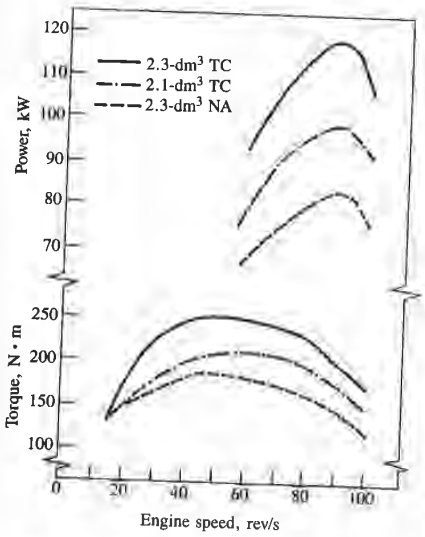

FIGURE 15-37
Power and torque as a function of engine speed for two turbocharged and one naturally aspirated four-cylinder spark-ignition engine. See Table 15.3.[52]

high engine speed; the details of this problem have already been discussed above. Even with the use of very rich mixtures and spark retard at WOT, lower compression ratios for turbocharged engines, and intercooling, knock avoidance requires that boost pressures (which would continue to rise with increasing engine speed in the absence of any control) be maintained approximately constant. This is normally achieved by reducing the exhaust flow through the turbine as speed increases by bypassing a substantial fraction of the exhaust around the turbine through the *wastegate* or flow control valve (see Sec. 6.8.4). A wastegate is a spring-loaded valve acting in response to the inlet manifold pressure on a controlling diaphragm. Although other methods of controlling boost can be used,[48] the wastegate is the most common. About 30 to 40 percent of the exhaust bypasses the turbine at maximum engine speed and load.

Figure 15-37 compares the performance of two turbocharged spark-ignition engines (four-cylinder, 2.1- and 2.3-dm³ displacement) with that of the base 2.3-dm³ engine in its naturally aspirated form. Table 15.3 gives details of these

TABLE 15.3
Turbocharged spark-ignition engine performance[52]

Type	2.1-dm³ TC	2.3-dm³ NA	2.3-dm³ TC/AC
Displacement, dm³	2.127	2.316	2.316
Bore × stroke, mm	92 × 80	96 × 80	96 × 80
Compression ratio	7.5	9.5	8.7
Maximum power, kW at rev/min	98 at 5400	83 at 5400	117 at 5300
Maximum torque, N · m at rev/min	210 at 3800	184 at 2800	250 at 2900
Maximum bmep, kPa	1241	998	1356

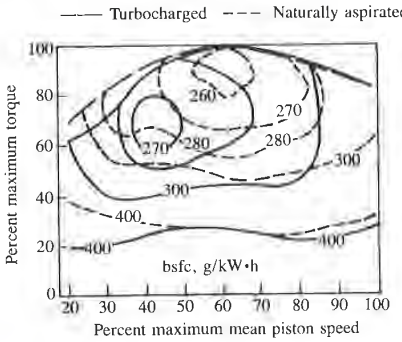

FIGURE 15-38
Comparison of bsfc contours (in grams per kilowatt-hour) on performance maps of turbocharged and naturally aspirated versions of the same spark-ignition engine, scaled to the same maximum torque and mean piston speed.[53]

three engines. The 2.1-dm^3 turbocharged but *not* intercooled engine (which also does not have a knock sensor to control spark advance) requires a lower compression ratio and achieves less of a bmep gain than the 2.3-dm^3 turbocharged intercooled engine with its knock-sensor spark-advance control, which together permit use of a higher compression ratio. Turbocharging the naturally aspirated 2.3-dm^3 engine, with the modifications indicated, results in a 36 percent increase in maximum engine torque and a flatter torque-versus-speed profile.

The brake specific fuel consumption contours of an engine produced in both naturally aspirated and turbocharged versions are shown in Fig. 15-38. The data have been scaled to represent engines of different displaced volume but the same maximum engine torque. The smaller-displacement low-compression-ratio turbocharged engine ($r_c = 6.9$) shows a reduction in bsfc at low speed and part load due to improved mechanical efficiency. At high speed and load the larger-displacement naturally aspirated engine has an advantage in bsfc due to its higher compression ratio (8.2), less enrichment, and more optimum timing.[53] In a vehicle context, the low-speed part-load advantage of the smaller size but equal power turbocharged engine should result in an average fuel economy benefit relative to the larger naturally aspirated engine. This benefit has been estimated as a function of load. At full load the average efficiencies should be comparable; at half load, the turbocharged engine should show a benefit of about 10 percent, the benefit increasing as load is decreased.[49]

15.6.2 Four-Stroke Cycle CI Engines

The factors that limit turbocharged diesel engine performance are completely different to those that limit turbocharged spark-ignition engines. The output of naturally aspirated diesel engines is limited by the maximum tolerable smoke emission levels, which occur at overall equivalence ratio values of about 0.7 to 0.8. Turbocharged diesel engine output is usually constrained by stress levels in critical mechanical components. These maximum stress levels limit the maximum cylinder pressure which can be tolerated under continuous operation, though the

thermal loading of critical components can become limiting too. As boost pressure is raised, unless engine design and operating conditions are changed, maximum pressures and thermal loadings will increase almost in proportion. In practice, the compression ratio is often reduced and the maximum fuel/air equivalence ratio must be reduced in turbocharged engines (relative to naturally aspirated engines) to maintain peak pressures and thermal loadings at acceptable levels. The fuel flow rate increases at a much lower rate than the air flow rate as boost pressure is increased. Limitations on turbocharged engine performance are discussed more fully by Watson and Janota.[48]

Small automotive indirect-injection (IDI) turbocharged engines are limited by structural and thermal considerations to about 130 atm maximum swirl- or pre-chamber pressure, 14 m/s maximum mean piston speed, and 860°C maximum exhaust temperature.[54] Smoke and NO_x emission standards are additional constraints. Figure 15-39 shows the full-load engine and turbocharger performance characteristics of a six-cylinder 2.38-dm^3 displacement Comet V swirl-chamber automobile diesel engine. The maximum boost pressure is controlled by a poppet-valve-type wastegate to 0.75 bar above atmospheric. The fuel consumption map for this engine is shown in Fig. 15-40. Superimposed on the turbocharged engine map is the map for the base naturally aspirated swirl-chamber IDI engine of the same geometry and compression ratio ($r_c = 23$). The turbocharged engine has a maximum torque 46 percent higher and a maximum power 33 percent higher than the naturally aspirated engine. The best bsfc values are closely comparable.

The different methods of supercharging internal combustion engines were reviewed in Sec. 6.8. Turbocharging, mechanical supercharging with a Roots blower, and pressure wave supercharging with the Comprex are alternative methods of boosting the performance of a small automotive swirl-chamber IDI

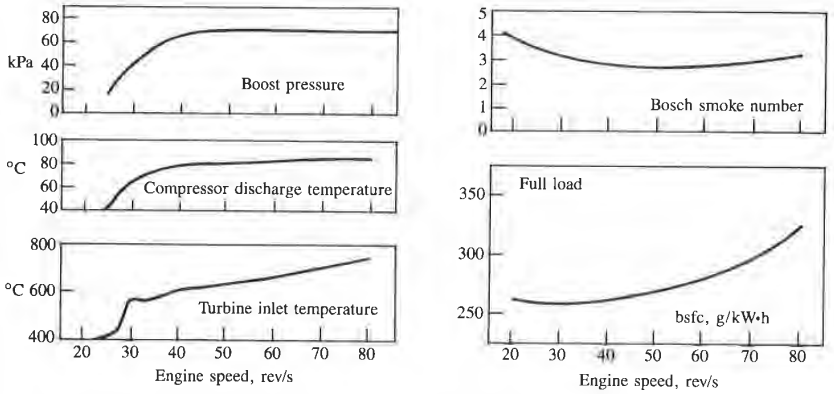

FIGURE 15-39
Engine and turbocharger characteristics of six-cylinder 2.38-dm^3 swirl-chamber IDI automotive diesel engine at full load.[54]

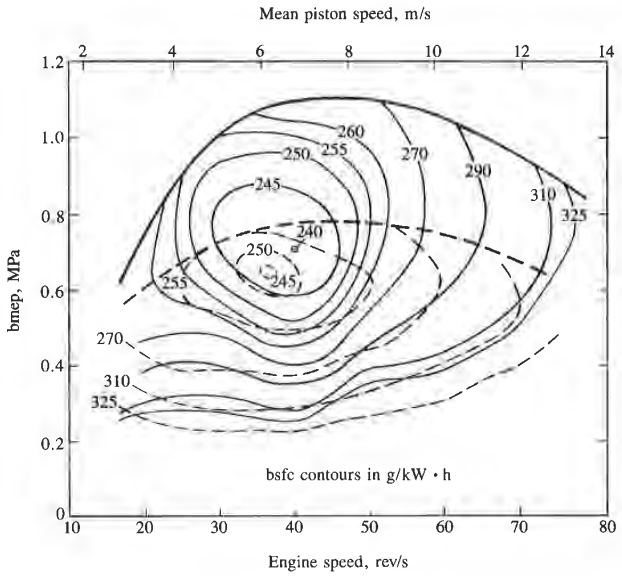

FIGURE 15-40
Fuel consumption map (bsfc in grams per kilowatt-hour) for turbocharged (——) and naturally aspirated (- - -) versions of 2.38-dm^3 six-cylinder swirl-chamber IDI diesel engine.[54]

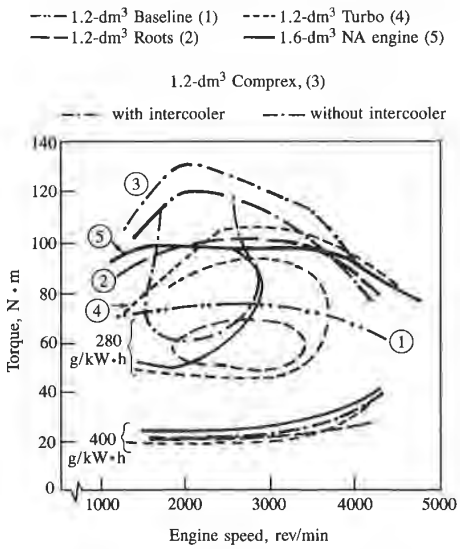

FIGURE 15-41
Torque and brake specific fuel consumption of naturally aspirated and supercharged 1.2-dm^3 swirl-chamber IDI diesel engine. Baseline (1): naturally aspirated. Supercharged with (2) Roots blower; (3) Comprex (with and without intercooler); (4) turbocharger. Larger displacement 1.6-dm^3 naturally aspirated engine (5).[55]

diesel engine. Figure 15-41 compares the torque and bsfc values obtained with each of these supercharging methods on a performance map for a 1.2-dm³ engine. Values for a 1.6-dm³ naturally aspirated IDI diesel engine are also shown. All three approaches achieve close to the desired maximum power of the 1.6-dm³ NA engine (40 kW at 4800 rev/min): e.g., 1.2-dm³ turbo, 41.2 kW at 4500 rev/min; 1.2-dm³ Comprex with intercooler, 42.3 kW at 3500 rev/min; 1.2-dm³ Roots, 37.6 kW at 4000 rev/min. The Comprex system produces the highest torque at low engine speeds, even under unsteady engine operating conditions. The density of the charge air determines the amount of charge, and hence the torque. Charge-air pressure and temperature for the three supercharging systems are shown in Fig. 15-42. The Comprex (here without an intercooler) must have the highest charge pressure because it has the highest charge temperature. Intercooling would be particularly effective in this case.[55]

Small high-speed high-swirl turbocharged direct-injection diesel engines (e.g., suitable for automobile or light-truck applications) have similar performance maps to those of equivalent IDI engines (Figs. 15-39 and 15-40). Maximum bmep values are closely comparable; usually slightly higher boost is required to offset the lower volumetric efficiency of the high-swirl-generating port and valve of the DI engine. Best bsfc values for the DI engine are usually about 15 percent lower than of comparable IDI engines (see Ref. 56).

The operating characteristics of larger medium-swirl turbocharged DI diesel engines are illustrated by the data shown in Fig. 15-43. The engine is a 12-dm³ displacement six-cylinder heavy-duty truck engine. The combustion chamber is similar to that shown in Fig. 15-32*c*, with a square combustion cavity and relatively low levels of swirl. The swirl is generated by a helical port in one of the two intake ports and a tangential port in the other in the four-valve cylinder head. Both the engine's operating map and the turbocharger compressor map with the boost pressure curve superposed are shown for two different compressor impellors. The adoption of the backward-vaned rake-type impellor compared to a more conventional design significantly increases low- and medium-speed per-

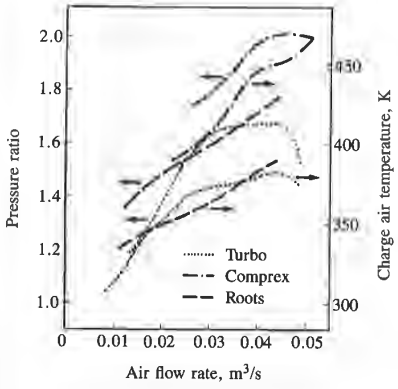

FIGURE 15-42
Charge pressure and temperature with the IDI diesel engine and different supercharging methods of Fig. 15-41.[55]

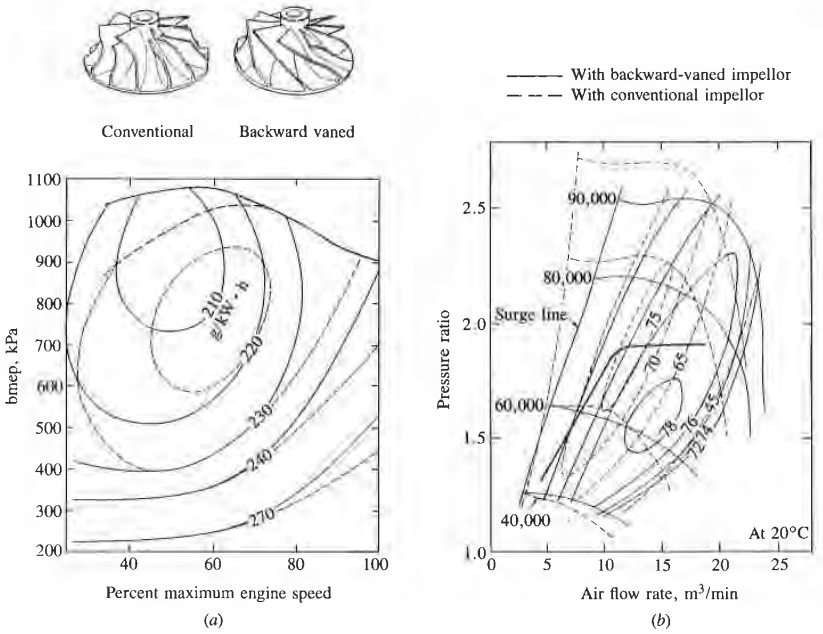

FIGURE 15-43
Performance characteristics of turbocharged 12-dm^3 six-cylinder medium-swirl heavy-duty truck DI diesel engine, with two different compressor impellors: (*a*) fuel consumption maps; (*b*) compressor maps with full-load boost operating line for engine with backward-vaned impellor superposed. Bore = 135 mm, stroke = 140 mm, $r_c = 16$.[57]

formance by improving the compressor efficiency over the engine's boost pressure curve (Fig. 15-43*b*). A wastegate is then used to control the boost level at high engine speeds. The improvement in low-speed engine torque is apparent in Fig. 15-43*a*. The dependence of the maximum torque curve on both engine and turbocharger design details is clear. With boost pressure ratios limited to below 2, in the absence of air-charge cooling, maximum bmep values of 1.1 MPa are typical of this size and type of diesel engine.

With structurally more rugged component designs, aftercooled turbocharged medium-speed diesel engines with swirl in this cylinder size range can utilize higher boost and generate much higher bmep. Wastegate control of boost is no longer required. Figure 15-44 shows the performance characteristics of a V-8 cylinder engine with its compressor map and full-load boost characteristic. This turbocharged intercooled engine achieves a maximum bmep of about 1.5 MPa and bsfc below 200 g/kW · h between the maximum torque speed and rated power. Boost pressure at full load increases continuously over the engine speed range.[58]

/ith backward-vaned impellor
/ith conventional impellor

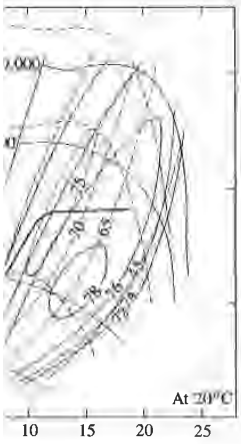

(*b*)

um-swirl heavy-duty truck DI
ımption maps; (*b*) compressor
d-vaned impellor superposed.

e engine's boost pressure
l the boost level at high
torque is apparent in
ırve on both engine and
ratios limited to below
values of 1.1 MPa are

gns, aftercooled turbo-
cylinder size range can
astegate control of boost
ance characteristics of a
oad boost characteristic.
ximum bmep of about
imum torque speed and
nuously over the engine

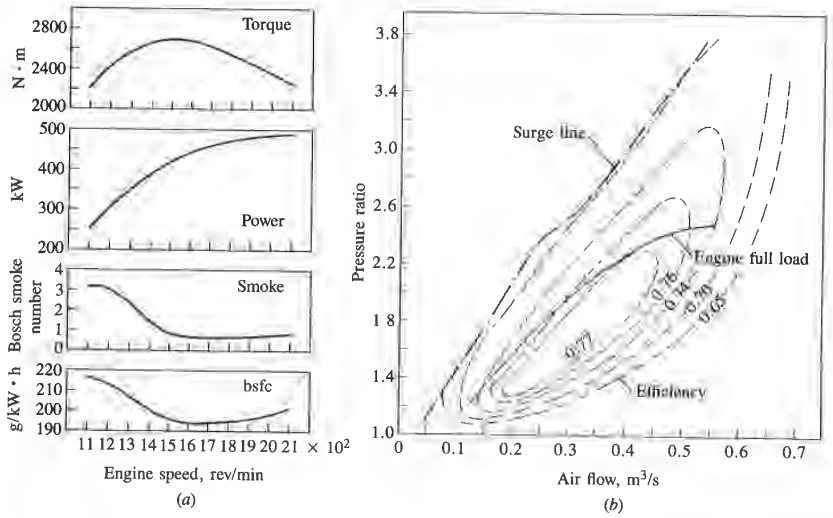

FIGURE 15-44
Performance characteristics of medium-speed turbocharged aftercooled DI diesel engine. (*a*) Torque, power, smoke number, and bsfc for V twelve-cylinder version. (*b*) Compressor characteristics and engine full-load line for V-8 cylinder version. Bore = 128 mm, stroke = 140 mm, $r_c = 15$.[58]

Examples of values of combustion-related parameters for this type of engine over the load range at its maximum rated speed are shown in Fig. 15-45 for a 14.6-dm³ six-cylinder turbocharged aftercooled DI diesel engine with a boost pressure ratio of 2 at rated power. The ignition delay decreases to about 10° (0.9 ms at 1800 rev/min) as load is increased. The bmep at 100 percent rated load at this speed is 1.2 MPa. Exhaust temperature increases substantially with increasing load: maximum cylinder pressure increases to about 10 MPa at the rated load. In this particular study it was found that these operating parameters were relatively insensitive to fuel variations. The cross-hatched bands show data for an additional nine fuels of varying sulfur content, aromatic content, 10 and 90 percent distillation temperatures.[59]

Higher outputs can be obtained with two-stage turbocharged aftercooled diesel engines, the arrangement shown in Fig. 6-37*d*. The performance characteristics of such a high bmep (1.74 MPa) six-cylinder engine of 14-dm³ displacement are shown in Fig. 15-46. The high air flow requires an overall pressure ratio of 3 at sea level ambient conditions (rising to 4 at 3658 m altitude). This was obtained at lower cost with two turbochargers in series than with a multistage single turbocharger. At rated conditions, the maximum cylinder pressure is 12.7 MPa and the maximum mean piston speed is 10.6 m/s.

Additional gains in efficiency with these heavy-duty automotive diesel engines can be achieved with turbocompounding: some of the available energy in the exhaust gases is captured in a turbine which is geared directly to the engine

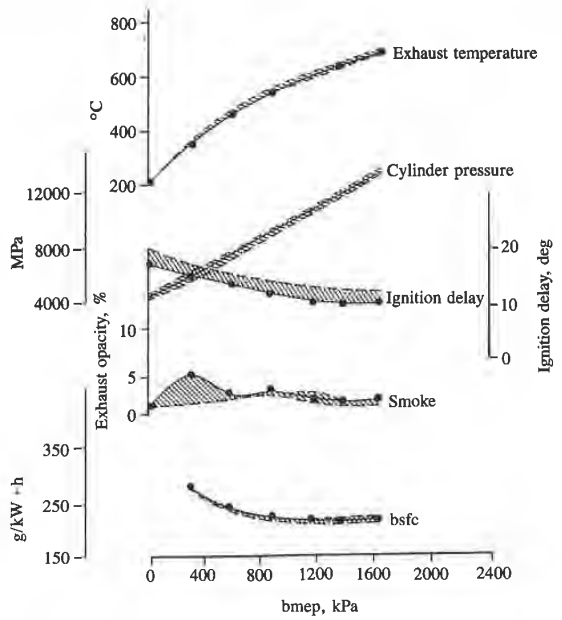

FIGURE 15-45
Operating parameters of 14.6-dm³ six-cylinder turbocharged aftercooled DI diesel engine as a function of load at maximum rated speed of 1800 rev/min. Maximum rated power = 261 kW at bmep = 1192 kPa. Points: standard diesel fuel. Shaded band: nine fuels of varying sulfur content, aromatic content, 10 and 90 per cent distillation temperatures.[59]

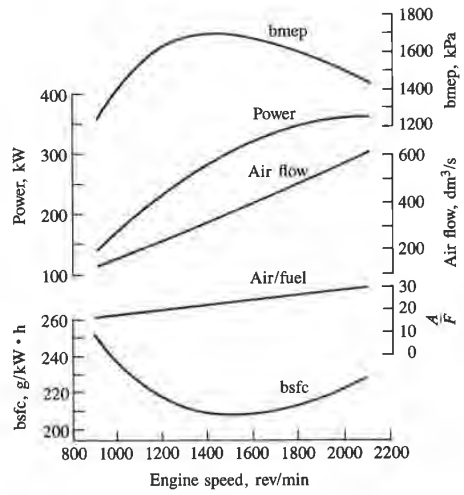

FIGURE 15-46
Operating characteristics of 14-dm³ six-cylinder two-stage turbocharged aftercooled quiescent-chamber DI diesel engine. Maximum bmep = 1.74 MPa. Boost pressure ratio at rated power = 3. Bore = 140 mm, stroke = 152 mm.[60]

drive shaft. The above discussion indicates that typical turbocharged DI diesel engines achieve bsfc levels of 210 to 220 g/kW · h (brake fuel conversion efficiencies of 0.4 to 0.38). With the increased cylinder pressure capability, higher fuel-injection pressures, and lower-temperature aftercooling of the above higher bmep engines, bsfc values of 200 g/kW · h (0.42 brake efficiency) or lower can be achieved. With turbocompounding, bsfc values can be reduced another 5 to 6 percent to about 180 g/kW · h, or a brake efficiency of 0.47, at rated power.[61]

The largest four-stroke cycle DI diesel engines are used for marine propulsion. An example is the Sulzer 400 mm bore 480 mm stroke engine which produces 640 kW per cylinder at 580 rev/min ($\bar{S}_p$ = 9.3 m/s). Very high bmep levels (2.19 MPa) are achieved at maximum continuous rated power through progress in turbocharger design and engine improvements which allow higher maximum cylinder pressures. These, combined with optimization of gas exchange and combustion processes, achieve bsfc values of 185 to 190 g/kW · h (45 to 46 percent brake efficiency).[62]

Many diesel system concepts are being examined which promise even higher output and/or efficiency. Variable-geometry turbocharger-turbine nozzles improve utilization of exhaust gas available energy at low engine speeds. The hyperbar turbocharging system—essentially a combination of a diesel engine with a free-running gas turbine (a combustion chamber is placed between the engine and the turbocharger turbine)—has the potential of much higher bmep. Diesel systems with thermally insulated combustion chambers which reduce heat losses and increase the available exhaust energy have the potential for improving efficiency and for increasing power through additional exhaust energy recovery in devices such as compounded turbines and exhaust-heated Rankine cycle systems.[48]

led DI diesel engine as a func-
ım rated power = 261 kW at
fuels of varying sulfur content,

15.6.3 Two-Stroke Cycle SI Engines

The two-stroke cycle spark-ignition engine in its standard form employs sealed crankcase induction and compression of the fresh charge prior to charge transfer, with compression and spark ignition in the engine cylinder after charge transfer. The fresh mixture must be compressed to above exhaust system pressures, prior to entry to the cylinder, to achieve effective scavenging of the burned gases. Two-stroke cycle scavenging processes were discussed in Sec. 6.6. The two-stroke spark-ignition engine is an especially simple and light engine concept and finds its greatest use as a portable power source or on motorcycles where these advantages are important. Its inherent weakness is that the fresh fuel-air mixture which short-circuits the cylinder directly to the exhaust system during the scavenging process constitutes a significant fuel consumption penalty, and results in excessive unburned hydrocarbon emissions.

15-46
characteristics of 14-dm^3 six-
wo-stage turbocharged after-
uiescent-chamber DI diesel
Maximum bmep = 1.74 MPa.
ssure ratio at rated power = 3.
0 mm, stroke = 152 mm.[60]

This section briefly discusses the performance characteristics of small crankcase compression two-stroke cycle SI engines. The performance characteristics (power and torque) of these engines depend on the extent to which the displaced volume is filled with fresh mixture, i.e., the charging efficiency [Eq. (6.24)]. The

fuel consumption will depend on both the trapping efficiency [Eq. (6.21)] and the charging efficiency. Figure 15-47*a* shows how the trapping efficiency η_{tr} varies with increasing delivery ratio Λ at several engine speeds for a two-cylinder 347-cm^3 displacement motorcycle crankcase compression engine. The delivery ratio increases from about 0.1 at idle conditions to 0.7 to 0.8 at wide-open throt-

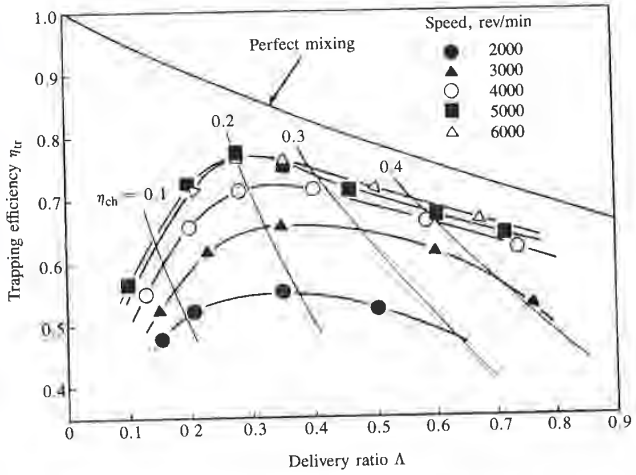

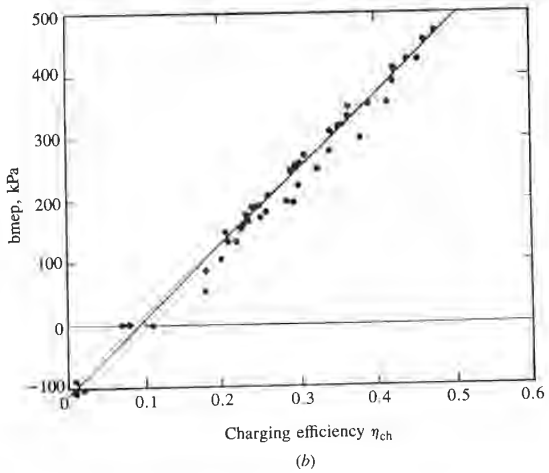

FIGURE 15-47
(*a*) Trapping and charging efficiencies as a function of the delivery ratio. (*b*) Dependence of brake mean effective pressure on fresh-charge mass defined by charging efficiency. Two-cylinder 347-cm^3 displacement two-stroke cycle spark-ignition engine.[63]

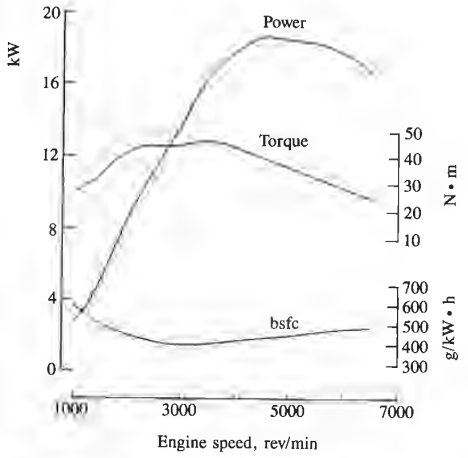

FIGURE 15-48
Performance characteristics of a three-cylinder 450-cm³ two-stroke cycle spark-ignition engine. Maximum bmep = 640 kPa. Bore = 58 mm, stroke = 56 mm.[64]

tle. Lines of constant charging efficiency η_{ch} [which equals $\Lambda\eta_{tr}$; see Eq. (6.25)] are shown. Figure 15-47*b* shows bmep plotted against these charging efficiency values and the linear dependence on fresh charge mass retained is clear.

Performance curves for a three-cylinder 450-cm³ two-stroke cycle minicar engine are shown in Fig. 15-48. Maximum bmep is 640 kPa at about 4000 rev/min. Smaller motorcycle engines can achieve slightly higher maximum bmep at higher speeds (7000 rev/min). Fuel consumption at the maximum bmep point is about 400 g/kW · h. Average fuel consumption is usually one-and-a-half to two times that of an equivalent four-stroke cycle engine.

CO emissions from two-stroke cycle engines vary primarily with the fuel/air equivalence ratio in a manner similar to that of four-stroke cycle engines (see Fig. 11-20). NO_x emissions are significantly lower than from four-stroke engines due to the high residual gas fraction resulting from the low charging efficiency. Unburned hydrocarbon emissions from carbureted two-stroke engines are about five times as high as those of equivalent four-stroke engines due to fresh mixture short-circuiting the cylinder during scavenging. Exhaust mass hydrocarbon emissions vary approximately as $\Lambda(1 - \eta_{tr})\phi$, where ϕ is the fuel/air equivalence ratio.[63]

15.6.4 Two-Stroke Cycle CI Engines

Large marine diesel engines (0.4 to 1 m bore) utilize the two-stroke cycle. These low-speed engines with relatively few cylinders are well suited to marine propulsion since they are able to match the power/speed requirements of ships with simple direct-drive arrangements. These engines are turbocharged to achieve high brake mean effective pressures and specific output. The largest of these engines can achieve brake fuel conversion efficiencies of up to 54 percent. An example of a large marine two-stroke engine is shown in Fig. 1-24. Over the past 25 years

the output per cylinder of such engines has increased by a factor of more than two, and fuel consumption has decreased by 25 percent. These changes have been achieved by increasing the maximum firing pressure to 13 MPa, and by refining critical engine processes such as fuel injection, combustion, supercharging, and scavenging. The uniflow-scavenging process is now preferred to loop scavenging since it achieves higher scavenging efficiency at high stroke/bore ratios and allows increases in the expansion stroke.[62]

The performance characteristics of a 580 mm bore Sulzer two-stroke marine diesel engine with a stroke/bore ratio of 2.9 are shown in Fig. 15-49. The solid lines show the standard turbocharged engine characteristics. The rated speed for the engine is 125 rev/min, corresponding to a maximum mean piston speed of 7.2 m/s. The rated bmep is 1.66 MPa. The minimum bsfc is 175 g/kW · h which equals a brake fuel conversion efficiency of 48 percent. For larger lower-speed engines, the efficiency is higher. The dashed lines show how the performance of this engine can be improved by turbocompounding. A proportion of the engine's exhaust flow, at loads higher than 50 percent, is diverted from the turbocharger inlet to a separate turbine coupled to the engine power takeoff gear via an epicyclic speed-reduction gear and hydraulic coupling. The additional power recovered in this manner from the engine exhaust flow improves bsfc by 5 g/kW · h. At part load, when the full exhaust flow passes through the turbocharger, an efficiency gain is also obtained, due to the higher scavenging pressure (and therefore increased cylinder pressure) obtained with the full exhaust flow.

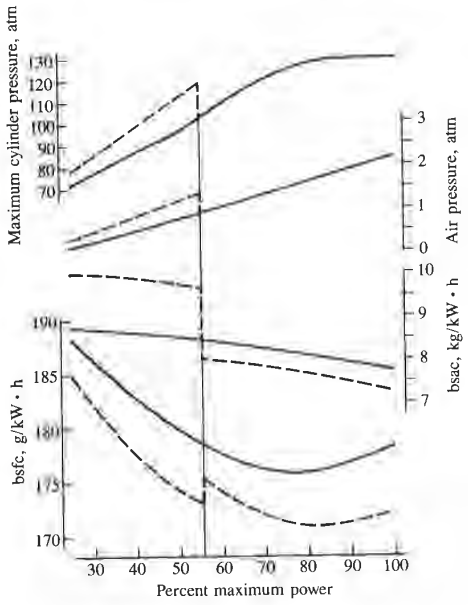

FIGURE 15-49
Performance characteristics of large marine two-stroke cycle uniflow-scavenged DI diesel engine. Bore = 580 mm, stroke/bore = 2.9, maximum rated speed = 125 rev/min (mean piston speed = 7.2 m/s), bmep (at rated power) = 1.66 MPa. Solid line: standard turbocharged configuration. Dashed lines: parallel turbocompounded configuration at greater than 50 percent load. bsac: brake specific air consumption.[62]

a factor of more than
hese changes have been
3 MPa, and by refining
on, supercharging, and
:red to loop scavenging
stroke/bore ratios and

)ore Sulzer two-stroke
1own in Fig. 15-49. The
aracteristics. The rated
maximum mean piston
minimum bsfc is 175
)f 48 percent. For larger
lines show how the per-
unding. A proportion of
:nt, is diverted from the
1gine power takeoff gear
)upling. The additional
t flow improves bsfc by
sses through the turbo-
gher scavenging pressure
the full exhaust flow.

15-49
:e characteristics of large
wo-stroke cycle uniflow-
DI diesel engine. Bore =
stroke/bore = 2.9, maximum
d = 125 rev/min (mean piston
? m/s), bmep (at rated power)
'a. Solid line: standard turbo-
:onfiguration. Dashed lines:
rbocompounded configuration
than 50 percent load. bsac:
ific air consumption.[62]

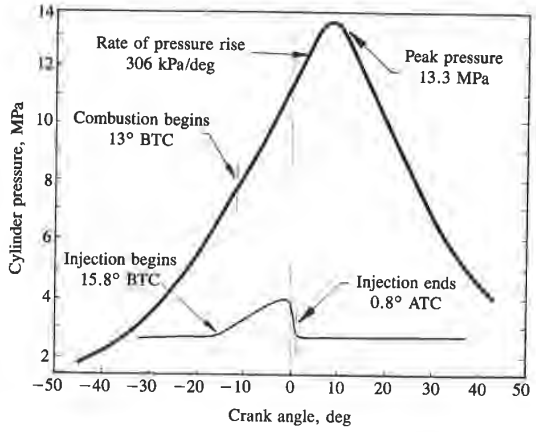

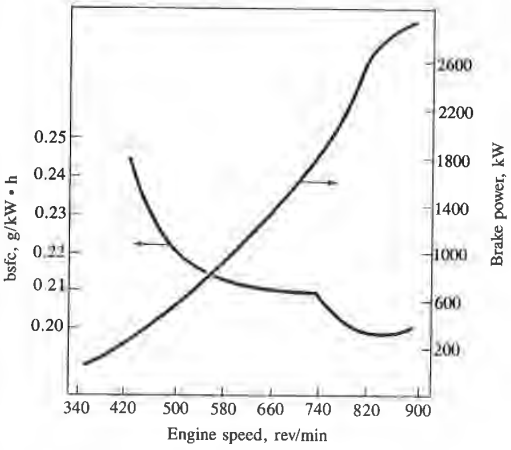

FIGURE 15-50
Injection, combustion, and performance characteristics of intermediate-size turbocharged two-stroke cycle uniflow-scavenged DI diesel engine. Bore = 230.2 mm, stroke = 279.4 mm and $r_c = 16$. Shallow dish-in-piston combustion chamber with swirl. At maximum rated power at 900 rev/min, bmep = 0.92–1.12 MPa depending on application.[65]

Both two-stroke and four-stroke cycle diesel engines of intermediate size (200 to 400 mm bore) are used in rail, industrial, marine, and oil drilling applications. The performance characteristics of a turbocharged two-stroke cycle uniflow-scavenged DI diesel engine (similar to the engine in Fig. 1-5), with 230.2 mm bore, 279.4 mm stroke, and a compression ratio of 16, are shown in Fig. 15-50. Combustion in the shallow dish-in-piston chamber with swirl occurs smoothly yielding a relatively low rate of pressure rise. The pressure curve shown with peak pressure of 13.3 MPa is for full-load operation. The bmep at rated power at 900 rev/min is 0.92 to 1.12 MPa depending on application. The maximum mean piston speed is 8.4 m/s. The bsfc of 200 g/kW · h corresponds to $\eta_{f,b} = 0.42$.

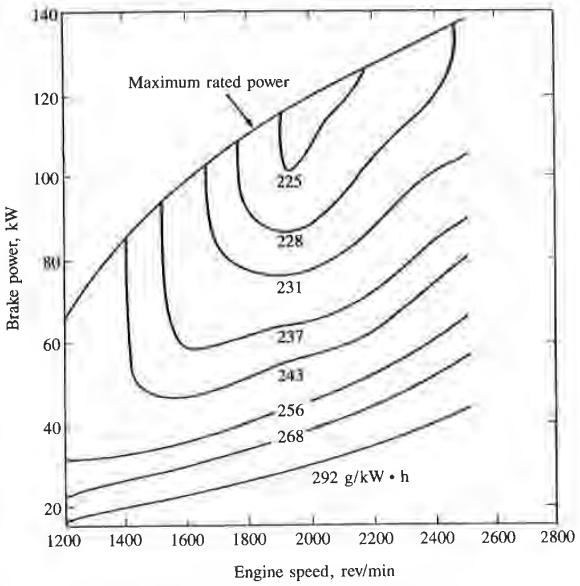

FIGURE 15-51
Brake power and specific fuel consumption (grams per kilowatt-hour) map of four-cylinder 3.48-dm^3 uniflow-scavenged two-stroke cycle DI diesel engine. Engine turbocharged at mid and high loads; Roots blown at low loads. Maximum boost pressure ratio = 2.6. Bore = 98.4 mm, stroke = 114.3 mm, $r_c = 18$.[66]

Smaller turbocharged two-stroke cycle DI diesel engines also compete with four-stroke cycle engines in the marine, industrial, and construction markets. The fuel consumption map of such a four-cylinder 3.48-dm^3 displacement uniflow-scavenged two-stroke cycle diesel engine is shown in Fig. 15-51. The engine uses a Roots blower to provide the required scavenging air pressure for starting and light-load operation. At moderate and high loads the turbocharger supplies sufficient boost and the blower is not needed; the blower is unloaded (air flow is bypassed around the blower) under these conditions. The engine generates 138 kW at its rated speed of 2500 rev/min (mean piston speed of 9.5 m/s) and a maximum bmep of 951 kPa at 1500 rev/min. The best bsfc is 225 g/kW · h and the maximum boost pressure ratio is 2.6.

15.7 ENGINE PERFORMANCE SUMMARY

The major performance characteristics of the spark-ignition and compression-ignition engines described in previous sections of this chapter are summarized here to highlight the overall trends. Table 15.4 lists the major design features of these engines, the bmep at maximum engine torque, bmep and the value of the mean piston speed $\bar{S}_p$ at maximum rated power, and the minimum value of bsfc

p of four-cylinder 3.48-dm^3
harged at mid and high
io = 2.6. Bore = 98.4 mm,

nes also compete with
struction markets. The
displacement uniflow-
15-51. The engine uses
ssure for starting and
ocharger supplies suffi-
unloaded (air flow is
The engine generates
peed of 9.5 m/s) and a
fc is 225 g/kW · h and

ion and compression-
apter are summarized
ajor design features of
p and the value of the
ninimum value of bsfc

TABLE 15.4
Performance of representative engines in different categories

Engine type†	Bore, mm	Stroke, mm	Stroke/bore	r_c	Volume per cylinder, dm^3	Number of cylinders	Maximum torque		Rated maximum power			Maximum efficiency			Reference
							bmep, kPa	Speed, rev/min	bmep, kPa	Speed, rev/min	Boost pressure ratio	$\bar{S}_p$, m/s	bsfc g/kW · h	$\eta_{f,b}$	
SI/4S/NA	96.8	86	0.88	8.6	0.632	6	910	2500	750	4300	—	12.3			1
SI/4S/NA	84.5	88	1.04	8.5	0.494	4	966	2800	767	5200	—	15.3			67
SI/4S/NA	86*	86*	1*	8.5*	0.5	4	910	3500	758	5000	—	14.3	274	0.30	13
SI/4S/NA	96	80	0.83	9.5	0.579	4	998	2800	796	5400	—	14.4			52
SI/4S/TC	92	80	0.87	7.5	0.532	4	1241	3800	1024	5400	1.6*	14.4			52
SI/4S/TCAC	96	80	0.83	8.7	0.579	4	1356	2900	1144	5300	1.6	14.1			52
SI/2S/C	58	56	0.97		0.144	3	654	3500	575	4500		8.4	~400*	~0.2	64
SI/2S/C	64	54	0.84		0.174	2	686	7000	590	8200		14.8	~340*	~0.24	63
IDI/4S/NA	76.5	86.4	1.13	23	0.397	5	850	3100	670	4800	—	13.8	280	0.30	35
IDI/4S/NA	84	82	0.98	22	0.454	4	675	2000	502	5000	—	13.7			4
IDI/4S/NA	102	100	0.98	19	0.817	4	848	2200	743	3500	—	11.7	251	0.34	46
IDI/4S/TC	76.5	86.4	1.13	23	0.397	6	1080	2400	840	4800	1.7	13.8	240	0.35	54
DI/4S/NA	76.5	80	1.05	18.5	0.368	4	735	2800	600	5000	—	13.3	246	0.34	34
DI/4S/NAA	102	100	0.98	18	0.817	8	784	2000	682	3200	—	10.7	220	0.39	33
DI/4S/NA	102	100	0.98	17	0.817	4	886	2200	782	3500	—	11.7	221	0.38	46
DI/4S/NA	115	135	1.17	16	1.40	6	851	1400	777	2700	—	12.2	204	0.42	3
DI/4S/NA	135	140	1.04		2.00	6	862	1400	763	2500	—	11.7			57
DI/4S/TC	115	135	1.17		1.40	6	1098	1500	941	2500		11.2	203	0.42	3
DI/4S/TCAC	115	135	1.17		1.40	6	1344	1600	1240	2300		10.4			3
DI/4S/TCAC	128	140	1.09	15	1.8	6–16	1560	1500	1280	2100	2.5	9.8	195	0.43	58
DI/4S/TC	135	140	1.04	16	2.00	6	1087	1300	911	2300	1.9	10.7	210	0.40	57
DI/4S/2TCAC	140	152	1.09		2.33	6	1740	1400	1445	2100	3	10.6	207	0.41	60
DI/4S/TCAC	400	480	1.20		60.3	6–18			2190	580		9.3	185	0.46	62
DI/2S/TC	98.4	114.3	1.16	18	0.870	3, 4, 6	1065	1500	952	2500	2.6	9.5	226	0.37	66
DI/2S/TC	230	279.4	1.21	16	11.6	8–20			920–1122	900	2.8	8.4	200	0.42	65
DI/2S/TCAC	380–840	1100–2900	2.9–3.4		125–1607	4–12			1660	196–90	3.5	7.2	180–160	0.47–0.53	62

† Engine type: SI = spark-ignition; IDI = indirect-injection compression-ignition; DI = direct-injection compression-ignition; 4S = four-stroke; 2S = two-stroke; NA = naturally aspirated; NAA = NA and air-cooled; C = crankcase compression of scavenging mixture; TC = turbocharged; TCAC = turbocharged and aftercooled; 2TC = two-stage turbocharged.
* Denotes estimated value.

and the corresponding brake fuel conversion efficiency. It should be stressed that there are many different engine configurations and uses, and that for each of these there are variations in design and operating characteristics. However, these representative values of performance parameters illustrate the following trends:

1. Within a given category of engines (e.g., naturally aspirated four-stroke SI engines) the values of maximum bmep, and bmep and $\bar{S}_p$ at maximum rated power, are closely comparable. Within an engine category where the range in size is substantial, there is an increase in maximum bmep and a decrease in minimum bsfc as size increases due to the decreasing relative importance of friction and heat loss per cycle. There is also a decrease in $\bar{S}_p$ at maximum power as engine size increases. Note the higher bmep of naturally aspirated SI engines compared to equivalent NA diesels due to the fuel-rich operation of the former at wide-open throttle.
2. Two-stroke cycle spark-ignition engines have significantly lower bmep and higher bsfc than four-stroke cycle SI engines.
3. The effect of increasing inlet air density by increasing inlet air pressure increases maximum bmep values substantially. Turbocharging with aftercooling gives increased bmep gains relative to turbocharging without aftercooling at the same pressure level. The maximum bmep of turbocharged SI engines is knock-limited. The maximum bmep of turbocharged compression-ignition engines is stress-limited. The larger CI engines are designed to accept higher maximum cylinder pressures, and hence higher boost.
4. The best efficiency values of modern automobile SI engines and IDI diesel engines are comparable. However, the diesel has a significant advantage at lower loads due to its low pumping work and leaner air/fuel ratio. Small DI diesels have comparable (or slightly lower) maximum bmep to equivalent IDI diesels. The best bsfc values for DI diesels are 10 to 15 percent better, however.
5. In the DI diesel category (which is used over the largest size range—less than 100 mm bore to almost 1 m), maximum bmep and best brake fuel conversion efficiency steadily improve with increasing engine size due to reduced impact of friction and heat loss per cycle, higher allowable maximum cylinder pressure so higher boost can be used, and (additionally in the larger engines) through turbocompounding.

PROBLEMS

15.1. The schematics show three different four-stroke cycle spark-ignition engine combustion chambers. A and B are two-valve engines, C is a four-valve engine (two inlet valves which open simultaneously, two exhaust valves). Dimensions in millimeters are indicated. A and C have normal inlet ports and do not generate any swirl. B has a helical inlet port and generates substantial swirl. Spark plug locations are indicated. All three engines operate at the same speed (3000 rev/min), with the same inlet mixture composition, temperature, and pressure, and have the same displaced volume.

(*a*) Rank the chambers 1, 2, 3 in the order of their volumetric efficiency (1 = highest η_v).
(*b*) Rank the chambers in order (1, 2, 3) of their flame frontal area (1 = highest) when the mass fraction burned is about 0.2 and the piston is at TC.
(*c*) Given this relative flame front area ranking, discuss whether the ranking by mass burning rate dm_b/dt will be different from the flame area ranking.
(*d*) Briefly discuss the knock implications of these three chamber designs. Which is likely to have the worst knock problem?

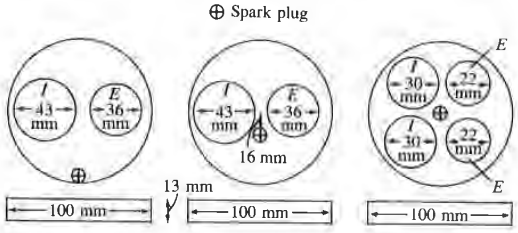

FIGURE P15-1

15.2. Figures 15-23 and 15-10 show the variation in brake specific fuel consumption (bsfc) for a swirl-chamber IDI automobile diesel (D) and a conventional automobile spark-ignition (SI) engine as a function of load and speed, respectively. From these graphs determine, and then plot, brake fuel conversion efficiency: (1) as a function of speed at *full load* and (2) as a function of load at a mid-speed of 2500 rev/min. Both engines are naturally aspirated. Assume the engine details are:

	Compression ratio	Equivalence ratio range	Displacement, dm^3
Diesel	22	0.3–0.8	2.3
SI engine	9	1.0–1.2	1.6

(*a*) List the major engine design and operating variables that determine brake fuel conversion efficiency.
(*b*) Explain briefly the reasons for the shapes of the curves you have plotted and the relative relationship of the D and SI curves.
(*c*) At 2500 rev/min, estimate which engine will give the higher maximum brake power.

15.3. The diesel system shown in the figure consists of a multicylinder reciprocating diesel engine, a turbocharger (with a compressor C and turbine T_T mechanically connected to each other), an intercooler (I), and a power turbine (T_P) which is geared to the engine drive shaft. The gas and fuel flow paths and the gas states at the numbered points are shown. You can assume that the specific heat at constant pressure c_p of the gas throughout the entire system is 1.2 kJ/kg·K and $\gamma = c_p/c_v = 1.333$. The engine operates at 1900 rev/min. The fuel has a lower heating value of 42 MJ/kg of fuel.

(*a*) What is the power (in kilowatts) which the turbocharger turbine (T_T) must produce? What is the gas temperature at exit to the turbocharger turbine?
(*b*) What is the power turbine power output?
(*c*) The heat losses in the engine are 15 percent of the fuel's chemical energy ($\dot{m}_f Q_{LHV}$). Find the engine power output, the total system power output, and the total system brake fuel conversion efficiency (friction effects in the engine and power turbine are internal to these devices and do not need to be explicitly evaluated).

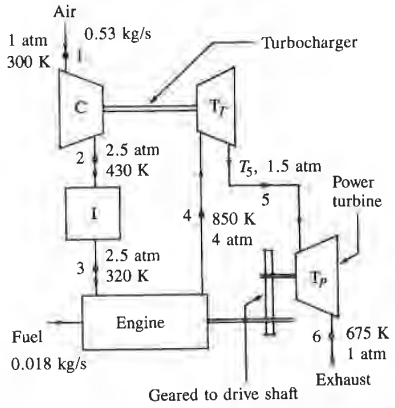

FIGURE P15-3

15.4. The attached graph shows how the brake power and specific fuel consumption of a four-stroke cycle single-cylinder spark-ignition engine vary with the fuel/air equivalence ratio at wide-open throttle. It also shows how the following efficiencies vary with equivalence ratio:

The volumetric efficiency: η_v
The mechanical efficiency: η_m [Eq. (2.17)]

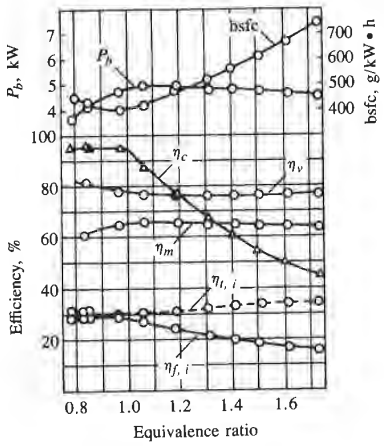

FIGURE P15-4

The combustion efficiency: η_c [Eq. (3.27)]
The indicated fuel conversion efficiency: $\eta_{f,i}$ [Eq. (2.23)]
The indicated thermal conversion efficiency: $\eta_{t,i}$ [Eq. (3.31)]

(*a*) Derive a relation between the variables $\eta_{f,i}$, η_c, and $\eta_{t,i}$.
(*b*) Derive an equation which relates the brake power P_b to η_v, η_m, η_c, $\eta_{t,i}$, and any other engine and fuel parameters required.
(*c*) Explain briefly why the variations of η_v, η_m, η_c, $\eta_{f,i}$, $\eta_{t,i}$ with equivalence ratio in the figure have the form shown (e.g., why the parameter is approximately constant, or has a maximum/minimum, or decreases/increases with increasing richness or leanness, etc.).

15.5. The diagram shows the layout of a low heat loss turbocharged turbocompounded diesel engine. The engine and exhaust system is insulated with ceramics to reduce heat losses to a minimum. Air flows steadily at 0.4 kg/s and atmospheric conditions into the compressor C, and exits at 445 K and 3 atm. The air is cooled to 350 K in the intercooler I. The specific heat of air, c_p, is 1 kJ/kg · K. In the reciprocating diesel engine, the fuel flow rate is 0.016 kg/s, the fuel heating value is 42.5 MJ/kg, and the heat lost through the ceramic walls is 60 kW.

The exhaust gases leave the reciprocating engine at 1000 K and 3 atm, and enter the first turbine T_A, which is mechanically linked to the compressor. The pressure between the two turbines is 1.5 atm. The second turbine T_B is mechanically coupled to the engine drive shaft and exhausts to the atmosphere at 800 K. The specific heat of exhaust gases, c_p, is 1.1 kJ/kg · K.

(*a*) Analyze the reciprocating diesel engine E and determine the indicated power obtained from this component of the total system. If the engine mechanical efficiency is 0.9 what is the brake power obtained from component E?
(*b*) Determine the power obtained from the power turbine T_B.
(*c*) Determine the total brake power obtained from the complete engine system and the fuel conversion efficiency of the system. You can neglect mechanical losses in the coupling between the power turbine and the engine drive shaft.

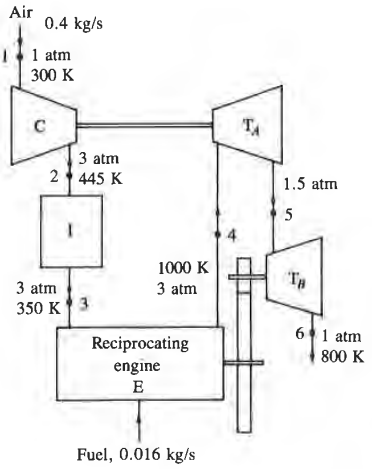

FIGURE P15-5

15.6. New automobile spark-ignition engines employ "fast-burn technology" to achieve an improvement in fuel consumption and reductions in hydrocarbon (HC) and oxides of nitrogen (NO_x) emissions. This question asks you to explain the experimental data which shows that faster-burning combustion chambers do provide these benefits relative to more moderate burn-rate chambers.

(*a*) Figure 9-36*b* shows the effect of increasing the percent of the exhaust gas recycled to the intake (for NO_x control) in a moderate burn-rate engine at constant speed and load, stoichiometric air/fuel ratio, with timing adjusted for maximum brake torque at each condition. COV_{imep} is the standard deviation in imep divided by the average imep, in percent. The different types of combustion are: *misfire*, *partial burn*, *slow burn*, *normal burn*, defined in Sec. 9.4.3. Frequency is percent of cycles in each of these categories. Use your knowledge of the spark-ignition engine flame-propagation process and HC emission mechanism to explain these trends in COV_{imep}, HC, and frequency as EGR is increased.

(*b*) The fast-burn combustion chamber uses two spark plugs and generates swirl inside the chamber by placing a vane in the inlet port to direct the air to enter the chamber tangentially. The swirl angular velocity in the cylinder at the end of intake is six times the crankshaft angular velocity. There is no swirl in the moderate burn-rate chamber which has a single spark plug and a relatively quiescent in-cylinder flow. The table shows spark timing, average time of peak pressure, average flame-development angle (0 to 10 percent mass burned) and rapid burning period (10 to 90 percent mass burned) for these two engines. Figures 11-29 and 15-9 show how the operating and emission characteristics of the fast burn and moderate burn-rate engines change as percent EGR is increased. Explain the reasons for the differences in these trends in COV_{imep}, bsfc (brake specific fuel consumption), and HC, and similarity in NO_x. The operating conditions are held constant at the same values as before.

	Fast burn	**Moderate burn**	
Spark timing	18°	40°	BTC
Crank angle for average p_{max}	15°	16°	ATC
0–10% burned	24°	35°	
10–90% burned	20°	50°	

15.7. Two alternative fuels, methanol and hydrogen, are being studied as potential future spark-ignition engine fuels which might replace gasoline (modeled by isooctane C_8H_{18}). The table gives some of the relevant properties of these fuels.

(*a*) For each fuel calculate the energy content per unit volume (in joules per cubic meter) of a stoichiometric mixture of fuel vapor and air at 1 atm and 350 K. The universal gas constant is 8314 J/kmol · K. What implications can you draw from these numbers regarding the maximum power output of an engine of fixed geometry operating with these fuels with stoichiometric mixtures?

(*b*) The octane rating of each fuel, and hence the knock-limited compression ratio of an engine optimized for each fuel, is different. Estimate the ratio of the maximum indicated mean effective pressure for methanol- and hydrogen-fueled

engines to that of the gasoline-fueled engine, allowing for energy density effects at intake (at 1 atm and 350 K), at the knock-limited compression ratio for each fuel, for stoichiometric mixtures. You can assume that the fuel-air cycle results for isooctane apply also for methanol and hydrogen cycles to a good approximation, when the energy density is the same.

(*c*) The lean operating limit for the three fuels is different as indicated. Estimate the ratio of indicated fuel conversion efficiency for methanol and hydrogen at their lean limit and knock-limited compression ratio, relative to gasoline at its lean limit and knock-limited compression ratio, at the same inlet pressure (0.5 atm). Under these conditions, rank the fuel-engine combinations in order of decreasing power output.

	Gasoline (isooctane) C_8H_{18}	Methanol CH_3OH	Hydrogen H_2
Stoichiometric F/A	0.066	0.155	0.0292
Lower heating value, MJ/kg	44.4	20.0	120.1
Molecular weight of fuel	114	32	2
Molecular weight of stoichiometric mixture	30.3	29.4	21
Research octane number	95	106	~90
Knock-limited compression ratio	9	12	8
Equivalence ratio at lean misfire limit	0.9	0.8	0.6

15.8. Small-size direct-injection (DI) diesel engines are being developed as potential replacements for indirect-injection (IDI) or prechamber engines in automobile applications. Figures 10-1*b* and 10-2 show the essential features of these two types of diesel. The DI engine employs high air swirl, which is set up with a helical swirl-generating inlet port (Fig. 8-13). The injector is centrally located over the bowl-in-piston combustion chamber and the injector nozzle has four holes, one in each quadrant. The IDI engine (a Ricardo Comet swirl chamber), in contrast, has no swirl in the main chamber, but generates high velocities and a rotating flow in the prechamber during compression.

Figures 15-21 and 15-23 show performance maps for typical versions of these two types of engines. Bmep, brake mean effective pressure, is plotted against engine speed. Brake specific fuel consumption contours are shown with the numbers in grams per kilowatt-hour.

The heat-release-rate profiles for these two types of engine at a typical mid-load mid-speed point are shown versus crank angle in the sketch. $\dot{Q}$ has units of joules per second.

(*a*) Explain the reasons for the differences in shape and relative timing in the cycle of the heat-release-rate profiles.

(*b*) Suggest reasons for the differences (magnitude and shape) in the maximum bmep versus mean-piston-speed line for the DI and IDI engines.

(*c*) Evaluate the brake fuel conversion efficiency of each engine at its maximum efficiency point, and at 2000 rev/min and road load (road load is the power requirement to maintain a vehicle at constant speed; it is 2 bar bmep at 2000 rev/min). Explain the origin of the observed differences in efficiency at these two operating conditions.

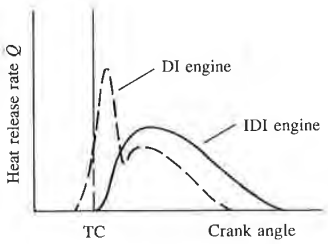

FIGURE P15-8

15.9. A four-stroke cycle naturally aspirated direct-injection diesel is being developed to provide 200 kW of power at the engine's maximum rated speed. Using information available in Chaps. 2, 5, and 15, on typical values of critical engine operating parameters at maximum power and speed for good engine designs, estimate the following:

(*a*) The compression ratio, the number of cylinders, the cylinder bore and stroke, and the maximum rated speed of an appropriate engine design that would provide this maximum power.

(*b*) The brake specific fuel consumption of this engine design at the maximum power operating point.

(*c*) The approximate increase in brake power that would result if the engine was turbocharged.

15.10. Natural gas (which is close to 100 percent methane, CH_4) is being considered as a spark-ignition engine fuel. The properties of methane and gasoline (assume the same properties as isooctane) and the engine details for each fuel are summarized below (ϕ is the fuel/air equivalence ratio).

	Natural gas	**Gasoline**
Composition	CH_4	C_8H_{18}
Heating value, MJ/kg	50.0	44.3
Research octane number	120	94
Compression ratio	14	8
Displaced volume, dm^3	2	2
Lean misfire limit	$\phi = 0.5$	$\phi = 0.8$
Part-load equivalence ratio	$\phi = 0.6$	$\phi = 0.9$
Full-load equivalence ratio	$\phi = 1.1$	$\phi = 1.2$

As indicated in the table, the displaced volume of the engine is unchanged when the conversion for natural gas is made; however, the clearance height is reduced to increase the compression ratio.

(*a*) Estimate the ratio of the volumetric efficiency of the engine operating on natural gas to the volumetric efficiency with gasoline, at wide-open throttle and 2000 rev/min. Both fuels are in the gaseous state in the intake manifold.

(*b*) Estimate the ratio of the maximum indicated power of the engine operating with natural gas to the maximum power of the gasoline engine.

(*c*) Estimate the ratio of the gross indicated fuel conversion efficiency of the natural gas engine to that of the gasoline engine, at the part-load conditions given.

(*d*) Explain whether the NO, CO, and hydrocarbon specific emissions (grams of pollutant per hour, per unit indicated power) at part-load conditions of the natural gas engine will be higher, about the same, or lower than the NO, CO, and HC emissions from the gasoline engine. Explain briefly why.

You can assume that the fuel-air cycle results derived for isooctane-air mixtures are also appropriate for methane-air mixtures.

15.11. Spark-ignition and prechamber diesel engines are both used as engines for passenger cars. They must meet the same exhaust emission requirements. Of great importance are their emission characteristics when optimized for maximum power at wide-open throttle (WOT) and when optimized at cruise conditions for maximum efficiency.

(*a*) Give typical values for the equivalence ratio for a passenger car spark-ignition engine and a prechamber diesel optimized for maximum power at WOT and 2000 rev/min, and optimized for maximum efficiency at part load (bmep = 300 kPa) and 1500 rev/min. Briefly explain the values you have chosen.

(*b*) Construct a table indicating whether at these two operating conditions the specific emissions of CO, HC, NO_x, and particulates are low (L), medium (M), or high (H) relative to the other load point and to the other engine. Explain your reasoning for each table entry.

15.12. For a naturally aspirated four-stroke cycle diesel engine:

(*a*) Show from the definition of mean effective pressure that

$$\text{bmep} \propto \eta_m \eta_{f,i} \eta_v (F/A)$$

where bmep = brake mean effective pressure
η_m = mechanical efficiency
$\eta_{f,i}$ = indicated fuel conversion efficiency
η_v = volumetric efficiency
F/A = fuel/air ratio

(*b*) Sketch carefully proportioned qualitative graphs of η_m, $\eta_{f,i}$, η_v, and $(F/A)/(F/A)_{\text{stoich}}$ versus speed N at full load, and explain the reasons for the shapes of the curves. Then explain why the maximum bmep versus speed curve has the shape shown in Fig. P15-12.

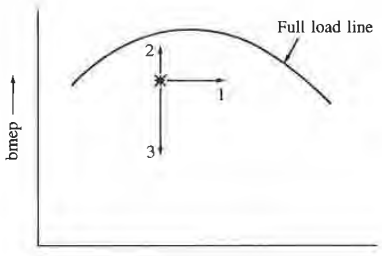

FIGURE P15-12

(*c*) The minimum brake specific fuel consumption point is indicated by the asterisk (*) in Fig. P15-12 (see Figs. 15-21 and 15-22). Explain why brake specific fuel consumption *increases* with (1) increasing speed, (2) increasing bmep, (3) decreasing bmep.

REFERENCES

1. Armstrong, D. L., and Stirrat, G. F.: "Ford's 1982 3.8L V6 Engine," SAE paper 820112, 1982.
2. "Engine Rating Code—Spark-Ignition," SAE Standard J245, in *SAE Handbook*.
3. Okino, M., Okada, K., and Abe, M.: "Isuzu New 8.4L Diesel Engine," SAE paper 850258, 1985.
4. Higashisono, M., Takeuchi, K., and Hara, H.: "The New Isuzu 1.8 Liter 4-Cylinder Diesel Engine for the United States Market," SAE paper 820116, *SAE Trans.*, vol. 91, 1982.
5. *General Motors Automotive Engine Test Code For Four Cycle Spark Ignition Engines*, 6th ed., 1975.
6. Heywood, J. B., Higgins, J. M., Watts, P. A., and Tabaczynski, R. J.: "Development and Use of a Cycle Simulation to Predict SI Engine Efficiency and NO_x Emissions," SAE paper 790291, 1979.
7. Heywood, J. B., and Watts, P. A.: "Parametric Studies of Fuel Consumption and NO Emissions of Dilute Spark-Ignition Engine Operation Using a Cycle Simulation," paper C98/79, in *Proceedings of Conference on Fuel Economy and Emissions of Lean Burn Engines*, Institution of Mechanical Engineers, London, 1979.
8. Quader, A. A.: "The Axially-Stratified-Charge Engine," SAE paper 820131, *SAE Trans.*, vol. 91, 1982.
9. Robison, J. A., and Brehob, W. M.: "The Influence of Improved Mixture Quality on Engine Exhaust Emissions and Performance," *J. Air Pollution Control Ass.*, vol. 17, no. 7, pp. 446–453, July 1967.
10. Thring, R. H., and Overington, M. T.: "Gasoline Engine Combustion—The High Ratio Compact Chamber," SAE paper 820166, *SAE Trans.*, vol. 91, 1982.
11. Hamburg, D. R., and Hyland, J. E.: "A Vaporized Gasoline Metering System for Internal Combustion Engines," SAE paper 760288, 1976.
12. Nakajima, Y., Sugihara, K., and Takagi, Y.: "Lean Mixture or EGR—Which is Better for Fuel Economy and NO_x Reduction?," paper C94/79, in *Proceedings of Conference on Fuel Economy and Emissions of Lean Burn Engines*, Institution of Mechanical Engineers, London, 1979.
13. Wade, W., and Jones, C.: "Current and Future Light Duty Diesel Engines and Their Fuels," SAE paper 840105, *SAE Trans.*, vol. 93, 1984.
14. Lavoie, G. A., and Blumberg, P. N.: "A Fundamental Model for Predicting Fuel Consumption, NO_x and HC Emissions of a Conventional Spark-Ignited Engine," *Combust. Sci. Technol.*, vol. 21, pp. 225–258, 1980.
15. Caton, J. A., Heywood, J. B., and Mendillo, J. V.: "Hydrocarbon Oxidation in a Spark-Ignition Engine Exhaust Port," *Combust. Sci. Technol.*, vol. 37, nos. 3 and 4, pp. 153–169, 1984.
16. Caton, J. A., and Heywood, J. B.: "Models for Heat Transfer, Mixing and Hydrocarbon Oxidation in an Exhaust Port of a Spark-Ignited Engine," SAE paper 800290, 1980.
17. Caris, D. F., and Nelson, E. E., "A New Look at High Compression Engines," *SAE Trans.*, vol. 67, pp. 112–124, 1959.
18. Kerley, R. V., and Thurston, K. W.: "The Indicated Performance of Otto-Cycle Engines," *SAE Trans.*, vol. 70, pp. 5–30, 1962.
19. Muranaka, S., Takagi, Y., and Ishida, T.: "Factors Limiting the Improvement in Thermal Efficiency of S.I. Engine at Higher Compression Ratio," SAE paper 870548, 1987.
20. Gruden, D. O.: "Combustion Chamber Layout for Modern Otto Engines," SAE paper 811231, 1981.
21. Barnes-Moss, H. W.: "A Designers Viewpoint," paper C343/73, in *Proceedings of Conference on Passenger Car Engines*, pp. 133–147, Institution of Mechanical Engineers, Conference publication 19, London, 1973.

22. Kuroda, H., Nakajima, Y., Sugihara, K., Takagi, Y., and Maranaka, S.: "Fast Burn with Heavy EGR Improves Fuel Economy and Reduces NO_x Emission," *JSAE Rev.*, no. 5, pp. 63–69, 1980.
23. Thring, R. H.: "The Effects of Varying Combustion Rate in Spark Ignited Engines," SAE paper 790387, 1979.
24. Harada, M., Kadota, T., and Sugiyama, Y.: "Nissan NAPS-Z Engine Realizes Better Fuel Economy and Low NO_x Emission," SAE paper 810010, 1981.
25. Poulos, S. G., and Heywood, J. B.: "The Effect of Chamber Geometry on Spark-Ignition Engine Combustion," SAE paper 830334, *SAE Trans.*, vol. 92, 1983.
26. Heywood, J. B.: "Combustion Chamber Design for Optimum Spark-Ignition Engine Performance," *Int. J. Vehicle Des.*, vol. 5, no. 3, pp. 336–357, 1984.
27. Novak, J. M., and Blumberg, P. N.: "Parametric Simulation of Significant Design and Operating Alternatives Affecting the Fuel Economy and Emissions of Spark-Ignited Engines," SAE paper 780943, *SAE Trans.*, vol. 87, 1978.
28. Amann, C. A.: "Control of the Homogeneous-Charge Passenger-Car Engine: Defining the Problem," SAE paper 801440, 1980.
29. Bell, A. G.: "The Relationship between Octane Quality and Octane Requirement," SAE paper 750935, 1975.
30. Leppard, W. R.: "Individual-Cylinder Knock Occurrence and Intensity in Multicylinder Engines," SAE paper 820074, 1982.
31. Ingamells, J. C., Stone, R. K., Gerber, N. H., and Unzelman, G. H.: "Effects of Atmospheric Variables on Passenger Car Octane Number Requirements," SAE paper 660544, *SAE Trans.*, vol. 75, 1966.
32. Gruden, D.: "Performance, Exhaust Emissions and Fuel Consumption of an IC Engine Operating with Lean Mixtures," paper C111/79, in *Proceedings of Conference on Fuel Economy and Emissions of Lean Burn Engines*, Institution of Mechanical Engineers, London, 1979.
33. Slezak, P. J., and Vossmeyer, W.: "New Deutz High Performance Diesel Engine," SAE paper 810905, 1981.
34. Neitz, A., and D'Alfonso, N.: "The M.A.N. Combustion System with Controlled Direct Injection for Passenger Car Diesel Engines," SAE paper 810479, 1981.
35. Sator, K., Buttgereit, W., and Sturzebecher, U.: "New 5- and 6-Cylinder VW Diesel Engines for Passenger Cars and Light Duty Trucks," SAE paper 790206, 1979.
36. Monaghan, M. L.: "The High Speed Direct Injection Diesel for Passenger Cars," SAE paper 810477, 1981.
37. Pischinger, R., and Cartellieri, W.: "Combustion System Parameters and Their Effect upon Diesel Engine Exhaust Emissions," SAE paper 720756, *SAE Trans.*, vol. 81, 1972.
38. Ball, W. F., and Hil, R. W.: "Control of a Light Duty Indirect Injection Diesel Engine for Best Trade-Off between Economy and Emissions," paper C122/82, in *Proceedings of Conference on Diesel Engines for Passenger Cars and Light Duty Vehicles*, Publication 1982-8, Institution of Mechanical Engineers, London, 1982.
39. Wade, W. R., Idzikowski, T., Kukkonen, C. A., and Reams, L. A.: "Direct Injection Diesel Capabilities for Passenger Cars," SAE paper 850552, 1985.
40. Greeves, G., and Wang, C. H. T.: "Origins of Diesel Particulate Mass Emission," SAE paper 810260, *SAE Trans.*, vol. 90, 1981.
41. Greeves, G., Khan, I. M., and Wang, C. H. T.: "Origins of Hydrocarbon Emissions from Diesel Engines," SAE paper 770259, *SAE Trans.*, vol. 86, 1977.
42. Greeves, G.: "Response of Diesel Combustion Systems to Increase of Fuel Injection Rate," SAE paper 790037, *SAE Trans.*, vol. 88, 1979.
43. Yu, R. C., and Shahed, S. M.: "Effects of Injection Timing and Exhaust Gas Recirculation on Emissions from a D.I. Diesel Engine," SAE paper 811234, *SAE Trans.*, vol. 90, 1981.
44. Khan, I. M., Greeves, G., and Wang, C. H. T.: "Factors Affecting Smoke and Gaseous Emissions from Direct Injection Engines and a Method of Calculation," SAE paper 730169, 1973.
45. Bassoli, C., Cornetti, G. M., and Cuniberti, F.: "IVECO Diesel Engine Family for Medium Duty Vehicles," SAE paper 820031, 1982.

46. Kawamura, H., Kihara, R., and Kinbara, M.: "Isuzu's New 3.27L Small Direct Injection Diesel," SAE paper 820032, 1982.
47. Arcoumanis, C., Bicen, A. F., and Whitelaw, J. H.: "Squish and Swirl-Squish Interaction in Motored Model Engines," *ASME Trans., J. Fluids Engng*, vol. 105, pp. 105–112, 1983.
48. Watson, N., and Janota, M. S.: *Turbocharging the Internal Combustion Engine*, Wiley-Interscience Publications, John Wiley, New York, 1982.
49. Hiereth, H., and Withalm, G.: "Some Special Features of the Turbocharged Gasoline Engine," SAE paper 790207, 1979.
50. Wallace, T. F.: "Buick's Turbocharged V-6 Powertrain for 1978," SAE paper 780413, *SAE Trans.*, vol. 87, 1978.
51. Allen, F. E., and Rinschler, G. L.: "Turbocharging the Chrysler 2.2 Liter Engine," SAE paper 840252, *SAE Trans.*, vol. 93, 1984.
52. Andersson, J., and Bengtsson, A.: "The Turbocharged and Intercooled 2.3 Liter Engine for the Volvo 760," SAE paper 840253, *SAE Trans.*, vol. 93, 1984.
53. Watson, N.: "Turbochargers for the 1980s—Current Trends and Future Prospects," SAE paper 790063, *SAE Trans*, vol. 88, 1979.
54. Grandinson, A., and Hedin, I.: "A Turbocharged Engine for a Growing Market," paper C119/82, in *Diesel Engines for Passenger Cars and Light Duty Vehicles*, Institution of Mechanical Engineers, Conference publication 1982–8, London, 1982.
55. Walzer, P., and Rottenkolber, P.: "Supercharging of Passenger Car Diesels," paper C117/82, in *Diesel Engines for Passenger Cars and Light Duty Vehicles*, Institution of Mechanical Engineers, Conference publication 1982–8, London, 1982.
56. Carstens, U. G., Isik, T., Biaggini, G., and Cornetti, G.: "Sofim Small High-Speed Diesel Engines—D.I. Versus I.D.I.," SAE paper 810481, 1981.
57. Okada, K., and Takatsuki, T.: "Isuzu's New 12.0L Turbocharged Diesel with Wastegate Boost Control for Fuel Economy," SAE paper 820029, 1982.
58. Schittler, M.: "MWM TBD 234 Compact High-Output Engines for Installation in Heavy Equipment and Military Vehicles," SAE paper 850257, 1985.
59. Barry, E. G., McCabe, L. J., Gerke, D. H., and Perez, J. M.: "Heavy-Duty Diesel Engine/Fuels Combustion Performance and Emissions—A Cooperative Research Program," SAE paper 852078, 1985.
60. Robinson, R. H., and Schnapp, J. P.: "Cummins NTC-475 Series Turbocharged Engine," SAE paper 820982, 1982.
61. Wilson, D. E.: "The Design of a Low Specific Fuel Consumption Turbocompound Engine," SAE paper 860072, 1986.
62. Lustgarten, G. A.: "The Latest Sulzer Marine Diesel Engine Technology," SAE paper 851219, 1985.
63. Tsuchiya, K., and Hirano, S.: "Characteristics of 2-Stroke Motorcycle Exhaust HC Emission and Effects of Air-Fuel Ratio and Ignition Timing," SAE paper 750908, 1975.
64. Uchiyama, H., Chiku, T., and Sayo, S.: "Emission Control of Two-Stroke Automobile Engine," SAE paper 770766, *SAE Trans.*, vol. 86, 1977.
65. Kotlin, J. J., Dunteman, N. R., Chen, J., and Heilenbach, J. W.: "The GM/EMD Model 710 G Series Turbocharged Two-Stroke Cycle Engine," ASME paper 85-DGP-24, 1985.
66. Fellberg, M., Huber, J. W., and Duerr, J. W.: "The Development of Detroit Diesel Allison's New Generation Series 53 Engines," SAE paper 850259, 1985.
67. Hisatomi, T., and Iida, H.: "Nissan Motor Company's New 2.0 Liter Four-Cylinder Gasoline Engine," SAE paper 820113, *SAE Trans.*, vol. 91, 1982.